Quantitative dissection of T cell negative selection mechanisms in the thymus

Jin Yan Yap

October 2017

A thesis submitted for the degree of Doctor of Philosophy
of The Australian National University

Australian National University

Department of Immunology and Infectious Disease,
The John Curtin School of Medical Research,
The Australian National University, Canberra, Australia

Statement of originality

This thesis presents research (experimental work, data analyses and thesis writing) completed in the Immunogenomics Laboratory (IGL), Department of Immunology and Infectious Disease, at the John Curtin School of Medical Research (JCSMR), Australian National University (ANU), Canberra, Australia. This research was performed under the supervision of Dr. Stephen Daley and Prof. Christopher Goodnow.

The data presented in this thesis was of my own work, unless indicated otherwise in figure legends.

JIN YAN YAP

Date: 19/10/2017

Acknowledgements

Dr. Stephen Daley
Principal PhD supervisor

First and foremost, I would like to express my heartfelt gratitude to my PhD supervisor Dr. Stephen Daley for his extensive academic support, financial support, guidance, ideas, feedback for my thesis writing and oral presentations and his inspiring enthusiasm in science throughout my PhD candidature. I would like to thank him for improving my critical thinking and scientific writing skills.

Prof. Christopher Goodnow
Co-supervisor / PhD supervisory panel member

I would also like to extend my gratitude to my co-supervisor/PhD supervisory panel member Prof. Christopher Goodnow for his intellectual suggestions on my project, especially during the first two years of my PhD candidature, and the abundance experimental resources provided throughout my PhD candidature.

Prof. Carola Vinuesa, Associate Prof. Anselm Enders and Prof. Christopher Parish
PhD supervisory panel members

I would like to thank all of my PhD supervisory panel members for their feedback during the yearly supervisory panel meetings and their encouragement, especially after the moving of my supervisors from JCSMR.

JCSMR PhD student co-ordinators and the HDR student administrators

I would like to thank all the past and present JCSMR PhD student co-ordinators **Associate Prof. Marco Casarotto, Associate Prof. Charani Ranasinghe and Dr. Anna Cowan** for giving wise advice and caring for students' welfare, especially during the challenging moments of my PhD journey. I would like to thank Marco for his assistance in providing the JCSMR scholarship during the last two months of my thesis writing. Also, I would like to thank **Tara Butler** and **Wendy Riley** for being such helpful and efficient HDR student administrators in processing all the forms.

Laboratory members associated to Daley's group

I would like to thank the following people for their technical assistance and their friendship:

Debbie Howard, who is an experienced senior laboratory technician, for her extremely efficient technical help in collecting organs, mashing thymi and counting cells, irradiating mice, injecting mice intravenously, all done in parallel with me, to speed up the experimental time required to complete big experiments. I would like to thank her for being such a helpful and wonderful person, and for the birthday cakes and cards and emotional support throughout my PhD journey.

Dr. Daniel Hu, an ex-PhD student, for teaching me EdU staining, EdU injections for a few experiments and his knowledge in answering some academic questions that puzzled me.

Mandeep Singh for sharing his molecular expertise in TCRα chain sequencing (from cDNA synthesis to the sequencing step) and teaching me some of the molecular techniques.

Zoe Marie for being a supportive and helpful friend and for proofreading some of my thesis chapters.

Dr. Rushika Wirasinha for proofreading a thesis chapter and providing feedback for my oral presentations.

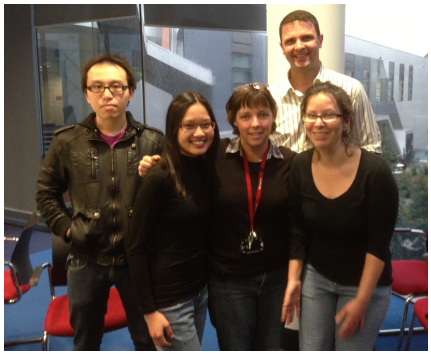

Daley's group

Past and present colleagues from Immunogenomics laboratory (IGL) and other JCSMR laboratories

I would also like to thank:

Dr. Zahra Sabouri-Thompson, Dr. Yogesh Jeellal, Dr. Shubhanshi Trivedi, Jayasree Ravichandran, my JCSMR sunshine, for being there whenever I needed to talk, for being encouraging and positive at all times, for their academic advice and friendship.

Dr. Kaveenda Samarasinghe for his company and emotional support especially during the challenging latter phase of my PhD journey.

Michelle Townsend, IGL laboratory manager for the smooth running of the laboratory.

IGL laboratory members - **Dr. James Wang, Dr. Keisuke Horikawa, Dr. Rebecca Sweet, Dr. Ian Parish, Dr. Mehmet Yabas, Hsei-Di Low, Sarp Kaya, Dr. Lisa Miosge, Hannes Burgmann, Mayura Wagle, Dr. Yovina Sontani;** and **Dr. Fui Jiun Choong, Dr. Candice Lee, Sarita Dhounchak, Dr. Alvin Pramata, Dr. David Simon Davis, James O'Connor, Ilenia Papa, Lorena Núñez Villacis** and **Paula Gonzales** for the social outings making my PhD days at JCSMR more colourful.

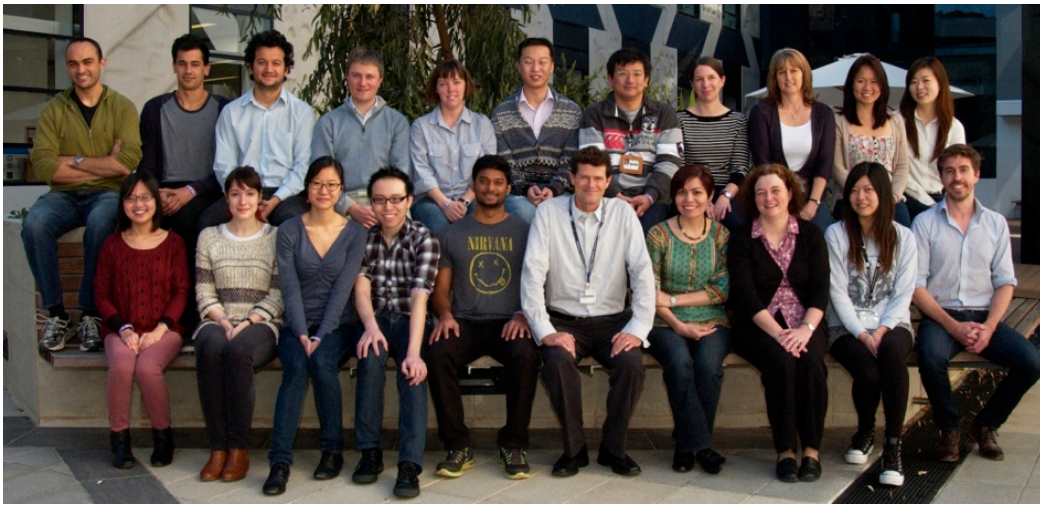

Immunogenomics laboratory members

Imaging and Cytometry Facility in JCSMR and
Australian Phenomics Facility (APF)

I would like to thank **Dr. Harpreet Vohra** and **Michael Devoy** for sorting the cells and being such helpful, especially when there was a blockage with the flow cytometry machines. I would also like to thank the staff in APF for mouse husbandry and genotyping.

The John Curtin School of Medical Research (JCSMR),
The Australian National University (ANU) and
Australian Government Research Training Program (RTP) Scholarship

I would like to thank JCSMR and ANU for giving me the opportunity to pursue a PhD degree in medical research and to attend local and international conferences, by offering the PhD scholarships and HDR student travel funds. This research is also supported by an Australian Government Research Training Program (RTP) Scholarship. I would like to thank JCSMR for organising the weekly Immunology seminar series by inviting the local and international speakers to broaden my knowledge, providing a world-class medical research facility, equipment, modern and comfortable laboratories and office furniture.

Past and present Toad Hall and University House buddies

Thank you for being such caring, sincere, supportive and wonderful hall friends, coming from all over the world, in particular **Dr. Nélida Villaseñor, Jeofrey Abalos, Dr. Dahlia Simangan, Shuang Zhang, Jo Leen Lim** and **Fui Swen Kuh**. It was nice to be able to share the joys and pains of a PhD student together and do fun indoor and outdoor activities together, making my PhD life much more vibrant.

Areli Rodriquez, Sita Wulan, Emma Roberts, Kitiphume Thammasiraphop, Jonas Rodekohr, Boon Lee, Zhou Yi, Ian Zhang, Dr. Su Yin Phua, Dr. Kai Xun Chan, Dr. Dony Alex, Dr. Cimo Chen, Sean Ang and **Ricardo Molina** for their long-lasting friendship, social gatherings and outings as well as emotional support in keeping me alive!

Family

I would definitely need to extend my indescribable gratitude to my parents **Mr. Keong Wah Yap** and **Madam Mei Kheng Yong** for their unconditional love and distant care; my siblings, **Jin Yie, Peng Cheng, Wan Li** and **Jin Ni**, for their support, all the way from Malaysia.

Last but not least, I would like to express my sincere gratitude to my partner, **Dr. Jason Liang Pin Ng**, whom I met during the most challenging phase of my PhD - after the moving of my supervisors and during thesis writing up phase. Thank you for being my guardian angel! Your company, immense support, optimism, grocery and food deliveries and daily travel to my hall, have made the final stages of my PhD more bearable.

Mice

Thank you for your sacrifice in helping humans to gain a deeper understanding on the mechanisms of thymic negative selection.

Without all the support, my PhD completion will not be possible.

Conference participation

This research has been presented in the following conferences:

Aug 2016 **International Congress of Immunology (ICI)**, Melbourne, Australia
Poster: Two waves of thymic deletion distinguished by differential dependence on thymic antigen-presenting cell subsets
Funded by ASI travel bursary

Dec 2015 **ASI Annual Scientific Meeting**, Canberra, Australia
Poster: MHC Class II induces Helios upregulation in more thymocytes than MHC Class I
Funded by Dr. Stephen Daley

Apr 2015 **Venice Thymus Meeting**, Italy
Talk: Thymic epithelial antigen abundance dictates the antigen presentation pathways available for $CD4^+$ T cell central tolerance
Funded by ANU/JCSMR HDR student travel fund, ANU Vice Chancellor's travel grant and Dr. Stephen Daley

Jan 2015 **4th SIgN-IFReC Network of Immunology Frontier (NIF) Winter School Immunology Program**, Singapore
Talk and poster: Thymic epithelial membrane antigen abundance dictates the routes available for MHCII-mediated central tolerance
Funded by 4th SIgN-IFReC NIF Travel fellowship

Dec 2014 **ASI Annual Scientific Meeting**, Wollongong, Australia
Poster: Thymic epithelial membrane antigen abundance dictates the routes available for MHCII-mediated central tolerance
Funded by ANU/JCSMR HDR student travel fund

Aug 2014 **ASI NSW & ACT Branch Meeting,** NSW, Australia
Talk: Effect of medullary thymic epithelial self-antigen abundance on T cell Tolerance
(PhD category first runner up prize)
Funded by Prof. Christopher Goodnow

June 2014 **The Australian Society of Medical Research (ASMR) ACT New Investigators Forum,** Canberra, Australia
Talk: Obligatory role of haematopoeitic antigen presenting cells in thymic T cell tolerance to low but not high abundance membrane-bound epithelial self-antigen

Sept 2013 **Australasian Society for Immunology (ASI) NSW & ACT Branch Meeting,** NSW, Australia
Talk: Thymic epithelial cells can delete the majority of strongly self-reactive $CD4^+$ thymocytes in the natural TCR repertoire
Funded by Prof. Christopher Goodnow

Publication

Hu, D.Y., Yap, J.Y., Wirasinha, R.C., Howard, D.R., Goodnow, C.C., and Daley, S.R. (2016). A timeline demarcating two waves of clonal deletion and Foxp3 upregulation during thymocyte development. Immunol Cell Biol *94*, 357-366.
Contributed Fig. 1.

Contents

List of abbreviations

A	Adenine nucleotide
A	Alanine amino acid
$Å^3$	Angstrom^3
AF	Alexa Fluor
Aire	Autoimmune regulator
APC	Allophycocyanin
APCs	Antigen presenting cells
APC-Cy7	Allophycocyanin and cyanine 7 tandem conjugate
APL	Altered peptide ligands
AP-1	Activator protein 1
Batf3	Basic Leucine Zipper ATF-Like Transcription Factor 3
BIM	BCL-2-interacting mediator of cell death
BM	Bone marrow
BM-APCs	Bone marrow-derived antigen presenting cells
bp	Base pair
BrdU	5-Bromo-2'-deoxyuridine
BSA	Bovine serum albumin
BV	Brilliant violet
B2m	Beta-2 microglobulin
C	Carboxyl-terminal
C	Cysteine amino acid
C	Cytosine nucleotide
Ca	Calcium
CCR7	C-C chemokine receptor type 7
CDRs	Complementarity-determining regions
CFSE	Carboxyfluorescein succinimidyl ester
CLIP	Class II-associated Li peptide
CMJ	Cortico-medullary junction
cTECs	Cortical thymic epithelial cells
CTV	Cell trace violet
CIITA	MHC class II transactivator
D	Aspartate amino acid
D	Diversity gene
D^b	Histocompatibility 2, class I D region, (also known as H2-K), b haplotype
DCs	Dendritic cells
DFF40/CAD	DNA fragmentation factor-40/caspase-activated DNase
DFF45/ICAD	DNA fragmentation factor-45/inhibitor of caspase-activated DNase
DMSO	Dimethyl sulfoxide
DN	$CD4^-$ $CD8^-$ double negative thymocyte
DP	$CD4^+$ $CD8^+$ double positive thymocyte
E	Glutamate amino acid
EDTA	Ethylenediaminetetraacetic acid
EdU	5-ethynyl-2'-deoxyuridine
ER	Endoplasmic reticulum
ERAD	Endoplasmic reticulum-associated protein degradation
ERK	Extracellular signal-regulated kinase
F	Phenylalanine amino acid
FACS	Fluorescence-activated cell sorting
FCS	Foetal calf serum

Fezf2	FEZ Family Zinc Finger 2
FITC	Fluorescein isothiocyanate
FOXO1	Forkhead Box O1
FoxP3	Forkhead box P3
FSC	Forward scatter
FTOC	Foetal thymic organ culture
g	Relative centrifugal force
G	Glycine amino acid
G	Guanine nucleotide
GADS	Growth factor receptor-bound protein 2 (GRB2)-related adaptor protein
GITR	Glucocorticoid-induced tumor necrosis factor receptor
H	Histidine amino acid
HEL	Hen egg lysozyme
HLA	Human leukocyte antigen
H2-Aa	Histocompatibility 2, class II antigen A, alpha
H2-Ab	Histocompatibility 2, class II antigen A, beta
I	Isoleucine amino acid
Lck	Lymphocyte-specific protein tyrosine kinase
IgG1	Immunoglobulin isotype G subclass 1
iIEL	CD8$\alpha\alpha^{+}$ small intestine intraepithelial lymphocytes
IL	Interleukin
insHEL	Expression of hen egg lysozyme transgene driven by insulin promoter
i.p.	Intraperitoneal
IRBP	Interphotoreceptor retinoid-binding protein
ITAMs	Immunoreceptor tyrosine-based activation motifs
ITK	Interleukin-2 inducible T cell kinase
i.v.	Intravenous
J	Joining gene
JNK	Jun amino-terminal kinase
K	Lysine amino acid
K^{b}	Histocompatibility 2, class I K region, (also known as H2-K), b haplotype
KO	Knock-out
L	Leucine amino acid
L	Litre
LAT	Linker for activation T cells
M	Methionine amino acid
MAITs	Mucosal-associated invariant T cells
MAPK	Mitogen-activated protein kinase
MFI	Mean fluorescence intensity
MHC	Major histocompatibility complex
MHCI	Major histocompatibility complex Class I
MHCII	Major histocompatibility complex Class II
M-J	Miyazawa-Jernigan matrix
mL	Millilitre
mM	Milimolar (number of moles of solute per litre of solution)
mRNA	Messenger ribonucleic acid
mTECs	Medullary thymic epithelial cells
µL	Microlitre
MIIC	Late endosomal MHC class II compartment

N	Amine-terminal
N	Asparagine amino acid
N	Non-templated nucletides
NFAT	Nuclear factor of activated T cells
NF-κB	Nuclear factor-kappa B
ng	Nanogram
NKT	Natural killer T cells
OVA	Ovalbumin
P	Proline amino acid
PBS	Phosphate buffered saline
PCR	Polymerase chain reaction
PD-1	Programmed cell death 1
PE	Phycoerythrin
PerCP	Peridinin chlorophyll protein complex
PerCP-Cy5.5	Peridinin-chlorophyll-protein and cyanine 5.5 tandem conjugate
PFA	Paraformaldehyde
PLCγ1	Phospholipase Cγ1
PLP	Proteolipid protein
pMHC	Peptide-MHC complex
Q	Glutamine amino acid
R	Arginine amino acid
RAG	Recombination activating gene
RFI	Relative fluorescence intensity
RIP	Rat insulin promoter
Rpm	Revolutions per minute
S	Serine amino acid
SA	Streptavidin
SFK	SRC family kinase
SIRP α	Signal regulatory protein α
SLP76	SH2 domain-containing leukocyte protein of 76 kDa
SP	$CD4^+CD8^-$/ $CD4^-CD8^+$ single positive thymocyte
SSC	Side scatter
SVM	Support vector machine
T	Threonine amino acid
T	Thymidine nucleotide
TAP	Transporter associated with antigen presentation
TBE	Tris/Borate/EDTA
T-bet	T-box transcription factor
TCR	T cell receptor
TCRα	TCR alpha chain
TCRβ	TCR beta chain
TCRδ	TCR delta chain
TCRγ	TCR gamma chain
TdT	Terminal deoxynucleotidyl transferase
TECs	Thymic epithelial cells
TetZap70	Tetracycline-inducible Zap70 transgene
Tg	Transgenic
thyroHEL promoter	Hen egg lysozyme transgene expression driven by thyroglobulin
TNF	Tumour necrosis factor
TRA	TCR alpha chain gene

TRAV	TCR alpha chain variable segment
TRAJ	TCR alpha chain joining segment
TRAC	TCR alpha chain constant segment
TRB	TCR beta chain gene
TRD	TCR delta chain gene
T-reg	$FoxP3^+$ regulatory T cell
TRG	TCR beta gamma gene
TSAs	Tissue-restricted antigens
TSCOT	Thymic stromal cotransporter
TSSP	Thymus-specific serine protease
TUNEL	Terminal deoxynucleotidyl transferase (TdT)-mediated 2'-deoxyuridine 5'-triphosphate (dUTP) nick end-labelling
V	Valine amino acid
V	Variable gene
W	Tryptophan amino acid
WT	Wild-type
W1	Wave 1 negative selection
W2	Wave 2 negative selection
XCL1	XC-chemokine ligand 1
Y	Tyrosine amino acid
ZAP70	ζ(zeta)-chain associated protein kinase of 70 kDa
7-AAD	7-aminoactinomycin D

Abstract

While many factors can influence the fate of developing T cells in the thymus, among the most influential are the strength and timing of signals transmitted by the T cell antigen receptor (TCR). Weak TCR binding to peptide/major histocompatibility complex (MHC) ligands induces thymocytes to develop into naïve T cells, a process called positive selection. Mechanisms that prevent naïve T cell development are termed "negative selection" and include apoptotic deletion and agonist selection into non-naïve T cell lineages. Strong TCR binding to pMHC ligands induces negative selection of thymocytes.

Thymocytes interact with two broad types of antigen-presenting cells (APCs): bone marrow (BM)-derived APCs and thymic epithelial cells (TECs). The traditional view of thymic selection is that positive selection occurs in the thymic cortex via interaction with TECs, followed by negative selection in the thymic medulla via interaction with BM-APCs. However, recent studies reveal that thymocytes can undergo either cortical or medullary negative selection, which differ in terms of the phenotypes of the thymocytes involved and their timing during T cell development. It remains unclear which APC types are required to mediate these two negative selection processes, which are called "Wave 1" and "Wave 2" of negative selection. In addition, the contributions of MHC class I (MHCI) and MHC class II (MHCII) to the two waves are unclear.

To dissect thymic selection, two assays were used in this study. First, the transcription factor, Helios, was used in a flow cytometry assay as a marker of negatively selected cells, in conjunction with chemokine receptor-7 (CCR7) to distinguish thymocyte maturation stages. Apoptosis-defective mice were used to inhibit death of negatively selected cells, allowing direct quantification of negative selection. Genetic ablation of MHCII expression within BM-APCs or autoimmune regulator (*Aire*$^{-/-}$) within TECs was used to examine the roles of APC types in thymic selection. Mice lacking expression of MHCI and/or MHCII were also examined. Second, a TCR sequencing assay was used to examine the characteristics of positively and negatively selected TCR repertoires in mice lacking expression of MHCI and/or MHCII.

In TCR transgenic and polyclonal models, MHCII^{+} BM-APCs were required to induce wave 1 negative selection. Ablation of MHCII^{+} BM-APCs either abrogated negative selection completely or delayed negative selection from wave 1 to wave 2. Although MHCI and MHCII were found to induce similar frequencies of TCR-signalled thymocytes, MHCII was found to make a greater contribution to negative selection than MHCI. Sequencing data revealed that TCRs that provoke negative selection at wave 1 are enriched with hydrophobic amino acids in the region expected to interact with the peptide component of pMHC ligands. Interestingly, hydrophobic amino acids are also enriched in the same region of TCRs that transmit a signal in mice lacking MHC expression. These results provide new insight into the determinants of thymic negative selection.

CHAPTER 1

General introduction

1.1 Function of the thymus

T lymphocytes (or T cells) play an essential role in defending organisms from threats such as infectious pathogens or cancerous cells. T cells develop in the **t**hymus. The function of the thymus was revealed only about 56 years ago as an organ required for the development of immunological competence (Miller, 1961). It is important to produce self-tolerant T cells that are not strongly reactive towards self-antigens to prevent autoimmune diseases. However, these T cells should be responsive towards foreign pathogens to fight against diseases.

During T cell development, developing thymocytes undergo a series of differentiation, T cell receptor (TCR) gene arrangement and selection mechanisms. All these mechanisms are supported by the thymic microenvironment containing different thymic antigen presenting cell (APC) types. Major histocompatibility complex (MHC) restriction is part of a crucial process during T cell selection. MHC restriction is defined as the obligatory recognition of MHC molecules on the surface of the APC by the TCR on T cells. MHC restriction was discovered 43 years ago in an experiment that revealed the requirement of virus-specific cytotoxic T cells to recognise antigen together with MHC class I in an antiviral response (Zinkernagel and Doherty, 1974).

During the selection process, the TCRs on thymocytes recognise linear self-peptides that are bound and presented by MHC molecules on thymic APCs (Davis and Bjorkman, 1988). Thymocytes with low TCR affinity for self-peptide-MHC are able to differentiate and mature into naïve T cells, a process known as positive selection (Germain, 2002; Klein et al., 2014) (Fig. 1.1). The mature T cells are eventually exported out of the thymus into the periphery to perform their immune function. Thymocytes with high TCR affinity for self-peptide-MHC, also described as self-reactive or autoreactive, are eliminated or inhibited in the thymus (Burnet, 1959, 1962) (Fig. 1.1), in order to acquire central tolerance in the thymus. This process is known as negative selection (Klein et al., 2014; Nossal, 1994). Thymocytes bearing non-functional TCRs or TCRs that are not able to recognise self-peptide-MHC, die by neglect (Fig. 1.1) (Hernandez et al., 2010; Surh and Sprent, 1994).

1.2 T cell differentiation and proliferation in the thymus

In mice and humans, the thymus can be broadly divided into two anatomical locations: the outer cortex and the inner medulla. The area that connects these two locations is

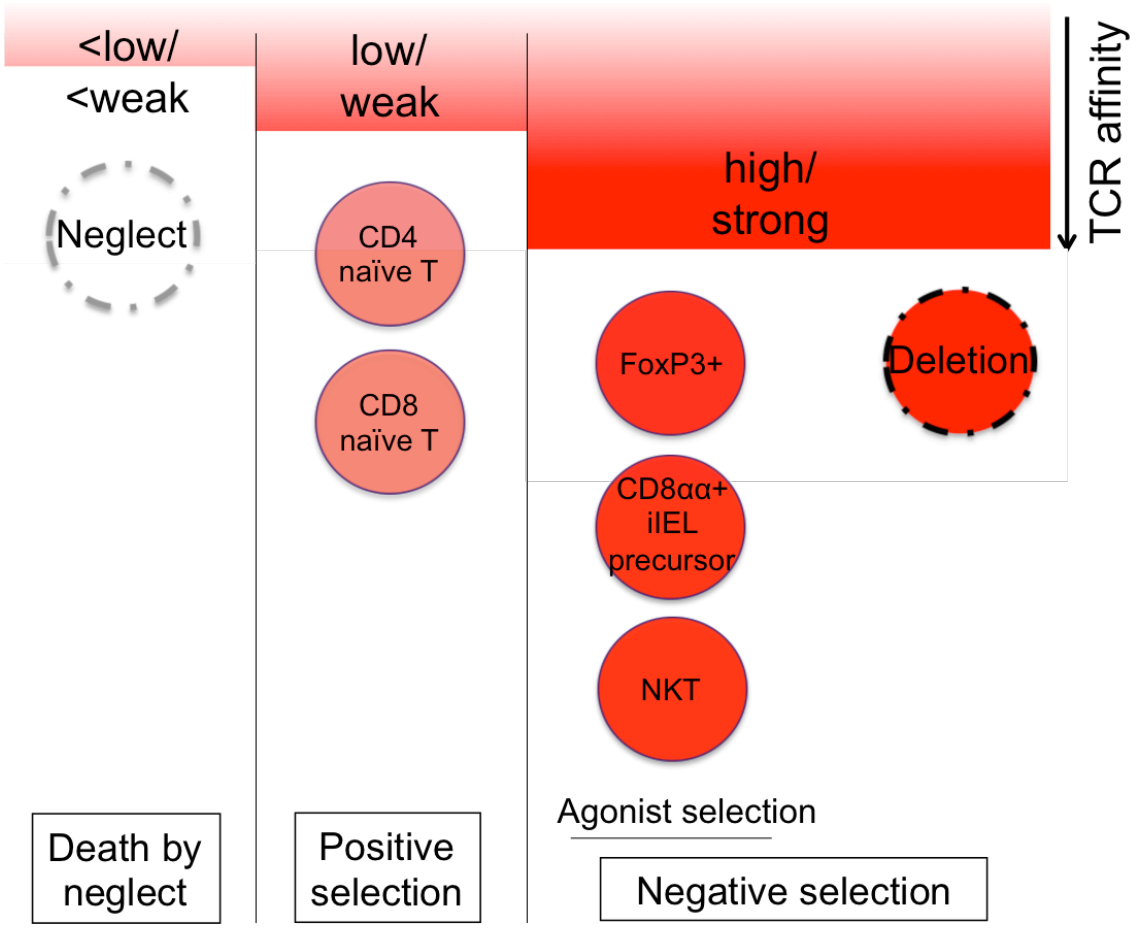

Figure 1.1. TCR affinity for self-peptide-MHC dictates thymocyte fate. Low TCR affinity or weak TCR interaction with self-peptide-MHC complexes mediates positive selection. Positive selection allows the maturation of thymocytes into single positive naïve T cells and prevents the thymocytes from dying by neglect. High TCR affinity or strong TCR interaction with self-peptide-MHC complexes mediates negative selection. Negative selection includes clonal deletion by apoptosis or clonal diversion (also known as agonist selection) into Forkhead box P3 transcription factor $(FoxP3)^+$ regulatory T (T-reg) cells, precursor of unconventional $CD8\alpha\alpha^+$ intestinal intraepithelial T cells (iIEL) or natural killer T (NKT) cells.

known as the cortico-medullary junction (CMJ). The thymic cortex contains a network of cortical thymic epithelial cells (cTECs) and some bone marrow (BM)-derived antigen presenting cells (APCs), including dendritic cells (DCs). The thymic medulla contains a network of medullary thymic epithelial cells (mTECs) and the majority of BM-derived APCs in the thymus (Barclay and Mayrhofer, 1981; Le Borgne et al., 2009; Raviola and Karnovsky, 1972; Takahama, 2006) (Fig. 1.2). CTECs and mTECs are also found in human thymus (Gotter et al., 2004; Takahama et al., 2017; Tomaru et al., 2009).

The circulating BM-derived lymphoid progenitors migrate to the thymus via blood vessels in the CMJ. Stages of thymocye differentiation can be categorised based on the surface expression of CD4 or CD8 molecules in thymocytes in mice and humans (Salomon et al., 1994). CD4 or CD8αβ molecules are also known as the coreceptors of T cells as they cooperatively bind to MHC molecules when the TCR engages peptide-MHC complexes. Thymocytes migrate from the thymic cortex to the medulla as they mature. Thymocyte differentiation begins with the absence of CD4 and CD8 coreceptors, known as the immature $CD4^{-}CD8^{-}$ double negative (DN) stage. Within the DN thymocytes, four sequential developmental stages were described based on the expression of CD44 and CD25: $CD44^{+}CD25^{-}$ (DN1), $CD44^{+}CD25^{+}$ (DN2), $CD44^{-}CD25^{+}$ (DN3) and $CD44^{-}CD25^{-}$ (DN4) (Godfrey et al., 1993). DN thymocytes can give rise to T cells that express either αβTCR or γδTCR heterodimers (Germain, 2002).

In both mice and humans, after the DN stage, thymocytes may upregulate both coreceptors to become $CD4^{+}CD8^{+}$ double positive (DP) cells (Fig. 1.2). Some DP thymocytes eventually differentiate into mature $CD4^{+}CD8^{-}$ CD4 single positive (CD4SP) or $CD8^{+}CD4^{-}$ CD8SP thymocytes (Fig. 1.2) (Salomon et al., 1994). The thymic cortex primarily contains DN and DP thymocytes, whereas the thymic medulla contains most of the SP thymocytes (Ehrlich et al., 2009; Kurd and Robey, 2016; Takahama, 2006; Xing and Hogquist, 2012).

During T cell development, thymocytes undergo up to three phases of proliferation. Two phases occur during the pre-selection stage and one during the post-selection stage. Also, thymocytes undergo up to two TCR gene rearrangement phases, giving rise to the expression of a mature TCR on the thymocyte surface. Two recombination-activating genes, named *RAG1* and *RAG2*, encoding the RAG1 and RAG2 proteins, are essential to cleave double-stranded DNA during the TCR gene rearrangement process (McBlane et al., 1995; Mombaerts et al., 1992; Shinkai et al., 1993) (Fig. 1.2).

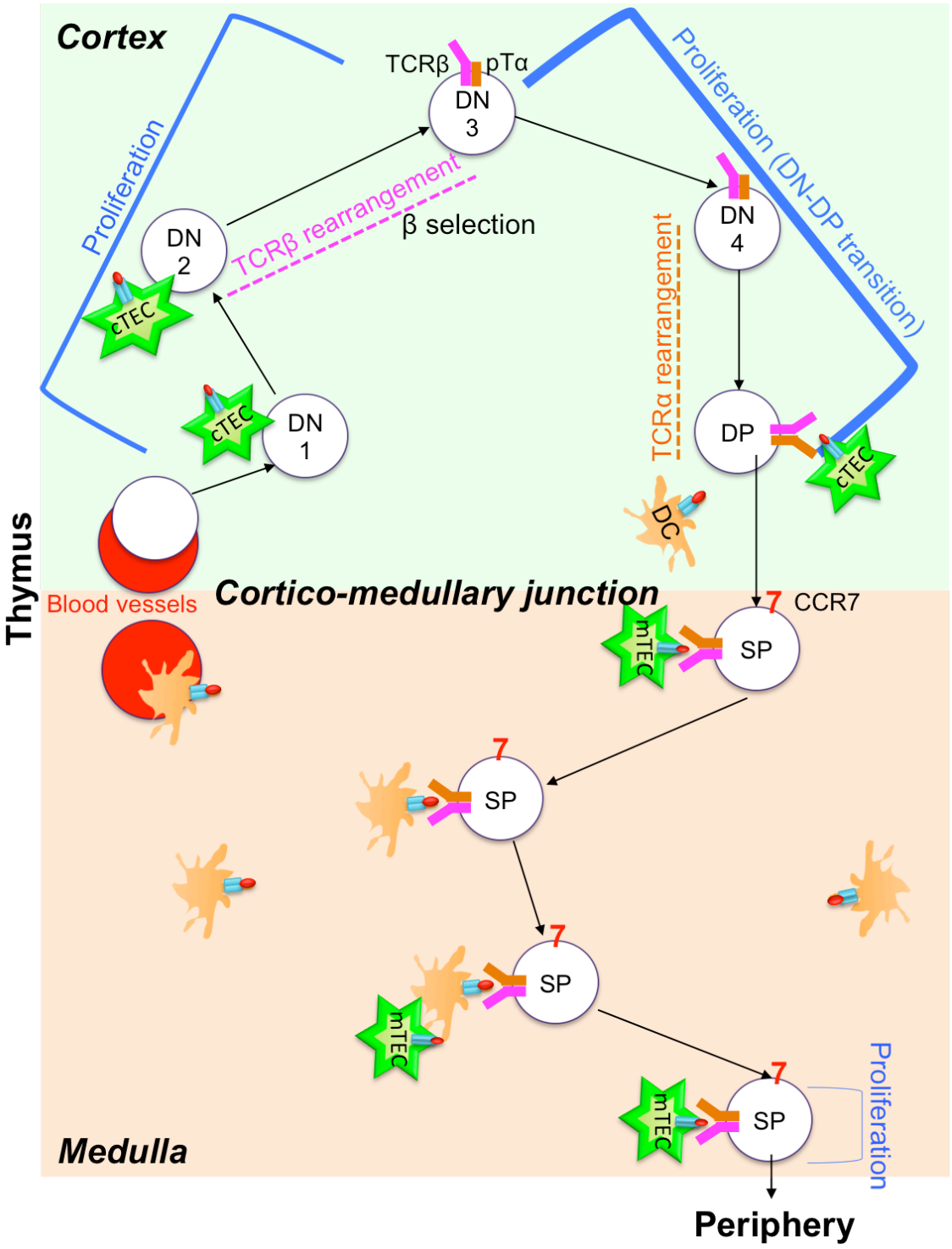
Cortex
TCRβ
pTα
DN 3
Proliferation
Proliferation (DN-DP transition)
DN 2
TCRβ rearrangement
β selection
DN 4
cTEC
TCRα rearrangement
cTEC
DN 1
DP
cTEC
DC
Thymus
Blood vessels
Cortico-medullary junction
7
CCR7
mTEC
SP
7
SP
7
SP
mTEC
7
SP
mTEC
Proliferation
Medulla
Periphery

Figure 1.2. αβT cell development in thymus. Thymic progenitor cells derived from bone marrow (BM) enter the thymus via blood vessels around the cortico-medullary junction (CMJ). Thymocytes undergo several stages of maturation starting as double negative (DN), lacking CD4 and CD8 coreceptor expression. DN cells are divided into four sequential stages: DN1 ($CD44^{+}CD25^{-}$), DN2 ($CD44^{+}CD25^{+}$), DN3 ($CD44^{-}CD25^{+}$) and DN4 ($CD44^{-}CD25^{-}$). Thymocytes undergo the first proliferation phase during DN1-DN3 stages. TCRβ gene arrangement commences at the DN2 and completes at the DN3 stage. Productive TCRβ chain expression in DN3 cells induces β-selection with progression through the DN4 stage and subsequently to the DP stage. During this DN to DP transition, thymocytes undergo a second (and largest) proliferative phase and also undergo TCRα gene rearrangement. DP cells which express the α and β TCR chains are subjected to selection processes. Positively selected DP cells differentiate into SP thymocytes and upregulate C-C chemokine receptor type 7 (CCR7). Some SP cells undergo a third proliferation phase in the medulla before they egress to the periphery.

Each pre-selection proliferation phase precedes a distinct phase of TCR gene rearrangement. During the DN1 to DN3 stages, thymocytes proliferate through ~2-3 cell divisions, as revealed by using bromodeoxyuridine (5-bromo-2'-deoxyuridine, BrdU), a thymidine analogue, to track cell proliferation *in vivo* (Pénit et al., 1995). Rearrangement of the TCRβ, γ and δ genes commences at the DN2 stage and completes at the DN3 stage (Hayday and Pennington, 2007; Livák et al., 1999; von Boehmer, 2004; Yui and Rothenberg, 2014) (Fig. 1.2). Thymocytes with unproductive TCR gene rearrangements undergo apoptosis at the DN3 stage (Mandal et al., 2005). Thymocytes that express a functional γδTCR at the DN3 stage diverge into the γδ T cell lineage (Prinz et al., 2006) and migrate out of the thymus to the periphery (Hayday and Pennington, 2007). Only 1-5% of T cells expresses γδ TCR (Vantourout and Hayday, 2013). Thymocytes with a productive TCRβ gene rearrangement, results in the pairing of TCRβ chain with an invariant pre-Tα (pTα) chain to form a pre-TCR (von Boehmer, 2005). The pre-TCR signaling allows the maturation of thymocytes from the DN3 stage into the DN4 and DP stages (Hayday and Pennington, 2007), and this process is known as β-selection (von Boehmer, 2005). Proliferation during β-selection occurs in between two phases of RAG1 and RAG2 expression (Hoffman et al., 1996; Wilson et al., 1994). TCRα mRNA molecules were detected in DP “blasts”, i.e. cells with large cell diameter, presumably still proliferating during β-selection (Guidos et al., 1990). Proliferation during β-selection occurs in the outer cortex (Penit, 1988) and contains the largest number of proliferating thymocytes, accounting for 98% of the thymocyte proliferation during T cell development (Pénit et al., 1995).

As thymocytes mature from the DN stage to the DP stage, thymocytes upregulate both CD4 and CD8 coreceptors to become DP cells, and the RAG1 and RAG2 proteins are re-expressed (Hoffman et al., 1996; Wilson et al., 1994). TCRα gene rearrangement commences during the DN-DP transition and completes at the DP stage, in which heterodimeric αβTCR are expressed on DP cells (Hogquist et al., 2005; Petrie et al., 1995). DP thymocytes have a life span of approximately 3.5 days to undergo selection (Egerton et al., 1990). Within this time frame, DP thymocytes bearing TCRs that are unable to recognise self-peptide-MHC complexes presented by cTECs die by neglect as they do not receive survival signals to undergo further maturation. It is estimated that up to 90% of DP thymocytes undergo death by neglect in the thymic cortex (Hernandez et al., 2010; Palmer, 2003). Apoptotic thymocytes in the cortex were found to be approximately as abundant in wild-type mice and mice lacking MHC Class I- and MHC Class II (Surh and Sprent, 1994). This is consistent with the hypothesis that most thymocytes undergo death by neglect.

DP thymocytes bearing TCRs that bind weakly to self-peptide-MHC complexes on cTECs mature to become CD4SP or CD8SP cells, a process known as positive selection (Germain, 2002; Klein et al., 2009). Weak binding between TCRs and peptide-MHC Class I (MHCI) complexes positively selects DP thymocytes into MHCI-restricted $CD8^+$ cytotoxic T cells. $CD8^+$ T cells are responsible for destroying infected cells (Germain, 2002). The weak binding between TCRs and peptide-MHC Class II (MHCII) complexes positively selects DP thymocytes into MHCII-restricted $CD4^+$ helper T cells (Fig. 1.5). $CD4^+$ T cells cooperate with other haematopoetic cells in the immune response to infection (Germain, 2002). Not all thymocytes abide by this rule of single MHC class restriction. Recent studies reported that some thymocytes are responsive to MHCI and also MHCII, termed as MHC class cross-reactive thymocytes (Huseby et al., 2005; McDonald et al., 2015). In addition, in the absence of both MHC classes and both CD4 and CD8 coreceptors, some thymocytes are able to differentiate into CD4SP or CD8SP cells (Van Laethem et al., 2007).

Cortical TECs are the only thymic APC type known to mediate positive selection of $CD4^+$ and $CD8^+$ T cells (Bill and Palmer, 1989; Cosgrove et al., 1992). MHC expression on BM-APCs is not sufficient for the development of SP thymocytes (Brocker et al., 1997; van Meerwijk et al., 1997). During the commitment of DP thymocytes to the CD4 or CD8 T cell lineage, DP thymocytes first downregulate both CD4 and CD8 coreceptors ($CD4^{lo}CD8^{lo}$). Then, the $CD4^{lo}CD8^{lo}$ thymocytes upregulate CD4 coreceptor while still remaining low for CD8 coreceptor, to attain an intermediate $CD4^+CD8^{lo}$ phenotype. Class II-restricted $CD4^+CD8^{lo}$ thymocytes continue to downregulate CD8 and become CD4SP ($CD4^+CD8^-$) cells, whereas Class I-restricted $CD4^+CD8^{lo}$ thymocytes reverse expression of their coreceptors to go through further intermediary stages ($CD4^{lo}CD8^{lo}$, then $CD4^{lo}CD8^+$), before becoming CD8SP ($CD4^-$ $CD8^+$) thymocytes (Fig. 1.3) (Lucas and Germain, 1996). Just before CD4SP or CD8SP thymocytes emigrate from the thymus, 2-5% of the SP cells with a mature phenotype ($TCR\beta^{hi}$ $CD24^-$ $Qa\text{-}2^{hi}$) undergo the third proliferative burst (Pénit and Vasseur, 1997).

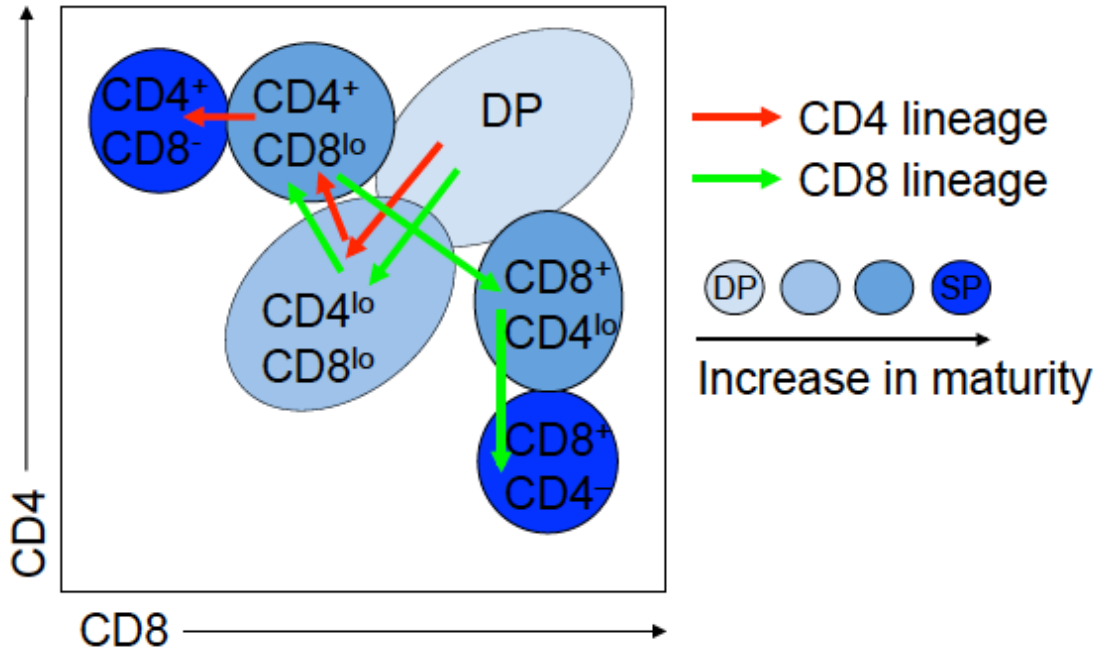

Figure 1.3. Maturation stages that characterise commitment of DP thymocytes to the CD4 or CD8 T cell lineage. DP thymocytes committed to CD4 or CD8 T cell lineage first downregulate both the CD4 and CD8 coreceptors ($CD4^{lo}CD8^{lo}$) and then upregulate the CD4 coreceptor while still remaining low for the CD8 coreceptor ($CD4^{+}CD8^{lo}$). DP thymocytes committed to CD4 T cell lineage mature into CD4SP ($CD4^{+}CD8^{-}$) thymocytes. On the other hand, thymocytes committed to CD8 T cell lineage downregulate both coreceptors again ($CD4^{lo}CD8^{lo}$), then upregulate the CD8 coreceptor while still maintaining low CD4 expression ($CD8^{+}CD4^{lo}$), and finally mature into CD8SP ($CD8^{+}CD4^{-}$) thymocytes.

1.3 Generation of TCRs via TCR gene recombination

The TCR is a disulfide-linked heterodimer comprised of either αβ or γδ chains (Raulet, 1989). TCR α and γ chains are composed of Variable (V), Joining (J) and Constant (C) regions, whereas TCRβ and δ chains are composed of V, Diversity (D), J and C regions (Livák et al., 1999; Petrie et al., 1995). Genes that encode αβTCRs are generated via somatic recombination at the TRA and TRB loci, encoding α chains and β chains, respectively. Similar rearrangements at TRG and TRD loci produce genes that encode the γ and δ chains of γδTCRs (Livák et al., 1999; Petrie et al., 1995). This thesis focuses on thymocytes bearing αβTCRs.

The human TRA locus contains 43-49 TRAV genes (also called V segments) and ~50 TRAJ genes (also called J segments) (Attaf et al., 2015; Rossjohn et al., 2015). The mouse TRA locus contains 72-82 TRAV genes (Bosc and Lefranc, 2003) and 60 TRAJ genes (Genolet et al., 2012). Productive TCRα chain genes contain one V segment joined to one J segment (Fig. 1.4A). The human TRB locus contains 40-48 TRBV segments, 2 TRBD segments and 12-13 TRBJ segments (Attaf et al., 2015; Rossjohn et al., 2015). Productive TCRβ chain genes contain one segment from each of the V, D and J segment clusters (Fig. 1.4B). In both TCRα and TCRβ chains, the intervening sequence between the J segment and a single C segment (i.e. TRAC or TRBC) is removed during mRNA splicing (Fig. 1.4) (Attaf et al., 2015). V(D)J somatic recombination generates about 10% of total TCR diversity (Cabaniols et al., 2001; Miles and Burrows, 2013). During V(D)J recombination, nucleotides are removed or non-templated nucleotides (N-nucleotides) are inserted at the junction between V and J gene segments (i.e. VJ junction) for TCRα chains or at the VD and/or DJ junctions for TCRβ chains (Fig. 1.4), in a process that requires the enzyme terminal deoxynucleotidyl transferase (TdT) (Cabaniols et al., 2001; Davis and Bjorkman, 1988) (Fig. 1.4). It is estimated that these deletions and insertions account for 90% of the diversity in TCR sequences (Cabaniols et al., 2001; Miles and Burrows, 2013).

Each TCR chain has three complementarity-determining regions (CDRs), namely CDR1, CDR2 and CDR3. CDR1 and CDR2 loops, encoded by the germline V gene segments, give rise to a limited TCR diversity and commonly contact the MHC molecule (Davis and Bjorkman, 1988) (Fig. 1.4). On the other hand, CDR3 loops are encoded by the more variable V(D)J junction(s) (Pannetier et al., 1993). The CDR3 loops are the portion of the TCR that commonly interacts with the peptide (Rudolph et al., 2006) (Fig. 1.4).

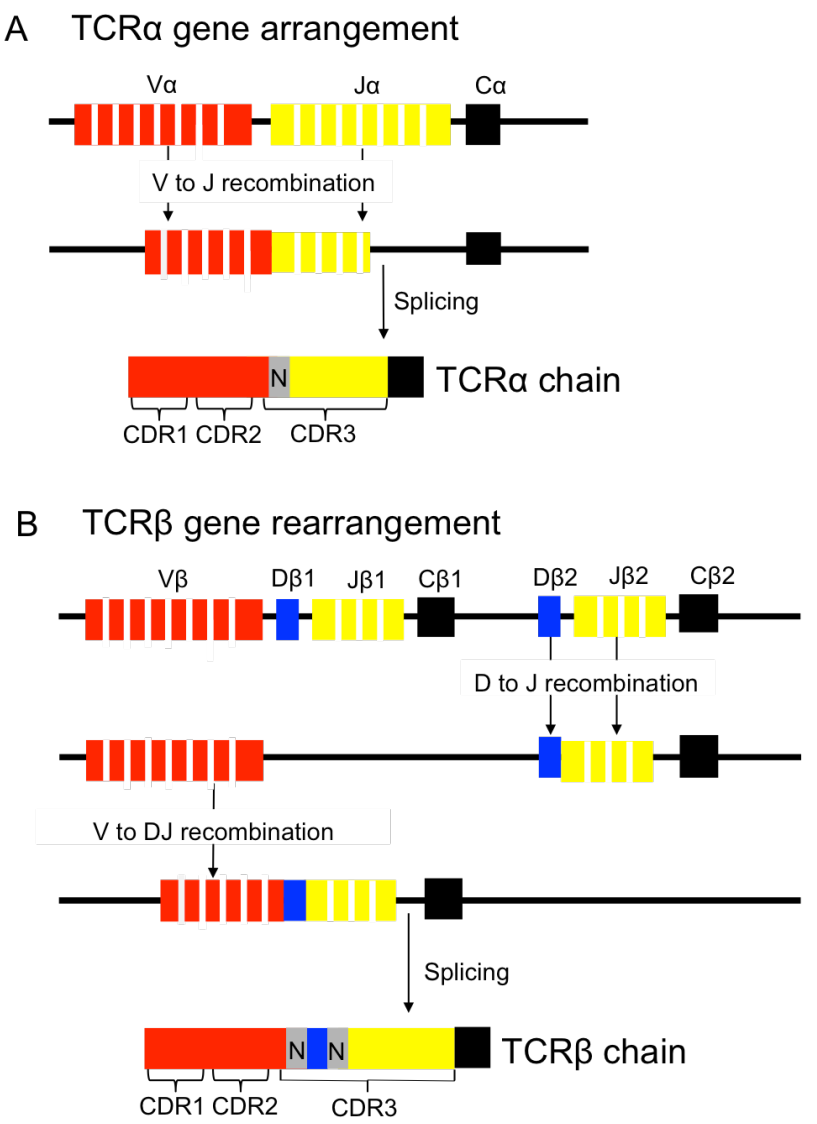

Figure 1.4. Generation of αβTCRs via TCRα and TCRβ gene recombination. (A) To produce TCRα chains, one segment of the Variable (V) gene is recombined with one segment of the Joining (J) gene, followed by a mRNA splicing process to join the Constant (C) gene. This forms TCRα chains containing a V, J and C region. (B) To produce TCRβ chains, one segment of the Diversity (D) gene is recombined with one segment of the J gene, which is known as DJ recombination. One segment of the V gene is recombined with the recombined DJ genes, which is known as V to DJ recombination. Messenger RNA splicing occurs to join the C gene with VDJ to form TCRβ chains containing a V, D, J and C region. (A, B) The rearranged TCR are further diversified by removal or insertion of non-templated nucleotides (N) at the V(D)J junctions. The germline V gene encodes the complementarity-determining region (CDR)1 and CDR2 loops. CDR1 and CDR2 loops recognise MHC molecules. The most variable CDR3 loops are mainly encoded by the J region (and D region) and partially encoded by the V region. CDR3 consists of the V region, N-nucleotides, and/or (D) region and J region that straddles the V(D)J junction. CDR3 loops recognise bound peptide.

1.4 MHC structure and antigen presentation to T cells

1.4.1 MHC Class I

MHC class I molecules (MHCI) are expressed on almost all nucleated cells (Ploegh et al., 1981) and on some non-nucleated cells such as platelets (Rowley et al., 2011). The MHC class I molecule is a heterodimer consisting of a polymorphic membrane-spanning α chain (also known as the heavy chain) and a non-membrane spanning β2-microglobulin (β2m, also known as the light chain) non-covalently bound to the α chain (Fig. 1.5A) (Klar and Hämmerling, 1989). The α chain folds into three domains. Two domains α1 and α2 (that form α1 and α2 helices) create a peptide-binding cleft (Bjorkman et al., 1987) that binds a short peptide of 8-10 amino acids. The peptide's N (amine)- and C (carboxyl)-terminal ends are anchored into the pockets at the ends of the peptide binding cleft (Rossjohn et al., 2015). The binding of peptide onto the MHCI is essential for the formation of stable MHCI protein (Bijlmakers et al., 1993). The third domain, the conserved α3 domain, spans the membrane (Fig. 1.5A). There are three classical polymorphic MHCI genes in humans (HLA-A, HLA-B and HLA-C) and mice (H2-K, H2-D and H2-L) (Rossjohn et al., 2015). The non-classical monomorphic MHCI-like molecules, CD1d and MR1, also require B2m for stable expression on the cell surface (Rossjohn et al., 2015).

The non-classical MHCI molecules, CD1d and MR1, are recognised by natural killer T (NKT) cells and mucosa-associated invariant T (MAIT) cells, respectively (Borrego et al., 2002; Kochan et al., 2013). CD1d presents lipid-based antigens that can be recognised by αβ (Matsuda et al., 2000) or γδ TCRs (Rossjohn et al., 2015). The NKT cells express an invariant TCRα chain and a restricted but not invariant TCRβ chain (Godfrey et al., 2004). MR1 presents vitamin B precursors or metabolites than can be recognised by MAIT cells, an innate-like T cell population (Kjer-Nielsen et al., 2012). MAIT cells were thought to express an invariant TCRα chain that pairs with a limited array of β chains (Kjer-Nielsen et al., 2012). Recently, MAIT cells are reported to have a semi-variable TCRα chain and fairly variable β chains (Gherardin et al., 2016; Kurioka et al., 2016; Napier et al., 2015).

1.4.2 MHC Class II

MHCII is a transmembrane heterodimer consisting of an α chain and a β chain. The α chain consists of α1 and α2 domains. Similarly, the β chain consists of β1 and β2 domains. α1 and β1 form the peptide-binding cleft, whereas α2 and β2 domains span

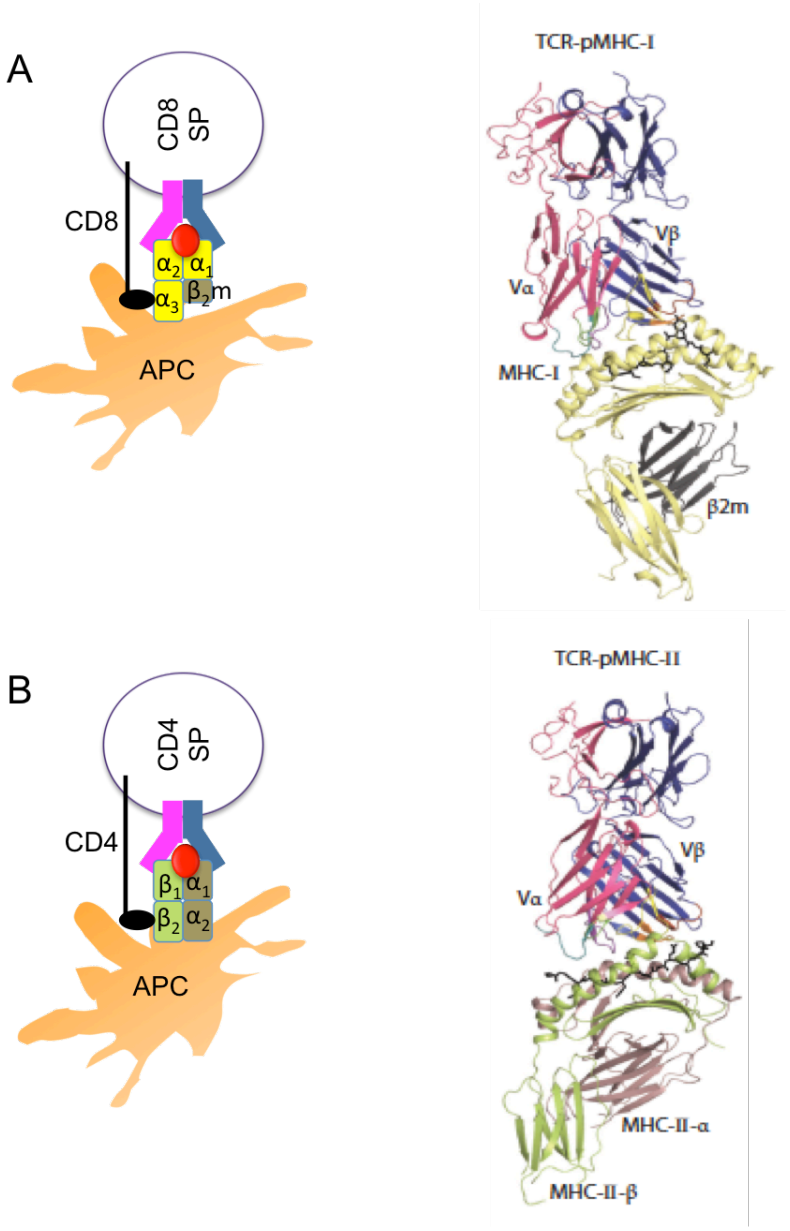

Figure 1.5. TCR recognition of self-peptide-MHC complexes. (A) Structure of MHC Class I (MHCI) and its recognition by $CD8^+$ T cells. MHCI consists of an α chain and a beta-2 microglobulin (β2m) chain. The α1 and α2 domains of α chain present the peptide, whereas the conserved α3 domain associates primarily with β2m necessary for MHC stability. The heterodimeric αβTCR of MHCI-restricted CD8SP thymocytes binds to the peptide presented on MHCI molecules by antigen presenting cells (APCs), with the simultaneous binding of CD8 coreceptor to the conserved region (α3 domain) of MHCI. (B) Structure of MHC Class II (MHCII) and its recognition by $CD4^+$ T cells. MHCII consists of an α chain and a β chain. Each chain of MHCII consists of two domains (i.e. α1 and α2, and β1 and β2). α1 and β1 domains of MHCII present the peptide to the TCR of MHCII-restricted CD4SP cells, with the simultaneous binding of the CD4 coreceptor to the conserved region of MHCII (α2 and β2 domains) during the TCR-recognition for self-peptide. Ribbon diagrams on the right of (A, B) are reproduced from Rossjohn et al. (2015).

the membrane (Fig. 1.5B). The peptide binding cleft of MHCII molecule is open at both ends, allowing the binding of a longer peptide (>11 amino acids) compared to MHCI (Rammensee et al., 1995). There are three MHC-II gene loci in humans (HLA-DR, HLA-DQ, and HLA-DP) and two in mice (H2-A and H2-E) (Rossjohn et al., 2015). H2-A is the only functional MHCII molecule in the C57BL/6 laboratory mouse strain, owing to an inactivating mutation in the promoter of H2-Ea gene, which encodes the α chain of the H2-E MHCII molecule (Mathis et al., 1983). The master regulator of MHCII expression is MHC class II transactivator (CIITA) (Reith et al., 2005). MHCII molecules are expressed on specialised APCs encompassing the haemapoeitic DCs, macrophages and B cells, and the non-haemapoetic cTECs and mTECs in the thymus (Holling et al., 2004).

1.4.3 Overview of antigen presentation by MHC Class I and MHC Class II

MHCI presents peptides derived from an endogenous (intracellular) source, with the exception of cross presentation, in which exogenously derived peptides are loaded on MHCI (Neefjes et al., 2011). By contrast, MHCII presents exogenous peptides, with the exception of macroautophagy. Macroautophagy is a process of bulk degradation of endogenous proteins encapsulated in autophagosomes (cytoplasmic vacuoles) following fusion with a lysosomal compartment. In the lysosomal compartment, the degraded endogenous peptides are loaded onto MHCII for antigen presentation (Klein et al., 2009). Bulk cytoplasmic autophagy usually occurs during starvation in other cell types, but the thymic tissue has an unusually high constitutive macroautophagy even without starvation (Mizushima et al., 2004).

Briefly, MHCI antigen presentation involves the degradation of cytosolic or nuclear proteins by the proteasome. Then the degraded proteins are translocated into the endoplasmic reticulum (ER) by transporter associated with antigen presentation (TAP) (Neefjes et al., 2011). The α chain and β2m of MHCI are assembled in the ER and are stabilised by chaperone proteins when no peptide is bound (Neefjes et al., 2011). The peptide-MHCI complexes are released from the chaperone proteins only after the loading of a peptide onto MHCI. They then leave the ER and are transported across the Golgi and to the plasma membrane for antigen presentation to $CD8^+$ T cells (Fig. 1.6). Peptides and MHCI that fail to form a complex are transported to the cytosol via the ER-associated protein degradation (ERAD) for degradation (Hughes et al., 1997; Neefjes et al., 2011) .

In MHCII antigen presentation, exogenous proteins can enter the endocytic pathway

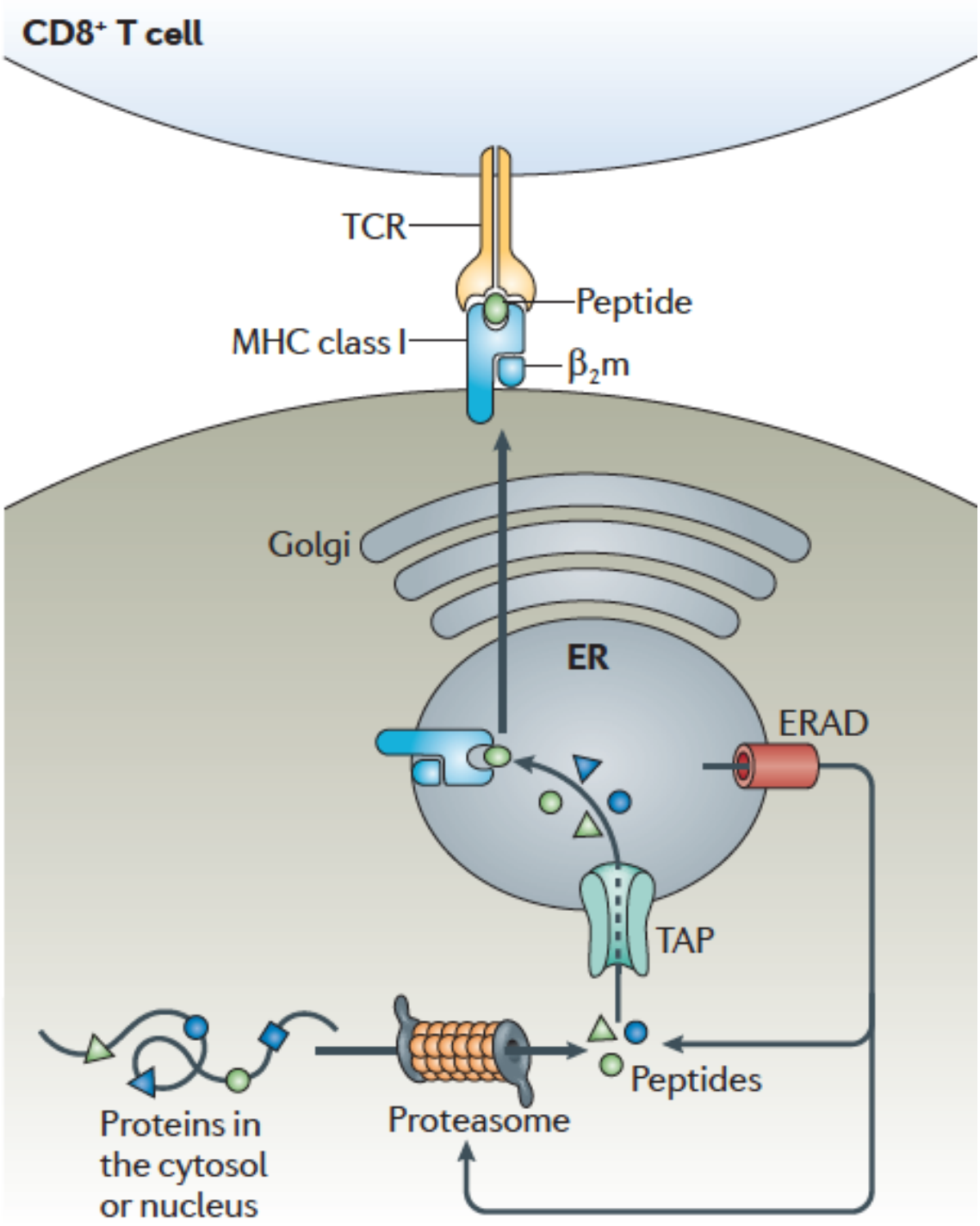

Figure 1.6. MHC Class I antigen presentation. Intracellular proteins are degraded by proteasomes. The degraded proteins are translocated into the endoplasmic reticulum (ER) via transporter associated with antigen presentation (TAP). The peptides are loaded onto MHCI molecules that are assembled in the ER. The peptide-MHC complexes are transported to the cell surface of APC, presenting to conventional $CD8^+$ T cells. Peptides and MHCI that are not bound to each other are transported to the cytosol for degradation via the ER-associated protein degradation (ERAD). Reproduced from Neefjes et al. (2011).

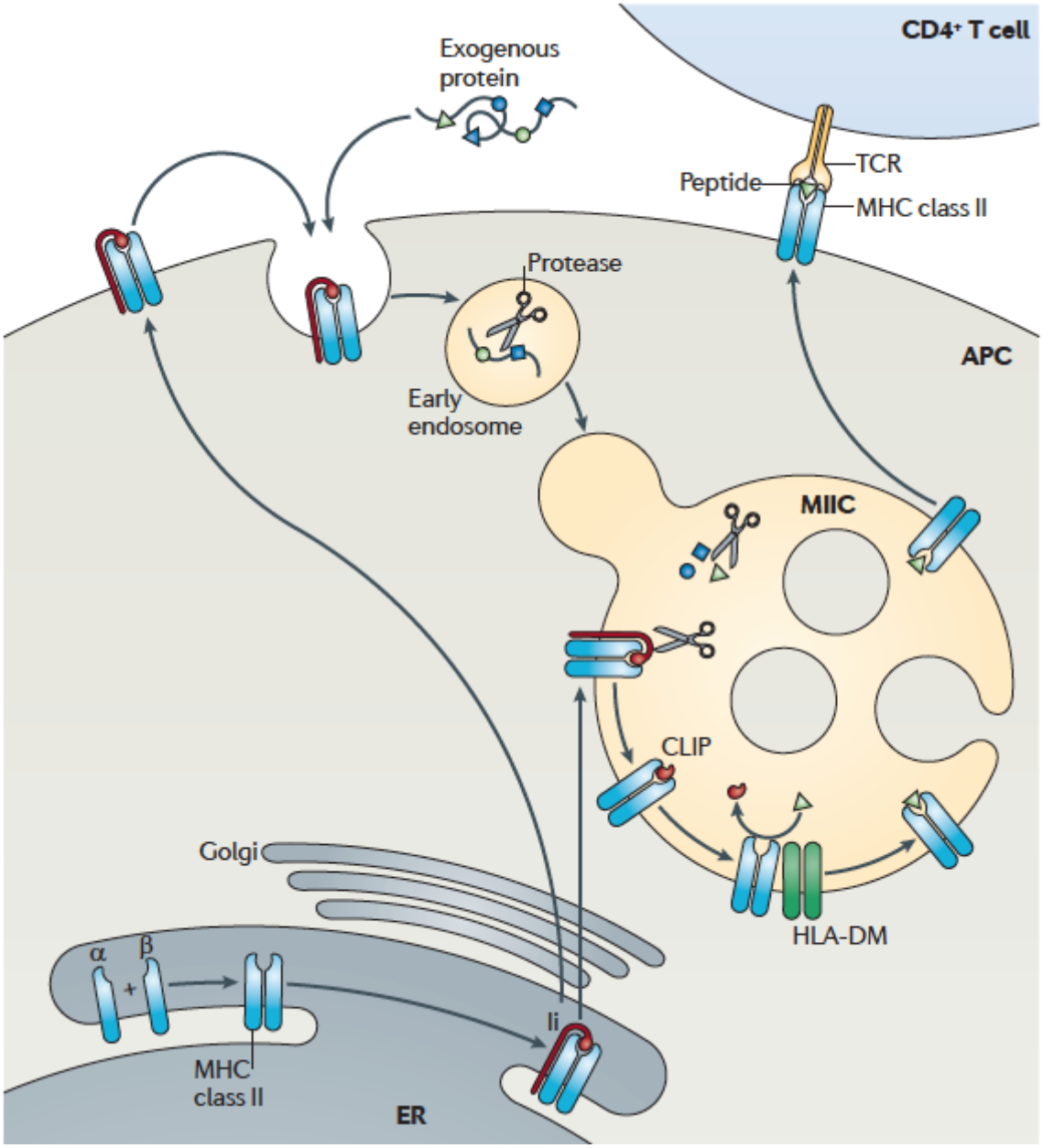

Figure 1.7. MHCII antigen presentation. Extracellular proteins are internalised and cleaved by proteases in an early endosome. Early endosomes fuse with the late endosomal-lysosomal antigen-processing compartment, also known as the MHC class II compartment (MIIC) for further antigen proteolysis and for the formation of peptide-MHCII complex. The α chain and β chain of MHCII are assembled in the ER and are associated with CD74 (MHC Class II invariant chain Ii). The MHCII-Ii complexes are transported to MIIC via Golgi or via Golgi and plasma membrane. In MIIC, the Ii is digested, producing the class II-associated Ii peptide (CLIP) in the peptide-binding groove of MHCII. A newly-formed peptide is exchanged with CLIP, with the help of HLA-DM. Finally, the peptide-MHCII complexes are transported to the plasma membrane for antigen presentation to the MHCII-restricted $CD4^+$ T cells. Reproduced from Neefjes et al. (2011).

via internalisation of proteins into an early endosome, in which the protein can be cleaved by protease. The early endosome fuses with a late endosomal-lysosomal antigen-processing compartment known as the MHC class II compartment (MIIC), for further antigen proteolysis (Neefjes et al., 2011; Roche and Furuta, 2015). The α chain and β chain of MHCII are assembled in the ER and are associated with CD74 (MHC Class II invariant chain Ii) (Fig. 1.7) (Stumptner-Cuvelette and Benaroch, 2002). The MHCII-Ii complex is transported to the MIIC via Golgi or via Golgi and plasma membrane. MIIC is also where the peptide-MHCII complex formation takes place. In MIIC, the Ii is digested, generating a residual fragment of Ii known as class II-associated Ii peptide (CLIP) in the peptide-binding groove of MHCII (Fig. 1.7) (Neefjes et al., 2011; Roche and Furuta, 2015). CLIP is removed from the CLIP-MHCII complex and replaced with peptide, facilitated by HLA-DM enzyme (Sloan et al., 1995). The peptide-MHCII complex is then transported to the plasma membrane for antigen presentation to $CD4^+$ T cells (Neefjes et al., 2011; Roche and Furuta, 2015).

1.5 Induction of TCR signalling

The extracellular domains of the CD4 or CD8 coreceptor bind to the non-polymorphic region of MHCII (Doyle and Strominger, 1987) and MHCI (Norment et al., 1988), respectively (Fig. 1.5, 1.8). CD8 binds to the MHCI α3 domain loop while CD4 binds to a hydrophobic region between MHCII α2 and β2 domains (Reinherz and Wang, 2015). The intracellular domains of the CD4 or CD8 coreceptor bind to Lck (also known as p56-Lck), a tyrosine kinase belonging to the SRC family kinase (SFK) (Brownlie and Zamoyska, 2013; Turner et al., 1990) (Fig. 1.8). Binding of the CD4 or CD8 coreceptor to Lck has been suggested to have role in initiating TCR signalling (Veillette et al., 1988; Veillette et al., 1989). A later study concluded that the principal function of CD4 and CD8 coreceptors is to enhance Lck recruitment, but not to stabilise TCR-peptide-MHC interactions (Artyomov et al., 2010).

An overview of TCR signaling is described as follows (Brownlie and Zamoyska, 2013; Li and Rudensky, 2016) and is depicted in Fig. 1.8. TCR signaling is initiated after the interaction of TCR with a peptide-MHC complex, with the simultaneous binding of the CD4 or CD8 coreceptor to the extracellular portion of MHCII and MHCI, respectively. Lck is the first molecule to be recruited to the TCR-CD3 complex after TCR engagement. Lck phosphorylates the immunoreceptor tyrosine-based activation motifs (ITAMs) of CD3δ-, γ-, ε-and ζ-chains, thereby initiating TCR signalling.

Phosphorylation of ITAMs allows the recruitment of the SYK family kinase Zap70 (ζ-chain associated protein kinase of 70 kDa) to the TCR-CD3 complex, and allows the phosphorylation of Zap70 by Lck. The phosphorylated Zap70 propagates TCR signalling by phosphorylating tyrosine residues on linker for activation T cells (LAT). The phosphorylated LAT recruits adaptor proteins including growth factor receptor-bound protein 2 (GRB2)-related adaptor protein (GADS), SH2 domain-containing leukocyte protein of 76 kDa (SLP76), phospholipase Cγ1 (PLCγ1) adhesion and interleukin-2-inducible T cell kinase (ITK), forming a multiprotein complex (Brownlie and Zamoyska, 2013; Li and Rudensky, 2016).

This multiprotein complex nucleated by LAT propagates TCR signalling to four major signalling pathways: (1) protein kinase AKT pathway, (2) calcium ($Ca2^{+}$) signalling, (3) transcription factor nuclear factor-κB (NF-κB) signalling pathway and (4) mitogen-activated protein kinase (MAPK)/extracellular signal-regulated kinase (ERK) pathway (MAPK/ERK pathway) (Brownlie and Zamoyska, 2013; Li and Rudensky, 2016). These signalling pathways result in the translocation of transcription factors to the nucleus and their activation, including Forkhead Box O1 (FOXO1), nuclear factor of activated T cells (NFAT), NF-κB and activator protein 1 (AP-1), respectively. These transcription factors are important for gene expression and T cell growth and differentiation (Brownlie and Zamoyska, 2013; Li and Rudensky, 2016).

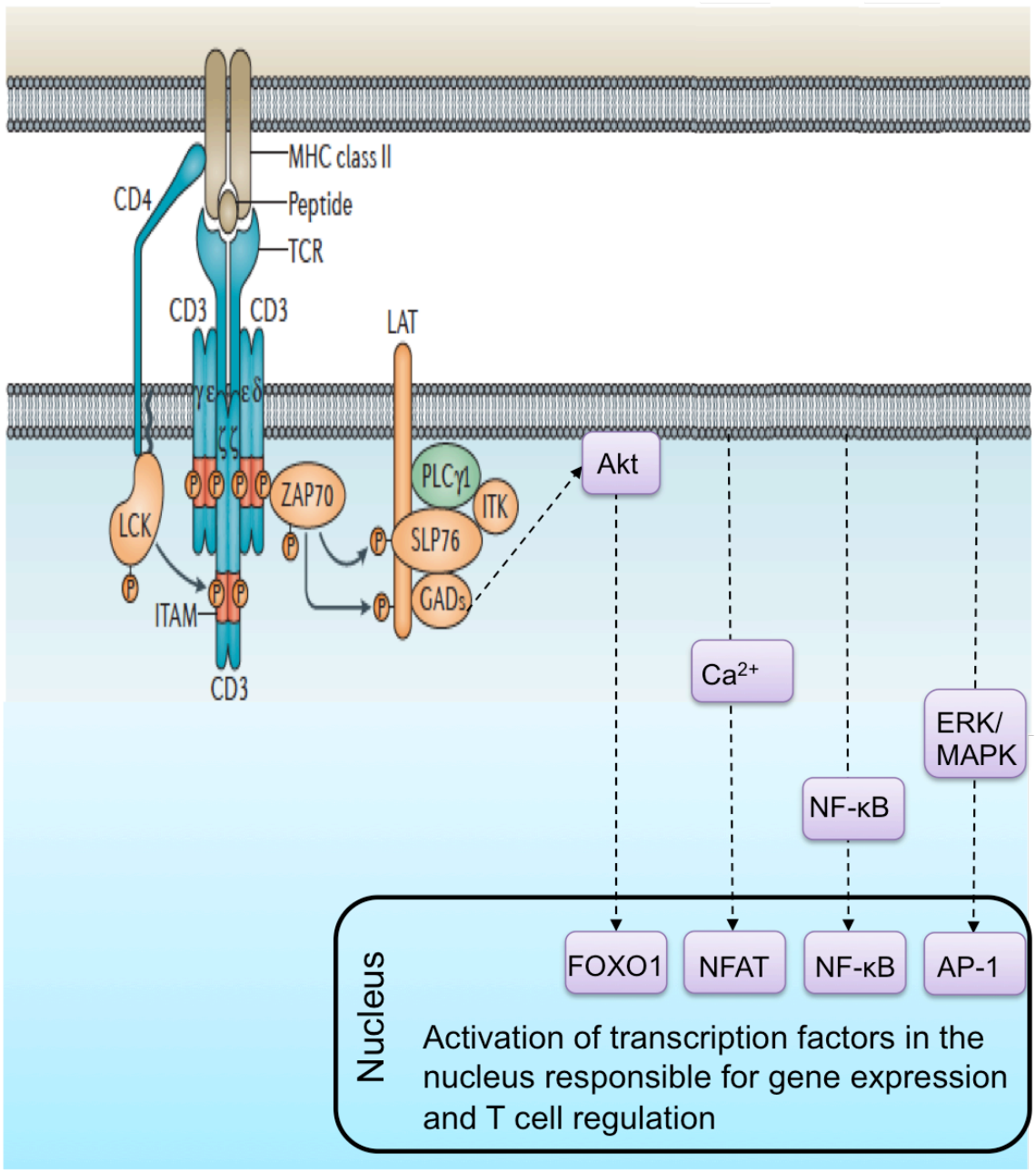
MHC class II
CD4
Peptide
TCR
CD3
CD3
LAT
LCK
ZAP70
PLCγ1
ITK
SLP76
GADs
ITAM
CD3
Akt
Ca2+
ERK/
MAPK
NF-κB
FOXO1
NFAT
NF-κB
AP-1
Nucleus
Activation of transcription factors in the nucleus responsible for gene expression and T cell regulation

Figure 1.8. Overview of TCR signalling. Upon TCR engagement, Lck (a tyrosine kinase) associates with the intracellular domain of the CD4 coreceptor (or CD8 coreceptor). Lck phosphorylates the CD3δ-, γ-, ε-and ζ-chains at the immunoreceptor tyrosine-based activation motifs (ITAMs) thereby initiating TCR signalling. Phosphorylation of ITAMs enables the recruitment of ζ-chain associated protein kinase of 70 kDa (Zap70) to the TCR-CD3 complex, and allows the phosphorylation of Zap70 by Lck. Zap70 phosphorylates multiple targets, including linker for activation T cells (LAT). The phosphorylated LAT recruits a few adaptor proteins including growth factor receptor-bound protein 2 (GRB2)-related adaptor protein (GADS), SH2 domain-containing leukocyte protein of 76 kDa (SLP76), phospholipase Cγ1 (PLCγ1) adhesion and interleukin-2-inducible T cell kinase (ITK), forming a multiprotein complex. This LAT multiprotein complex propagates TCR signalling to four major signalling pathways. These signalling pathways are the (1) protein kinase AKT pathway, (2) $Ca2^{+}$ signalling, (3) transcription factor nuclear factor-κB (NF-κB) signalling pathway and (4) mitogen-activated protein kinase (MAPK)/extracellular signal-regulated kinase (ERK) pathway (MAPK/ERK pathway), which in turn translocate or activate the transcription factors Forkhead Box O1 (FOXO1), nuclear factor of activated T cells (NFAT), NF-κB and activator protein 1 (AP-1), respectively, in the nucleus. These transcription factors are essential for gene expression and T cell growth and differentiation. P, phosphorylated. Modified from Li and Rudensky (2016).

1.6 Characteristics of TCR-signalling during positive and negative selection

Previous studies revealed that the patterns of TCR signalling of negatively selected thymocytes are different from positively selected thymocytes. In a foetal thymic organ culture (FTOC) system, one study stimulated ovalbumin (OVA) peptide-specific OT-I ($TAP^{-/-}$) transgenic T cells arrested at DP stage with different OVA-derived peptides. This study reported that the negative selecting ligands induce a rapid and robust ERK activation, whereas the positive selecting ligands stimulate a lower intensity but sustained ERK activation (McNeil et al., 2005). These observations indicate that the kinetics of ERK activation in negative selection are different from positive selection (McNeil et al., 2005). Another study used a similar system by incubating OT-I Tg *Rag*$^{-/-}$ *B2m*$^{-/-}$ cells arrested at the DP stage with tetramers of H2-K^b loaded with a positive selecting or negative selecting peptide (Daniels et al., 2006). This study demonstrated that phosphorylated ERK, and several molecules "upstream" of ERK in the TCR signaling pathway, accumulated at the plasma membrane during negative selection, whereas these molecules were either undetectable or distributed throughout the cytoplasm during positive selection (Daniels et al., 2006). By contrast, phosphorylated Jun amino-terminal kinase (JNK) accumulated throughout the cytoplasm in both positive and negative selecting conditions. This study concluded that the subcellular localisation of ERK and JNK is different in negative selection and positive selection.

Another study reported distinct temporal patterns of TCR signalling and motility in positively selected versus negatively selected thymocytes (Melichar et al., 2013). This study used multi-photon imaging to observe thymocytes undergoing positive or negative selection in thymic slices. Two TCR transgenic MHCI-restricted models were used: OVA peptide specific-OT-I thymocytes and male peptide specific-HY^{CD4} thymocytes. Positive selection was characterised by low cytosolic Ca^{2+} concentration with brief and infrequent signalling events separated by periods of migration of thymocytes. Negative selection was characterised by persistent increase in intracellular Ca^{2+} concentration with prolonged signalling events and migratory arrest of thymocytes (Melichar et al., 2013).

1.7 Positive selection

Before 2008, the traditional view of thymic selection is that positive selection occurs in the cortex, followed by negative selection (in particular clonal deletion) in the medulla of the thymus (Fig. 1.9A). The classical definition of positive selection is the induction of immature DP thymocytes with low/intermediate TCR affinity to self-peptide-MHC complexes to differentiate into mature SP thymocytes (Klein et al., 2014). This process commences in the cortex and the positively selected cells may be subsequently negatively selected in the medulla (Moran and Hogquist, 2012) (Fig. 1.9A). In this thesis, the intent is to formulate a binary scheme to distinguish positive selection from negative selection. Towards this end, positive selection refers to the complete maturation of $CCR7^{-}$ (similar to DP) thymocytes into $CCR7^{+}$ (similar to naïve SP) thymocytes in the medulla (Fig. 1.9B). Negative selection is any process that prevents a self-reactive thymocyte from undergoing positive selection. In this scheme, negative selection comprises two separate mechanisms: apoptotic deletion and agonist selection (Fig. 1.9B) (section 1.8).

1.8 Negative selection

1.8.1 Negative selection occurs in the thymic medulla

Negative selection is commonly used synonymously with clonal deletion, which is defined as the apoptosis of self-reactive TCRs with high affinity for self-antigens (Germain, 2002; Klein et al., 2009; Klein et al., 2014; Xing and Hogquist, 2012). In this thesis, negative selection is defined as mechanisms that prevent strongly TCR-signalled self-reactive thymocytes from maturing into naïve T cells. Negative selection in this context encompasses clonal deletion and agonist selection (Fig. 1.9B). Agonist selection is the clonal diversion of strongly TCR-signalled cells by agonist ligands into non-naïve T cell lineages such as $TCR\alpha\beta^{+}$ DN intestinal intraepithelial lymphocyte (iIEL) precursors (Pobezinsky et al., 2012), Forkhead box P3 transcription factor $(FoxP3)^{+}$ T-regulatory (T-reg) cells (Kawahata et al., 2002; Moran et al., 2011), NKT cells or MAIT cells (Moran et al., 2011; Stritesky et al., 2012) (Fig. 1.1, 1.9B). This concept of negative selection is consistent with previous views that include anergy (Nossal, 1994) and survivors of self-reactive thymocytes that differentiate into iIEL precursors (Pobezinsky et al., 2012), as negative selection.

Clonal deletion was thought to occur primarily in the medulla of the thymus (Fig. 1.9A). This view was based on the first direct evidence of clonal deletion, demonstrating that

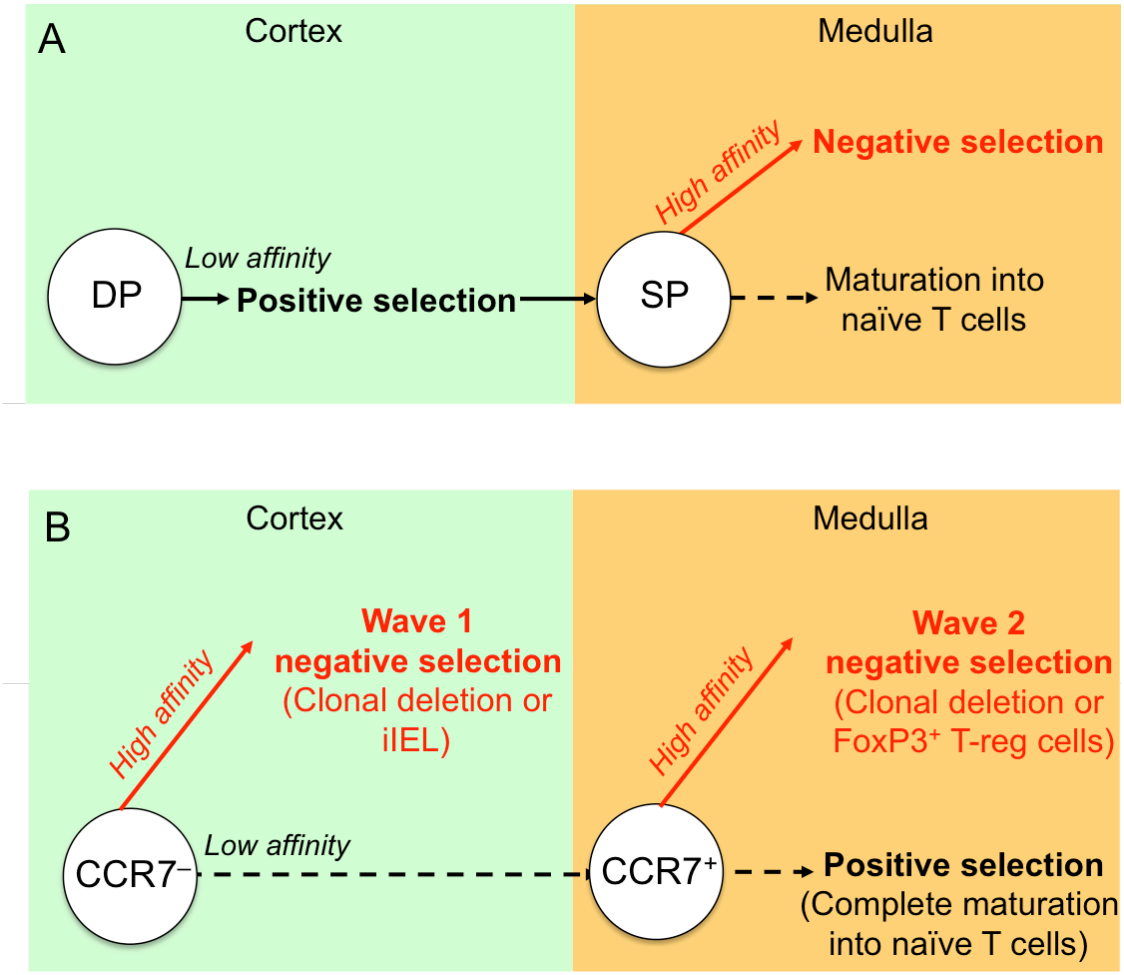

Figure 1.9. Terminology used to describe thymic selection events. (A) The traditional view of thymic selection before 2008. DP thymocytes with low TCR affinity for self-peptide-MHC complexes undergo positive selection in the thymic cortex, and continue to mature into naïve SP cells in the thymic medulla. In the medulla, positively selected SP thymocytes with high TCR affinity for self-peptide-MHC complexes undergo negative selection in the thymic medulla. (B) The terminology used in this thesis. Positive selection is the process by which $CCR7^{-}$ (~DP) thymocytes with low TCR affinity for self-peptide-MHC complexes in cortex completely mature into naïve $CCR7^{+}$ (~SP) cells in the medulla. Thymocytes with high TCR affinity for a self-peptide-MHC complex may undergo negative selection either at the $CCR7^{-}$ (~DP) stage, termed as wave 1 negative selection or at the $CCR7^{+}$ stage, termed as wave 2 negative selection. Waves 1 and 2 negative selection comprise two separate mechanisms: apoptotic deletion and agonist selection into precursors of intestinal intraepithelial lymphocytes (iIELs) in wave 1 or $FoxP3^{+}$ T-regulatory cells in wave 2.

T cells bearing Vβ17a$^+$ TCR that are specific to superantigen in the presence of MHC class II protein (IE) were selectively eliminated from mature SP thymocytes in mice expressing IE, but did not affect the immature DP thymocytes (Kappler et al., 1987). This indicates that clonal deletion of superantigen-reactive thymocytes occurs at the SP stage and therefore is thought to occur in the thymic medulla (Kappler et al., 1987). Superantigen is a protein that binds to and activates all T cells that express a particular set of Vβ TCR genes (Klein et al., 2009). Terminal deoxynucleotidyl transferase (TdT)-mediated 2'-deoxyuridine 5'-triphosphate (dUTP) nick end-labelling (TUNEL) assay has been used to label apoptotic nuclei in the thymus, which allows visualisation of apoptotic thymocytes *in situ* (Surh and Sprent, 1994). In another study, the deletion of superantigen specific-TCR Vβ5 transgenic thymocytes in H-2E$^+$ mice showed that a large number of apoptotic TUNEL$^+$ cells was observed in the thymic medulla based on the immunohistochemistry (Surh and Sprent, 1994), suggesting that thymic deletion occurs in the medulla. Furthermore, early study showed that BM-APCs were sufficient to delete superantigen-reactive Vβ17α$^+$ T cells (Marrack et al., 1988) and most BM-APCs are located in the thymic medulla (Barclay and Mayrhofer, 1981). These findings support the view that clonal deletion occurs in the thymic medulla.

Later, a study suggested that ectopic expression of a specific isoform of a tissue-specific antigen (TSA), known as proteolipid protein (PLP), in the thymic epithelium is important in mediating central tolerance and preventing autoimmune encephalomyelitis in mice (Klein et al., 2000). TSAs are normally found in the periphery but are also expressed ectopically in the thymic medulla, particularly in the mTECs (Derbinski et al., 2001). This ectopic expression of TSAs is partly regulated by autoimmune regulator (Aire), a crucial transcription factor in the thymus (Anderson et al., 2002). Studies also demonstrated that the hen egg lysozyme (HEL)-specific 3A9 transgenic (Tg) TCR (Liston et al., 2003) and the ovalbumin (OVA)-specific OT-II Tg TCR (Anderson et al., 2005) undergo negative selection at the SP stage in which the TSAs are Aire-dependent. These findings suggest that the expression of Aire and TSAs in the thymic medulla facilitates negative selection in the medulla.

A few studies used two-photon microscopy to observe thymocyte migration and cellular interactions in a 3-dimensional thymic tissue slices, in the presence of positive or negative selecting ligands. In the thymic medulla, the negatively selected F5 TCR transgenic thymocytes that are specific to $NP_{366–374}$ peptide (derived from influenza nucleoprotein) underwent rapid calcium flux and migratory arrest when the thymic slices were perfused with medium containing $NP_{366–374}$ peptide (Dzhagalov et al., 2013). This observation is consistent with the hallmark of negatively selected thymocytes

(Melichar et al., 2013). Although negatively selected MHCI-restricted OT-I Tg thymocytes specific for an Aire-dependent membrane-OVA (mOVA) self-antigen (Anderson et al., 2005; Gallegos and Bevan, 2004; Kurts et al., 1997) did not show migratory arrest, the migration of these thymocytes was slower than positively selected thymocytes and occurred in a confined environment (Le Borgne et al., 2009).

1.8.2 Negative selection occurs in the thymic cortex

Early studies showed that clonal deletion could occur at the immature DN to DP transition in 2C transgenic TCR (Sha et al., 1988) and in transgenic TCR specific to ubiquitous HY self-antigen expressed in male mice (i.e. HY model) (Kisielow et al., 1988). This early clonal deletion was possibly due to premature expression of the transgenic TCR at the DN stage. In 2008, a detailed analysis revealed that thymic negative selection can occur in the thymic cortex in a HY^{cd4} transgenic model (McCaughtry et al., 2008). In the HY and HY^{cd4} transgenic models, the CD8 Tg TCR binds strongly to a self-antigen expressed ubiquitously in male but not female mice (McCaughtry et al., 2008). In the HY^{cd4} transgenic model, the onset of TCRα expression occurs at the physiological stage in DP cells, resulting in deletion at the DP to SP transition (Baldwin et al., 2005), unlike the early clonal deletion at the DN to DP transition in HY model (Kisielow et al., 1988).

An antibody that binds to active caspase 3 has been used to identify thymocytes undergoing apoptosis (McCaughtry et al., 2008; Stritesky et al., 2013). Caspase 3 is an effector caspase that is responsible for proteolytic cleavage of cellular targets leading to apoptosis (Shi, 2002). During apoptosis, inactive caspase 3 is required to be proteolytically cleaved at aspartic acid (position 175) to produce the active form of caspase 3 (Nicholson et al., 1995). Active caspase 3 mediates apoptosis in mammalian lymphocytes and promyelocytes (Fernandes-Alnemri et al., 1994). Active caspase 3 has been used as a marker of apoptotic thymocytes. Active caspase 3^+ cells were reported to be 4.8-fold higher in HY^{cd4} male mice (that facilitate clonal deletion) compared to HY^{cd4} female mice (that facilitate positive selection) (McCaughtry et al., 2008). In addition, immunofluorescent staining on a thymic tissue section of a male mouse demonstrated that the self-reactive HY^{cd4} Thy 1.2^+ thymocytes were found to be co-localised with active caspase 3^+ staining throughout the thymic cortex, but not in the medulla (McCaughtry et al., 2008). This provides evidence that clonal deletion could occur in the thymic cortex. This observation raises the possibility that apoptosis detected in the thymic cortex by Surh and Sprent (1994) may include cells dying by deletion.

The two-photon microscopy on thymic slices reported that negatively selected $NP_{366–374}$-specific F5 TCR Tg DP thymocytes exhibited rapid calcium flux and migratory arrest in the thymic cortex (Dzhagalov et al., 2013). Similarly, OVA specific OT-I Tg DP thymocytes undergoing negative selection in the thymic cortex increased intracellular Ca^{2+} concentrations, resulting in migratory arrest and translocation of the transcription factor NFAT to the nucleus (Melichar et al., 2013). These patterns of TCR signaling and migration of the negatively selected thymocytes observed in the thymic cortex provide real time evidence supporting negative selection can occur in the thymic cortex.

The discovery of cortical negative selection has led scientists to revisit negative selection at the immature developmental stage. Characterisation of thymocyte deletion at the immature DP or $CCR7^{–}$ stage has advanced with the advent of molecular markers, Nur77 and Helios, which identify strongly TCR-signalled thymocytes (Daley et al., 2013; Stritesky et al., 2013). These two studies used mice lacking pro-apoptotic protein BCL-2-interacting mediator of cell death (BIM; also known as BCL2L11) (*Bim*$^{–/–}$) (Bouillet et al., 2002). In *Bim*$^{–/–}$ mice, instead of undergoing rapid deletion, strongly TCR-signalled thymocytes persist and can be quantified. The first study used transgenically expressed GFP under the control of the promoter of the *Nr4a1* gene, which encodes Nur77 (Stritesky et al., 2013). In these $Nur77^{GFP}$ reporter mice, the GFP expression correlates to the TCR signal strength (Moran et al., 2011). Compared to pre-selection DP thymocytes, Nur77 transcription factor is expressed 10-fold higher in negatively selected thymocytes but it is also expressed 2-fold higher in positively selected thymocytes (Baldwin and Hogquist, 2007). Bim-deficient $Nur77^{GFP}$ mice had an increased number of thymocytes expressing high levels of $Nur77^{GFP}$ at the immature DP stage, and at the more mature SP stage (Stritesky et al., 2013).

The second study used an endogenously expressed Helios transcription factor as a marker to quantify negative selection (Daley et al., 2013). Helios is upregulated in strongly TCR-signalled thymocytes as evident in the Bim-deficient HEL-specific 3A9 TCR × insHEL double Tg mouse model in which CD4SP thymocytes undergo negative selection. In contrast, Helios is downregulated in weakly TCR-signalled thymocytes as shown in Bim-deficient 3A9 TCR single Tg mice modeling positive selection (Daley et al., 2013). Using Helios in conjunction with CCR7 to mark maturation stages of developing thymocytes, our group revealed that negative selection occurs in the superantigen specific $CCR7^{–}$ immature thymocytes and in the self-antigen specific $CCR7^{+}$ mature thymocytes (Fig. 1.9B), similar to DP and SP stages, respectively (Daley et al., 2013).

CCR7 is important for localisation of SP thymocytes within the medulla and for migration of developing thymocytes from the cortex to the medulla. Mice deficient in CCR7 or double deficient in the medullary CCR7 ligands CCL19/CCL21, resulted in the accumulation of SP cells in the cortex (Kwan and Killeen, 2004; Ueno et al., 2004). In another study using two-photon microscopy to visualise migration of DN, DP and CD4SP thymocytes on thymic slices also revealed that CCR7 is important in mediating the chemotaxis of CD4SP thymocytes towards the medulla (Ehrlich et al., 2009). Thymocytes that exhibit the phenotype of Helios^{+} CCR7^{-} are characterised as wave 1 negative selection, whereas thymocytes exhibiting Helios^{+} CCR7^{+} phenotype are characterised as wave 2 negative selection by our group (Fig. 1.9B) (Daley et al., 2013). Wave 1 and wave 2 thymocytes were also detected in the polyclonal thymocyte repertoire (Hu et al., 2016).

Based on the use of Nur77^{GFP} as a negative selection marker, it was reported that 57% of thymocytes undergo DP cortical negative selection (Stritesky et al., 2013). Similarly, ~55% of CD69^{+} TCR-signalled nascent thymocytes labelled with BrdU were deleted (with Helios upregulation) at the CCR7^{-} (similar to the DP) stage (Daley et al., 2013). 20% (Daley et al., 2013) to 60% (Stritesky et al., 2013) of thymocytes were estimated to undergo negative selection at the CCR7^{+} or SP stage in the CD4 lineage. The proportion of cells undergoing negative selection at the immature stage is higher than positive selection, and higher than the proportion of cells undergoing negative selection at the more mature stage of thymocyte development (Daley et al., 2013; Stritesky et al., 2013). Within the active caspase 3^{+} CD69^{+} CD5^{+} thymocyte population undergoing TCR-signalled apoptosis (i.e. deletion), the proportion of DP thymocytes exceeds SP thymocytes by 2-3 fold (Stritesky et al., 2013). These studies indicate that developing thymocytes are constantly exposed to negatively selected self-antigens and are eliminated by apoptotic deletion at multiple stages of thymocyte development in the normal thymus (Fig. 1.9B).

Although the proportions of selectable thymocytes undergoing apoptotic deletion have been studied, the proportions of selectable (i.e. TCR-signalled) thymocytes responsive to MHCI or MHCII, and the proportions of strongly TCR-signalled thymocytes induced by MHCI or MHCII, remain unclear. Sinclair et al. (2013) tracked the Zap70-dependent thymocyte differentiation or cell death contributed by MHCI or MHCII throughout T cell development using mice bearing a tetracycline-inducible Zap70 (TetZap70) transgene. In TetZap70 mice, *Zap70*$^{-/-}$ thymocytes were arrested at the DP stage but the Zap70 expression within the *Zap70*$^{-/-}$ thymocytes could be turned on by administration of tetracycline (Saini et al., 2010). BM chimeras were generated by reconstituting the

irradiated *B2m*$^{-/-}$ *Rag1*$^{-/-}$ and *H2-Ab1*$^{-/-}$ (referred to as *MHCII*$^{-/-}$ by the authors) *Rag1*$^{-/-}$ hosts with wild-type TetZap70 BM cells. This study concluded that the proportion of selectable thymocytes induced by MHCII or MHCI was similar at the initiation stage (Sinclair et al., 2013). However, as the BM cells transferred into the single MHC-deficient hosts expressed both MHC Class I and II, it is possible that some TCR signalling events were mediated by the MHC class that was supposed to be "absent" on BM-APCs. Furthermore, the transgenic Zap70 expression does not replicate physiological Zap70 expression. Therefore, whether MHCI and MHCII have equivalent or different capacities to induce TCR signalling in thymocytes remains unclear.

1.8.3 Characteristics and timing of the two waves of negative selection

The two waves of negative selection are phenotypically distinctive. Like negatively selected DP thymocytes in the HY^{cd4} Tg model, the wave 1 (Helios^{+} CCR7^{-}) negatively selected thymocytes in a superantigen-mediated model (Daley et al., 2013) and in the polyclonal repertoire (Hu et al., 2016), upregulate program death inhibitory receptor (PD-1) expression, and downregulate both CD4 and CD8 coreceptors, also termed as coreceptor dulling (Daley et al., 2013; Hu et al., 2016; McCaughtry et al., 2008). The coreceptor dulling phenotype is also consistent with *in vitro* TCR-activated DP thymocytes undergoing apoptosis (Page et al., 1993; Swat et al., 1991). By contrast, wave 2 (Helios^{+} CCR7^{+}) negatively selected thymocytes, like SP thymocytes in the 3A9 TCR × insHEL double Tg mouse model, activate a TCR-Card11-NF-κB response which opposes Bim-mediated apoptosis (Daley et al., 2013). The TCR-Card11-NF-κB responses include the upregulation of CD25 (also known as Interleukin-2 receptor alpha chain, IL-2RA), OX40 (CD134, tumour necrosis factor (TNF) receptor), glucocorticoid-induced TNF receptor (GITR) and c-Rel (Daley et al., 2013). Wave 2 negative selection is reported to be the stage in which FoxP3^{+} T-reg differentiation occurs (Hu et al., 2016), consistent with the upregulation of CD25, OX40 and GITR in FoxP3^{+} T-reg cells (McHugh et al., 2002).

Wave 1 negatively selected thymocytes are also temporally and spatially separable from wave 2 negatively selected thymocytes based on studies using BrdU or 5-ethynyl-2'-deoxyuridine (EdU) to label proliferating cells *in vivo* and *in vitro* (Salic and Mitchison, 2008; Yu et al., 2009). EdU is a compound chemically similar to BrdU, a novel alternative to BrdU (Buck et al., 2008). BrdU and EdU are thymidine analogues that are incorporated into newly synthesised DNA in cells during S (synthesis) phase of the cell cycle (Gratzner, 1982). EdU uses a click-it reaction in which copper (I) catalyses the reaction between the alkane group in EdU and the azide which contains

the fluorochrome (Buck et al., 2008). BrdU/EdU has a half-life of 15-30 min in mice injected with a single bolus (Cheraghali et al., 1994; Matiašová et al., 2014; Packard Jr et al., 1973).

EdU time course experiments conducted by our group recently showed that wave 1 induction peaked at day 2, whereas wave 2 induction peaked at day 5 (but detected at days 4-7), after the major proliferation phase at the DN to DP transition (i.e. after EdU injection) (Hu et al., 2016). Given that $BrdU^+$ thymocytes were detected exclusively in the thymic cortex after 2 days of BrdU injection (Penit, 1986), and apoptotic (active caspase 3^+) negatively selected $CCR7^-$ DP MHCI-restricted TCR Tg thymocytes were detected in the thymic cortex (McCaughtry et al., 2008), all these findings indicate that wave 1 negative selection occurs in the thymic cortex. A few $BrdU^+$ thymocytes were detected in thymic medulla at 3 days after BrdU injection, whereas all $BrdU^+$ thymocytes were detected in the thymic medulla 5-7 days after BrdU injection (Penit, 1986). Given the requirement for CCR7 in facilitating the migration of thymocytes from the cortex to medulla (Kwan and Killeen, 2004; Ueno et al., 2004), these findings suggest that wave 2 thymocytes occur in the thymic medulla.

Although these studies demonstrated that wave 1 and wave 2 negatively selected thymocytes are phenotypically distinctive in wild-type mice based on cellular studies, it has not been shown whether there are qualitative differences between the wave 1 TCR repertoire and the positively selected CD4SP and CD8SP TCR repertoires using a TCR sequencing approach.

1.8.4 Early agonist selection: iIEL precursors develop at wave 1

Precursors of the unconventional $CD8\alpha\alpha^+$ $CD4^-$ iIELs found in the small intestinal epithelium have been identified in the thymus where they undergo agonist selection (Gangadharan et al., 2006; Klose et al., 2014; Leishman et al., 2002). Thymocytes forced to express a TCR derived from $CD8\alpha\alpha^+$ $CD4^-$ iIEL attained a $TCR\alpha\beta^+$ $CD4^{lo}CD8^{lo}$ $PD\text{-}1^{hi}$ phenotype (Mayans et al., 2014; McDonald et al., 2014), characteristic of strongly TCR-signalled wave 1 $CCR7^-$ thymocytes (Fig. 1.9B) (Daley et al., 2013; McDonald et al., 2015). $CD4^{lo}CD8^{lo}$ $PD\text{-}1^{hi}$ thymocytes are referred to as iIEL precursors hereafter. The self-reactive thymocytes that survive clonal deletion either in the absence of CD28 co-stimulation or in transgenic overexpression of anti-apoptotic proteins Bcl-2 or Mcl-1 are clonally diverted into $TCR\alpha\beta^+$ $CD4^{lo}CD8^{lo}$ $PD\text{-}1^{hi}$ iIEL precursors (Pobezinsky et al., 2012).

1.8.5 Late agonist selection: T-reg differentiation occurs at wave 2

FoxP3$^+$ CD25$^+$ CD4$^+$ T-reg cells have roles in suppressing autoimmune inflammation (Sakaguchi et al., 1995; Takahashi et al., 2000). Our group demonstrated that FoxP3$^+$ induction predominantly occurs in strongly TCR-signalled wave 2 (Helios$^+$ CCR7$^+$) thymocytes (Fig. 1.9B), at 4-8 days after proliferation at the DN-DP transition, based on EdU time course analyses (Hu et al., 2016). Previous studies also reported that Helios is expressed in thymic FoxP3$^+$ T-reg cells (Thornton et al., 2010) and in the peripherally induced T-reg cells (Gottschalk et al., 2012). Consistently, FoxP3 induction was also reported to occur at the CCR7$^+$ CCR9$^-$ CD4SP mature stage by quantitative PCR and flow cytometry (Cowan et al., 2013). Altogether, these findings suggest that the thymic medulla is the site where thymocytes upregulate FoxP3. Surprisingly, the absence of CCR7 increased FoxP3$^+$ T-reg numbers in the thymus (Cowan et al., 2014). This was explained recently by the role of CCR7 in limiting peripheral T-reg recirculation back to the thymus (Cowan et al., 2016).

1.9 Types of thymic APCs involved in T cell selection

The interaction between thymocytes and different types of thymic APCs in the thymus is important in facilitating positive or negative selection. Thymic APCs can be broadly divided into BM-derived APCs (DCs, macrophages and B cells) and non-BM-derived APCs (cTECs and mTECs). Cortical TECs in the thymic cortex are important for positive selection, whereas mTECs and DCs in the medulla are important for negative selection (Klein et al., 2014; Xing and Hogquist, 2012).

1.9.1 Cortical thymic epithelial cells (cTECs) are important for positive selection

Cortical TECs are the major thymic APCs that mediate positive selection as evident by the following observation: In MHCII-deficient (*H2-Ab*$^{-/-}$) mice reconstituted with one of a panel of transgenes restoring MHCII expression to different cell types, only transgenes that drove MHC Class II expression on cTECs enhanced CD4SP thymocyte formation (Bill and Palmer, 1989; Cosgrove et al., 1992).

Precisely why cTECs are required for positive selection is unclear. However, cTECs do have unique properties in terms of antigen presentation via MHCI and MHCII molecules. For instance, the β5t (PSMB11) protein is exclusively expressed in cTECs

and forms one subunit of a “thymoproteasome” (Florea et al., 2010). The thymoproteasome is thought to play a role in positive selection of $CD8^+$ T cells, as mice lacking β5t have impaired $CD8^+$ T cell development (Murata et al., 2007).

Cortical TECs also express a unique thymus-specific serine protease (TSSP) (Bowlus et al., 1999) that is thought to be involved in generating MHCII positively selecting ligands, as TSSP-deficiency decreased the positive selection of MHCII transgenic TCRs (Gommeaux et al., 2009). Cathepsin L, a unique lysosomal protease in MHCII antigen processing, preferentially expressed in the cTECs (Nakagawa et al., 1998), plays a role in producing positively selecting peptide ligands (Honey et al., 2002) and in positive selection of polyclonal $CD4^+$ T cells (Nakagawa et al., 1998).

Although cTECs express MHCII, cTECs are not efficient in presenting the exogenous proteins on MHCII molecules via the classical MHCII endocytic pathway (Klein et al., 2009; Klein et al., 2001). Instead, cTECs use an unconventional processing of endogenous peptides in the context of MHCII, known as macroautophagy. Macroautophagy is an antigen processing mechanism that involves the sequestration of cytoplasm into autophagosomes of non-lysosomal origin followed by the loading of intracellular peptides onto MHCII (Nedjic et al., 2009). It has been shown that macroautophagy occurs constitutively in 70% of cTECs (Nedjic et al., 2008). Thymocytes expressing certain TCRs fail to develop into CD4SP cells in mice lacking macroautophagy in TECs due to inactivation of the autophagy-related gene 5 ($Atg5^{-/-}$), suggesting that macroautophagy is important for positive selection (Nedjic et al., 2008).

1.9.2 Medullary thymic epithelial cells (mTECs) are important for negative selection

Medullary TECs express a large number of TSAs which are dependent on Aire (Anderson et al., 2002; Derbinski et al., 2001) or transcriptional regulator FEZ Family Zinc Finger 2 (Fezf2) (Takaba et al., 2015). Each TSA is expressed only by 1-3% of mTECs at any give time as revealed by RNA *in situ* hybridisation on thymic sections (Klein et al., 2014). Aire is expressed in the medullary region (Klein et al., 2014), exclusively by a subset of mTECs (Hubert et al., 2008) with a mature ($MHCII^{hi}$ $CD80^{hi}$) phenotype (Derbinski et al., 2005). Fezf2 is also expressed in mTECs (Takaba et al., 2015). In addition to their role as an antigen reservoir, mTECs can serve as APCs in inducing negative selection (Hinterberger et al., 2010).

In *C2TAkd* mice, partial (~90%) reduction of MHCII expression on mTECs by

microRNA-mediated CIITA degradation suggested an autonomous role of mTECs in inducing negative selection of $CD4^+$ T cells (Hinterberger et al., 2010). This study measured the frequency of CD4SP thymocytes in 4 groups of chimeric mice. Two groups, namely, wild-type hosts bearing MHCII-deficient BM, and *C2TAkd* hosts bearing wild-type BM, had significantly higher CD4SP frequencies (at different levels) than control wild-type hosts with wild-type BM-APCs. This suggests that the impairment of clonal deletion mediated by BM-APCs or by mTECs occurs at a different extent, thus revealing the non-redundant roles of mTECs and BM-APCs in mediating clonal deletion (Hinterberger et al., 2010). The same study also studied DO11.10 × Aire-OVA double Tg mice in which the DO11.10 Tg T cells are specific to the OVA peptide specifically expressed in mTECs. The authors showed that DCs are not required to mediate clonal deletion in this model. However, combined deficiency of DCs and MHCII-deficiency in mTECs (Aire-OVA × *C2TAkd* recipients with DO11.10 × ΔDC bone marrow) caused an increase in $DO11.10^+$ $FoxP3^-$ Tg T cells. This indicates the role of mTECs in clonal deletion (Hinterberger et al., 2010). In another study, sequencing of TCRα chains with a fixed transgenic TCRβ chain concluded that 5% $Foxp3^-$ CD4SP TCRs failed to undergo negative selection in *C2TAkd* mice (Perry et al., 2014).

Like cTECs, mTECs are extremely inefficient in delivering epitopes derived from exogenous antigens onto MHC class II (conventional pathway), a characteristic that is different from thymic DCs (Klein et al., 2001). 5-10% of mTECs (particularly the mature $CD80^{hi}$ $MHCII^{hi}$ $Aire^+$ subset) showed evidence of macroautophagy with high numbers of autophagosomes (Nedjic et al., 2008). Macroautophagy in mTECs has been shown to play a role in inducing $CD4^+$ T cell negative selection (Aichinger et al., 2013).

1.9.3 Dendritic cells (DCs) are important in mediating negative selection

There are three distinct subsets of thymic DCs. Two DC subsets belong to the conventional DCs (cDCs), i.e. $CD8^+$ cDCs (also known as resident DCs) and signal regulatory protein α $(SIRPα)^+$ cDCs (also known as migratory DCs). The third subset is plasmacytoid DCs (pDCs) (Klein et al., 2014; Perry and Hsieh, 2016; Wu and Shortman, 2005). The intrathymically developed $CD8^+$ cDCs comprise ~50% of all thymic DCs, whereas the extra-thymically developed $SIRPα^+$ cDCs and plasmacytoid DCs that migrate to the thymus account for 20% and 30%, respectively, of all thymic DCs (Oh and Shin, 2015; Wu and Shortman, 2005).

Thymic DCs can acquire antigens from mTECs, from the blood, or from peripheral tissues and home to the thymus (Oh and Shin, 2015). $SIRPα^+$ migratory DCs found in

CMJ perivascular space and around small vessels, have been shown to be able to present blood-borne antigens (Baba et al., 2009). $CD8^+$ resident cDCs are found predominantly in the thymic medulla (Klein et al., 2014; Lei et al., 2011). Plasmacytoid DCs (and potentially $SIRP\alpha^+$ DCs) can transport peripheral (extrathymic) antigens and migrate to the thymus to promote tolerance (Bonasio et al., 2006; Hadeiba et al., 2012).

Self-antigens can be presented directly by BM-APCs or mTECs (direct presentation), or indirectly presented via antigen transfer from mTECs to BM-APCs (indirect presentation), to induce tolerance. An early BM chimera experiment showed that superantigen-reactive $V\beta17\alpha^+$ T cells were reduced when MHCII I-E expression was confined to BM-APCs but not when I-E expression was confined to radioresistant thymic epithelium, suggesting that BM-APCs are important in clonal deletion (Marrack et al., 1988). Later studies showed that MHCII-deficiency on BM-APCs (Hinterberger et al., 2010; van Meerwijk et al., 1997) or *in vivo* ablation of CD11c-expressing DCs using a diphtheria toxin α chain transgene (Ohnmacht et al., 2009) resulted in increased CD4SP thymocytes. These findings indicate the role of BM-APCs, in particular DCs, in mediating clonal deletion.

Based on TCRα sequencing in mice with a fixed transgenic TCRβ, 20% of CD4SP TCRs were found to depend on $MHCII^+$ BM-APCs for deletion (Perry et al., 2014). The TCRs dependent on $MHCII^+$ BM-APCs for deletion were partly distinct from the TCRs that were dependent on high MHCII expression in mature mTECs, revealing the non-redundant roles of BM-APCs and mTECs in inducing negative selection (Perry et al., 2014).

Antigen transfer (also called indirect presentation or antigen handover) from mTECs to BM-APCs is an important antigen-presenting mechanism underlying negative selection in the thymus. APCs purified from the thymus can induce T cells to proliferate *in vitro*, if they present a peptide that is recognised by the T cells. In such an assay, purified thymic DCs were found to stimulate more T-cell proliferation than purified mTECs, even when the peptide was expressed within mTECs and not DCs (Koble and Kyewski, 2009). This suggests that antigen handover can "amplify" the T-cell stimulatory capacity of mTEC-derived self-antigens. *In vivo* studies have shown that some mTEC-derived self-antigens require antigen handover in order to induce thymocyte deletion (Aichinger et al., 2013; Hubert et al., 2011; Taniguchi et al., 2012). Antigen handover is also important for T-reg selection in the thymus, as a TCR sequencing approach revealed that almost half of the TCRs that required Aire to undergo T-reg

differentiation, also required MHCII^{+} BM-APCs in order to meet this fate (Perry et al., 2014). It is thought that CD8^{+} cDCs can contribute to indirect presentation in the thymus. This is because mTECs are the only thymic stromal cells that express the Aire-dependent XC-chemokine ligand 1 (XCL1) and XCL1 is important in localising DCs in the medulla, and CD8^{+} cDCs express the XCL1 receptor (Lei et al., 2011). Furthermore, Perry et al. (2014) also showed a role for Batf3 (Basic Leucine Zipper ATF-Like Transcription Factor 3)-dependent CD8^{+} cDCs in inducing negative selection by indirectly presenting Aire-induced self-antigens to thymocytes.

The above studies (sections 1.9.2 and 1.9.3) revealed the roles of mTECs and/or BM-APCs in mediating thymic medullary negative selection, either via direct presentation or indirect presentation (antigen handover mechanism). As increases in CD4SP thymocytes were observed when mTECs and/or BM-APCs were defective, it was inferred that these APC types mediate negative selection at or around the DP-SP transition. However, these studies did not directly measure negative selection by using markers of negatively selected thymocytes, such as Helios or Nur77. It remains unclear which thymic APC is important in mediating the large amount of negative selection that occurs at wave 1 and whether different APC types are required to mediate waves 1 and 2 negative selection during thymocyte development.

1.10 Aims

The contributions of thymic APC types to negative selection have largely been focused at the mature CD4SP developmental stage. It remains elusive whether different APC types mediate negative selection at different stages of thymocyte development. Although the proportion of thymocytes undergoing apoptotic deletion has been studied, the proportions of positively selected and negatively selected thymocytes responsive to MHCI or MHCII, remain unclear. Finally, the TCR repertoires that provoke positive or negative selection in response to one MHC class, or in the absence of both MHC classes, have not been defined.

This thesis aimed to dissect thymic negative selection mechanisms by examining:

i) the role of thymic APC types ($MHCII^+$ BM-APCs versus Aire) in thymic negative selection (Chapter 3);

ii) the role of MHC Class I and MHC Class II in inducing TCR signalling and thymic negative selection (Chapter 4); and

iii) the comparison between TCR repertoires in wild-type mice and in mice lacking one or both MHC classes using a TCR sequencing approach (Chapter 5).

CHAPTER 2

Materials and methods

2.1 Mice

All mice used in this study were bred and housed in the Australian Phenomics Facility (APF), The Australian National University (ANU), Canberra. The strains used were B10.BR (H-2^k); C57BL/6 (H-2^b); 3A9 TCR (Ho et al., 1994), insHEL and thyroHEL (initially called ILK-3 and TLK-2, respectively) (Akkaraju et al., 1997) ; *Bim*$^{-/-}$ (*Bcl2l1*^{tm1Ast}); *Tg(Vav-BCL2)*^{1Jad} (called *Bcl-2* Tg here) (Ogilvy et al., 1999); *Aire*$^{-/-}$ (*Aire*^{tm1Pltn}); *B2m*$^{-/-}$ (*B2m*^{tm1Jae}); *H2-Aa*$^{-/-}$ (*H2-Aa*^{tm1Blt}); *Tcra*$^{-/-}$ (Tcra^{tm1Mom}) and Yae62β transgenic mice (62b-Tg, with a transgenic TCRβ chain) (Stadinski et al., 2011). Mice were genotyped for transgenes and mutations by the APF Genotyping Laboratory using PCR assays. Mice were used between 7 and 28 weeks (predominantly between 10 and 16 weeks) after birth. All mice were hemizygous for the 3A9, insHEL, thyroHEL, *Bcl-2* Tg and 62b-Tg transgenes. The Animal Experimentation Ethics Committee of the ANU approved all procedures.

2.2 Materials

2.2.1 Antibodies

Table 2.1. List of extracellular antibodies for flow cytometry

Extracellular Antibody	Clone	Conjugate	Vendor
Anti-mouse CD4	RM4-5	F700	Biolegend, BD Pharmingen*
Anti-mouse CD4	GK1.5	FITC	BD Biosciences
Anti-mouse B220	RA3-6B2	APC	BD Biosciences
Anti-mouse CD8	53-6.7	APC-Cy7	Biologend
Anti-mouse CD197 (CCR7)	4B12	APC	eBioscience
		Biotin, PE	Biolegend
Anti-mouse CD5	53-7.3	APC	eBioscience
		Biotin, PerCP	BD Biosciences
Anti-mouse CD24	M1/69	PerCPCy5.5	eBioscience
Anti-mouse CD45.1	A20	FITC, PE	BD Pharmingen
Anti-mouse CD45.2	104	APC	eBioscience
		Pacific Blue	Biolegend
		PerCP	BD Pharmingen
Anti-mouse CD69	H1.2F3	Biotin	BD Pharmingen
		FITC	BD Biosciences
Anti-mouse CD11b	M1/70	FITC	BD Biosciences
Anti-mouse CD11c	N418	APC Cy7	Biolegend
Anti-mouse OX40	OX-86	PE	Biolegend
Anti-mouse PD-1 (CD279)	29F.1A12	BV421	Biolegend
	J43	PE	eBioscience
Anti-mouse TCRβ	H57-597	Biotin	BD Pharmingen
		FITC, PerCPCy5.5	eBioscience
Anti-mouse I-A/I-E (MHC Class II)	M5/114.15.2	APC	Biolegend
		eFlour 450	eBioscience
**Streptavidin-	-	BV605	Biolegend
7-AAD viability staining solution	-	-	BD Biosciences
Anti-mouse IgG1	A85-1	Biotin	BD Pharmingen
Anti-mouse B220	APC	RA3-6B2	BD Biosciences
1G12	1G12 hybridoma cells obtained from *American Type Culture Collection (*ATCC) were cultured in 5% FCS-RPMI until the medium was exhausted. Tissue culture supernatant was then harvested, azide was added at 0.1% (m/v) and stored at -20°C until use.		

Table 2.2. List of intracellular antibodies for flow cytometry

Intracellular antibody	Clone	Conjugate	Vendor
Anti-mouse FoxP3	FJK-16s	FITC eFlour 450 PerCP-Cy5.5	eBioscience
Anti mouse/human Helios	22F6	FITC Pacific blue PE	Biolegend
Anti-Cleaved Caspase-3 (Asp 175) rabbit monoclonal antibody	D3E9	AF488 AF647	Cell Signalling Technology

Abbreviations for Table 2.1 and 2.2: AF, alexa fluor; APC, Allophycocyanin; APC-Cy7, Allophycocyanin and cyanine 7 tandem conjugate; BV, Brilliant Violet; FITC, Fluorescein isothiocyanate; IgG1, Immunoglobulin isotype G1; PE, Phycoerythrin; PerCP, Peridinin chloroplast protein; PerCP-Cy5.5, peridinin-chlorophyll-protein and cyanine 5.5 tandem conjugate; 7-AAD, 7-aminoactinomycin D.

*compulsory to use when staining TCR^{3A9} Tg cells. This is because the comparable reagent purchased from BioLegend contains mouse IgG1, being harvested from ascites fluid in mice. Since the 1G12 antibody is also a mouse IgG1, the non-specific mouse IgG1 in the BioLegend reagent absorbed anti-mouse IgG1 during the final layer of extracellular staining, preventing detection of 1G12-labelled cells.

**to detect biotinylated antibodies.

2.2.2 Solutions, chemicals or buffers (unless specified in section 2.3)

1× Phosphate buffered saline (PBS) (The John Curtin School of Medical Research (JCSMR) Media Facility)

Dulbecco's PBS (also known as commercial PBS) (Sigma)

Roswell Park Memorial Institute RPMI-1640 medium (Gibco or Sigma)

Heat-inactivated fetal calf serum (FCS) (Sigma)

Heat-inactivated bovine serum (BS) (Thermo Fisher Scientific)

Bovine serum albumin (BSA) (Bovogen Biologicals)

16% Paraformaldehyde (formaldehyde) aqueous solution (Electron Microscopy Sciences)

RNAse Zap (Ambion or Invitrogen)

Agarose, Molecular Grade (Bioline)

EDTA (Sigma or VMR)

Sodium azide solution 10% (Australian Chemical Reagents, ARC)

Trypan blue solution 0.4% (Sigma)

Culture supernatant from the 1G12 hybridoma (specific for TCR^{3A9}; American Type Culture Collection), diluted 1 in 4 with FACS buffer during flow cytometry staining.

Turks solution
2% (v/v) acetic acid and 0.01% crystal violet in deionised water.

FACS buffer PBS containing 2% (v/v) heat-inactivated bovine serum and 0.01% (v/v) sodium azide solution.

FACS sort buffer
Commercial Dulbecco's PBS containing 0.5% (v/v) 0.5M EDTA and 1% (v/v) FCS.

Red blood cell (RBC) lysis buffer (10×)
8.3 g ammonium chloride (Ajax Finechem, Thermo Fisher Scientific), 1 g potassium bicarbonate (Ajax Finechem, Thermo Fisher Scientific), 37 mg EDTA disodium salt (VWR) in 100 mL deionised water. Buffer was diluted with deionised water to 1× concentration prior to use and adjusted to pH 7.3 with hydrochloric acid solution.

Tris-borate-EDTA (TBE) buffer (10×)
108 g Tris base (Trizma® base, Sigma), 55 g boric acid (Amresco, reorder from ASTRAC) and 40 mL 0.5M EDTA (pH8.0) were added in 2 L with MilliQ water. Buffer was diluted to 1× concentration with MilliQ water prior to use.

2.2.3 Common consumables (unless specified in section 2.3)

70 µm nylon cell strainer (Falcon)

96-well round bottom plate (Corning)

Flat 8 cap strips for 96-well PCR plate (Thermo scientific)

96-well PCR Plates, skirted (green colour) (Eppendorf)

Sterile filter pipette tips:
10 µL; 1-20 µL; 1-200 µL; 1000 µL Maxymum Recovery (Axygen)

Non-sterile non-filter pipette tips:
White TXL-10 (0.1-10 µL); Yellow T-200-Y; Bluo\e T-1000-B (Axygen)

15mL and 50mL tubes (Falcon)

5 mL Polypropylene tubes (Falcon)

0.5 mL and 1.5 mL microtubes (Axygen)

Disposable sterile 5 mL, 10 mL and 25 mL pipettes (Corning and Coaster)

2.3 Methods

2.3.1 Flow cytometry

2.3.1.1 Isolation of thymocytes or splenocytes for flow cytometry

Dissected thymus or spleen was collected in FACS buffer stored on ice, broken into single cell suspensions by mechanical agitation against a 70 uM cell strainer. Single cell thymocyte suspensions were mixed 1:20 with Turks solution for cell counting using haemocytometer. 3-4 × 10^6 thymocytes per well were added into a round-bottom 96 well plate. Thymocytes were centrifuged at 1300 rpm, 8°C for 4 min. This is the standard centrifugal condition unless specified elsewhere.

The standard sequence of antibody staining is as follow: Chemokine receptor CCR7 labelling (section 2.3.1.2), 1G12 supernatant labelling (only for 3A9 transgenic TCRs) (section 2.3.1.3), extracellular antibody staining (section 2.3.1.4), intracellular antibody staining (section 2.3.1.5 or 2.3.1.6) and EdU staining (if required) (section 2.3.3).

2.3.1.2 Chemokine receptor CCR7 labelling

The cell pellet on 96-well plate was stained with 50 µL of CCR7-fluorochrome conjugated antibody for 60 mins, at 37°C in the dark. Cells were pelleted by centrifugation and were washed once with 150 µL of FACS buffer. If polyclonal cells were used, proceed to section 2.3.1.4. If 3A9 TCR transgenic cells were used, proceed to section 2.3.1.3.

2.3.1.3 1G12 labelling

After CCR7 labelling, if 3A9 TCR transgenic thymocytes were analysed, cells were incubated in 50 µL of culture supernatant from the 1G12 hybridoma (diluted with FACS buffer, 1 in 4) for 30 min at 4°C. Cells were pelleted by centrifugation.

2.3.1.4 Extracellular antibody staining

Cells were stained with 50 µL of extracellular antibody cocktail and/or or mouse IgG1 (to detect 1G12) for 30 mins, at 4°C in the dark. Cells were pelleted by centrifugation and were washed once with FACS buffer.

2.3.1.5 Intracellular antibody staining

Prior to intracellular antibody staining, cells were first fixed by adding 50 µL fixation buffer (containing 4× fixation concentrate diluted with fixation diluent, 1 in 4; eBioscience FoxP3 staining kit) into each well and incubated for 30 mins, at 4°C in the dark. Cells were pelleted by centrifugation and washed once with FACS buffer, followed by permeabilization in 50 µL of permeabilisation buffer (containing 10× permeabilisation buffer diluted with Milli-Q water, 1 in 10; eBioscience FoxP3 staining kit) for 10 mins at 4°C in the dark. Cells were pelleted by centrifugation and incubated with 50 µL of intracellular antibody cocktail, including streptavidin-BV 605 conjugate to detect biotinylated antibodies, for 30 mins, at 4°C in the dark. Cells were pelleted by centrifugation and washed once with 150 µL permeabilization buffer, and washed once with FACS buffer.

2.3.1.6 Active caspase 3 intracellular staining

If active caspase 3 staining was required, after extracellular staining in section 2.3.1.4, thymocytes were fixed and permeabilized using 100 µL BD Cytofix/Cytoperm fixation and permeabilization solution (BD Bioscience) for 10 min, at 4°C in the dark, followed by two washes with 150 µL BD Perm/Wash buffer (containing 10× Perm/Wash buffer concentrate diluted with Milli-Q water, 1 in 10). Cells were stained intracellularly with Cleaved Caspase-3 (Asp 175) rabbit monoclonal antibody (Cell Signalling Technology) for 30 min, at room temperature in dark, and washed once with 150 µL BD Perm/Wash buffer.

2.3.1.7 Flow cytometry data acquisition

Stained cells were resuspended in 40 µL FACS buffer per sample in each cluster tube. Single colour stained and unstained compensation controls were resuspended in 150 µL FACS buffer. FACS samples were acquired by BD LSRFortessa^{TM} or BD LSRII cytometer.

2.3.2 Cell sorting

Thymus or spleen was collected in 5 mL of FACS sort buffer. Single cell suspensions of thymocytes or splenocytes were obtained through 70 uM cell strainer in FACS sort buffer. Single cell suspensions were pelleted by centrifugation at 1300 rpm, 8°C for 4

min (standard centrifugal condition unless specified elsewhere). Splenocytes were lysed by adding 1 mL of 1× RBC lysis buffer for ~2-4 mins. Lysis reaction was stopped by topping up to 10 mL with FACS sort buffer. Cells were pelleted by centrifugation. The lysed splenocytes were washed again with FACS sort buffer and pelleted by centrifugation.

Approximately 100 × 10^6 of thymocytes or splenocytes from each mouse were stained with 1.5 mL of extracellular antibody cocktail under similar condition and washed as described (section 2.3.1.4), except by using 4 mL FACS sort buffer in each wash. The pelleted stained cells were resuspended in 1.5 mL of FACS sort buffer and filtered via 70 nμ nylon cell strainer into a 5 mL polyprolylene tube prior to cell sort. Cells were sorted using BD FACSAria I and FACSAria II cell sorters (BD biosciences). Sorted cells were collected in polyprolylene tube containing 500 μL FCS.

2.3.3 *In vivo* EdU pulse labelling

5-ethynyl-2'-deoxyuridine (EdU) is a thymidine analogue that is incorporated into DNA during DNA synthesis (Fig. 2.1) (Salic and Mitchison, 2008). EdU labelling was performed using Click-iT® EdU AF488, AF647 or Pacific Blue Flow Cytometry Assay Kits (Molecular Probe Life Technology) according to the manufacturer's instructions with slight modification. All reagents are provided in the kits unless specified.

Briefly, 0.25 mg EdU was injected intraperitonally (0.1 mL of a 2.5 mg/mL m/v in DMSO solution (Sigma)) into each mouse. 1h to 7 days post-EdU injection, thymus was collected. After intracellular staining as described above (section 2.3.1.5 or 2.3.1.6), cells were washed in 150 μL 1% (w/v) bovine serum albumin (BSA) in PBS (1% BSA-PBS, not from kit). Thymocytes were refixed with 50 μL of 4% (v/v) paraformaldehyde (PFA) in PBS for 5 min at room temperature, and were centrifuged and washed with 150 μL 1% BSA-PBS. Cells were then re-permeabilised with 150 μL permeabilisation buffer (containing 10× saponin-based permeabilisation buffer diluted with 1% BSA-PBS, 1 in 10). Cells in each well were resuspended in 100 μL of fresh Click-iT® reaction buffer containing 95.5% of 1× PBS, 2% 100 mM copper sulphate, 2% 1× Click-iT® EdU buffer additive (Component G, which was used at one-fifth of the concentration recommended), 0.5% of azide conjugated with fluorescent dye. Cells were incubated for 30 min at room temperature, in the dark. The buffer addictive reduces Cu^{2+} ions into Cu^{+} ions. Cu^{+} ions catalyse the covalent reaction between azide (that is coupled to a fluorescent dye) and alkyne (that is found in the ethynyl moiety of

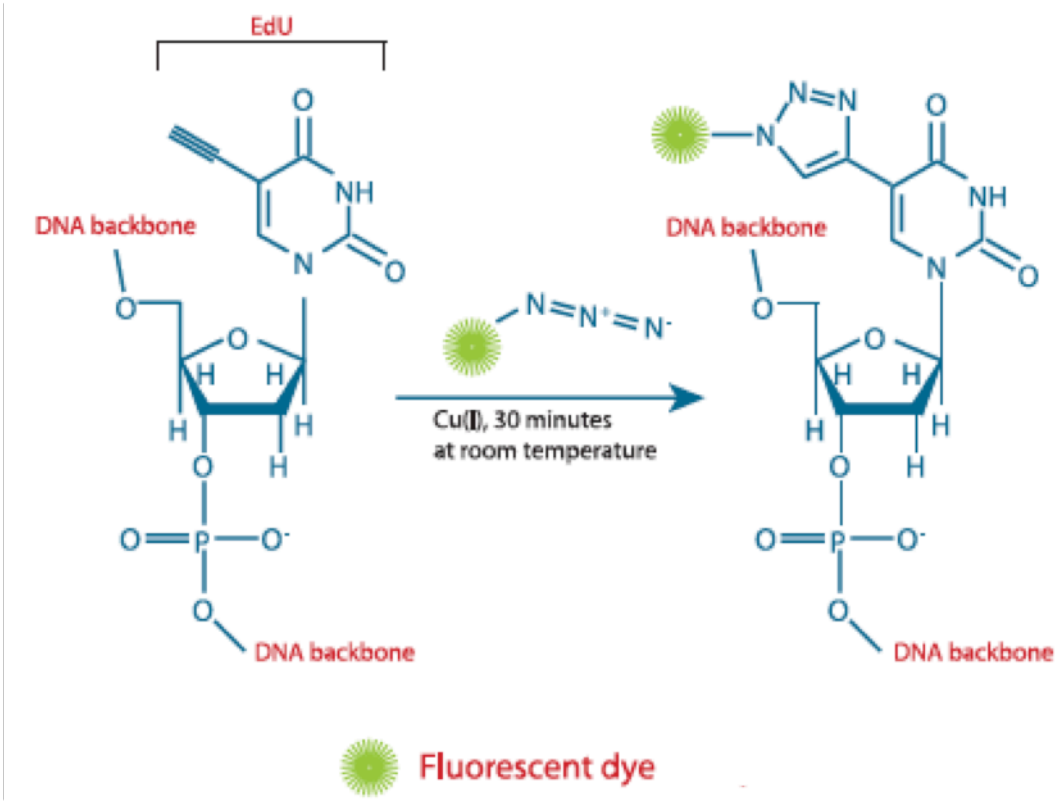

Figure 2.1. Click-iT® reaction between EdU and azide-conjugated with flurorescent dye. The detection of EdU is based on a click reaction. The EdU incorporated into the DNA contains an alkyne. Azide is conjugated to a fluorescent dye for detection. Upon the addition of buffer addictive and copper sulphate, copper (I) causes the alkyne in EdU to react with the azide conjugated with fluorochrome, to form a stable triazole ring, enabling EdU detection using flow cytometry. The small size of the detection azide allows the use of mild conditions to access the EdU incorporated into the DNA. Adapted from EdU manual (Molecular Probes) (revised July 2010, MP10044).

EdU) (Salic and Mitchison, 2008) (Fig. 2.1). 100 µL of Click-iT® reaction buffer without azide component was added to the single stained and the unstained compensation controls for flow cytometry. After incubation, cells were washed once with permeabilisation buffer, and washed once with 1% BSA-PBS, and resuspended in FACS buffer for flow cytometry.

2.3.4 Thymic stromal cell Isolation for individual thymus

This procedure was performed as previously described with adaption (Gray et al., 2002). Fat and connective tissue of each thymus were trimmed off thoroughly. Each thymic lobe was dissected. The capsule of each lobe was nicked 6-10 times on both sides (top and bottom) with fine scissors (Kaisers). Each thymus was agitated in 3 mL of RPMI using a wide-bore transfer pipette to gently flush out thymocytes until the media was visibly cloudy. The supernatant (containing thymocytes) was collected and kept on ice. The thymic fragment (pellet) was incubated at 37°C for 15 min in 2 mL digestion buffer containing 0.125% (w/v) Collagenase D (from *Clostridium histolyticum*, Roche Diagnostics) and 0.5 mL of 0.1% (w/v) DNAse I (from Bovine pancreas (grade II), Roche Diagnostics) in RPMI. The thymic fragments were with agitated gently using wide-bore transfer pipette for 12 times at every 5 min during the 15 min incubation interval. After 15 min, fragments were allowed to settle. The supernatant was collected (and labelled as “Digest 1”) and kept on ice. The same digestion buffer was added into the remaining settled thymic fragments and incubated for 15 min with gentle agitation every 5 min, and the supernatant collected was and labelled as “Digest 2”). This digestion procedure was repeated for a third time, supernatant collected was labeled as “Digest 3”. Digest 1, 2 and 3 were kept on ice.

After 3 digestions, the remaining aggregates were incubated in 3 mL of digestion buffer containing 0.125% (w/v) Collagenase/Dispase (from *Vibrio alginolyticus/ Bacillus polymyxa*, Roche Diagnostics) and 0.3 mL of 0.1% (w/v) DNAse I in RPMI for 20-25 min, with gentle agitation every 5 min during the incubation interval. The supernatant was collected and pooled with “Digest 3”, and were centrifuged at 1200 rpm, 8°C for 5 min. The pellet was resuspended in 1 mL cold EDTA/FACS buffer (containing 5mM EDTA in PBS, 5% FCS and and 0.1% NaN_3). Cells were filtered through 100 µm cell strainer and counted by mixing with Turks solution (1 in 20). Approximately 3-4 × 10^6 cells per well were stained for flow cytometry.

2.3.5 Generation of bone marrow chimeras

2.3.5.1 Isolation and freezing of bone marrow cells

Bones from the tibia, femur and pelvis of mice were collected, while muscles attached to the bones were removed using scissors and forceps in a laminar flow cabinet. Bones were then immersed in RPMI medium containing 5% FCS (FCS-RPMI) and stored at 4°C. Bone marrow (BM) was harvested by flushing out cells using 1 mL syringe and 26 Gauge needle under sterile condition. Single cell suspensions were prepared by teasing the tissues apart through a 70 µm nylon cell strainer with a 1 mL syringe plunger. BM cells were topped up to 20 mL with FCS-RPMI. BM cells were counted on haemocytometer using Turks solution. Cells were pelleted by centrifugation for 10 min, 1200 rpm, at 8°C. Cells were resuspended in 3 mL of BM freezing media comprising FCS and 10% (v/v) of DMSO, and were added into two Nunc vials, 1.5 mL per vial. The vials were placed in dry ice for ~10 mins, followed by storage at -80°C.

2.3.5.2 Thawing of frozen BM

Frozen BM were quick thawed by immersion in a 37°C waterbath. BM cells for each vial were resuspended in 13.5 mL of RPMI with 5% FCS for counting. BM cell suspensions was mixed with Trypan blue (1:1 dilution). The non-blue (i.e. colourless) cells, identified as the viable marrow cells, were counted using haemocytometer under the microscope. Absolute cell number was determined. Cells were pelleted by centrifugation for 10 mins, 1200 rpm, at 8°C and resuspended with 1x commercial PBS and filtered using 70µm nylon cell strainer.

2.3.5.3 Mouse irradiation

Mice (minimum 8 weeks of age) to be irradiated were fed with blue antibiotic water containing polymyxin, neomycin and blue dye, at least 48h before irradiation. Mice were sub-lethally irradiated for 2 doses at 450 cGy, with the second dose 4h apart from the first irradiation dose. This is to deplete the recipients' haematopoietic cells. Mice were heated under a lamp for ~2 mins. A minimum of 2×10^6 BM cells, resuspended in commercial 1x PBS, were injected intravenously (iv) into each recipient mouse. Mice were allowed to recover for a four to six-week period before analysis.

2.3.6 High-throughput sequencing of TCRα chains

2.3.6.1 RNA extraction

50,000 cells of each FACS sorted population ($CD4^{lo}$ $CD8^{lo}$ $PD1^{hi}$ $CCR7^{-}$, non- DN CD4SP $CCR7^{+}$ and non- DN CD8SP $CCR7^{+}$ thymocytes, or splenocytes $TCR\beta^{+}$ $B220^{-}$ Fig. 5.2) were extracted for RNA using RNAeasy Kit (Qiagen) according to the manufacturer's instructions with slight modifications. Briefly, sorted cells were pelleted by centrifugation in 1.5 mL microcentrifuge tubes. 350 µL of Buffer RLT was added followed by a quick 10 sec votex to disrupt the membrane of the cells. 350 µL of 70% ethanol was added to the lysate, and mixed well by pipetting. 700 µL of the sample were transferred to a RNeasy Mini spin column containing silica-based membrane placed in a 2 mL collection tube. The column was centrifuged for 1 min at ≥8000 x g (standard centrifugation condition in section 2.3.6.1 unless specified). The flow-through was discarded. 700 µL Buffer RW1 was added to the column followed by centrifugation and removal of the flow-through. 500 µL Buffer RPE was added to the column and centrifuged. The flow-through was discarded. 500 µL Buffer RPE was added again to the column, but was centrifuged for 2 min at ≥8000 x g. Column was centrifuged at full speed for 2 min to dry the membrane. The column was placed in a new 1.5 mL collection tube. Finally, 23 µL RNase-free water was added directly to the centre of column membrane and centrifuged to elute the RNA. The purity and concentration of RNA were determined using Nanodrop 2000c Spectrophotometer (Thermo Scientific) by using 1 µL of extracted RNA.

2.3.6.2 cDNA synthesis

cDNA from the extracted RNA was generated using iScript™ cDNA Synthesis Kit (Bio-Rad), stored at -20°C. In each reaction, 15 µL RNA template (max 1 µg total RNA) was added to 5 µL of master mix containing 1 µL iScript reverse transcriptase and 4 µL of 5x iScript reaction mix, summing up to a total volume of 20 µL per reaction. A negative control containing 5 µL of master mix and 15 µL of ultrapure nuclease-free distilled water (Invitrogen) was included. cDNA was synthesised using polymerase chain reaction (PCR) Mastercycler ep Gradient S (Eppendorf) with the following conditions: 1 cycle at 25°C for 5 min, 1 cycle at 42°C for 30 min, 1 cycle at 85°C for 5 min and on hold at 4°C.

2.3.6.3 PCR amplification of TCRα chain (first PCR)

The TCRα chain sequence of the synthesised cDNA was amplified using Q5® High Fidelity PCR Kit (New England BioLabs Inc), 14 forward internal primers and one reverse internal primer (GeneWorks) (Table 2.3) specific for TCRα chain (Fig. 2.2A). Each individual forward primer stock was reconstituted to 70 µM. Each of the 14 forward primers was combined (14 forward primers × 5 µL of each) in a 0.5 mL microtube, collectively known as TRAV (TCRα chain variable region) forward primers, to a working stock concentration of 5 µM. The reverse primer is also known as TRAC (TCRα chain constant region) primer. The working stocks of forwards and reverse primers were stored at -20°C. Some of the TRAV primers are degenerate primers, which are defined as a mix of oligonucleotide sequences in which some positions contain a number of possible bases, giving a population of primers with similar sequences that cover all possible nucleotide combinations for a given protein sequence (Iserte et al., 2013).

The forward primers and reverse primers contain a 5' adapter sequence which was used as a target, in a second PCR amplification (also known as indexing PCR, section 2.3.6.6), for the addition of sample-specific "barcodes" plus P5/P7 sequences to facilitate binding of amplicons to the Illumina flowcell (Fig. 2.2A, B).

In each reaction, 5 µL cDNA template was added to 20 µL of master mix containing 12.5 µL of Q5® High-fidelity 2× master mix, 0.25 µL of 5 µM forward primers, 0.25 µL of 5 µM reverse primer and 7 µL of nuclease-free water, constituting a total of 25 µL per reaction (or per sample). The TCRα chain was PCR amplified using Mastercycler ep Gradient S (Eppendorf) with the following conditions: 1 cycle at 98°C for 5 min; followed by 35 cycles of 95°C for 30 sec, 55°C for 30 sec, 72°C for 1 min; 1 cycle at 72°C for 5 min, and on hold at 4°C. Amplified cDNA samples were stored at -80°C if not used immediately for indexing PCR (section 2.3.6.6).

Table 2.3 Sequences of 14 Vα forward internal primers and one Cα reverse primer

Primer name	Sequence (5' to 3')
Forward primers	
TRAV1 INT ADP	**TCG TCG GCA GCG TCA GAT GTG TAT AAG AGA CAG** CTC CAC ATT CCT GAG CC
TRAV2 INT ADP	**TCG TCG GCA GCG TCA GAT GTG TAT AAG AGA CAG** ACT CTG AGC CTG CCC T
TRAV5(D)-4 INT ADP	**TCG TCG GCA GCG TCA GAT GTG TAT AAG AGA CAG** AGA ATC CTA AGC TCA TCA TTG AC
TRAV6.5_6.6(D) INT ADP	**TCG TCG GCA GCG TCA GAT GTG TAT AAG AGA CAG** GTK CRR TAT CCY GGA GAA GGT C
TRAV8 INT ADP	**TCG TCG GCA GCG TCA GAT GTG TAT AAG AGA CAG** AGA GCC ACC CTT GAC AC
TRAV11 INT ADP	**TCG TCG GCA GCG TCA GAT GTG TAT AAG AGA CAG** AAC AGG ACA CAG GCA AAG
TRAV12 INT ADP	**TCG TCG GCA GCG TCA GAT GTG TAT AAG AGA CAG** GGT TCC ACG CCA CTC
TRAV13 INT ADP	**TCG TCG GCA GCG TCA GAT GTG TAT AAG AGA CAG** CCT TGG TTC TGC AGG AG
TRAV14 INT ADP	**TCG TCG GCA GCG TCA GAT GTG TAT AAG AGA CAG** CTC TGA CAG TCT GGG AAG G
TRAV15 INT ADP	**TCG TCG GCA GCG TCA GAT GTG TAT AAG AGA CAG** AYT CTG TAG TCT TCC AGA AAT CAC
TRAV16 INT ADP	**TCG TCG GCA GCG TCA GAT GTG TAT AAG AGA CAG** ATT ATT CTC TGA ACT TTC AGA AGC
TRAV18 INT ADP	**TCG TCG GCA GCG TCA GAT GTG TAT AAG AGA CAG** CAA GAT TTC ACC GCA CG
TRAV19 INT ADP	**TCG TCG GCA GCG TCA GAT GTG TAT AAG AGA CAG** GCT GAC TGT TCA AGA GGG A
TRAV21 INT ADP	**TCG TCG GCA GCG TCA GAT GTG TAT AAG AGA CAG** AAT AGT ATG GCT TTC CTG GC
Reverse primer	
TRAC INT ADP	**GTC TCG TGG GCT CGG AGA TGT GTA TAA GAG ACA G**GC ACA TTG ATT TGG GAG TC

All primers were ordered from GeneWorks, with the 3' portion of the sequences based on Dash et al. (2011) with modifications by those authors, communicated with permission to the host laboratory by Nicole La Gruta, Monash University, Melbourne, Australia. Nucleotide symbols in bold represent 5' overhang adapter sequence, which allows the binding of index adapter primers, adopted by Mandeep Singh and Yogesh Jeelall in the host laboratory. 5' **TCG TCG GCA GCG TCA GAT GTG TAT AAG AGA CAG,** Read 1 adapter; 5' **GTC TCG TGG GCT CGG AGA TGT GTA TAA GAG ACA G,** Read 2 adapter.

Mixed (or degenerate) base codes according to The *International Union of Pure and Applied Chemistry* (IUPAC): R(A or G), Y(C or T), K(G or T).

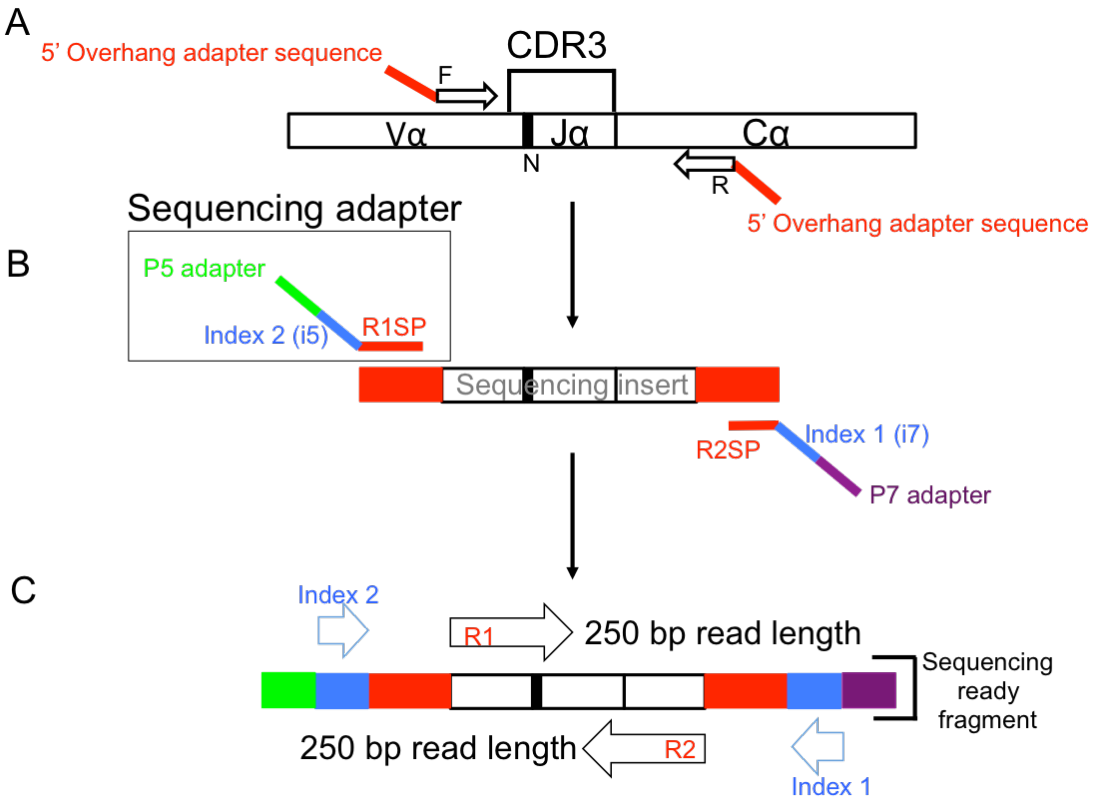

Figure 2.2. Primers and region of interest for PCR amplifications and sequencing of TCRα chain. (A) CDR3 region of TCRα chain, consists of TRAV, TRAV-TRAJ junction and TRAJ, was amplified via first round of PCR using 14 TRAV forward primers and one TRAJ reverse primer. Each of the forward and reverse primers contains a 5' overhang adapter sequence (red). First round PCR also adds 5' overhang adapter sequences to the PCR amplified region. (B) Second round of PCR known as indexing PCR add sequencing adapters to the CDR3 region of TCRα chain to barcode each sample prior to sequencing. Each sequencing adapter contains (i) a P5 (green) or P7 adapter sequence (purple) to make template compatible to flow cell, (ii) unique 8-bp index 1 or index 2 sequence (blue), and (iii) sequence that binds to 5' overhang adaptor sequence, also known as read 1 or read 2 sequencing primer (R1SP and R2SP, respectively) (red). (C) After the second PCR, the sample is ready for a 2 x 250 bp paired-end sequencing using Illumina MiSeq. The read sequence in forward direction up to 250 bp (known as Read 1, R1), the read sequence in reverse direction up to 250 bp (known as Read 2, R2). Information obtained from Illumina Adapter Sequences (February 2016, Document # 1000000002694 v01), and Illumina Data sheet: DNA Sequencing Nextera® DNA Library Preparation Kits (January 2016).

2.3.6.4 Gel electrophoresis of amplified TCRα chain

To confirm the successful amplification of TCRα chain (after first PCR, section 2.3.6.3), or successful indexed cDNA samples (second PCR, section 2.3.6.6), 2% (w/v) agarose gel was prepared by mixing 2g of agarose powder with 100 mL of 1× TBE buffer and microwaved for 2 min until the gel was completely dissolved. Gel was slightly cooled down before adding 1 µL of 10x GelRed™ nucleic acid gel stain (Biotium) into the gel to enable DNA viewing. Gel was poured into a gel cast with combs and left for at least 30 mins to solidify. 5 µL of amplified DNA or 5 µL of Quick-Load® Purple 2-Log DNA ladder (0.1-10kb bp, Fig. 2.3) (NEB) was mixed with 1 µL of 6× gel purple loading dye (NEB), and loaded into each gel well. Gel was run at 120 volts for ~1h in 1x TBE running buffer. Gel was viewed under UV transilluminator (GeneGenius Bioimaging System) and image was taken to determine the size of each band based on the DNA ladder loaded. PCR product between 300-400bp was expected after the first PCR, whereas product size between 500-600bp was expected after the second PCR.

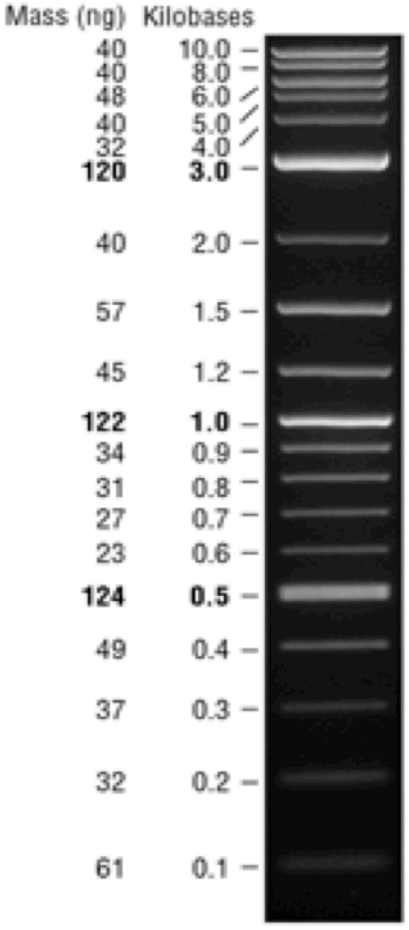

Figure 2.3. The mass and size of individual fragment of 19 fragments of Quick-Load® Purple 2-Log DNA ladder (NEB).

2.3.6.5 Post-PCR clean up

To remove oligonucleotides <100bp in length, amplified cDNA (section 2.3.6.3) or amplified indexing cDNA samples (section 2.3.6.6) were “cleaned up” using AMpure XP beads (Beckman Coulter) (Fig. 2.4). The Agencourt AMPure XP Reagent (brown colour) containing magnetic beads stored 4°C was left at room temperature for ~30 min. The 96-well PCR plate containing the amplified products was centrifuged for 1 min, at 1500 rpm. Beads were resuspended thoroughly before added into the amplified products at a ratio of 0.8, namely 20 µL of reagent containing beads into 25 µL of PCR product per well. The 96-well plate was placed onto a magnetic stand (Ambion) for 2.5-3 min until the reagent turned clear. Supernatant was removed carefully without disturbing the bead pellet held on to the magnetic stand. While still on the magnetic stand, samples were washed twice with 200 µL of 80% ethanol ensuring the beads were fully covered. Beads were incubated for 30 sec in each ethanol wash before removing the ethanol with a pipette. The samples were left to dry for 15 minutes on magnetic stand. The plate was removed from the magnetic stand. Sample in each well was resuspended with 23 µL of ultrapure distilled water (Invitrogen), mixed thoroughly and incubated at room temperature for 5 min. The plate was placed onto the magnetic stand again and left for 5 min. While still on the magnetic stand, 20 µL of the supernatant was collected into a new 96-well PCR plate, preventing from capturing the beads. The cleaned up samples were stored at stored at -80°C if not used immediately.

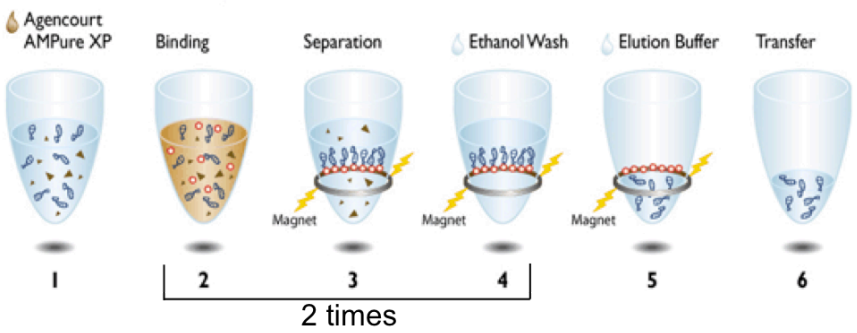

Figure 2.4. PCR product purification via Agencourt AMPure XP purification system. (1) Agencourt AMPure XP Reagent containing magnetic beads was left at room temperature for 30 min and (2) added to PCR amplicons to allow binding of PCR amplicons to magnetic beads. (3) PCR amplicons bound to magnetic beads held by a magnetic bar were separated from contaminants. (4) PCR amplicons were washed with ethanol. Steps 2-4 were repeated once. (5) Nuclease-free water was used to elute of PCR amplicons from the magnetic particles. (6) The purified PCR amplicons were transferred away from the beads into a new plate. Modified from Beckman Coulter website: Agencourt AMPure XP - PCR Purification.

2.3.6.6 Indexing PCR (second PCR)

Indexing PCR (limited-cycle amplification) was performed using the 96-sample Nextera™ Index Kit (Ilumina) that contains the following index primers:

Index 1 Read
5' CAAGCAGAAGACGGCATACGAGAT[i7]GTCTCGTGGGCTCGG, which corresponds to 5' P7 sequencing adapter [index 1] Read 2

Index 2 Read
5' AATGATACGGCGACCACCGAGATCTACAC[i5]TCGTCGGCAGCGTC, which corresponds to 5' P5 sequencing adapter [index 2] Read 1

These index primers append the three following components: (1) Read 1 or Read 2 sequencing primers (which were added into the beginning of each sequencing read; (2) two 8-bp index sequences (or dual index barcodes), which are index 1 (i7) and index 2 (i5)) (Table 2.4), and (3) two Illumina sequencing adapters (P7 and P5 adapter), to each sample. Index 1 (i7) primers (orange caps) were used to add Read 2 sequencing primer, i7 index and P7 adapter (all adjacent to each other, Fig. 2.2B) to each sample. Index 2 (i5) primers (white caps) were used to add Read 1 sequencing primer, i5 index and P5 adapter (Fig. 2.2B) to each sample. This kit contains 12 different Index 1 (i7) adapters (N701–N712), corresponding to columns (1-12) in a 96-well plate, as well as 8 different Index 2 (i5) (N502-N508 and N517) adapters, corresponding to rows (A-H). This dual indexing therefore allows a sample to have a unique combination of indexes. In the Index adapter name, N or refers to Nextera XT sample preparation, 7 or 5 refers to Index 1 (i7) or Index 2 (i5), respectively. The 01-12 refers to the Index number (Table 2.4).

Prior to the addition of indexing PCR master mix, 2.5 µL of one of the twelve i7 index primers was pipetted into each well of corresponding column, and 2.5 µL of one of the eight i5 index primers was pipetted into each well of the corresponding row. In short, each reaction for indexing PCR contained 2.5µL of i7 index primer, 2.5 µL of i5 index primer, 20 µL of the purified cDNA after first PCR (section 2.3.6.3), 25 µL of Q5 High-fidelity 2× master mix, summed to a final volume 50 µL per reaction.

The indexing PCR was performed using PCR Mastercycler ep Gradient S (Eppendorf) under the following conditions: 1 cycle at 72°C for 3 min, 1 cycle at 98°C for 30 sec; followed by 5 cycles of 98°C for 10 sec, 63°C for 30 sec, 72°C for 3 min; on hold at 4°C. Indexed samples following PCR were cleaned up for the second time as described in section 2.3.6.5, except that 40 µL of beads were added to 50 µL of indexed PCR product. The purified indexed PCR products were subjected to gel electrophoresis (section 2.3.6.4). The remaining products were stored at -80°C.

Table 2.4 List of Index 1 (i7) and Index 2 (i5) sequences. Adapted from Illumina Adapter Sequences (October 2015, Document # 1000000002694 v00, page 10-11).

i7 Bases in Adapter	i7 Index Name	i7 Bases for Sample Sheet
TCGCCTTA	N701	TAAGGCGA
CTAGTACG	N702	CGTACTAG
TTCTGCCT	N703	AGGCAGAA
GCTCAGGA	N704	TCCTGAGC
AGGAGTCC	N705	GGACTCCT
CATGCCTA	N706	TAGGCATG
GTAGAGAG	N707	CTCTCTAC
CCTCTCTG	N708	CAGAGAGG
AGCGTAGC	N709	GCTACGCT
CAGCCTCG	N710	CGAGGCTG
TGCCTCTT	N711	AAGAGGCA
TCCTCTAC	N712	GTAGAGGA

i5 Bases in Adapter	i5 Index Name	i5 Bases for Sample Sheet HiSeq 2000/2500 and MiSeq
TAGATCGC	[N/S/E]501	TAGATCGC
CTCTCTAT	[N/S/E]502	CTCTCTAT
TATCCTCT	[N/S/E]503	TATCCTCT
AGAGTAGA	[N/S/E]504	AGAGTAGA
GTAAGGAG	[N/S/E]505	GTAAGGAG
ACTGCATA	[N/S/E]506	ACTGCATA
AAGGAGTA	[N/S/E]507	AAGGAGTA
CTAAGCCT	[N/S/E]508	CTAAGCCT
GCGTAAGA	[N/S/E]517	GCGTAAGA

2.3.6.7 Pooling of TCRα chain cDNA library and sequencing

2 µL of each purified indexed sample from section 2.3.6.6 was analysed on the LabChip® GXII (Perkin Elmer) by JCSMR Biomolecular Resource Facility (BRF) to determine the concentration and the size of individual cDNA segments (bands) per sample. LabChip® GX is a high throughput microfluidics platform that performs high-resolution, reproducible electrophoretic separation. The individual bands of cDNA of TCRα chain were estimated to be between 380 and 610 bp in each sample. The concentrations of cDNA with the size ranging from 380-610 bp in each sample were summed up to determine the total concentration of TCRα chain cDNA in each sample.

5 µL of each purified indexed sample was diluted in the appropriate amount of water to give a final concentration of cDNA to 2 nM in each sample. 5 µL of 2 nM cDNA from each sample was pooled into a single library in a 1.5 mL microtube. This TCRα library was sent to BRF for TCRα deep sequencing using the Illumina MiSeq sequencer performing 250 paired-end read (Fig. 2.2C).

2.3.7 Data analyses

2.3.7.1 Flow cytometry data analysis

Flowjo Tree Star 9.6.4 and 9.9 were used to analyse the flow cytometry data in fcs format.

2.3.7.2 Statistical analyses

PRISM 6 was used to perform the following statistical analyses:

i) Unpaired Student's t-tests;
ii) Multiple t-tests without assuming a consistent standard deviation, but with correction for multiple testing using the Holm-Sidak method;
iii) 1-way ANOVA with Tukey's or Dunn's post-tests;
iv) 2-way-ANOVA with Tukey's post-tests;
v) r^2 and two-tailed P values from the Pearson correlation coefficient

2.3.7.3 TCRα chain sequencing analyses

i) PANDAseq

PANDAseq (PAired-eND Assembler for Illumina sequences) software was used to assemble the raw TCRα chain Illumina paired-end sequence reads (forward read (read 1) and reverse read (read 2)) in FASTQ file into a single sequence (Masella et al., 2012).

ii) MiTCR

MiTCR (V-(D)-J mapping software) was used to convert the assembled sequencing reads into TCR "nucleotypes" by aligning to V and J segments of the *Tcra* locus (Bolotin et al., 2013).

iii) VDJtools

VDJtools software package (Version 1.0.9) was used to analysis TCR sequencing data after converting data in MiTCR format into VDJtools format. TCR sequencing data were analysed and reported using different routines in VDJtools (Shugay et al., 2015). The following VDJtools routines were used in Chapter 5: *CalcBasicStats*, *Correct, FilterNonFunctional*, *CalcPairwiseDistances, ClusterSamples*, *SelectTop*, *TrackClonotypes*, *PoolSamples*, *OverlapPair*, *CalcSegmentUsage* and *CalcCdrAAProfile.* Further detail on these routines is provided in Chapter 5.

CalcPairwiseDistances and ClusterSamples routines used F pairwise similarities metric (formula below), which is the geometric mean of relative clonotype overlapping frequencies in first and second sample in pair, to measure how similar the TCR repertoire is between the two samples.

The formula of F metric: Geometric mean of relative overlap frequencies

$$F_{ij} = \sqrt{f_{ij} f_{ji}}$$

where $f_{ij} = \sum_{k=1}^{N} \phi_{ik}$ is the total frequency of clonotypes that overlap between samples i and j in sample i.

Adapted from Shugay, M. (December 2015), vdjtools Documentation, Release SNAPSHOT.

2.3.7.4 CDR3α amino acid sequence analysis

IceLogo software (http://iomics.ugent.be/icelogoserver/create) was used to provide visualisation of CDR3 amino acid sequences and intuitive comparison between two datasets (the experimental set and the reference set) (Colaert et al., 2009; Maddelein et al., 2015).

CHAPTER 3

Contributions of MHCII^{+} BM-APCs and Aire to the two waves of thymic negative selection

3.1 Introduction

T cell clonal deletion occurs when strong binding to a thymic APC results in thymocyte death (Kappler et al., 1987). Strong TCR-signalling can trigger thymocyte deletion to prevent thymocytes with cross-reactive TCRs from becoming mature naive T cells (Huseby et al., 2003; Huseby et al., 2005; McDonald et al., 2015). Although thymocytes may be deleted at any stage after they first express an αβ TCR (Baldwin et al., 1999), it is unclear whether deletion at different stages of T cell development requires distinct thymic APC subsets.

The two major thymic APC types are TECs and BM-APCs. Medullary TECs (mTECs) express a broad array of tissue-specific self-antigens (TSAs), some of which are regulated by the transcription factor, Aire (Anderson et al., 2002; Derbinski et al., 2005; Sansom et al., 2014). MTEC-derived self-antigens can be presented to thymocytes by the mTECs directly (Hinterberger et al., 2010; Klein et al., 2001) or mTEC-derived self-antigens can be presented indirectly via antigen handover to BM-APCs (Aschenbrenner et al., 2007; Gallegos and Bevan, 2004; Hubert et al., 2011; Koble and Kyewski, 2009; Taniguchi et al., 2012). In the thymus, BM-APCs, particularly DCs, can also present self-antigens that they express themselves (Apostolou et al., 2002), blood-borne self-antigens (Atibalentja et al., 2009; Baba et al., 2009) or peripheral tissue antigens captured by migratory or plasmacytoid DCs in the periphery (Bonasio et al., 2006; Hadeiba et al., 2012).

The crucial role of BM-APCs in deletion has been revealed by studies demonstrating that depletion of BM-APCs, or defective MHCII expression on BM-APCs, markedly increases the number of CD4SP thymocytes (Ohnmacht et al., 2009; Shimoda et al., 2006; van Meerwijk et al., 1997) or self-antigen-binding $CD4^+$ T cells (Chu et al., 2010). While diminished MHCII expression within mature mTECs in *C2TAkd* mice (Hinterberger et al., 2010) and ablation of Aire-expressing mTECs also increases CD4SP thymocyte number (Metzger et al., 2013), no such effect is observed in Aire-deficient mice (Anderson et al., 2002). In a TCRβ transgenic mouse strain, TCRα chain sequencing of $CD4^+$ $V\alpha2^+$ T cells revealed that 25% of TCRs are deleted by $MHCII^+$ BM-APCs, whereas 7% of TCRs are deleted in an Aire-dependent manner (Perry et al., 2014). Almost half of the TCRs that required Aire also required $MHCII^+$ BM-APCs to undergo deletion (Perry et al., 2014). While these findings show that $MHCII^+$ BM-APCs and Aire have autonomous and cooperative roles in thymocyte deletion, it is unclear whether these APC types delete self-reactive T cells at distinct stages of thymocyte development.

The experiments described in this chapter aimed to quantify the contributions of $MHCII^+$ BM-APCs and Aire to thymocyte deletion at the $CCR7^-$ and $CCR7^+$ developmental stages, characterised respectively as “wave 1” and “wave 2” of thymocyte deletion. Two different types of experimental models were used. Some experiments used TCR transgenic models, which provide a setting in which the self-reactive TCR and the self-antigen responsible for mediating thymocyte deletion are known. One advantage of TCR transgenic models is that the self-reactive thymocytes are identifiable, in this case using a monoclonal antibody, called 1G12, which binds to the 3A9 TCR (Van Parijs et al., 1998). The 3A9 TCR is stimulated by the MHCII molecule, $I\text{-}A^k$, complexed with the $HEL_{46\text{-}61}$ peptide (Brooks et al., 1991). 3A9 TCR (TCR^{3A9}) transgenic thymocytes are deleted earlier in development, and fewer T cells escape deletion, when membrane bound-HEL is expressed under the thyroglobulin (thyroHEL) promoter compared to the insulin (insHEL) promoter (Akkaraju et al., 1997; Liston et al., 2004a; Liston et al., 2004b). TCR^{3A9} thymocyte deletion by insHEL and thyroHEL is absolutely dependent on Aire (Liston et al., 2004a), but whether BM-APCs have roles in these deletion mechanisms had not been examined. The second type of experimental model examines mice with natural TCR repertoires. As these latter experiments rely on the use of Helios and CCR7, one goal of the TCR transgenic experiments was to compare findings based on the conventional approach of staging thymocyte deletion using CD4 and CD8 with an alternative approach that uses Helios and CCR7.

3.2 Results

3.2.1 Crucial roles for MHCII^{+} BM-APCs in TCR^{3A9} transgenic thymocyte deletion mediated by insHEL and thyroHEL

3.2.1.1 Differential escape from wave 1 deletion in insHEL versus thyroHEL mice with intact APCs

To define the stages of T cell development at which insHEL and thyroHEL mediate deletion, thymocytes from 3A9 x insHEL or 3A9 x thyroHEL double-transgenic (Tg) mice were compared to 3A9 single-Tg and non-Tg controls (i.e. carrying neither 3A9 nor HEL transgenes) using flow cytometry. In mice bearing the 3A9 TCR transgene, 10-20% of thymocytes were stained by the 1G12 antibody, versus <0.05% of thymocytes in non-Tg mice (Fig. 3.1A), which indicates that the 1G12 antibody binds specifically to the 3A9 TCR (TCR^{3A9}). TCR^{3A9+} FoxP3^{-} thymocytes were analysed for CD4/CD8 expression to define different thymocyte maturation stages (Fig. 3.1B). All 3A9 TCR Tg groups had similar numbers of TCR^{3A9+} FoxP3^{-} thymocytes at the least mature CD4^{-} CD8^{-} double-negative (DN) stage (Fig. 3.1B). Compared to 3A9 mice, 3A9 x insHEL mice had a 68% reduction in the number of DP cells and a 93% reduction in CD4SP cells (Fig. 3.1B, middle and right). The corresponding reductions in 3A9 x thyroHEL mice were 88% at the DP stage and 99% at the CD4SP stage (Fig. 3.1B). The use of CCR7 alone as a maturation marker yielded similar results, as 3A9 x insHEL mice had 61% fewer CCR7^{-} cells and 92% fewer CCR7^{+} cells than 3A9 controls (Fig. 3.1C). Compared to 3A9 mice, 3A9 x thyroHEL mice had 81% fewer CCR7^{-} cells and 99% fewer CCR7^{+} cells than 3A9 mice (Fig. 3.1C). The difference in CCR7^{+} thymocyte number indicates that escape from wave 1 deletion is less common in 3A9 x thyroHEL mice than in 3A9 x insHEL mice (Fig. 3.1C).

In 3A9 single-Tg mice without HEL antigen, Helios expression was significantly lower in the CCR7^{+} subset than in the CCR7^{-} subset (Fig. 3.1D), consistent with Helios downregulation as thymocytes mature into naïve T cells (Daley et al., 2013). Compared to 3A9 single-Tg controls, Helios expression was significantly higher in 3A9 x insHEL thymocytes only at the CCR7^{+} stage (Fig. 3.1D). Helios expression was significantly higher in 3A9 x thyroHEL mice at both CCR7^{-} and CCR7^{+} stages (Fig. 3.1D). Decreased escape from wave 1 deletion in 3A9 x thyroHEL mice was thus associated with high Helios expression in CCR7^{-} thymocytes.

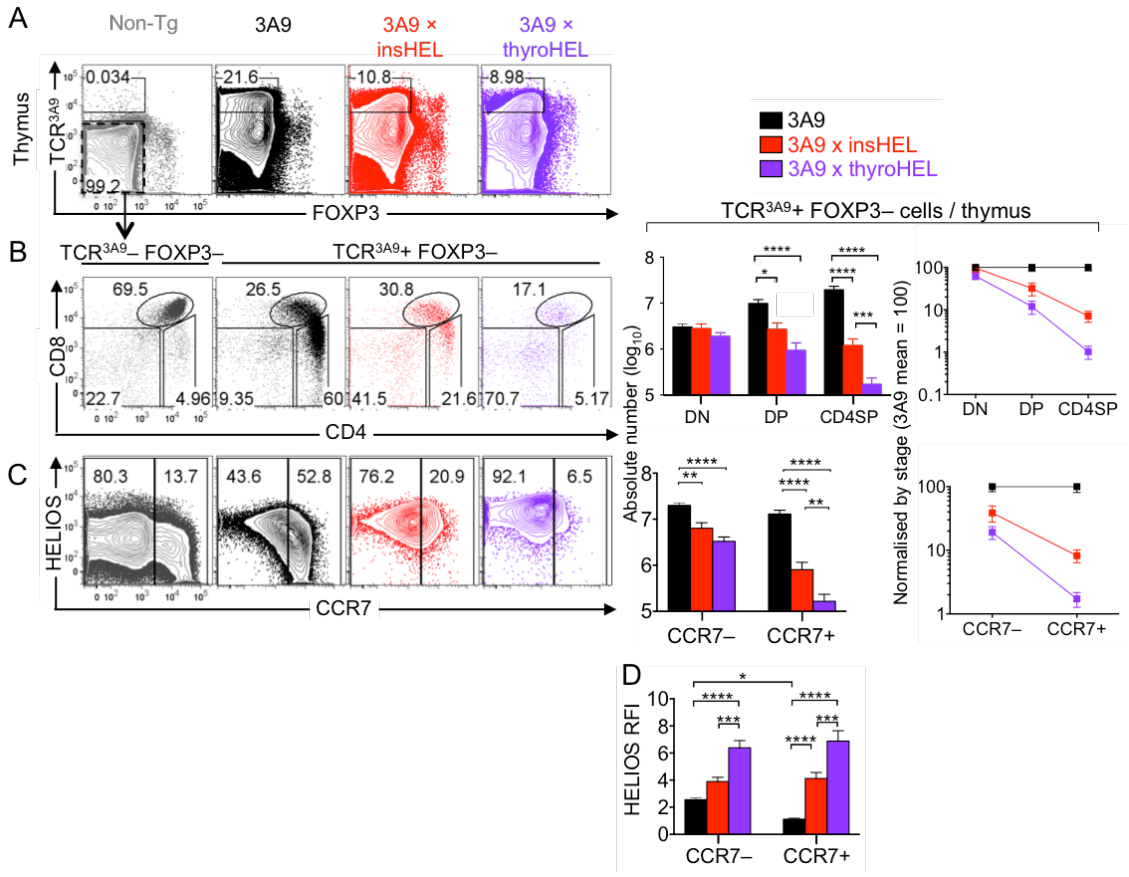

Figure 3.1. Differential escape from wave 1 deletion mediated by insHEL and thyroHEL self-antigens. (A) Representative flow cytometry plots show expression of the 3A9 TCR (TCR^{3A9}) versus FoxP3 on thymocytes from non-Tg, 3A9, 3A9 × insHEL and 3A9 × thyroHEL mice, with gates enclosing the TCR^{3A9+} $FoxP3^{-}$ population. (B, C) TCR^{3A9+} $FoxP3^{-}$ population was analysed for CD4 and CD8 (B left) and Helios and CCR7 (C left). Column graphs show the number of TCR^{3A9+} $FoxP3^{-}$ cells per thymus at the indicated stages of development (middle). To visualise the extent of self-reactive thymocyte deletion within the different stages, line graphs (right) show the same data with the 3A9 group normalised to 100. (D) Helios relative fluorescence intensity (RFI) on $CCR7^{-}$ and $CCR7^{+}$ subsets of TCR^{3A9+} $FoxP3^{-}$ thymocytes normalised to non-Tg $FoxP3^{-}$ DP thymocytes, as gated in (A, B). (B-D) Columns or symbols show the group mean and error bars the SEM compiled from 3 independent experiments with a total of 6-7 mice per group. Statistical analyses used one-way ANOVA (B, C) or (D) 2-way ANOVA and Tukey's post-tests; only statistical significant P values are shown with symbols: * <0.05; ** <0.01; *** <0.001; **** <0.0001.

Bim$^{-/-}$ mice were used to investigate the consequences of an apoptosis defect on thymocyte deletion in the two models. Mixed chimeras were generated by reconstituting non-Tg, insHEL and thyroHEL hosts with 5% *Bim*$^{-/-}$ TCR^{3A9} (CD45$^{2/2}$) and 95% *Bim*$^{+/+}$ (CD45$^{1/1}$ or CD45$^{1/2}$) BM. Among CD45$^{2/2}$ (*Bim*$^{-/-}$) TCR^{3A9+} FoxP3^{-} thymocytes, compared to non-Tg and insHEL hosts, thyroHEL hosts had a significantly lower frequency of CCR7^{+} cells (Fig. 3.2A). This indicates that thyroHEL recognition prevented the self-reactive thymocytes from fully upregulating CCR7, whereas insHEL recognition did not (Fig. 3.2A). ThyroHEL hosts had the highest frequency of CD4^{lo}CD8^{lo} cells among *Bim*$^{-/-}$ TCR^{3A9+} FoxP3^{-} thymocytes and also induced the highest level of PD-1 expression (Fig. 3.2B, C). Since thyroHEL induced coreceptor dulling and high PD-1 expression, which are the hallmarks of strong TCR-signalling at wave 1 (Daley et al., 2013; McCaughtry et al., 2008), and thyroHEL recognition prevented self-reactive thymocytes from upregulating CCR7, it is concluded that thyroHEL predominantly mediates deletion at wave 1.

3.2.1.2 The insHEL and thyroHEL transgene products responsible for deletion are not BM-APC-derived

3A9 thymocytes are not deleted when only the BM-APCs carry the insHEL transgene (Liston et al., 2005). To test whether BM-APCs carrying the thyroHEL transgene can mediate deletion directly, mixed chimeras were made by reconstituting non-Tg hosts with BM from non-Tg, insHEL or thyroHEL mice that was mixed 9:1 with 3A9 BM. Six weeks later, the CD4SP cell frequency among TCR^{3A9+} FoxP3^{-} thymocytes was similar in all groups (~75%) (Fig. 3.3). This finding demonstrates that neither insHEL nor thyroHEL deletes 3A9 thymocytes via direct presentation by BM-APCs when the transgenes are confined to only the BM-APCs.

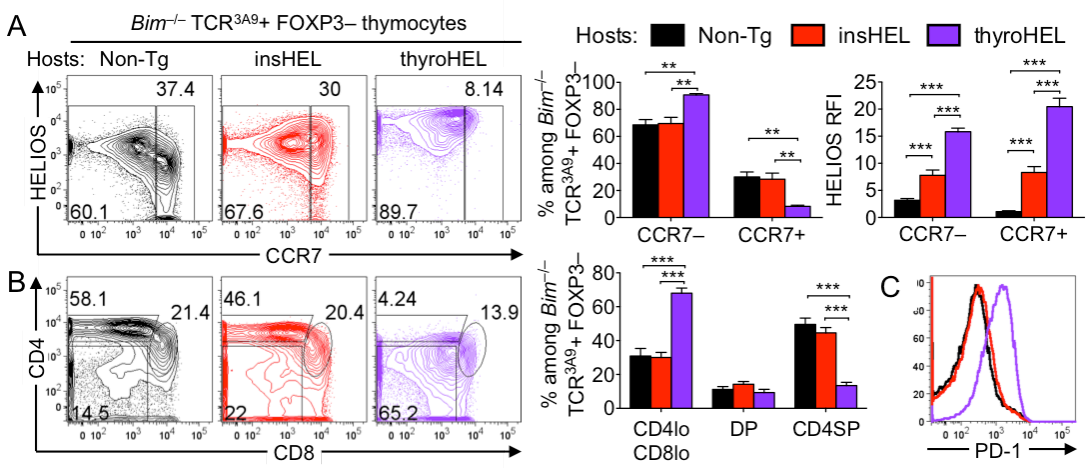

Figure 3.2. ThyroHEL but not insHEL triggers coreceptor dulling and PD-1 upregulation when apoptosis is defective. Mixed BM chimeras were generated by reconstituting irradiated non-Tg (n=12), insHEL (n=13) or thyroHEL (n=9) hosts with a mixture consisting of 5% *Bim*$^{-/-}$ TCR^{3A9} BM (CD45$^{2/2}$) and 95% *Bim*$^{+/+}$ BM (CD45$^{1/1}$ or CD45$^{1/2}$). Six week post-reconstitution, *Bim*$^{-/-}$ TCR^{3A9+} FoxP3^{-} thymocytes were analysed for Helios and CCR7 (A left). (A) Summaries show frequency of CCR7^{-} and CCR7^{+} cells among *Bim*$^{-/-}$ TCR^{3A9+} FoxP3^{-} population (middle) and Helios RFI on CCR7^{-} and CCR7^{+} subsets normalised to non-Tg FoxP3^{-} DP thymocytes (right). (B) CD4/CD8 phenotype (left) and summary shows frequency of gated CD4^{lo}CD8^{lo}, DP and CD4SP subsets among *Bim*$^{-/-}$ TCR^{3A9+} FoxP3^{-} thymocytes (right). (C) Representative histogram of PD-1 expression on *Bim*$^{-/-}$ TCR^{3A9+} FoxP3^{-} thymocytes. (A, B) Graphs show mean and error bars the SEM. Statistical analyses used one-way ANOVA and Tukey's post-tests; only statistical significant P values are shown with symbols: ** <0.01; *** <0.001.

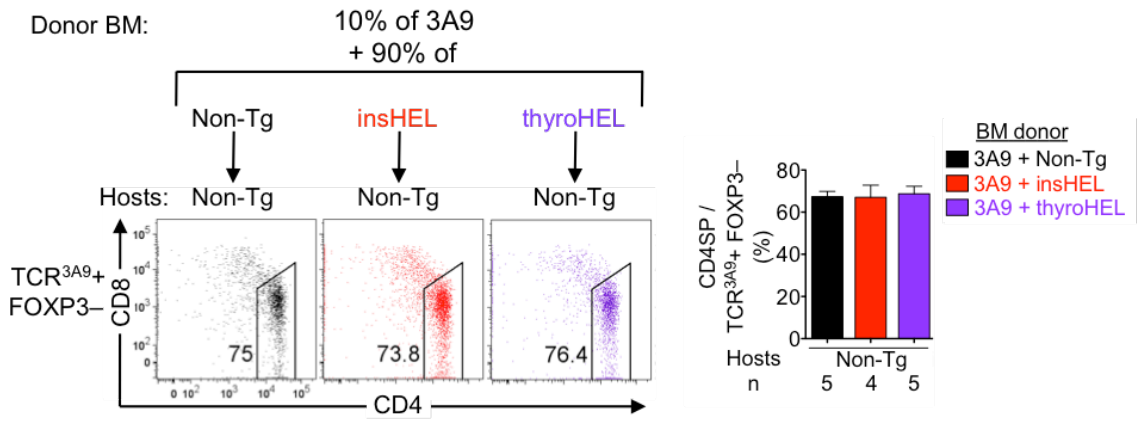

Figure 3.3: Neither insHEL nor thyroHEL mediates deletion when confined to only the BM-APCs. Irradiated non-Tg hosts ($CD45^{2/2}$) were reconstituted with non-transgenic, insHEL or thyroHEL ($CD45^{1/1}$) BM mixed with 3A9 ($CD45^{1/2}$) BM at a ratio of 9:1. Six weeks later, $CD45^{1/2}$ TCR^{3A9+} $FoxP3^{-}$ thymocytes were analysed for CD8/CD4 phenotype (left) and the CD4SP cell frequency (group mean and error bars the SEM) was determined (right).

3.2.1.3 MHCII-deficiency within BM-APCs abrogates insHEL-mediated deletion and shifts thyroHEL-mediated deletion towards wave 2

To test whether indirect presentation by BM-APCs (antigen handover mechanism from mTECs to BM-APCs, which present the antigen to thymocytes) influences thymocyte deletion by insHEL or thyroHEL, chimeras were generated using wild-type or MHCII-deficient (*H2-Aa*$^{-/-}$) 3A9 BM. InsHEL and thyroHEL hosts with wild-type BM-APCs had thymocyte CD4/CD8 and CCR7/Helios profiles (Fig. 3.4A, B) similar to non-chimeric 3A9 x insHEL and 3A9 x thyroHEL mice (Fig. 3.1B, C), indicative of thymocyte deletion as expected.

i) MHCII^{+} BM-APCs are essential for Helios induction and deletion in insHEL mice

Strikingly, insHEL hosts with MHCII-deficient BM-APCs were indistinguishable from non-Tg hosts in terms of the number of DP and CD4SP (Fig. 3.4A) or CCR7^{-} and CCR7^{+} thymocytes (Fig. 3.4B). Helios expression at CCR7^{-} and CCR7^{+} stages was also indistinguishable between these two groups (Fig. 3.4C). MHCII-deficiency within BM-APCs thus completely abrogates insHEL-mediated deletion. Taken together with the inability of BM-APCs to produce the self-antigen that mediates thymocyte deletion (Fig. 3.3), the data indicate that indirect presentation by MHCII^{+} BM-APCs is absolutely required for insHEL to induce Helios in, and delete, 3A9 thymocytes.

ii) MHCII^{+} BM-APCs enhance Helios induction and are required for wave 1 deletion mediated by thyroHEL

The number of CD4SP and CCR7^{+} thymocytes in thyroHEL hosts with MHCII-deficient BM-APCs was lower than in non-Tg hosts with MHCII-deficient BM-APCs, but higher than in thyroHEL hosts with wild-type BM-APCs (Fig. 3.4A, B). This finding suggests that MHCII^{+} BM-APCs enhance thyroHEL-mediated deletion at wave 1. MHCII-deficiency within BM-APCs significantly decreased, but did not abolish, Helios induction in thyroHEL hosts (Fig. 3.4C).

Considering all chimeras, the number of CCR7^{+} thymocytes was inversely correlated with Helios expression in CCR7^{-} thymocytes (Fig. 3.4D). At one extreme, non-Tg hosts, as well as insHEL hosts of MHCII-deficient BM-APCs, had high numbers of CCR7^{+} thymocytes and low Helios expression in CCR7^{-} thymocytes, a pattern consistent with the absence of thymocyte deletion (Fig. 3.4D). At the other extreme,

thyroHEL hosts with wild-type BM-APCs had low numbers of CCR7^{+} thymocytes and high Helios expression in CCR7^{-} thymocytes, indicative of effective deletion at wave 1 (Fig. 3.4D). In the intermediate zone, thyroHEL hosts with defective BM-APCs were clustered with insHEL hosts bearing wild-type BM-APCs (Fig. 3.4D).

iii) Increased OX40 expression in self-reactive CCR7^{+} thymocytes compared to CCR7^{-} thymocytes

OX40 is a protein highly expressed in FoxP3^{+} T-reg cells (Takeda et al., 2004). OX40 expression was low to undetectable in TCR^{3A9+} FoxP3^{-} CCR7^{-} thymocytes regardless of host genotype (Fig. 3.5A). When compared to the analysis of Helios expression above (Fig. 3.4B, C), it is evident that TCR^{3A9+} FoxP3^{-} CCR7^{-} thymocytes can upregulate Helios without upregulating OX40. In non-Tg hosts, most TCR^{3A9+} FoxP3^{-} CCR7^{+} thymocytes were also negative for OX40, although a subset did express OX40 at intermediate levels (Fig. 3.5A). Consistent with the Helios and CCR7 analyses (Fig. 3.4B, C), OX40 expression in insHEL hosts with MHCII-deficient BM-APCs was indistinguishable from non-Tg hosts. In the other 3 groups of chimeras (i.e. insHEL hosts with wild-type BM-APCs, thyroHEL hosts with wild-type or MHCII-deficient BM-APCs), a subset of TCR^{3A9+} FoxP3^{-} thymocytes expressed OX40 at high levels (Fig. 3.5A). In these 3 groups, cells that expressed OX40 at high levels tended to also express high levels of CCR7 (Fig. 3.5A). In self-reactive thymocytes, the capacity to express high levels of OX40 is associated with reaching the CCR7^{+} stage of development.

ThyroHEL hosts with MHCII-deficient BM-APCs had a significant increase in FoxP3^{+} T-reg cells compared to thyroHEL hosts with wild-type BM-APCs (Fig. 3.5B). Nascent FoxP3^{+} thymocytes are a mixture of CCR7^{-} CD24^{+} and CCR7^{+} cells whereas non-nascent thymic FoxP3^{+} cells are predominantly CCR7^{-} CD24^{-} cells (Hu et al., 2016). Among the TCR^{3A9+} FoxP3^{+} thymic T-reg cells, only the CCR7^{+} subset was significantly increased in thyroHEL mice with MHCII-deficient BM-APCs compared to thyroHEL mice wild-type BM-APCs (Fig. 3.5C). This suggests that MHCII-deficiency in BM-APCs increases nascent FoxP3^{+} thymocyte induction in thyroHEL hosts.

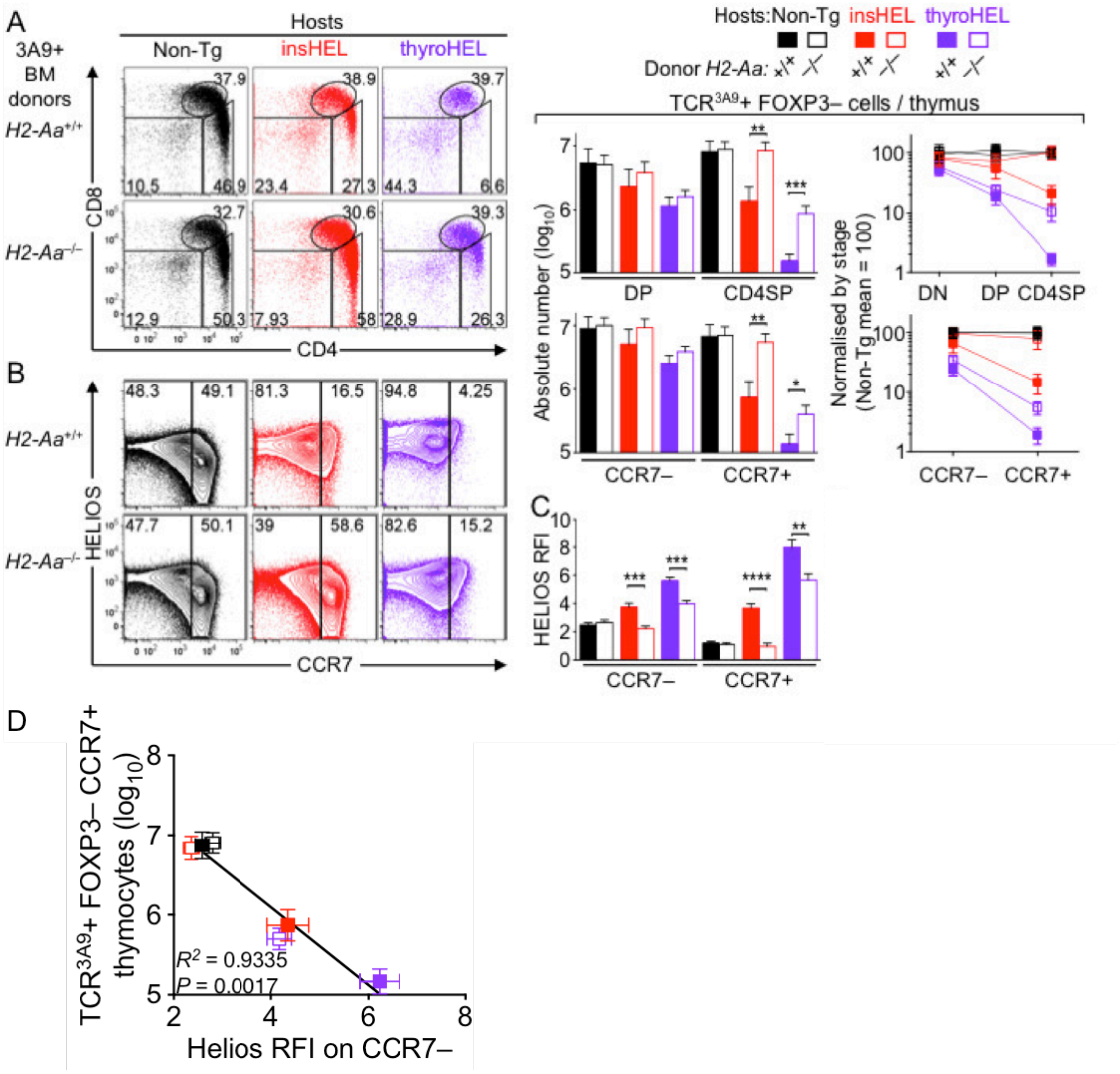
A
Hosts
Non-Tg
insHEL
thyroHEL
3A9+ BM donors
H2-Aa+/+
H2-Aa–/–
CD8
CD4
37.9
38.9
39.7
10.5
46.9
23.4
27.3
44.3
6.6
32.7
30.6
39.3
12.9
50.3
7.93
58
28.9
26.3
B
HELIOS
CCR7
48.3
49.1
81.3
16.5
94.8
4.25
47.7
50.1
39
58.6
82.6
15.2
Hosts:Non-Tg insHEL thyroHEL
Donor H2-Aa:
TCR3A9+ FOXP3– cells / thymus
Absolute number (log10)
DP
CD4SP
CCR7–
CCR7+
Normalised by stage (Non-Tg mean = 100)
DN
DP
CD4SP
C
HELIOS RFI
D
TCR3A9+ FOXP3– CCR7+ thymocytes (log10)
R2 = 0.9335
P = 0.0017
Helios RFI on CCR7–

Figure 3.4. MHCII-deficiency within BM-APCs abrogates insHEL-mediated deletion and shifts thyroHEL-mediated deletion towards wave 2. Irradiated Non-Tg, insHEL or thyroHEL hosts were reconstituted with 3A9 BM that was either MHCII-sufficient (*H2-Aa*$^{+/+}$) or MHCII-deficient (*H2-Aa*$^{-/-}$) and analysed 4-6 weeks later. (A, B) Gated TCR^{3A9+} FoxP3^{-} thymocytes were analysed for (A) CD4/CD8 expression to distinguish DN, DP and CD4SP subsets and (B) Helios/CCR7 expression to distinguish CCR7^{-} and CCR7^{+} subsets. (A, B) Column graphs (middle) show number + SEM of TCR^{3A9+} FoxP3^{-} cells within each stage per thymus and line graphs (right) show the same data normalised by stage with Non-Tg mean = 100. (C) Helios RFI on CCR7^{-} and CCR7^{+} subsets of TCR^{3A9+} FoxP3^{-} thymocytes relative to Non-Tg (i.e. non-HEL and non-3A9 Tg) DP thymocytes. (D) For each group of chimeras (represented by a square symbol), the Helios RFI on CCR7^{-} cells was plotted against the number of TCR^{3A9+} FoxP3^{-} CCR7^{+} cells per thymus. (A-D) Graphs show mean and SEM. In (A-C), *H2-Aa*$^{+/+}$ and *H2-Aa*$^{-/-}$ groups were compared using t tests for each T cell stage (DP, CD4SP, CCR7^{-} or CCR7^{+}) and host genotype (Non-Tg, insHEL or thyroHEL) combination, without assuming a consistent standard deviation, but with correction for multiple testing using the Holm-Sidak method. In (D), group mean and error bars the SEM obtained in (B) and (C) were plotted as XY pairs. The r^2 and two-tailed P values were calculated from the Pearson correlation coefficient by GraphPad Prism. Data were compiled from 2 independent cohorts of chimeras with a total of 6-8 mice per group. P value symbols: * <0.05; ** <0.01; *** <0.001; **** <0.0001.

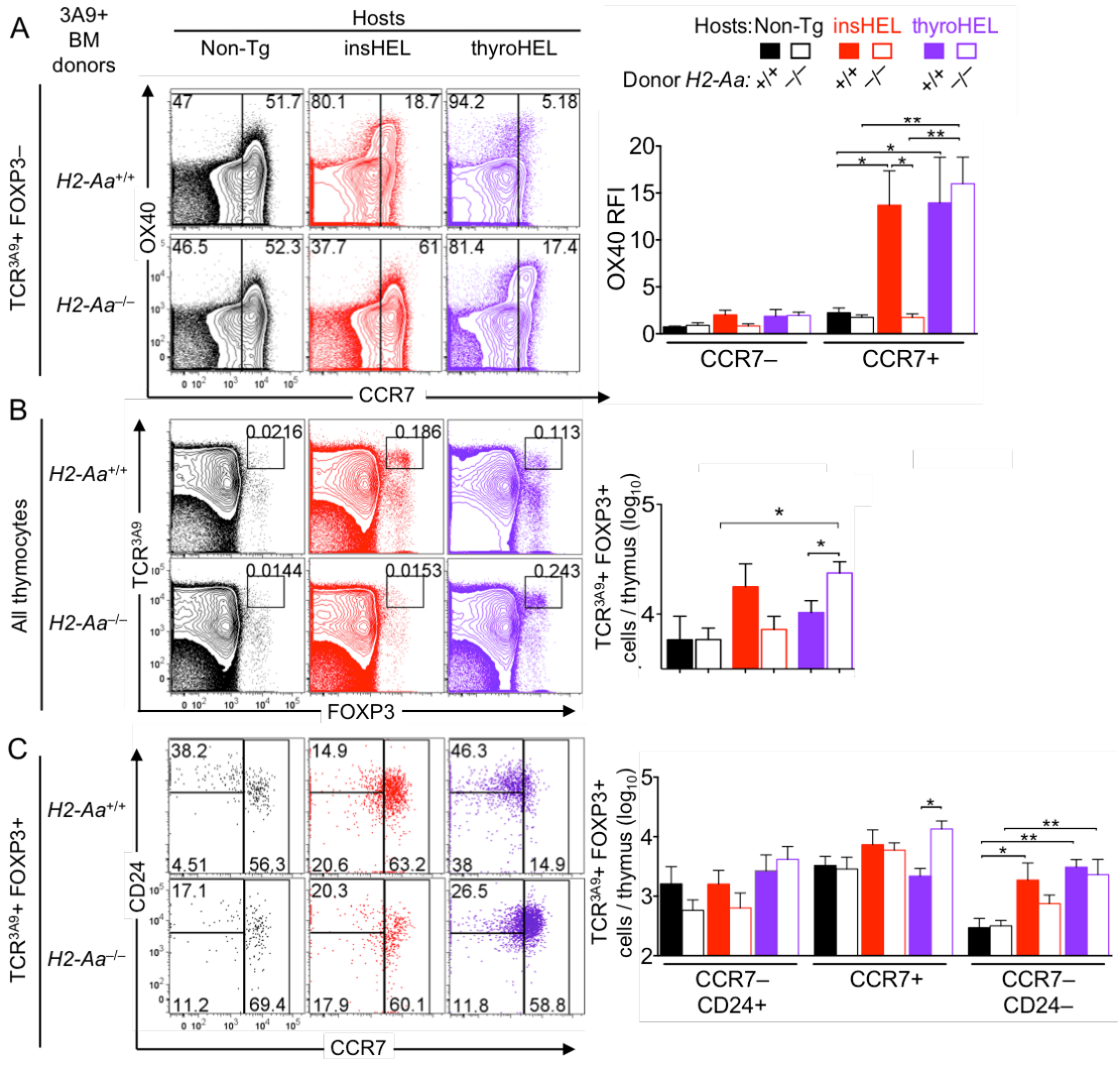

Figure 3.5. In self-reactive thymocytes, the capacity to express high levels of OX40 is associated with reaching the CCR7$^+$ stage of development. From the chimeras described in Fig. 3.4, (A) TCR^{3A9+} FoxP3$^-$ thymocytes were analysed for OX40/CCR7 (left) and summary (right) shows OX40 RFI for the CCR7$^-$ and CCR7$^+$ subsets, relative to Non-Tg (i.e. non-HEL and non-3A9 Tg) FoxP3$^-$ DP thymocytes; (B) total thymic TCR^{3A9+} FoxP3$^+$ cells were gated (left) and enumerated (right), and (C) thymic TCR^{3A9+} Foxp3$^+$ cells were divided into 3 subsets based on CD24/CCR7 expression (left) and the absolute number of cells within each subset per thymus were enumerated (right). (A-C) Statistical analysis used two-way ANOVA and Tukey's post-tests. Columns show the group mean and error bars the SEM compiled from 2 independent cohorts of chimeras with 6-8 mice per group in total. P value symbols: * <0.05; ** <0.01.

3.2.2 Contributions of MHCII$^+$ BM-APCs and Aire to the induction of the two waves of polyclonal thymocyte negative selection

3.2.2.1 MHC expression is important to induce Helios and CCR7 expression in polyclonal thymocytes

In mice with natural TCR and self-antigen repertoires, a Helios$^+$ CCR7$^-$ phenotype marks wave 1 thymocytes, Helios$^+$ CCR7$^+$ marks wave 2 thymocytes, Helios$^-$ CCR7$^+$ identifies thymocytes that have received a weak TCR signal conducive to naïve T cell formation, and a Helios$^-$ CCR7$^-$ phenotype identifies thymocytes with no evidence of a TCR signal (Daley et al., 2013; Hu et al., 2016). To analyse thymocytes that would normally be deleted by apoptosis, mice expressing human *Bcl-2* under the mouse *Vav1* promoter (*Bcl-2* Tg) (Ogilvy et al., 1999) were used. To focus the analysis on newly formed thymocytes, mice were injected with with 5-ethynyl-2'-deoxyuridine (EdU). This procedure labels DNA-synthesising thymocytes, which are predominantly at the stage immediately before they express an αβ TCR (Lucas et al., 1993).

3 days after the EdU injection, EdU$^+$ thymocytes were analysed for Helios and CCR7 expression. Among the EdU$^+$ cohorts, the frequencies of Helios$^+$ CCR7$^-$, Helios$^+$ CCR7$^+$ and Helios$^-$ CCR7$^+$ thymocytes were markedly decreased in *H2-Aa*$^{-/-}$*B2m*$^{-/-}$ *Bcl-2* Tg mice compared to *Bcl-2* Tg control mice with normal MHC expression (Fig. 3.6). This indicates that induction of Helios and CCR7 expression in nascent thymocytes largely depends on MHC expression.

3.2.2.2 A role for MHCII$^+$ BM-APCs in wave 1 negative selection

To quantify effects of MHCII-deficiency within BM-APCs on thymocyte negative selection (deletion), chimeras were generated using either *H2-Aa*$^{+/+}$ or *H2-Aa*$^{-/-}$ BM donors. To verify that Helios$^+$ thymocytes are susceptible to deletion by apoptosis, the BM donors were either *Bim*$^{+/+}$ or *Bim*$^{-/-}$. To confine the analysis to MHCII-responsive thymocytes, the irradiated hosts (on C57BL/6 background) were β2-microglobulin (B2m)-deficient so that the thymic epithelial cells would lack MHCI expression (Zijlstra et al., 1990).

This and subsequent experiments excluded mature T cells by considering only EdU$^+$ cells with high CD24 expression. CD24 is downregulated starting ~3 days after the main phase of thymocyte proliferation (Lucas et al., 1993). Five weeks after BM reconstitution, and 3 days after EdU injection, the EdU$^+$ CD24$^+$ thymocyte frequency in

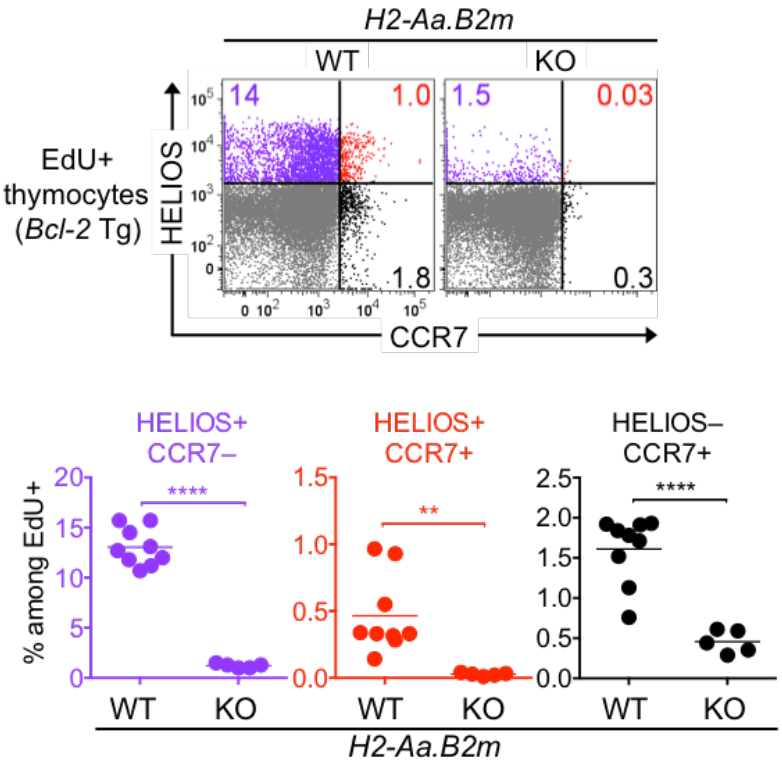

Figure 3.6. MHC-dependence of Helios and CCR7 induction in nascent thymocytes. *Bcl-2* Tg MHC wild-type (n=9) and *Bcl-2* Tg *H2-Aa*$^{-/-}$*B2m* (n=5) mice were injected with EdU 3 days before EdU^{+} thymocytes were analysed for Helios/CCR7 expression (top) with summaries (bottom) showing the frequency among EdU^{+} thymocytes of Helios^{+} CCR7^{-}, Helios^{+} CCR7^{+} and Helios^{-} CCR7^{+} subsets. Each symbol represents one mouse and each line represents mean. Data were compiled from two independent experiments. Statistical analyses used unpaired Student's t-tests. P value symbols: ** <0.01; **** <0.0001.

the *Bim*$^{-/-}$ *H2-Aa*$^{-/-}$ group was significantly higher than in the *Bim*$^{+/+}$ *H2-Aa*$^{-/-}$ group (Fig. 3.7A). Otherwise, the nascent thymocyte cohorts under analysis were similar in size.

The EdU^{+} CD24^{+} thymocyte cohorts were analysed for Helios and CCR7 expression. Comparing the two *Bim*$^{+/+}$ groups with normal apoptosis, the frequency of Helios^{-} CCR7^{+} cells in hosts with *H2-Aa*$^{-/-}$ BM was significantly higher than hosts with *H2-Aa*$^{+/+}$ BM (6.7% vs 4.0%, respectively) (Fig. 3.7B). This increase in naïve T cell induction provides indirect evidence that thymocyte deletion was impaired when the BM-APCs lacked MHCII. However, the Helios^{+} CCR7^{-} and Helios^{+} CCR7^{+} cell frequencies were similar in *Bim*$^{+/+}$ groups with *H2-Aa*$^{+/+}$ versus *H2-Aa*$^{-/-}$ BM (Fig. 3.7B).

Comparing the two groups with *H2-Aa*$^{+/+}$ BM (filled circles), Bim-deficiency significantly increased the frequencies of Helios^{+} CCR7^{-} and Helios^{+} CCR7^{+} thymocytes (Fig. 3.7B), showing that the apoptosis defect caused by Bim-deficiency prolongs the survival of strongly TCR-signalled Helios^{+} cells. This allows direct quantification of strongly TCR-signalled Helios^{+} cells in the nascent thymocyte cohort.

In the two *Bim*$^{-/-}$ groups with defective apoptosis (open circles), the Helios^{+} CCR7^{-} cell frequency was 8.6% in hosts with *H2-Aa*$^{+/+}$ BM versus 4.6% in hosts with *H2-Aa*$^{-/-}$ BM (Fig. 3.7B). This finding provides direct evidence that MHCII-deficiency within BM-APCs decreased wave 1 negative selection. In subsequent experiments, induction of waves 1 and 2 was considered to be 100% efficient in chimeras with normal APCs but apoptosis-defective thymocytes. By these criteria, MHCII-deficiency within BM-APCs caused a 46.5% decrease in wave 1 negative selection [calculated as (8.6 – 4.6 / 8.6) × 100].

Helios^{+} CCR7^{+} cell frequencies in *Bim*$^{-/-}$ groups with *H2-Aa*$^{+/+}$ or *H2-Aa*$^{-/-}$ BM (both ~0.7%) were significantly higher than in the *Bim*$^{+/+}$ groups with *H2-Aa*$^{+/+}$ and *H2-Aa*$^{-/-}$ (both ~0.2%) (Fig. 3.7B), indicating that nascent thymocytes with the potential to become wave 2 cells are normally deleted in a Bim-dependent manner. However, MHCII-deficiency within BM-APCs did not change wave 2 quantitatively.

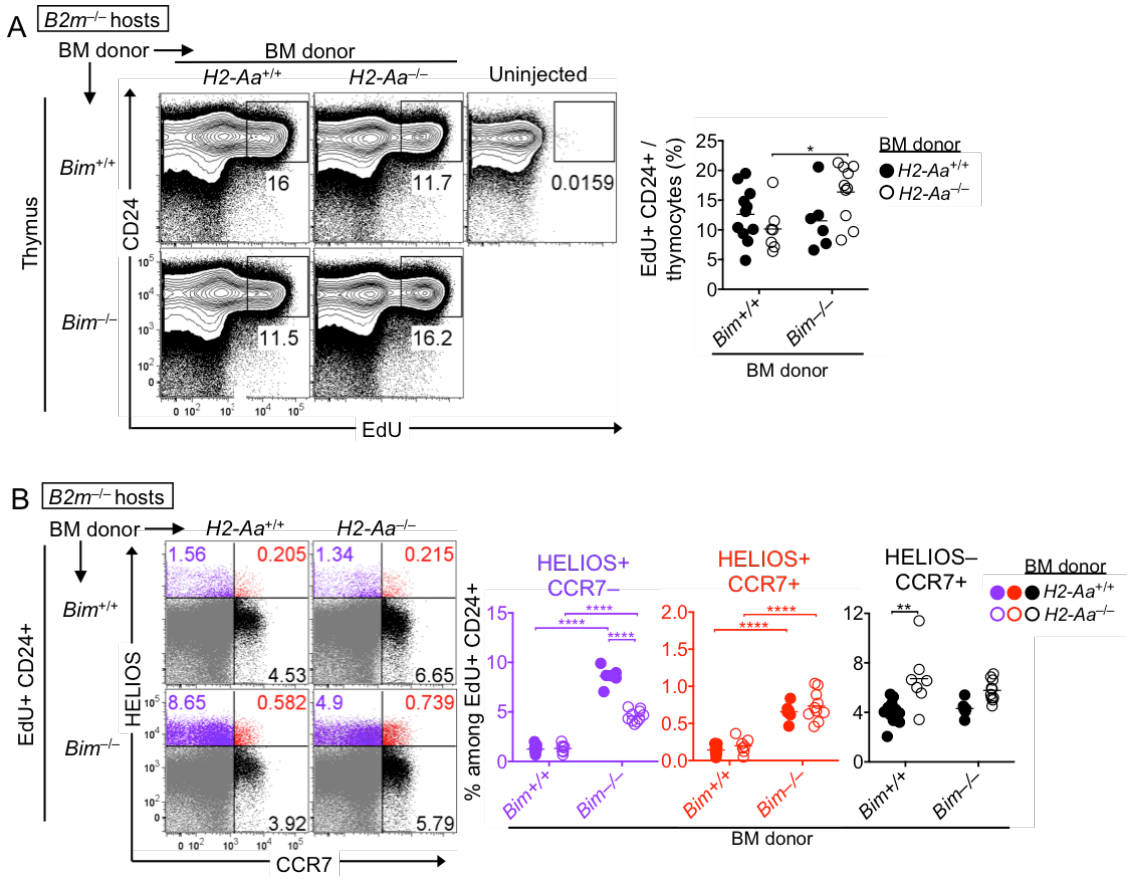

Figure 3.7. Apoptosis defect reveals the role for MHCII^{+} BM-APCs in wave 1 negative selection. (A) Irradiated *B2m*$^{-/-}$ (C57BL/6, H-2^{b}) hosts were reconstituted with *Bim*$^{+/+}$ or *Bim*$^{-/-}$ BM, which was additionally either *H2-Aa*$^{+/+}$ (filled circles) or *H2-Aa*$^{-/-}$ (open circles), resulting in 4 groups of chimeras analysed 5 weeks later and 3 days after a single EdU injection. Thymocytes were analysed for CD24 and EdU expression (left) and the summary (right) shows the frequency of EdU^{+} CD24^{+} cells among all thymocytes. (B) Plots (left) show EdU^{+} CD24^{+} thymocytes subdivided using Helios/CCR7 expression with summaries (right) showing frequencies of each Helios/CCR7 subset. (A, B) Data were compiled from 2 independent experiments. Each symbol represents one mouse; each line represents group mean. Statistical analyses used two-way ANOVA with Tukey's post tests; P value symbols: * <0.05; ** <0.01; **** <0.0001.

3.2.2.3 Reduction of MHCII expression within BM-APCs in chimeras reconstituted with MHCII-deficient BM

The frequency of BM-derived APCs (DC and macrophages) in the four groups of BM chimeras described above (Fig. 3.7) was determined. After thymic stroma digestion, viable 7AAD$^-$ cells that were TCRβ^{lo} and of haemapoeitic origin as indicated by CD45$^+$, were analysed to identify CD11c$^+$ cells (DCs) and CD11b$^+$ CD11c$^-$ cells (predominantly macrophages) (Fig. 3.8A) (Gray et al., 2002). The frequency of CD11c$^+$ among CD45$^+$ cells was similar in all four groups (Fig. 3.8B). Among CD45$^+$ cells, the frequency of CD11b$^+$ CD11c$^-$ cells was also similar in all groups (Fig. 3.8C). These data suggest that the frequencies of BM-APCs are similar in the presence of absence of Bim or MHCII within the haemapoetic compartment.

The MHCII expression on BM-APCs in the four groups of chimeras was analysed. The frequencies of MHCII^{hi} cells within CD45$^+$ CD11c$^+$ cells (Fig. 3.9A) were significantly reduced in chimeras reconstituted with *H2-Aa*$^{-/-}$ BM compared to *H2-Aa*$^{+/+}$ BM, regardless of *Bim* genotype. Similarly, the frequencies of MHCII^{hi} cells within CD45$^+$ CD11b$^+$ CD11c$^-$ cells were reduced in chimeras reconstituted with *H2-Aa*$^{-/-}$ BM compared to *H2-Aa*$^{+/+}$ BM (Fig. 3.9B). These findings confirm that the transplantation procedure depleted MHCII$^+$ BM APCs from the host mice. Comparing the two groups receiving *H2-Aa*$^{+/+}$ BM, Bim-deficiency seems to increase the frequency of MHCII^{hi} cells in CD11c$^+$ cells and CD11b$^+$ CD11c$^-$ cells (Fig. 3.9).

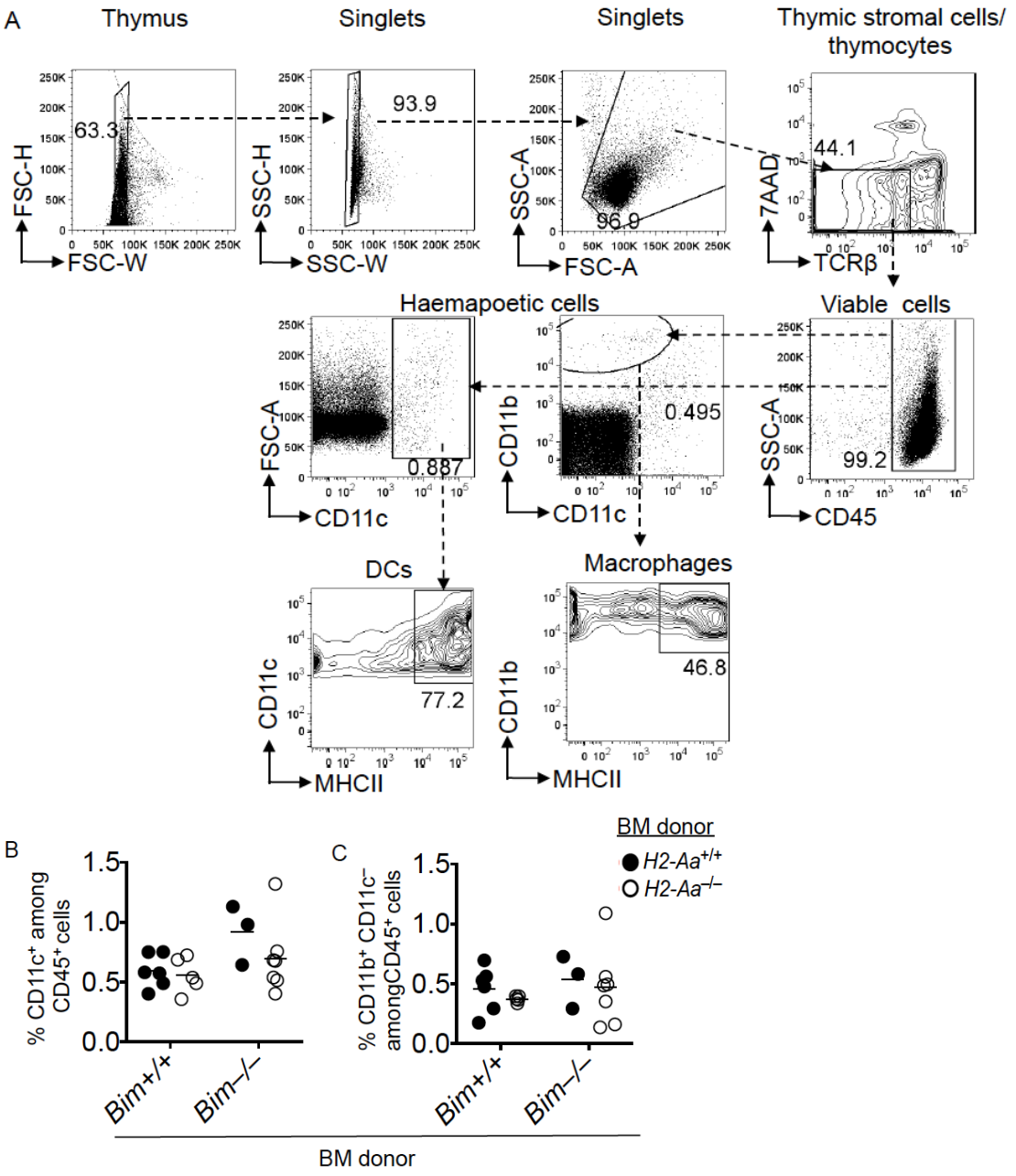

Figure 3.8. MHCII-deficiency within BM-APCs did not affect the frequency of DCs and macrophages regardless of the Bim genotype. Five weeks after BM reconstitution, thymic stromal cells of the irradiated *B2m*$^{-/-}$ (C57BL/6, H-2^{b}) hosts bearing BM of the indicated *Bim* and *H2-Aa* genotypes were collagenase digested. (A) The digested thymic samples were gated for singlets, followed by 7AAD^{-} TCRβ^{lo} cells to exclude the non-viable cells. 7AAD^{-} TCRβ^{lo} cells were gated for CD45^{+} haematopoietic cells were gated for CD11c^{+} to identify DCs and gated for CD11b^{+} CD11c^{-} to identify macrophages. Finally, CD11c^{+} and CD11b^{+} CD11c^{-} cells were analysed for MHCII^{hi} cells. (B, C) Summaries show frequency of (B) CD11c^{+} and (C) CD11b^{+} CD11c^{-} among CD45^{+} 7AAD^{-} TCRβ^{lo} cells. A total of n = 3-7 mice per group compiled from a cohort of chimeras. Lines represent mean; non-significant statistical values were obtained between all comparison groups using two-way ANOVA with Tukey's post-tests.

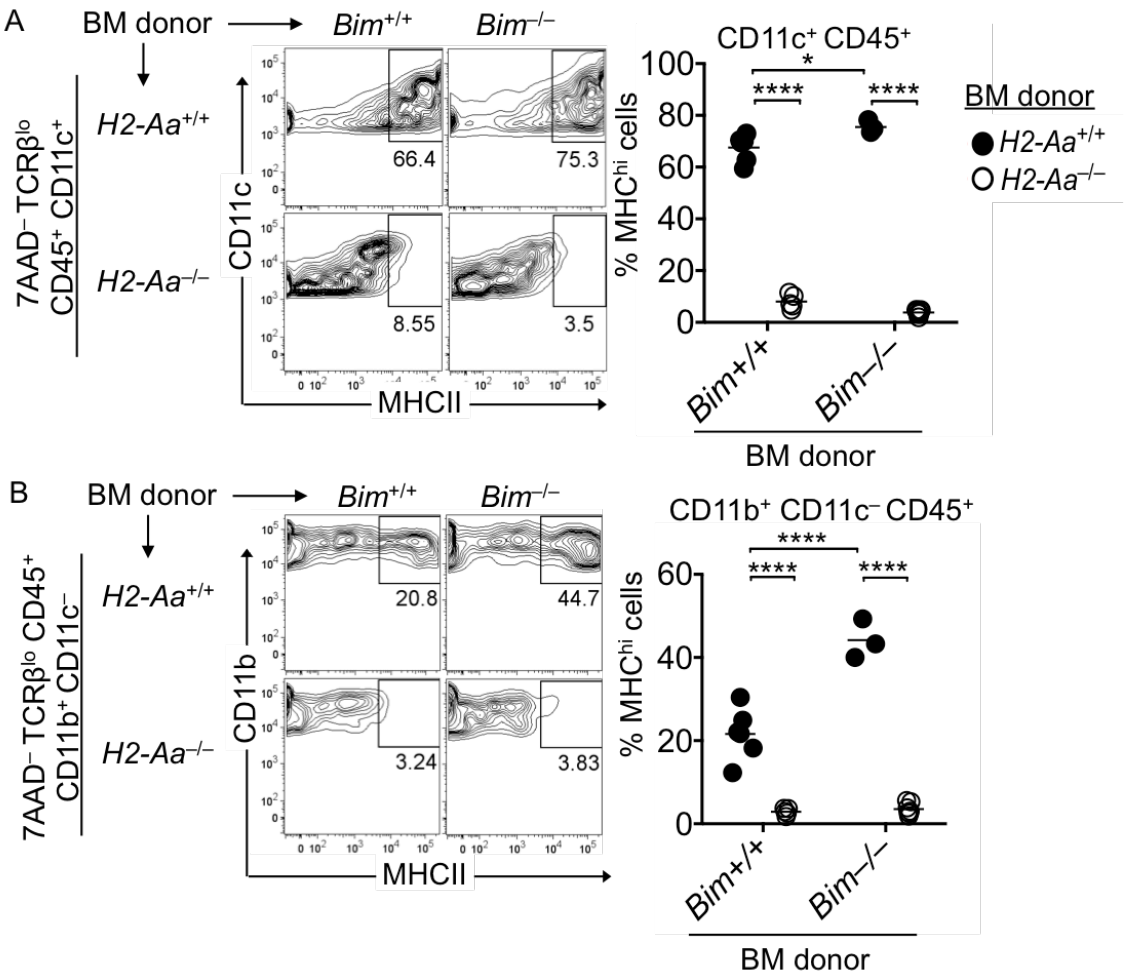

Figure 3.9. Reduced MHCII expression on DCs and macrophages in thymus of chimeras bearing *H2-Aa*$^{-/-}$ BM. Five weeks after BM reconstitution, thymic stromal cells of the irradiated *B2m*$^{-/-}$ (C57BL/6, H-2^{b}) hosts bearing BM of the indicated *Bim* and *H2-Aa* genotypes were collagenase digested. 7AAD^{-} TCRβ^{lo} cells were gated for CD45^{+} haematopoietic cells. CD45^{+} cells were gated for CD11c^{+} (A), and gated for CD11b^{+} CD11c^{-} (B), and analysed for MHCII^{hi} cells. (Right of A and B) Summaries show frequency of MHCII^{hi} cells among CD11c^{+} CD45^{+} 7AAD^{-} TCRβ^{lo} cells and CD11b^{+} CD11c^{-} CD45^{+} 7AAD^{-} TCRβ^{lo} cells. A total of n = 3-7 mice per group compiled from a cohort of chimeras. Lines represent mean; statistical analyses used two-way ANOVA with Tukey's post tests; P value symbols: * <0.05; **** <0.0001.

3.2.2.4 A possible role for Aire in Helios$^+$ thymocyte induction in mice on the B10.BR genetic background

To test the effect of Aire-deficiency within non-BM-APCs on the two waves of thymocyte negative selection, *Bim*$^{-/-}$ BM was used to reconstitute irradiated *Aire*$^{+/+}$, *Aire*$^{+/-}$ and *Aire*$^{-/-}$ hosts on the B10.BR genetic background, and the resulting chimeras were analysed as above (section 3.2.2.2). The *Aire*$^{+/-}$ hosts were not significantly different from *Aire*$^{+/+}$ controls in all three Helios/CCR7 subsets analysed (Fig. 3.10).

Among EdU$^+$ CD24$^+$ thymocytes, the mean frequency of Helios$^+$ CCR7$^-$ cells was significantly reduced in *Aire*$^{-/-}$ hosts (9.2%) compared to *Aire*$^{+/+}$ hosts (11.6%) (Fig. 3.10), representing a 21% decrease in wave 1 negative selection. The mean frequency of Helios$^+$ CCR7$^+$ cells was 1.1% in *Aire*$^{-/-}$ hosts versus 2.1% in *Aire*$^{+/+}$ hosts (Fig. 3.10), revealing a 48% decrease in wave 2 cells due to Aire-deficiency. The mean frequency of Helios$^-$ CCR7$^+$ cells was similar at ~10% regardless of host *Aire* genotype (Fig. 3.10). These results suggest that Aire is required for normal Helios$^+$ thymocyte induction in mice on the B10.BR background.

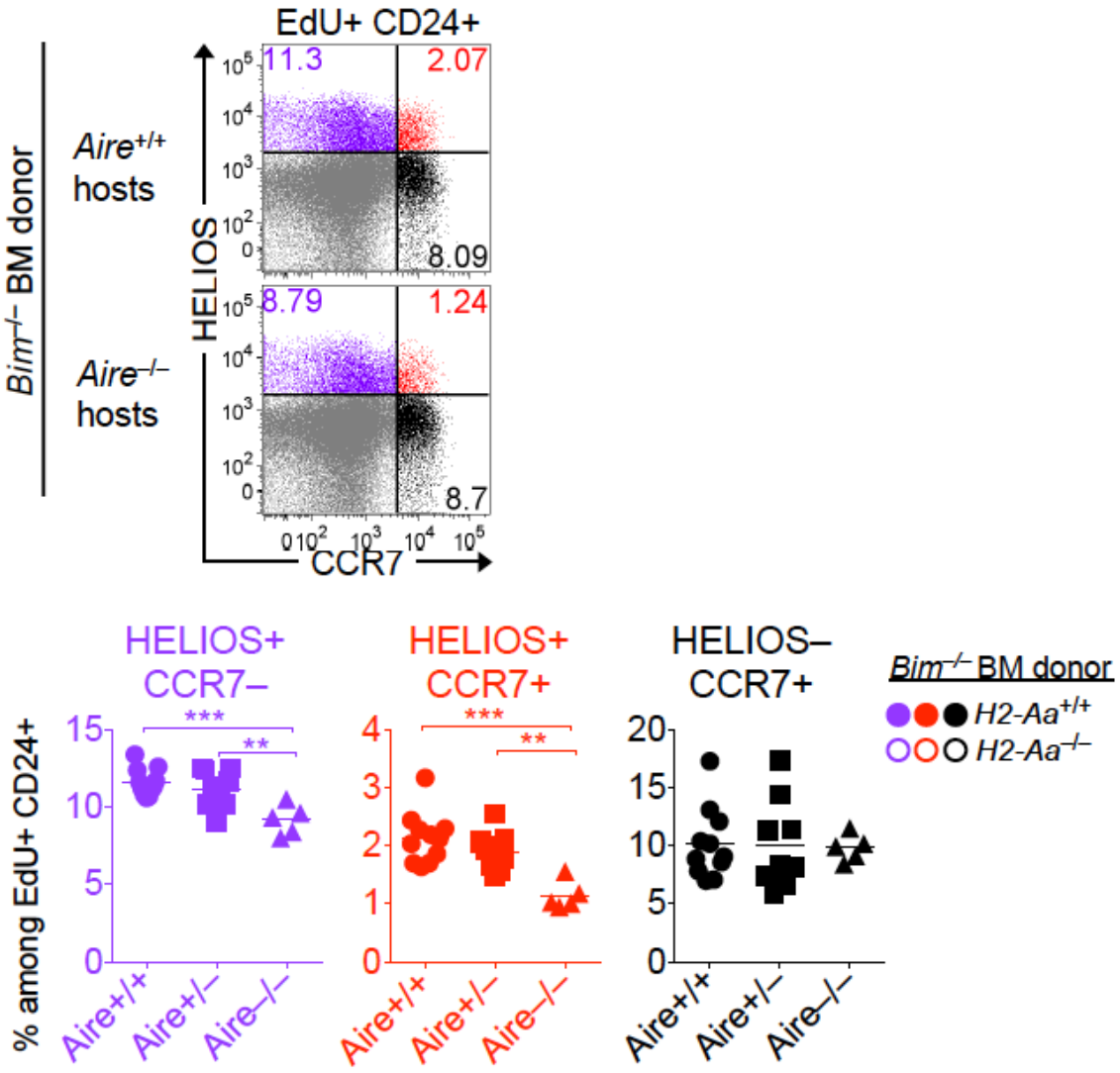

Figure 3.10. A role for Aire in Helios^{+} thymocyte induction in B10.BR mice. Irradiated *Aire*$^{+/+}$, *Aire*$^{+/-}$ or *Aire*$^{-/-}$ hosts were reconstituted with *Bim*$^{-/-}$ BM [all on the B10.BR (H-2^{k}) background] and chimeras were analysed 5 weeks later, 3 days after a single EdU injection. Flow cytometry phenotype (top) and summaries (bottom) show frequencies of three subsets defined using Helios and CCR7 expression among EdU^{+} CD24^{+} thymocytes. Data were compiled from 2 independent cohorts of chimeras. Each symbol represents one mouse in summaries; each line represents group mean. Statistical analyses used one-way ANOVA with Tukey's post tests; P value symbols: ** <0.01, *** <0.001.

3.2.2.5 The contribution of Aire to Helios$^+$ thymocyte induction requires the BM-APCs to express MHCII

To test requirements for MHCII$^+$ BM-APCs and Aire in parallel, chimeras were generated by transferring *Bcl-2* Tg donor BM that was additionally either *H2-Aa*$^{+/+}$ (filled circles) or *H2-Aa*$^{-/-}$ (open circles), into irradiated *Aire*$^{+/+}$ or *Aire*$^{-/-}$ hosts (Fig. 3.11). This resulted in four groups of chimeras with C57BL/6 genetic background: (1) thymic APCs were normal, (2) MHCII-deficiency within BM-APCs, (3) Aire-deficiency within non-BM-APCs and (4) both thymic APC types were defective (MHCII-deficiency within BM-APCs and Aire-deficiency within non-BM-APCs).

Comparing the two *Aire*$^{+/+}$ groups, the mean frequency of Helios$^+$ CCR7$^-$ cells in the EdU$^+$ CD24$^+$ cohort was significantly reduced by 37.4% in hosts bearing *H2-Aa*$^{-/-}$ BM-APCs (5.7%) compared to *H2-Aa*$^{+/+}$ BM-APCs (9.1%) (Fig. 3.11). This recapitulates the findings above using B2m-deficient hosts (Fig. 3.7B) and confirms that MHCII$^+$ BM-APCs are necessary for normal negative selection at wave 1.

The Helios$^+$ CCR7$^-$ cell frequency in *Aire*$^{-/-}$ hosts with *H2-Aa*$^{+/+}$ BM-APCs (8%) was significantly higher than in *Aire*$^{+/+}$ hosts with *H2-Aa*$^{-/-}$ BM-APCs (5.7%) (Fig. 3.11), demonstrating that wave 1 relies more on MHCII$^+$ BM-APCs than on Aire, at least in quantitative terms.

When the BM-APCs were wild-type, Aire-deficiency did not significantly affect the Helios$^+$ CCR7$^-$ frequency in these chimeras on the B6 background (Fig. 3.11). One mouse in the *Aire*$^{-/-}$ group had a very high Helios$^+$ CCR7$^-$ cell frequency, while the remaining mice in the *Aire*$^{-/-}$ group did appear to have slightly lower Helios$^+$ CCR7$^-$ frequencies than the *Aire*$^{+/+}$ group (Fig. 3.11).

In chimeras with wild-type BM-APCs, the Helios$^+$ CCR7$^+$ frequency was significantly decreased in *Aire*$^{-/-}$ hosts compared to *Aire*$^{+/+}$ hosts (1.0% vs 1.5%) (Fig. 3.11), indicating a 33% decrease in wave 2 cells due to Aire-deficiency. This is consistent with the result in the B10.BR background and strengthens the evidence that Aire is required for normal Helios$^+$ CCR7$^+$ thymocyte induction (Fig. 3.10). Comparing groups with defective BM-APCs (open circles), Aire-deficiency did not have any significant effect on the parameters examined (Fig. 3.11). This suggests the contribution of Aire to Helios$^+$ thymocyte induction requires the BM-APCs to express MHCII.

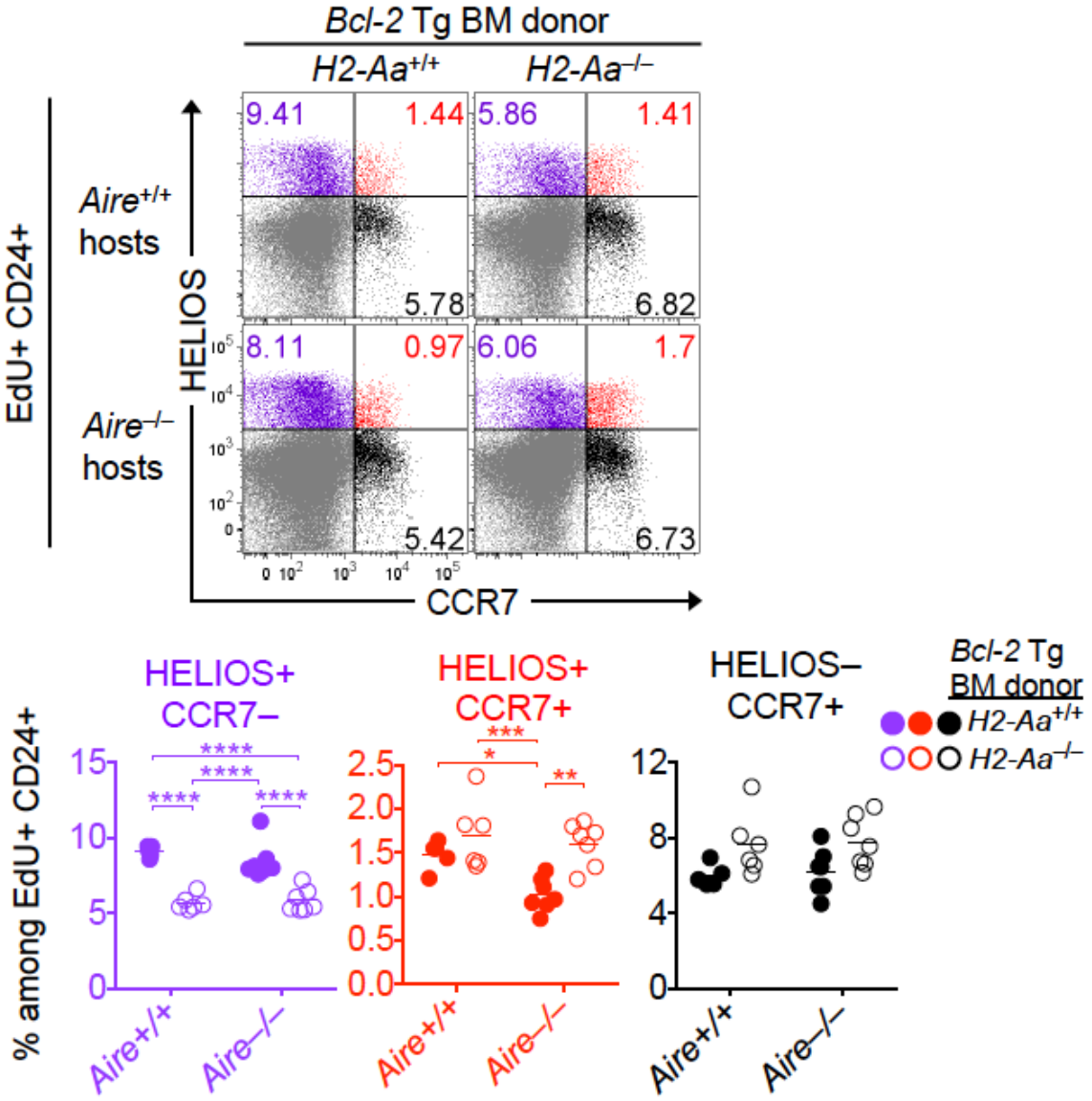

Figure 3.11. MHCII^{+} BM-APCs are required to detect Aire's contribution to Helios^{+} thymocyte induction. Irradiated *Aire*$^{+/+}$ or *Aire*$^{–/–}$ [C57BL/6 (B6), H-2^{b}] hosts were reconstituted with *Bcl-2* Tg BM that was either *H2-Aa*$^{+/+}$ or *H2-Aa*$^{–/–}$. Chimeras were analysed 5 weeks later, 3 days after a single EdU injection. Flow cytometry phenotype (top) and summaries (bottom) show frequencies of subsets defined using Helios and CCR7 expression among EdU^{+} CD24^{+} thymocytes. Each symbol represents one mouse in summaries; lines represent group means. Statistical analyses used two-way ANOVA with Tukey's post tests; P value symbols: * <0.05, ** <0.01, *** <0.001, **** <0.0001.

3.2.3 Contributions of BM-APCs and/or Aire to the induction of $CD4^{lo}CD8^{lo}$ PD-1^{hi} polyclonal thymocytes

While strong TCR signalling in DP or $CCR7^{-}$ thymocytes induces deletion, some thymocytes survive this type of stimulus and subsequently differentiate into small intestinal intraepithelial lymphocytes (iIEL) (Gangadharan et al., 2006; Mayans et al., 2014; McDonald et al., 2015; McDonald et al., 2014; Pobezinsky et al., 2012). The DN $TCR\beta^{+}$ thymocyte population, which is thought to contain iIEL precursors, is expanded in apoptosis-defective mice and in mice lacking CD28 or CD80 and CD86 (Pobezinsky et al., 2012). As wave 1 was reduced by 46.5% in mice with MHCII-deficient BM-APCs based on Helios/CCR7 approach (Fig. 3.7B), the same samples were interrogated for possible effects on the thymic IEL precursor population using $CD4^{lo}CD8^{lo}$ PD-1^{hi} approach.

3.2.3.1 High PD-1 expression in $CD4^{lo}CD8^{lo}$ $TCR\beta^{+}$ thymocytes

DN $TCR\beta^{+}$ thymocytes in CD80/CD86-deficient mice on the B6 background express the PD-1 protein at extremely high levels (Pobezinsky et al., 2012). In B6 mice, using a $CD24^{+}$ $Foxp3^{-}$ gate to exclude mature ($CD24^{-}$) and T-reg ($Foxp3^{+}$) cells from the analysis, the $CD4^{lo}CD8^{lo}$ population was found to contain a discrete $TCR\beta^{+}$ population (Fig. 3.12A). The $CD4^{lo}CD8^{lo}$ $TCR\beta^{+}$ population contained 79.3% of PD-1^{hi} cells [(6.7 / 6.7+1.74) ×100] in wild-type mice with normal apoptosis and 81.9% of PD-1^{hi} cells in *Bcl-2* Tg mice (Fig. 3.12A). The $CD4^{lo}CD8^{lo}$ PD-1^{+} population contained 48.3% of $TCR\beta^{+}$ cells [(6.7/ 7.17+6.7) ×100] in wild-type mice and 92.7% of $TCR\beta^{+}$ cells in *Bcl-2* Tg mice (Fig. 3.12A). This suggests that that among $CD4^{lo}CD8^{lo}$ thymocytes in apoptosis-defective mice, PD-1 and TCRβ expression correlate closely. In wild-type mice however, there is a PD-1^{+} $TCR\beta^{-}$ subset that makes up a large proportion of the PD-1^{+} population.

3.2.3.2 Role for $MHCII^{+}$ BM-APCs in $CD4^{lo}CD8^{lo}$ PD-1^{hi} thymocyte induction in B2m-deficient hosts

This analysis was performed on samples from the chimeric B2m-deficient hosts bearing *Bim*$^{+/+}$ or *Bim*$^{-/-}$ BM that was additionally either *H2-Aa*$^{+/+}$ or *H2-Aa*$^{-/-}$ (as described in section 3.2.2.2). The PD-1^{hi} subset of $CD24^{+}$ $Foxp3^{-}$ $CD4^{lo}CD8^{lo}$ thymocytes was enumerated as a percentage of all thymocytes and in absolute numbers. Comparing the two groups with $MHCII^{+}$ BM-APCs (filled black circles), Bim-deficiency significantly increased the frequency and number of $CD4^{lo}CD8^{lo}$ PD-1^{hi}

thymocytes (Fig. 3.12B). This indicates that $CD4^{lo}CD8^{lo}$ $PD\text{-}1^{hi}$ thymocytes are normally susceptible to Bim-mediated apoptosis, including when the thymic epithelial cells lack B2m expression.

Comparing $CD24^{+}$ $FoxP3^{-}$ $CD4^{lo}CD8^{lo}$ $PD\text{-}1^{hi}$ thymocytes in the two Bim-deficient groups, MHCII-deficiency within BM-APCs reduced their frequency by 66.5% (1.8 versus 5.5%) and their absolute number by 68% (2.13×10^{6} versus 6.65×10^{6}) (Fig. 3.12B). No significant differences were detected when comparing the two Bim-sufficient groups (Fig. 3.12B). The PD-1 versus Helios plots show that the $CD24^{+}$ $FoxP3^{-}$ $CD4^{lo}CD8^{lo}$ $PD\text{-}1^{hi}$ population in Bim-sufficient mice contains a mixture of $Helios^{intermediate}$ and $Helios^{+}$ cells, whereas this population is predominantly $Helios^{+}$ in Bim-deficient mice (Fig. 3.12B). These findings, which do not rely on the use of Helios as a molecular marker, indicate that $MHCII^{+}$ BM-APCs are required to induce the formation of strongly TCR-signalled $CD4^{lo}CD8^{lo}$ $PD\text{-}1^{hi}$ thymocytes, consistent with the conclusion of the analysis using Helios and CCR7.

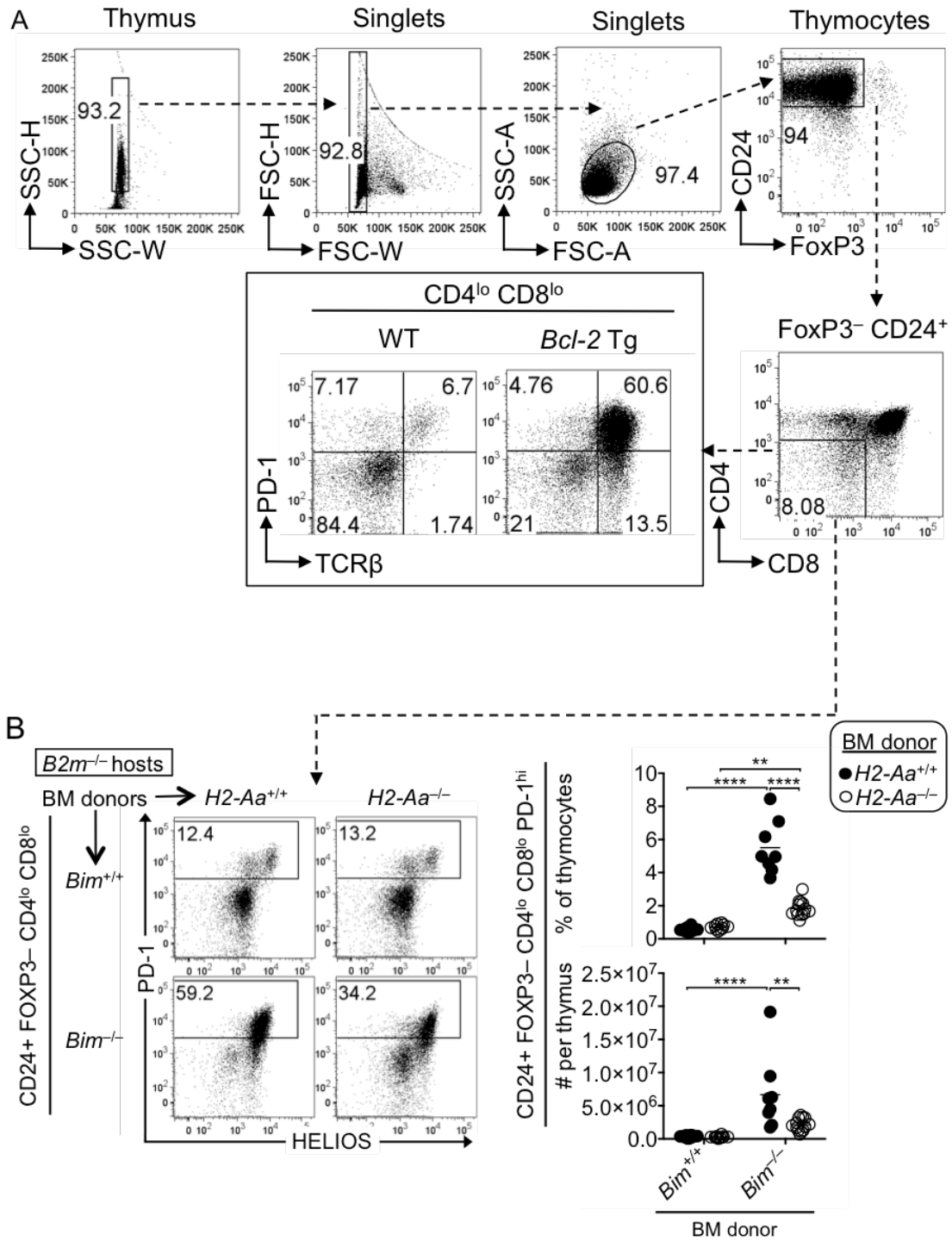
A
Thymus
Singlets
Singlets
Thymocytes
SSC-H
SSC-W
93.2
FSC-H
FSC-W
92.8
SSC-A
FSC-A
97.4
CD24
FoxP3
94
CD4lo CD8lo
WT
Bcl-2 Tg
PD-1
TCRβ
7.17
6.7
84.4
1.74
4.76
60.6
21
13.5
FoxP3– CD24+
CD4
CD8
8.08
B
B2m–/– hosts
BM donors
H2-Aa+/+
H2-Aa–/–
Bim+/+
Bim–/–
CD24+ FOXP3– CD4lo CD8lo
PD-1
HELIOS
12.4
13.2
59.2
34.2
BM donor
H2-Aa+/+
H2-Aa–/–
CD24+ FOXP3– CD4lo CD8lo PD-1hi
% of thymocytes
# per thymus
****
**
Bim+/+
Bim–/–
BM donor

Figure 3.12. Quantification of requirement for MHCII^{+} BM-APCs in inducing strongly TCR-signalled CD4^{lo}CD8^{lo} PD-1^{hi} thymocytes. The same cohort of BM chimeras described in Fig. 3.7 was analysed. (A) Gating strategy for analysis CD24^{+} FoxP3^{-} CD4^{lo}CD8^{lo} PD-1^{hi} population. After doublets exclusion using FSC-W (forward scattered light-width) versus FSC-H (FSC-height) and SSC (side scattered light)-W versus SSC-H gates, thymocytes were analysed for CD24 and FoxP3 expression. CD24^{+} FoxP3^{-} thymocytes were gated for CD4^{lo}CD8^{lo} population. CD4^{lo}CD8^{lo} population was analysed for PD-1 and TCRβ in wild-type and *Bcl-2* Tg mice. Alternatively, the gated immature CD24^{+} FoxP3^{-} CD4^{lo}CD8^{lo} thymocytes were analysed for (B, left) PD-1 expression (PD-1 versus Helios). Helios expression is irrelevant to the enumeration of PD-1^{+} cells. (B, right) Summaries show the frequency and number of CD24^{+} FoxP3^{-} CD4^{lo}CD8^{lo} PD-1^{hi} events among all thymocytes. Data were compiled from two independent experiments with a total of n = 8-13 mice per group. Lines represent mean. Statistical analyses used 2-way ANOVA and Tukey's post-tests; P value symbol: **** <0.0001; ** <0.01.

3.2.3.3 No evidence of a role for Aire in $CD4^{lo}CD8^{lo}$ PD-1^{hi} induction in B10.BR mice

The *Aire*$^{+/+}$, *Aire*$^{+/-}$ and *Aire*$^{-/-}$ BM chimeras on the B10.BR background described in section 3.2.2.4 were analysed as above (Fig. 3.12). The $CD24^{+}$ $FoxP3^{-}$ $CD4^{lo}CD8^{lo}$ PD-1^{hi} thymocyte populations made up a similar frequency of all thymocytes across the three groups ~3.5%. However, the absolute number of cells was significant reduced in the *Aire*$^{-/-}$ group (1.66×10^{6}) compared to *Aire*$^{+/+}$ controls (3.70×10^{6}) (Fig. 3.13). The effect on $CD4^{lo}CD8^{lo}$ PD-1^{hi} thymocyte number may reflect a requirement for Aire in the overall thymus size or architecture (Yano et al., 2008) rather than a specific role in inducing thymic iIEL precursors.

3.2.3.4 A role for $MHCII^{+}$ BM-APCs in $CD4^{lo}CD8^{lo}$ PD-1^{hi} induction in B6 mice with normal B2m expression

The same four groups of BM chimeras (*Bcl-2* Tg BM donor *H2-Aa*$^{+/+}$ or *H2-Aa*$^{-/-}$ → *Aire*$^{+/+}$ or *Aire*$^{-/-}$ hosts) generated in section 3.2.2.5 were analysed. Comparing the *Aire*$^{+/+}$ groups, the mean frequency of $CD24^{+}$ $FoxP3^{-}$ $CD4^{lo}CD8^{lo}$ PD-1^{hi} among all thymocytes was significantly reduced in hosts bearing *H2-Aa*$^{-/-}$ BM-APCs (1.9%) compared to *H2-Aa*$^{+/+}$ BM-APCs (5.8%) by 67% (Fig. 3.14). Likewise, the number of $CD24^{+}$ $FoxP3^{-}$ $CD4^{lo}CD8^{lo}$ PD-1^{hi} thymocytes was significantly decreased in hosts bearing *H2-Aa*$^{-/-}$ BM-APCs (15.5×10^{6}) compared to *H2-Aa*$^{+/+}$ (15.5×10^{6}) by 76% (Fig. 3.14). These results recapitulated the findings in section 3.2.3.2, indicating the requirement of $MHCII^{+}$ BM-APCs in inducing strongly TCR-signalled $CD4^{lo}CD8^{lo}$ PD-1^{hi} thymocytes.

Comparing the two groups with MHCII-deficient BM-APCs, Aire-deficiency had no detectable effect on the frequency or number of $CD24^{+}$ $FoxP3^{-}$ $CD4^{lo}CD8^{lo}$ PD-1^{hi} thymocytes (Fig. 3.14). Comparing the two groups with wild-type BM-APCs, Aire-deficiency did not significantly affect the frequency of $CD24^{+}$ $FoxP3^{-}$ $CD4^{lo}CD8^{lo}$ PD-1^{hi} cells among all thymocytes, but did significantly reduce the absolute number of these cells by ~50% (7.8×10^{6} versus 15.5×10^{6}) (Fig. 3.14). This is consistent with the result observed in B10.BR mice (section 3.2.3.3).

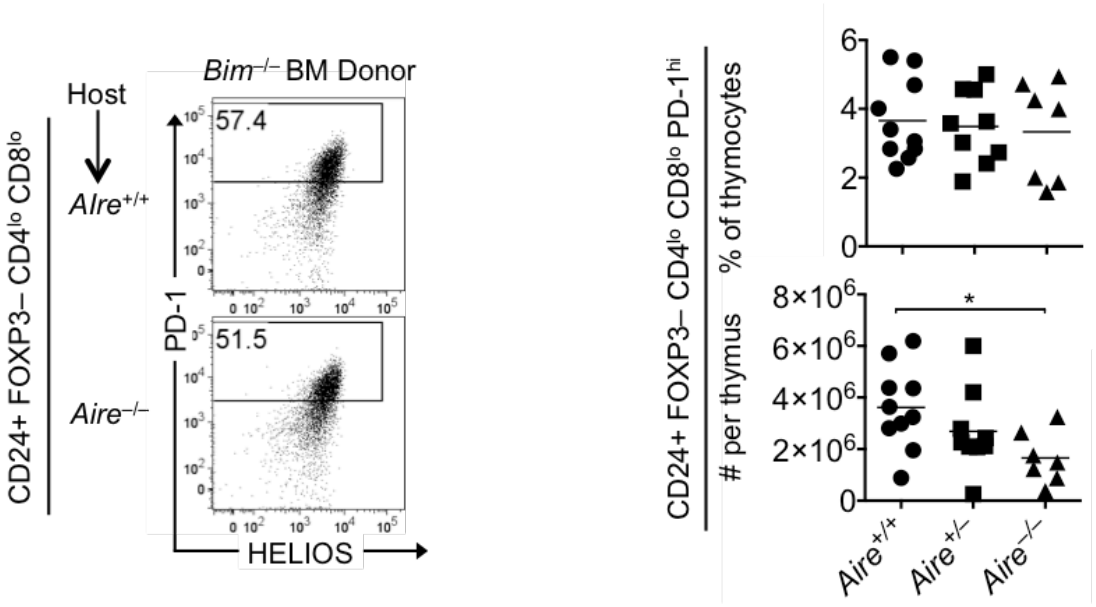

Figure 3.13. Quantification of requirement for Aire in inducing strongly TCR-signalled CD4^{lo}CD8^{lo} PD-1^{hi} thymocytes. The gated immature CD24^{+} FoxP3^{-} CD4^{lo}CD8^{lo} thymocytes in the same cohort of BM chimeras described in Fig. 3.10 were analysed for PD-1 expression (left). Summaries show the frequency and number of CD24^{+} FoxP3^{-} CD4^{lo}CD8^{lo} PD-1^{hi} events among all thymocytes (right). Data were compiled from two independent experiments with a total of n = 7-9 mice per group. Lines represent mean. Statistical analyses used 1-way ANOVA and Tukey's post-tests; P value symbol: * <0.05.

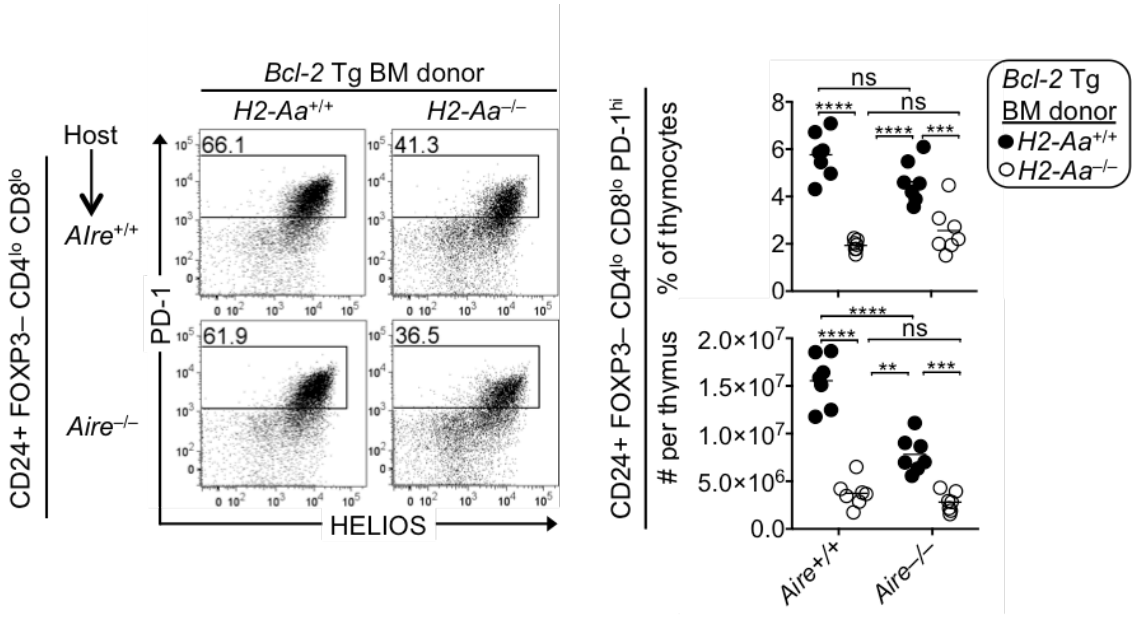

Figure 3.14. A role for MHCII^{+} BM-APCs in CD4^{lo}CD8^{lo} PD-1^{hi} thymocyte induction. The gated CD24^{+} FoxP3$^{–}$ CD4^{lo}CD8^{lo} thymocytes in the same cohort of BM chimeras described in Fig. 3.11 were analysed for PD-1 expression (left). Summaries (right) show the frequency and number of CD24^{+} FoxP3$^{–}$ CD4^{lo}CD8^{lo} PD-1^{hi} events among all thymocytes. Data were compiled from one experiment with a total of n = 7 mice per group. Lines represent mean. Statistical analyses used 2-way ANOVA and Tukey's post-tests; P value symbols: **** <0.0001; *** <0.001; ** <0.01; ns, non-significant.

3.3 Discussion

This study examined how defects in MHCII^{+} BM-APCs and Aire affect the induction of Helios^{+} thymocytes at CCR7^{-} and CCR7^{+} stages of T cell development, which are characterised as waves 1 and 2 negative selection, respectively. The 3A9 TCR Tg results show that MHCII-deficiency within BM-APCs impaired deletion at wave 1 by causing a shift towards deletion at wave 2, or a complete abrogation of deletion. In polyclonal thymocytes, wave 1 was markedly impaired by MHCII-deficiency in BM-APCs. These findings indicate the requirement for MHCII^{+} BM-APCs in inducing wave 1 negative selection. Preliminary evidence suggests that Aire has a role in mediating wave 2 negative selection in the polyclonal thymocyte repertoire. However, further experiments are required to confirm this preliminary evidence.

The similar phenotypes of non-transgenic thymic grafts in non-transgenic and insHEL transgenic hosts exclude circulating HEL as a potential source of the insHEL self-antigen that deletes 3A9 thymocytes (Liston et al., 2005). In addition, the similar thymic phenotypes of non-transgenic hosts implanted with 3A9 versus 3A9 x insHEL BM excludes BM-APCs as a potential source of the insHEL that deletes 3A9 thymocytes (Liston et al., 2005 and Fig. 3.3 above). However, the level of insHEL mRNA expression within CD45^{-} thymic stromal cells and the extent of mature CD4SP thymocyte deletion are proportional to the *Aire* gene dose (Liston et al., 2004a) and Aire-deficiency abrogates insHEL-mediated deletion (Liston et al., 2003). The latter observations suggest that TECs contribute to Aire-dependent insHEL-mediated deletion. MHCII-deficiency within BM-APCs completely abolished insHEL-mediated deletion, suggesting that insHEL^{+} TECs do not directly delete 3A9 thymocytes, but instead they rely entirely on self-antigen transfer from TECs to BM-APCs to induce deletion. The Aire-dependent self antigens such as RIP-OVA^{hi} (Hubert et al., 2011), Aire-GCL$_{G120A}$ (Aichinger et al., 2013) and the natural self-antigen, interphotoreceptor retinoid-binding protein (IRBP) (Taniguchi et al., 2012) are also co-dependent on TECs and MHCII^{+} BM-APCs to delete CD4^{+} thymocytes. As about half of all TCRs that require Aire also require MHCII^{+} BM-APCs to undergo deletion (Perry et al., 2014), insHEL, RIP-OVA^{hi}, Aire-GCL$_{G120A}$ and IRBP may represent an extensive class of self-antigens for which thymocyte deletion requires both TECs and BM-APCs, but only BM-APCs actually present the self-antigen to thymocytes to induce deletion.

The serum HEL protein concentration is lower in thyroHEL mice than in insHEL mice (0.5 ng/mL and 1.2 ng/mL, respectively) (Akkaraju et al., 1997), suggesting that circulating HEL is an unlikely source of the thyroHEL self-antigen that triggers 3A9

thymocyte deletion. The similar thymic phenotypes of non-transgenic hosts implanted with 3A9 versus 3A9 x thyroHEL BM excludes BM-APCs as a source of thyroHEL that deletes 3A9 thymocytes. Unlike insHEL-mediated deletion, thyroHEL-mediated deletion still occurred when BM-APCs lacked MHCII expression, indicating that thyroHEL$^+$ TECs directly present HEL self-antigen to 3A9 thymocytes. However, thyroHEL-mediated deletion was detectably shifted towards wave 2 (later T cell developmental stage) instead of wave 1 in the absence of MHCII$^+$ BM-APCs. In thyroHEL hosts, Helios induction was greater, and fewer thymocytes escaped from wave 1 deletion, when the BM-APCs expressed MHCII, suggesting that BM-APCs also present HEL self-antigen in thyroHEL hosts. The effect on Helios expression indicates that BM-APCs amplify thyroHEL-induced TCR-signalling. This finding has a precedent, as mTEC-derived self-antigens elicited more T cell proliferation when presented by thymic DCs than by the mTECs themselves (Koble and Kyewski, 2009). The finding that BM-APCs enable thymocyte deletion to occur earlier in T cell development could explain why the ePCC transgenic self-antigen, which is predominantly expressed within mTECs (Aichinger et al., 2013), causes an 83% reduction in CD4SP thymocytes in mice expressing the AD10 TCR, whereas it causes a 51% reduction when the BM-APCs lack MHCII (Oehen et al., 1996). ThyroHEL thus represents a class of self-antigens for which TECs alone can delete thymocytes, but for which stringent deletion at wave 1 requires cooperation between TECs and BM-APCs (i.e. indirect presentation by BM-APCs).

Dampening of thymocyte deletion can be accompanied by increased FoxP3$^+$ thymocyte induction (Cozzo Picca et al., 2009; Hinterberger et al., 2010), as observed in thyroHEL hosts with defective BM-APCs compared to functional BM-APCs. The blunting of thyroHEL-mediated Helios induction by MHCII-deficiency within BM-APCs is fully consistent with the “avidity model”, which postulates that strong TCR signalling triggers deletion whereas intermediate TCR signalling induces FoxP3 upregulation (Hinterberger et al., 2010). However, it is also relevant that MHCII-deficiency within BM-APCs shifted thyroHEL-mediated deletion towards wave 2, at which a marked increase in induction of the T-reg-associated protein, OX40 (Takeda et al., 2004), was observed, compared to wave 1. FoxP3 upregulation has also been reported to occur in wave 2 (Helios$^+$ CCR7$^+$ CD4SP) thymocytes (Hu et al., 2016). The stage of T cell development is another key variable in the deletion versus Treg selection “decision”. It is possible that MHCII$^+$ BM-APCs limit thyroHEL-mediated T-reg differentiation by inducing deletion at wave 1, before the thymocytes are mature enough to respond to strong TCR signalling in a manner that enables T-reg differentiation to occur.

In BM chimeras bearing 3A9 thymocytes, Helios expression in CCR7^{-} thymocytes correlated negatively with the absolute number of CCR7^{+} thymocytes. Based entirely on thymocytes with normal apoptosis, this correlation extends the evidence that a Helios^{+} phenotype marks thymocytes susceptible to deletion. However, when apoptosis is normal, enumerating Helios^{+} thymocytes is not a sensitive method to quantify the overall amount of deletion occurring in the thymus. This is highlighted in the investigation of polyclonal thymocytes with normal apoptosis, in which MHCII-deficiency within BM-APCs had no effect on wave 1 or wave 2 cell frequencies. However, when the lifespan of Helios^{+} thymocytes was extended by defective apoptosis, MHCII-deficiency within BM-APCs decreased wave 1 by 46.5%, indicating the crucial role of MHCII^{+} BM-APCs in mediating wave 1. Enumerating Helios^{+} cells within apoptosis-defective thymocyte cohorts thus provides a sensitive method to measure thymocyte deletion in the polyclonal repertoire.

It is possible that B2m-deficiency in TECs may not capture all of the normal wave 1 negative selection and could have altered the amount of wave 1 negative selection. However, MHCII-deficiency within BM-APCs consistently reduced wave 1 cells by a comparable frequency, 46.1% and 37.4% in the irradiated bone marrow recipients with *B2m*$^{-/-}$ and *B2m*$^{+/+}$ within the TECs, respectively. Therefore, B2m-deficiency in TECs made no obvious difference to the amount of negative selection, at least within the limits of the assay employed. These consistent results confirm that MHCII^{+} BM-APCs are necessary for normal negative selection at wave 1.

Wave 1 cells are characterised by coreceptor dulling and PD-1 induction (Daley et al., 2013; McCaughtry et al., 2008). Using the published method independent of Helios/CCR7 to identify strongly TCR-signalled CD4^{lo}CD8^{lo} PD-1^{hi} thymocytes (Mayans et al., 2014; McDonald et al., 2015; McDonald et al., 2014; Pobezinsky et al., 2012) that are mostly CCR7^{-} (McDonald et al., 2015), MHCII-deficiency within BM-APCs reduced the number of these cells by 68% (in *Bim*$^{-/-}$) and ~76% (in *Bcl-2* Tg). Consistent with the Helios/CCR7 analysis, this indicates that MHCII^{+} BM-APCs are required to induce negative selection in immature thymocytes yet to upregulate CCR7.

Thymocytes reside in the thymic cortex for at least 2 days after they proliferate as precursors with no or low $\alpha\beta$ TCR expression (Penit, 1986). Progression from the proliferating precursor stage to the Helios^{+} CCR7^{-} stage peaks at 2 days (Hu et al., 2016), suggesting that wave 1 thymocytes are located in the thymic cortex. The reduction in wave 1 caused by MHCII-deficiency within BM-APCs suggests that cortical BM-APCs are crucial for inducing wave 1. Consistent with this, imaging analysis of

cortical deletion *in situ* demonstrated that thymocytes were arrested and signalled adjacent to DCs, implicating DCs in mediating cortical deletion (Melichar et al., 2013). It remains unclear which types of DCs are found in the thymic cortex. Migratory DCs have been reported to accumulate around blood vessels in the cortex (Baba et al., 2009), from which they take up proteins circulating in the blood (Baba et al., 2009; Raviola and Karnovsky, 1972). A small subset (~2%) of cortical DCs was observed to migrate actively within the thymic cortex (Ladi et al., 2008). Alternatively, migratory DCs could potentially transport self-antigens derived from outside the thymus (Baba et al., 2009; Bonasio et al., 2006) or from mTECs (Koble and Kyewski, 2009) into the cortex.

Unexpectedly, ~40-50% of wave 1 (Helios$^+$ CCR7$^-$) or CD24$^+$ FoxP3$^-$ CD4^{lo}CD8^{lo} PD-1^{hi} induction still occurred when the BM-APCs lacked MHCII and the non-BM-APCs lacked Aire or B2m. This observation could be explained by four non-mutually exclusive possibilities. First, the remaining wave 1 thymocytes may be induced by MHCII$^+$ non-BM-APCs based on the evidence that they delete Vα11$^+$ T cells in C57BL/6 mice (Stadinski et al., 2011). Consistent with this line of evidence, cortical epithelial cells have been demonstrated to deliver a strong TCR signal and induce phenotypic changes associated with thymocyte deletion including PD-1 upregulation (McCaughtry et al., 2008). TSCOT (thymic stromal cotransporter)$^+$ CDR1$^+$ cTECs have been reported to delete neo-antigen-specific T cells in the cortex without depending on Aire, mTECs or DCs (Ahn et al., 2008). Second, host-derived MHCII$^+$ BM-APCs that survived irradiation may be responsible for inducing the remaining wave 1 thymocytes. This seems unlikely because MHCII^{hi} expression was severely reduced in DCs and macrophages in BM chimeras bearing MHCII-deficient BM. Third, donor-derived B2m$^+$ BM-APCs may be responsible. In support of this, DP thymocytes are sufficient to induce negative selection of co-resident Ag-specific DP thymocytes (Melichar et al., 2015). Fourth, BM-APCs may acquire MHCII molecules from epithelial cells by intercellular transfer (Koble and Kyewski, 2009; Millet et al., 2008).

Although MHCII-deficiency within BM-APCs did not diminish wave 2 (Helios$^+$ CCR7$^+$) quantitatively, this does not exclude TCR repertoire (qualitative) changes within the wave 2 thymocyte cohort. The results in 3A9 TCR Tg chimeras with MHCII-deficient BM-APCs suggest that wave 2 would lose self-antigens that behave like insHEL, and gain self-antigens that behave like thyroHEL, when the BM-APCs lack MHCII.

Aire-deficiency had variable effects on wave 1, reducing it by 21% in mice on the B10.BR background, yet failing to significantly reduce wave 1 induction in mice on the C57BL/6 background. Aire-deficiency did not decrease the frequency of CD4^{lo}CD8^{lo}

PD-1^{hi} polyclonal thymocytes. It is currently not clear that Aire plays an essential role in wave 1 negative selection, but any potential contribution of Aire to wave 1 appears to be dependent on BM-APCs. If migratory DCs that acquire self-antigens derived from mTECs (Koble and Kyewski, 2009) transport them into the cortex, this may provide an explanation for how Aire, which is expressed within mTECs (Heino et al., 1999), contributes to wave 1 in the cortex. It is hypothesised that wave 1 deletion occurs in the cortex. Aire may have indirect effects on thymocytes in the thymic cortex. For example, Aire may impact chemokine expression and/or haemopoietic APC migration patterns (Lei et al., 2011), which could affect wave 1 deletion.

The only setting in which a decrease in wave 2 was detected was when the BM-APCs were normal and the non-BM-APCs lacked Aire. Aire-deficiency diminished the frequency of wave 2 cells by 48% in mice on the B10.BR background, and by 33% in mice on the C57BL/6 background. This suggests that wave 2 depends crucially on Aire, presumably due to its role in diversifying self-antigen expression within mTECs (Anderson et al., 2002; Derbinski et al., 2005; Sansom et al., 2014) and perhaps by promoting the normal localisation or migration of BM-APCs in the thymic medulla (Lei et al., 2011). Time course experiments revealed that it takes ~5 days for thymocytes to progress from the proliferating precursor stage into wave 2 (Hu et al., 2016). As the frequency of wave 2 cells detected at 3 days after EdU injection was rather low, future experiments should be performed at 5 days after EdU injection to determine whether Aire-deficiency impacts wave 2 in a quantitative manner.

A self-reactive thymocyte may first receive a strong TCR signal at the CCR7^{-} or CCR7^{+} stage of development, due to differences in the self-antigen repertoires and APC networks encountered at these two stages. Thymocytes bound for deletion at the immature CCR7^{-} stage express very high levels of PD-1 (Daley et al., 2013; McDonald et al., 2015), whereas more mature CCR7^{+} thymocytes bound for deletion commonly upregulate CD25 and OX40 (Cozzo Picca et al., 2009; Daley et al., 2013; Wirnsberger et al., 2009). This phenotypic divergence of the two waves seems central to self-reactive thymocyte fate, as CCR7^{-} CD4^{lo}CD8^{lo} PD-1^{hi} iIEL thymic survivors colonise the small intestinal epithelium (Mayans et al., 2014; McDonald et al., 2015; McDonald et al., 2014), whereas wave 2 survivors upregulate FoxP3 and differentiate into the T-reg lineage (Cowan et al., 2013; Hu et al., 2016).

On quantitative terms, this study concludes that MHCII^{+} BM-APCs are crucial in mediating wave 1 negative selection in monoclonal or polyclonal thymocyte repertoires.

Preliminary evidence suggests that Aire has a role in mediating wave 2 negative selection in the polyclonal thymocyte repertoire.

CHAPTER 4

Quantification of the thymocyte repertoire that depends on MHC Class I and/or MHC Class II for TCR-signalling

4.1 Introduction

In mice, naïve $CD8^+$, but not $CD4^+$, T cell development is markedly reduced in the absence of B2m (Koller et al., 1990; Zijlstra et al., 1990). Naïve $CD4^+$, but not $CD8^+$, T cell development is markedly reduced in the absence of MHCII expression (Cosgrove et al., 1991; Grusby et al., 1991). These findings demonstrate the requirement for B2m, which is required for stable expression of MHCI on the cell surface (Zijlstra et al., 1990), in $CD8^+$ T cell development and the requirement for MHCII in $CD4^+$ T cell development.

There are more $CD4^+$ T cells than $CD8^+$ T cells in the thymus and peripheral lymphoid organs of healthy and young mice and humans. The mechanism that gives rise to this imbalance is unclear. In theory, two factors could be at play. First, more MHCII-binding T cells may initiate development. In other words, of all the thymocytes that receive a TCR signal in the thymus, the MHCII-responsive fraction exceeds the MHCI-responsive fraction. A second possibility is that, once initiated, completion of T cell development may be more common in $CD4^+$ T cells than in $CD8^+$ T cells.

Sinclair et al. (2013) concluded that there is no imbalance at the initiation step. These authors used mice lacking endogenous Zap70, but bearing a tetracycline-inducible Zap70 (TetZap70) transgene, to track Zap70-dependent developmental events in thymocytes. Zap70 is essential for mature T cell development and T cell signaling (Negishi et al., 1995). In TetZap70 mice, Zap70 expression is able to be switched on (or off) in *Zap70*$^{-/-}$ thymocytes by administration (or withholding) of tetracycline (Saini et al., 2010). This model revealed that DP thymocytes could be delineated into three substages, namely the DP1 ($CD5^{lo}TCR\beta^{lo}$) pre-selection stage, the DP2 ($CD5^{hi}TCR\beta^{int}$) stage, which contains CD4SP precursors and CD8SP precursors, and the DP3 ($CD5^{int}TCR\beta^{hi}$) stage, which contains the direct precursors of CD8SP cells only (Saini et al., 2010). The authors used TetZap70 BM cells to reconstitute irradiated *B2m*$^{-/-}$ *Rag1*$^{-/-}$ and *H2-Ab1*$^{-/-}$ (referred to as *MHCII*$^{-/-}$ by the authors) *Rag1*$^{-/-}$ hosts to track the maturation of MHCII-responsive cells and MHCI-responsive cells, respectively. Upon tetracycline feeding, the maturation rates from DP1 to DP2 cells were similar in the two groups of hosts, suggesting MHCII can induce a TCR signal in a similar proportion of thymocytes as can MHCI (Sinclair et al., 2013).

Sinclair et al. (2013) concluded that cell death during the maturation of TCR-signalled thymocytes is higher in MHCI-responsive cells than in MHCII-responsive cells. Specifically, the rate of cell death at the DP2 stage was higher in *MHCII*$^{-/-}$ *Rag1*$^{-/-}$

hosts than in *B2m*$^{-/-}$ *Rag1*$^{-/-}$ hosts. The authors concluded the imbalance between CD4^{+} and CD8^{+} T cells arises from a higher cell death rate in TCR-signalled MHCI-responsive thymocytes compared to TCR-signalled MHCII-responsive thymocytes.

Transgenic overexpression of the pro-apoptotic protein, Bax, in T cells increases apoptosis in thymocytes (Brady et al., 1996; Williams et al., 1998). Endogenous Bax mRNA expression levels are similar throughout thymocyte development (Sinclair et al., 2013). The authors studied mice expressing a transgene encoding Bax controlled by human CD2 promoter, which drives transgene expression throughout thymocyte development (de Boer et al., 2003). Transgenic Bax expression in T cells exaggerated the numeric imbalance in favour of CD4^{+} T cells over CD8^{+} T cells among CD24^{hi} T cells in the thymus and spleen (Sinclair et al., 2013). This led the authors to conclude that increasing apoptotic stress preferentially impairs development of MHCI-responsive T cells. However, the opposite effect is not observed when apoptosis is impaired, as CD4^{+} T cells still outnumber CD8^{+} T cells in *Bim*$^{-/-}$ and *Bcl-2* Tg mice (Daley et al., 2013). Thus, it is not entirely clear that the CD4:CD8 imbalance is explained by differential sensitivity to apoptosis after thymocytes have received TCR signalling.

Several points should be considered when interpreting the results using the TetZap70 experimental system. First, the Zap70 expression in DP1 TetZap70 thymocytes is broader than in wild-type thymocytes, ranging from the low level observed in wild-type DP1 thymocytes to the higher levels observed in wild-type DP2 thymocytes (Saini et al., 2010). This could potentially change the sensitivity of pre-selection DP1 thymocytes to antigen, altering the frequency of thymocytes that initiate development. Second, the stage-dependent regulation of Zap70 expression observed in wild-type mice is absent in TetZap70 mice. Zap70 expression increases progressively as thymocytes develop from DP1 to DP3 in wild-type mice. By contrast, TetZap70 mice exhibit the lowest Zap 70 expression at DP3 (Saini et al., 2010). This results in a partial developmental block of CD8SP thymocytes (Saini et al., 2010). Third, since BM-derived cells in the chimeric mice were capable of expressing both MHC classes, some thymocytes may have received pro-survival or pro-death TCR signals from the MHC class that was supposed to be absent on BM-derived cells.

Results in chapter 3 revealed that nascent thymocyte cohorts contain a much higher proportion of Helios^{+} cells in apoptosis-defective mice compared to mice with normal apoptosis. It was inferred that defective apoptosis enabled the identification and enumeration of strongly TCR-signalled Helios^{+} thymocytes, which would have undergone apoptosis or been phagocytosed in mice with normal apoptosis (Dzhagalov

et al., 2013). Impairing apoptosis is thus a promising strategy to preserve and enumerate TCR-signalled thymocytes in a way that is difficult to achieve in mice with normal apoptosis.

Recent research has provided evidence that the $CD4^{lo}CD8^{lo}$ $TCR\beta^{+}$ $PD\text{-}1^{hi}$ thymocyte population contains cells that are susceptible to clonal deletion, yet this population also contains precursors of T cells that colonise the small intestinal epithelium. The absolute number of $CD4^{lo}CD8^{lo}$ $TCR\beta^{+}$ $PD\text{-}1^{hi}$ thymocytes increases in the absence of costimulatory receptor CD28 or costimulatory ligands CD80 and CD86, and when apoptosis is inhibited by Bcl-2 transgene expression in haemopoietic cells (Pobezinsky et al., 2012). Compared to conventional $CD4^{+}$ and $CD8^{+}$ T cells in the thymus and lymph nodes, $CD4^{lo}CD8^{lo}$ $TCR\beta^{+}$ $PD\text{-}1^{hi}$ thymocytes and $CD8\alpha\alpha^{+}$ small intestinal intraepithelial lymphocytes ($CD8\alpha\alpha^{+}$ iIEL) are enriched in cells expressing superantigen-reactive TCRs (Pobezinsky et al., 2012), which are known to be susceptible to clonal deletion (Kappler et al., 1987). Most thymocytes forced to express TCRs derived from $CD8\alpha\alpha^{+}$ iIEL attain a $CD4^{lo}CD8^{lo}$ $TCR\beta^{+}$ $PD\text{-}1^{hi}$ phenotype before undergoing apoptosis in the thymus (Mayans et al., 2014; McDonald et al., 2015; McDonald et al., 2014). However, some $CD4^{lo}CD8^{lo}$ $TCR\beta^{+}$ $PD\text{-}1^{hi}$ thymocytes survive and colonise the small intestinal epithelium in a manner that requires the transcription factors, Runx3 and T-bet (Klose et al., 2014; Pobezinsky et al., 2012). These findings outline a putative differentiation pathway, which involves strong TCR signalling at the DP stage of thymocyte development inducing a $CD4^{lo}CD8^{lo}$ $TCR\beta^{+}$ $PD\text{-}1^{hi}$ intermediate population that contains cells susceptible to clonal deletion by apoptosis, but from which a small subset of cells survives and ultimately colonises the small intestinal epithelium. Hereafter in this thesis, the term “iIEL precursors” refers to the $CD4^{lo}CD8^{lo}$ $PD\text{-}1^{hi}$ thymocyte population.

Some information is available regarding the MHC molecules that induce the formation of iIEL precursors. One study identified 19 TCRs that induced thymocytes to attain a $CD4^{lo}CD8^{lo}$ phenotype. These 19 TCRs all consisted of one of 3 $TCR\beta$ chains paired with various $TCR\alpha$ chains derived in various ways, including from pre-selection thymocytes. Out of these 19 TCRs, approximately 25% recognised B2m-dependent ligands, 40% recognised MHCII, and 35% recognised both B2m-dependent ligands and MHCII (McDonald et al., 2015). Another study found that 5 out of 5 iIEL-derived TCRs recognised B2m-dependent ligands (but not MHCII) in the thymus (Mayans et al., 2014). No information is available on the relative contributions of MHCI versus MHCII to induction of iIEL precursors across the natural TCR repertoire.

The experiments below investigated the contributions of MHCI and MHCII to the induction of TCR-signalling in thymocytes. As the focus of this study concerns mechanisms underlying nascent T cell development, mature T cells that have recirculated into the thymus from the periphery (such as memory T cells and T-reg cells) (McCaughtry et al., 2007; Thiault et al., 2015) or have resided in thymus long term (such as NKT cells) (Berzins et al., 2006; Godfrey et al., 2010) may confound the results. Thus, EdU was used to label a nascent cohort of thymocytes undergoing DNA synthesis *in vivo*. All experimental animals expressed wild-type Zap70. To capture thymocytes that would normally be lost through apoptosis, mice with defective apoptosis were analysed alongside mice with normal apoptosis. The data show that in mice with normal apoptosis, while the absence of both MHC classes markedly diminished the size of the TCR-signalled cohort, the absence of one MHC class had no significant effect. However, results from apoptosis-defective mice indicate that the absence on one MHC class does have an effect, and the fraction of the thymocyte repertoire that requires MHCII to receive a TCR-signal is similar in size to the fraction that requires B2m-dependent ligands to receive a TCR signal. The apoptosis-defective dataset revealed that induction of Helios^{+} thymocytes was diminished to a significantly greater extent by the absence of MHCII compared to the absence of MHCI. These results reveal novel contrasts between the contributions of MHCI and MHCII to the induction of strong TCR-signalling within thymocytes.

4.2 Results

4.2.1 Characterisation of the phenotypic transitions in thymocyte cohorts labelled during DNA synthesis *in vivo*

To examine the expansion and reduction of the progeny of a single cohort of DNA synthesizing thymocytes *in vivo* over time, each mouse was injected intraperitoneally with a single bolus of 250 µg EdU from 0.04 (1 hour) to 7 days before flow cytometric analysis. It is assumed that thymocytes labelled with EdU were synthesising DNA within a short interval at the time of injection or shortly afterwards. Wild-type and apoptosis-defective *Bcl-2* Tg mice were injected with EdU at various time points and their thymocytes were all analysed by flow cytometry on the same day (Fig. 4.1A). Uninjected mice were included to ensure the detection of EdU^+ cells was specific (Fig. 4.1A). The frequency and number of EdU^+ thymocytes per mouse were determined at different time points after EdU injection. Thymocytes synthesising DNA at the time of EdU injection, identified as EdU^+ thymocytes, are also referred to as nascent thymocytes in this thesis.

In non-Tg mice the EdU^+ thymocyte frequency increased from 0.04 (1 hour) to 2 days after EdU injection, when it peaked at a mean frequency of 16.4% (Fig. 4.1B). The mean frequency of EdU^+ thymocytes declined from 2 to 7 days after EdU injection, with a sharp decrease from 12.5% at 3 days to 0.6% at 5 days after EdU injection. The number of EdU^+ thymocytes in non-Tg mice increased by 17-fold from 1 hour to 2 days after EdU injection, and declined by 59-fold from 2 to 7 days after EdU injection (Fig. 4.1B). This shows that within a cohort of nascent thymocytes, addition of cells via proliferation outweighs subtraction of cells for about 2 days in non-Tg mice. After 2 days, subtraction outweighs addition.

In *Bcl-2* Tg mice the frequency of EdU^+ thymocytes increased from 1 hour to 3 days after EdU injection, when it peaked at 13.6% (Fig. 4.1B). A 16-fold increase in number of EdU^+ thymocytes was observed between 1 hour and 3 days after EdU. This suggests that addition of nascent cells to the thymocyte pool outweighs subtraction for about 3 days in *Bcl-2* Tg mice, 1 day longer than in non-Tg mice.

At early time points (1 hour to 2 days) after EdU injection, non-Tg mice had up to ~2-fold higher frequency of EdU^+ thymocytes, and 1.3 to 2.7-fold higher number of EdU^+ thymocytes than *Bcl-2* Tg mice (Fig. 4.1B). Although not statistically significant, the data suggest that *Bcl-2* Tg expression may blunt thymocyte proliferation during the DN-

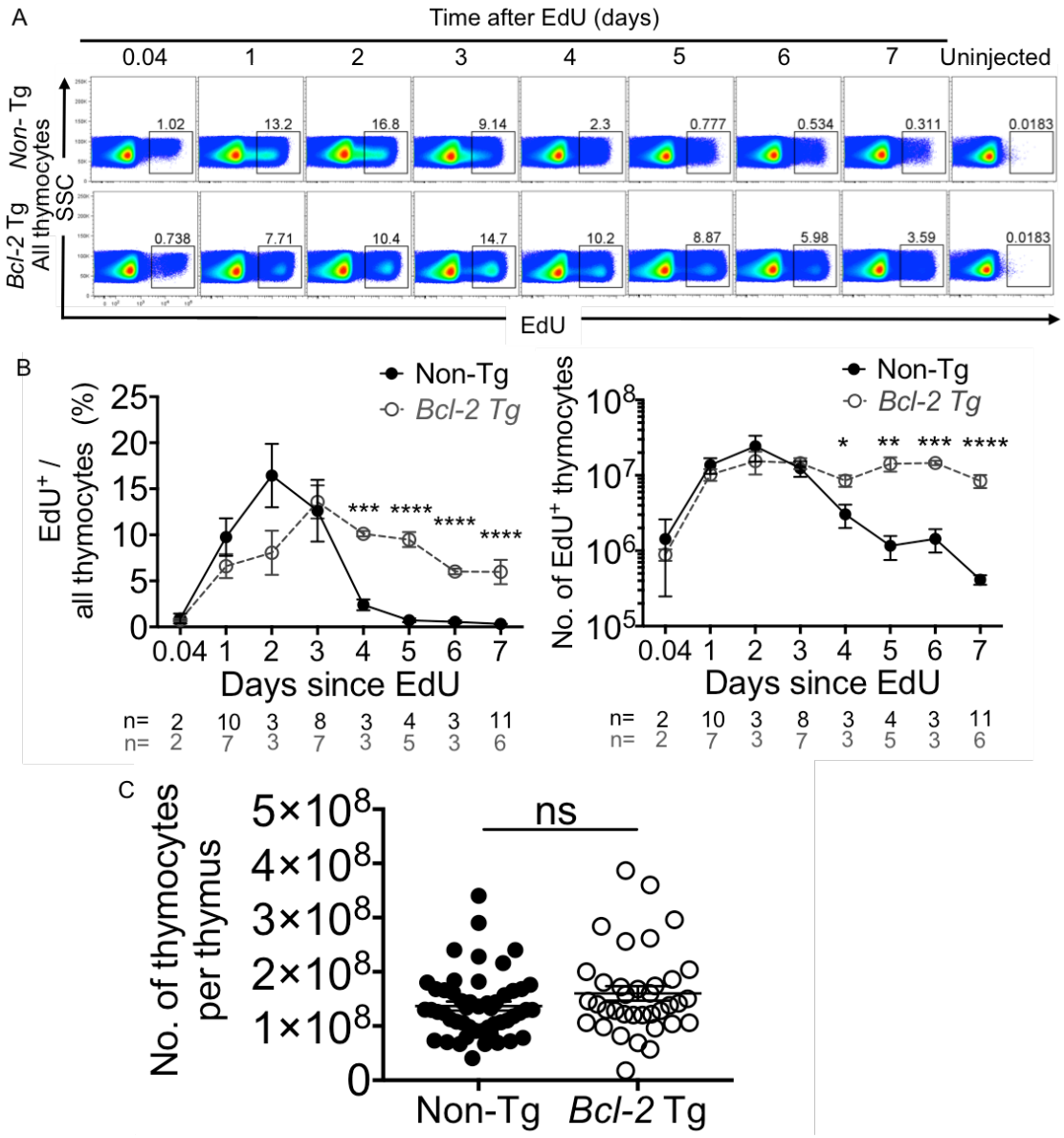
A
Time after EdU (days)
0.04
1
2
3
4
5
6
7
Uninjected
Non- Tg
Bcl-2 Tg
All thymocytes SSC
1.02
13.2
16.8
9.14
2.3
0.777
0.534
0.311
0.0183
0.738
7.71
10.4
14.7
10.2
8.87
5.98
3.59
0.0183
EdU
B
Non-Tg
Bcl-2 Tg
EdU+ / all thymocytes (%)
Days since EdU
No. of EdU+ thymocytes
n= 2 10 3 8 3 4 3 11
n= 2 7 3 7 3 5 3 6
C
No. of thymocytes per thymus
ns
Non-Tg
Bcl-2 Tg

Figure 4.1. Expansion and reduction of DNA synthesising thymocytes over 1 week. Non-Tg and *Bcl-2* Tg mice were injected with EdU from 1 hour (0.04d) to 7 days before flow cytometric analysis of thymocytes. Uninjected mice were analysed in parallel as a control. (A) All thymocytes were analysed for SSC/EdU (top). (B) Summaries show percentages of EdU^+ events among all thymocytes (left) and absolute number of EdU^+ thymocytes (right) over time after EdU injection. Only P values <0.05 between non-Tg and *Bcl-2* Tg groups were indicated with asterisk(s). (C) Graph shows total number of cells per thymus in wild-type (n = 51) and *Bcl-2* Tg (n = 36) mice. Data were compiled from 1 to 4 independent experiments with a total of n = 2-11 mice per group. Symbols and error bars represent mean and SEM. Statistical analyses used unpaired Student's t-tests comparing between non-Tg and *Bcl-2* Tg groups; P value symbols: **** <0.0001; *** <0.001; ** <0.01; * <0.05; ns (non-significant) >0.05. EdU was used in three independent experiments and BrdU was used in one experiment. Mice in all four experiments were EdU or BrdU injected by Daniel Hu, and two experiments were performed by Daniel Hu.

DP transition. At 3 days after EdU injection, *Bcl-2* Tg mice had a similar frequency and number of EdU^+ thymocytes to non-Tg mice (Fig. 4.1B).

In *Bcl-2* Tg mice the frequency of EdU^+ thymocytes decreased by only 2-fold from 3-7 days after EdU injection. The number of EdU^+ thymocytes did not change detectably during the same interval (Fig. 4.1B). While *Bcl-2* Tg mice did not have significantly higher number of total thymocytes than non-Tg mice (Fig. 4.1C), the frequency and the number of EdU^+ thymocytes were significantly higher in *Bcl-2* Tg mice than in non-Tg mice between 4 and 7 days after EdU injection. These findings show that *Bcl-2* transgene prolongs the lifespan of nascent thymocytes.

4.2.1.1 Characterisation of thymocytes expressing TCRβ and CD5

i) Nearly all DNA synthesising (EdU^+) thymocytes are $TCR\beta^-$ $CD5^-$

TCRβ and CD5 are upregulated in DP thymocytes by Zap70-dependent signalling (Saini et al., 2010). TCRβ and CD5 are also expressed by CD4SP and CD8SP thymocytes (Azzam et al., 1998) and post-selection $TCR\alpha\beta^+$ $CD4^{lo}CD8^{lo}$ thymocytes (Pobezinsky et al., 2012). This suggests that TCRβ and CD5 expression may be sensitive markers of TCR-signalled thymocytes generally, not just within the DP population. It follows that TCRβ and CD5 may be useful markers to measure the percentage of TCR-signalled cells within nascent thymocyte cohorts.

Thymocytes undergoing proliferation either before TCRβ gene recombination (DN2-DN3) or before TCRα gene recombination (DN-DP) would be expected to have a $TCR\beta^-$ $CD5^-$ phenotype (Pénit et al., 1995), whereas those proliferating in the last 24 hours before emigration would be expected to have a $TCR\beta^+$ $CD5^+$ phenotype (Pénit and Vasseur, 1997). To define the phenotype of DNA synthesising thymocytes, the EdU^+ population was examined 1 hour after EdU injection. In non-Tg mice, ~1% of the EdU^+ thymocytes were $TCR\beta^+$ $CD5^+$ at 1 hour after EdU injection, whereas ~10% of EdU^- thymocytes were $TCR\beta^+$ $CD5^+$ (Fig. 4.2A, B). Likewise in *Bcl-2* Tg mice, ~3% of EdU^+ thymocytes were $TCR\beta^+$ $CD5^+$ at 1 hour after EdU injection (Fig. 4.2A, B). This demonstrates that most DNA synthesising thymocytes are $TCR\beta^-$ $CD5^-$.

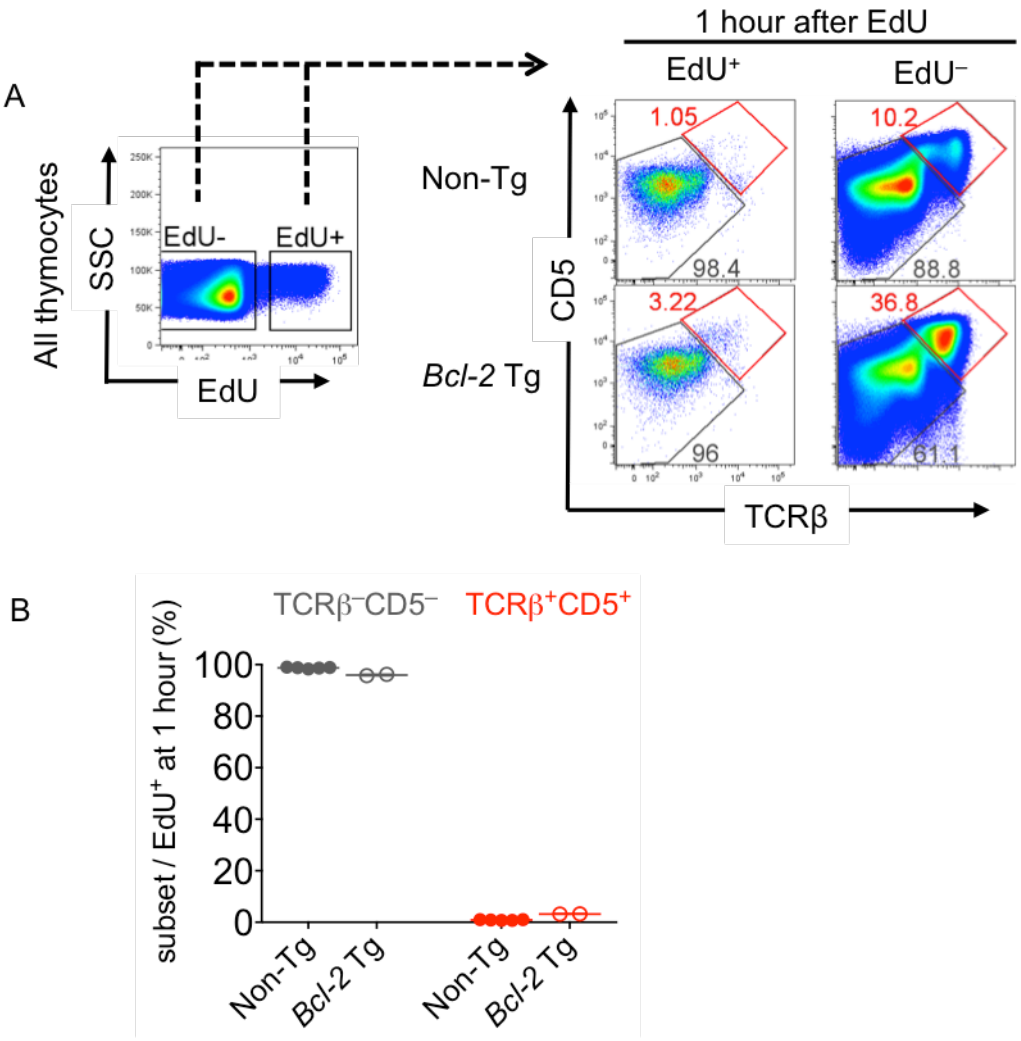

Figure 4.2. DNA synthesising thymocytes have a TCRβ$^-$ CD5$^-$ phenotype. Non-Tg and *Bcl-2* Tg mice were injected with EdU 1 hour before flow cytometric analysis of thymocytes. (A) All thymocytes were first gated for EdU$^+$ and EdU$^-$ populations. These two populations were analysed for TCRβ and CD5 expression. (B) Summaries show the frequencies of TCRβ$^+$ CD5$^+$ (red) and TCRβ$^-$ CD5$^-$ (grey) cells among EdU$^+$ thymocytes in the indicated genotypes. Data were compiled from 2 independent experiments in non-Tg mice (n = 4), and one experiment for *Bcl-2* Tg mice (n = 2). Lines represent mean.

ii) A subset of EdU$^+$ thymocytes attains a TCRβ$^+$ CD5$^+$ phenotype after DNA synthesis

To track phenotypic changes during thymocyte development, EdU$^+$ thymocytes were analysed throughout the time course (Fig. 4.3A). In non-Tg mice, the number of EdU$^+$ TCRβ$^+$ CD5$^+$ thymocytes increased sharply from 1 hour (mean = 2.1 × 10^4) to 2 days (mean = 1.4 × 10^6) after EdU injection (Fig. 4.3B), representing a 67-fold expansion. In theory, this order of population expansion could be achieved if every EdU$^+$ TCRβ$^+$ CD5$^+$ cell underwent 6 mitoses in the 47-hour interval and all its progeny survived (since 2^6 = 64). The number of EdU$^+$ TCRβ$^-$ CD5$^-$ thymocytes increased from 2.5 × 10^6 to 1.4 × 10^7 within the same time interval (Fig. 4.3C). This represents a ~6-fold expansion requiring 2-3 mitoses. The EdU$^+$ TCRβ$^+$ CD5$^+$ cells and EdU$^+$ TCRβ$^-$ CD5$^-$ cells had a similar mean fluorescence intensity (MFI) of EdU labeling (Fig. 4.4A, B). As the EdU MFI would be expected to halve with every round of mitosis, this finding excludes the possibility that EdU$^+$ TCRβ$^+$ CD5$^+$ cells underwent 3 or 4 more mitoses than the EdU$^+$ TCRβ$^-$ CD5$^-$ cells. These data favour an alternative interpretation, which is that a subset of EdU$^+$ TCRβ$^-$ CD5$^-$ thymocytes became EdU$^+$ TCRβ$^+$ CD5$^+$ cells between 1 hour and 2 days after EdU injection. Notably, the MFI of EdU labelling in EdU$^+$ thymocytes was higher in *Bcl-2* Tg mice than in non-Tg mice throughout the time course, regardless of TCRβ/CD5 phenotype (Fig. 4.4A, B).

In non-Tg mice, the number of EdU$^+$ TCRβ$^-$ CD5$^-$ thymocytes decreased from 3 days (mean = 8.5 × 10^6) to 5 days (mean = 3.4 × 10^5) after EdU injection, representing a 25-fold reduction (Fig. 4.3C). The number of EdU$^+$ TCRβ$^+$ CD5$^+$ thymocytes decreased from 1.5 × 10^6 to 5.5 ×10^5, representing a 2.7-fold reduction within the same interval (Fig. 4.3B). The steep decline in the major population of EdU$^+$ TCRβ$^-$ CD5$^-$ thymocytes, without a corresponding increase in EdU$^+$ TCRβ$^+$ CD5$^+$ thymocytes, demonstrates that most EdU$^+$ TCRβ$^-$ CD5$^-$ thymocytes die 3-5 days after incorporating EdU without ever attaining an EdU$^+$ TCRβ$^+$ CD5$^+$ phenotype.

From 3 to 7 days after EdU injection in non-Tg mice, the number of EdU$^+$ TCRβ$^+$ CD5$^+$ thymocytes declined by 3.7-fold (Fig. 4.3B), compared to a 78-fold decline in the number of EdU$^+$ TCRβ$^-$ CD5$^-$ thymocytes (Fig. 4.3C). The lower disappearance rate demonstrates that a greater fraction of the EdU$^+$ TCRβ$^+$ CD5$^+$ thymocytes persist in the thymus >3 days after incorporating EdU. This is consistent with onward differentiation in EdU$^+$ TCRβ$^+$ CD5$^+$ thymocytes.

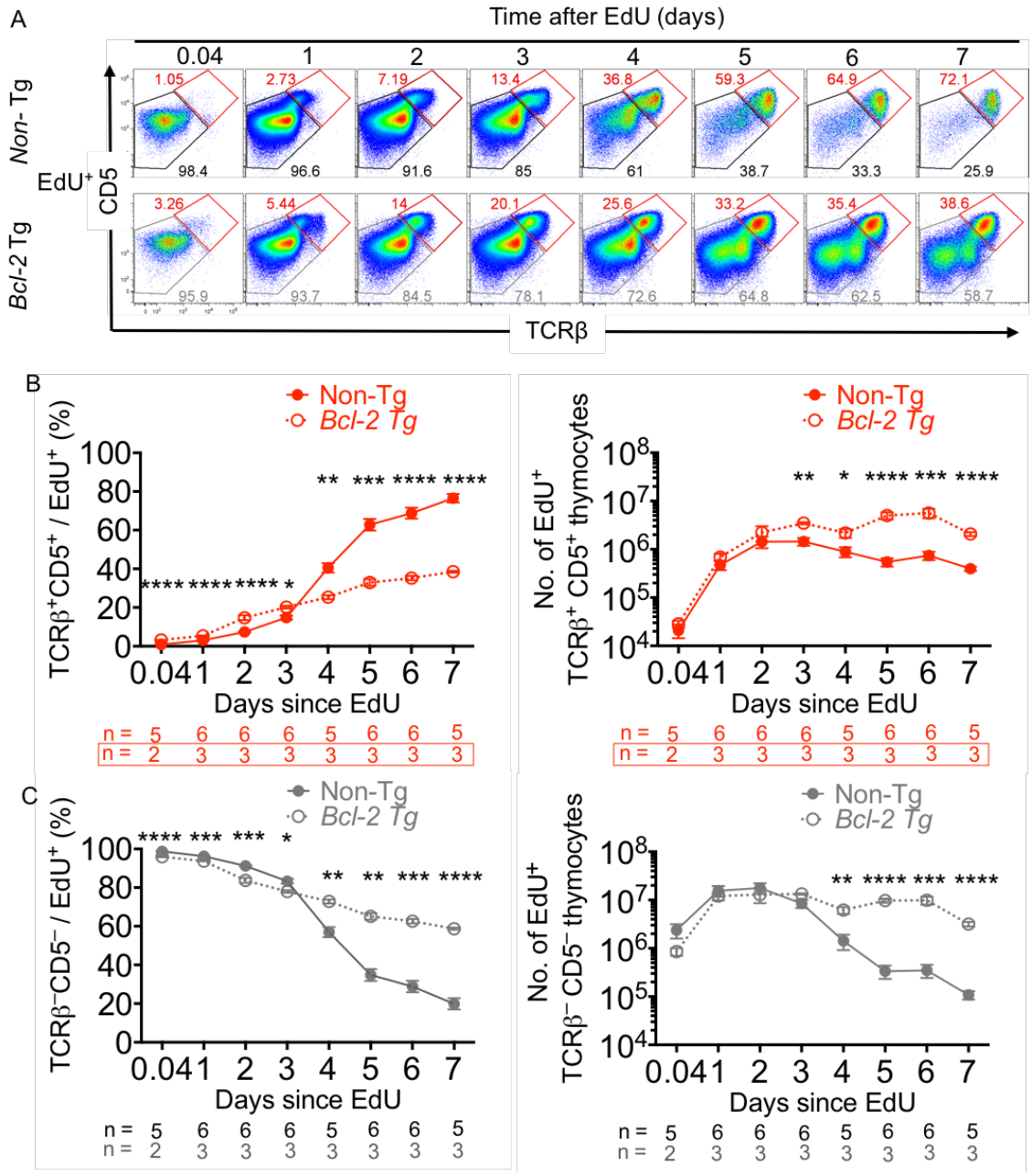

Figure 4.3. Some nascent TCRβ⁻ CD5⁻ thymocytes differentiate into TCRβ⁺ CD5⁺ thymocytes. As part of the time course experiment described in Fig. 4.1, (A) EdU⁺ thymocytes were divided into TCRβ⁺ CD5⁺ (red) and TCRβ⁻ CD5⁻ (grey) subsets. (B) Summaries show the frequency of TCRβ⁻ CD5⁻ cells among EdU⁺ thymocytes (left) and the number of EdU⁺ TCRβ⁻ CD5⁻ thymocytes (right) enumerated over time after EdU injection. (C) Summaries show the frequency of TCRβ⁺ CD5⁺ cells among EdU⁺ thymocytes (left) and the number of EdU⁺ TCRβ⁺ CD5⁺ thymocytes (right) enumerated over time after EdU injection. Data were compiled from 2 independent experiments in non-Tg mice (n = 5-6 per group), and one experiment for *Bcl-2* Tg mice (n = 2-3 per group). Symbols and error bars represent mean and SEM. Statistical analyses used unpaired Student's t-tests comparing between non-Tg and *Bcl-2* Tg groups at individual time point; P value symbols: **** <0.0001; *** <0.001; ** <0.01; * <0.05.

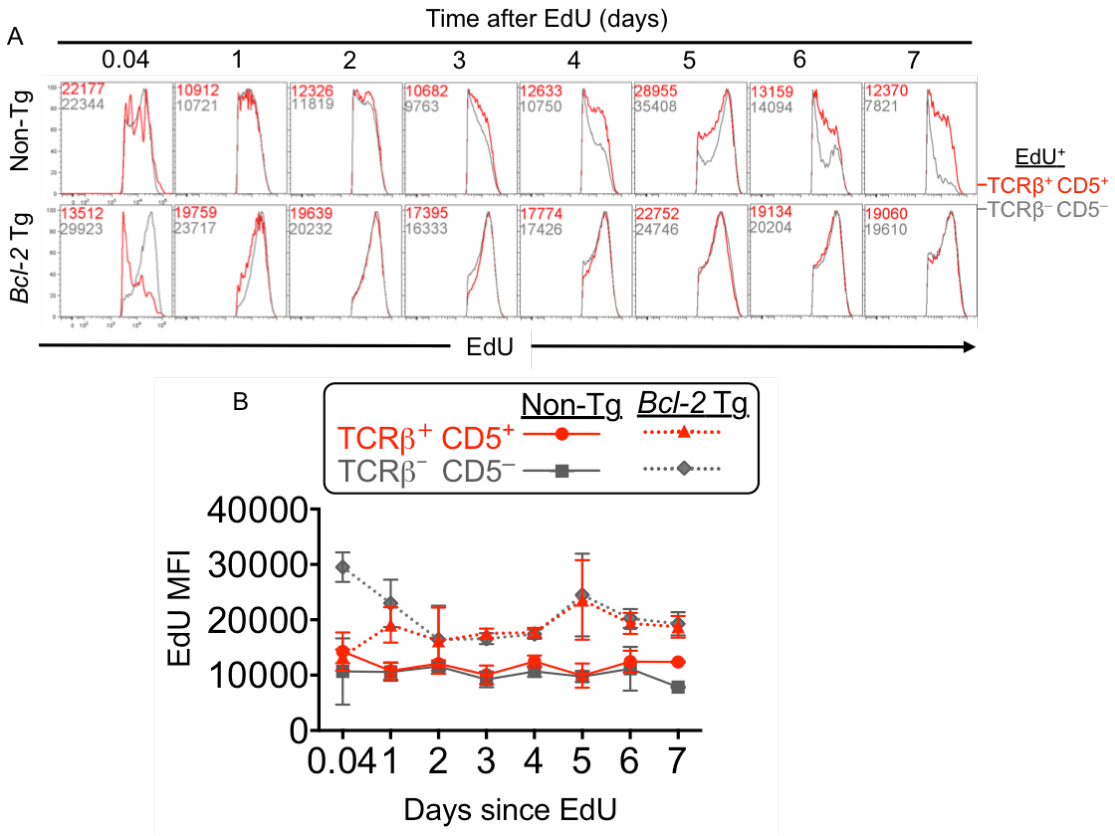

Figure 4.4. The EdU$^+$ TCRβ$^+$ CD5$^+$ thymocytes and EdU$^+$ TCRβ$^-$ CD5$^-$ thymocytes have a similar mean fluorescence intensity (MFI) of EdU labeling. As part of the time course experiment described in Fig. 4.1, the level of EdU labeling in (A) EdU$^+$ TCRβ$^+$ CD5$^+$ cells (red) and EdU$^+$ TCRβ$^-$ CD5$^-$ (grey) cells was analysed in non-Tg and *Bcl-2* Tg mice over time after EdU injection. Numbers on histograms represent mean fluorescence intensity (MFI) of gated TCRβ/CD5$^+$ or TCRβ/CD5$^-$ events. (B) Summary shows the EdU MFIs of EdU$^+$ TCRβ$^+$ CD5$^+$ (red) and EdU$^+$ TCRβ$^-$ CD5$^-$ (grey) of non-Tg mice (solid line) and *Bcl-2* Tg (dotted line). Data were compiled from an experiment with a total of n = 3 mice per group, except n = 2 mice per group for 0.04 day after EdU for non-Tg and *Bcl-2* Tg, and for 7 days after EdU in non-Tg mice. Symbols and error bars represent mean and SEM.

In *Bcl-2* Tg mice, the number of EdU^+ $TCR\beta^-$ $CD5^-$ thymocytes increased from 1 hour (mean = 8.5×10^5) to 3 days (mean = 1.3×10^7) after EdU injection (Fig. 4.3C), representing a 16-fold expansion. The number of EdU^+ $TCR\beta^+$ $CD5^+$ thymocytes increased from 2.9×10^4 to 3.5×10^6 within the same time interval (Fig. 4.3B), representing a 121-fold expansion. Based on the logic outlined above, this data suggests that a subset of EdU^+ $TCR\beta^-$ $CD5^-$ thymocytes became EdU^+ $TCR\beta^+$ $CD5^+$ cells between 1 hour and 3 days after EdU injection.

There are large differences between non-Tg and *Bcl-2* Tg genotypes in the latter section of the time course. During the interval 3-7 days after EdU injection, the number of EdU^+ $TCR\beta^-$ $CD5^-$ thymocytes declined by only 4-fold in *Bcl-2* Tg mice, compared to 79-fold in non-Tg mice (Fig. 4.3C). In the case of EdU^+ $TCR\beta^+$ $CD5^+$ thymocytes, the *Bcl-2* Tg mice only had a 1.7-fold decline compared to 3.7-fold in non-Tg mice between 3 and 7 days after EdU injection (Fig. 4.3B). The difference observed for EdU^+ $TCR\beta^+$ $CD5^+$ thymocytes between the two genotypes is much smaller than observed for EdU^+ $TCR\beta^-$ $CD5^-$ thymocytes. These findings demonstrate that the most pronounced extension in lifespan afforded by *Bcl-2* Tg expression is within thymocytes that remain $TCR\beta^-$ $CD5^-$ after incorporating EdU.

iii) EdU^+ $TCR\beta^-$ $CD5^-$ thymocytes commonly retain a DP phenotype, whereas EdU^+ $TCR\beta^+$ $CD5^+$ thymocytes commonly attain non-DP phenotypes

To further characterise the phenotypic divergence of $TCR\beta^-$ $CD5^-$ and $TCR\beta^+$ $CD5^+$ thymocytes, the CD4/CD8 profile of these two subsets among the nascent EdU^+ cohorts was analysed. EdU^+ $TCR\beta^-$ $CD5^-$ (Fig. 4.5A) and EdU^+ $TCR\beta^+$ $CD5^+$ (Fig. 4.6A) subsets were subdivided into four populations, namely DP, $CD4^{lo}CD8^{lo}$ (coreceptor dull), CD4SP and CD8SP. DP cells dominated the $TCR\beta^-$ $CD5^-$ subset in both non-Tg (Fig. 4.5B) and *Bcl-2* Tg mice (Fig. 4.5C) throughout the time course, despite a gradual decrease in DP cells at day 4-7 in non-Tg mice (Fig. 4.5B). This demonstrates that nascent $TCR\beta^-$ $CD5^-$ thymocytes commonly retain a DP phenotype.

EdU^+ $TCR\beta^+$ $CD5^+$ thymocytes had a wider spectrum of CD4/CD8 phenotypes. In non-Tg mice, although EdU^+ $TCR\beta^+$ $CD5^+$ thymocytes were predominantly DP cells at 1-2 days after EdU injection, a progressive increase in the frequency of CD4SP cells was observed from 1-4 days after EdU injection (Fig. 4.6B). The frequency of $CD4^{lo}CD8^{lo}$ and CD8SP thymocytes remained relatively low throughout the time course, although the CD8SP frequency increased between 4 and 7 days after EdU injection (Fig. 4.6B). These findings show that attainment of non-DP phenotypes is more common in $TCR\beta^+$

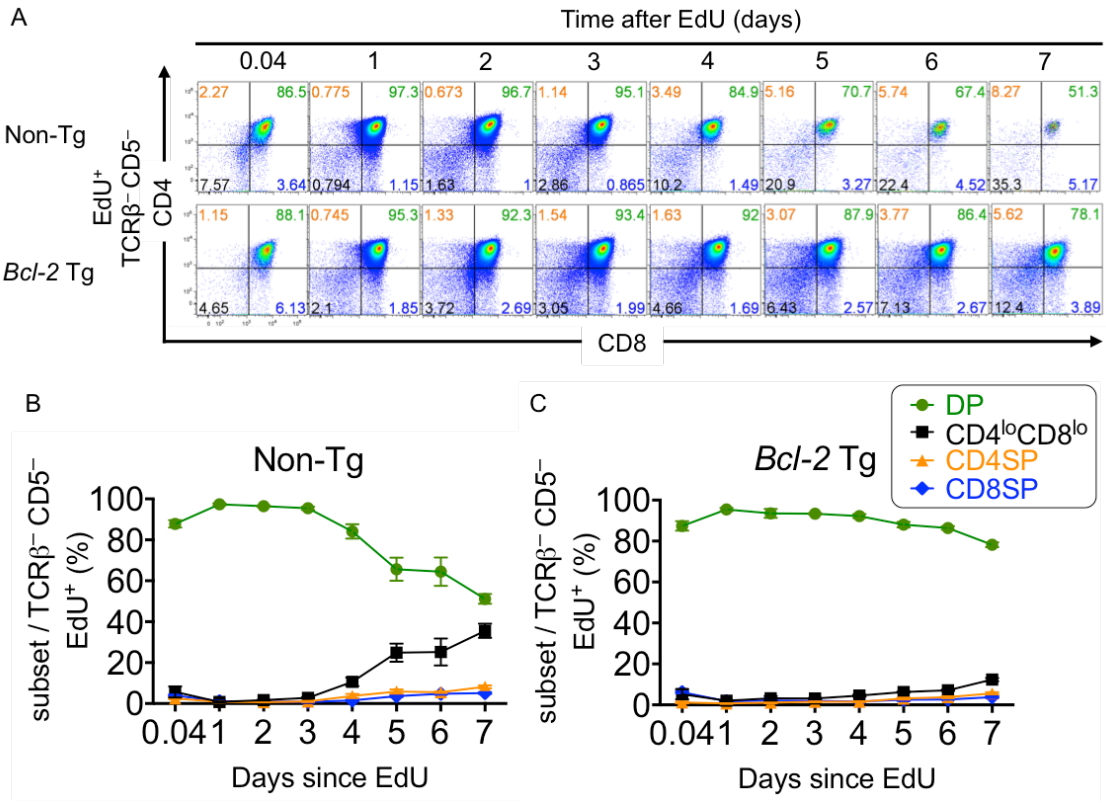

Figure 4.5. Retention of DP phenotype is common in TCRβ$^-$ CD5$^-$ thymocytes. As part of the time course experiment described in Fig. 4.1, (A) EdU$^+$ TCRβ$^-$ CD5$^-$ thymocytes were analysed for CD4/CD8 over time after EdU injection. (B) Summaries show the frequency of DP (green), CD4^{lo}CD8^{lo} (black), CD4SP (orange) and CD8SP (blue) subsets among EdU$^+$ TCRβ$^-$ CD5$^-$ thymocytes over time after EdU injection. Data were compiled from an experiment with a total of n = 3 mice per group, except n = 2 mice for 0.04 day in both genotypes and for 7 days after EdU in non-Tg mice. Symbols and error bars represent mean and SEM.

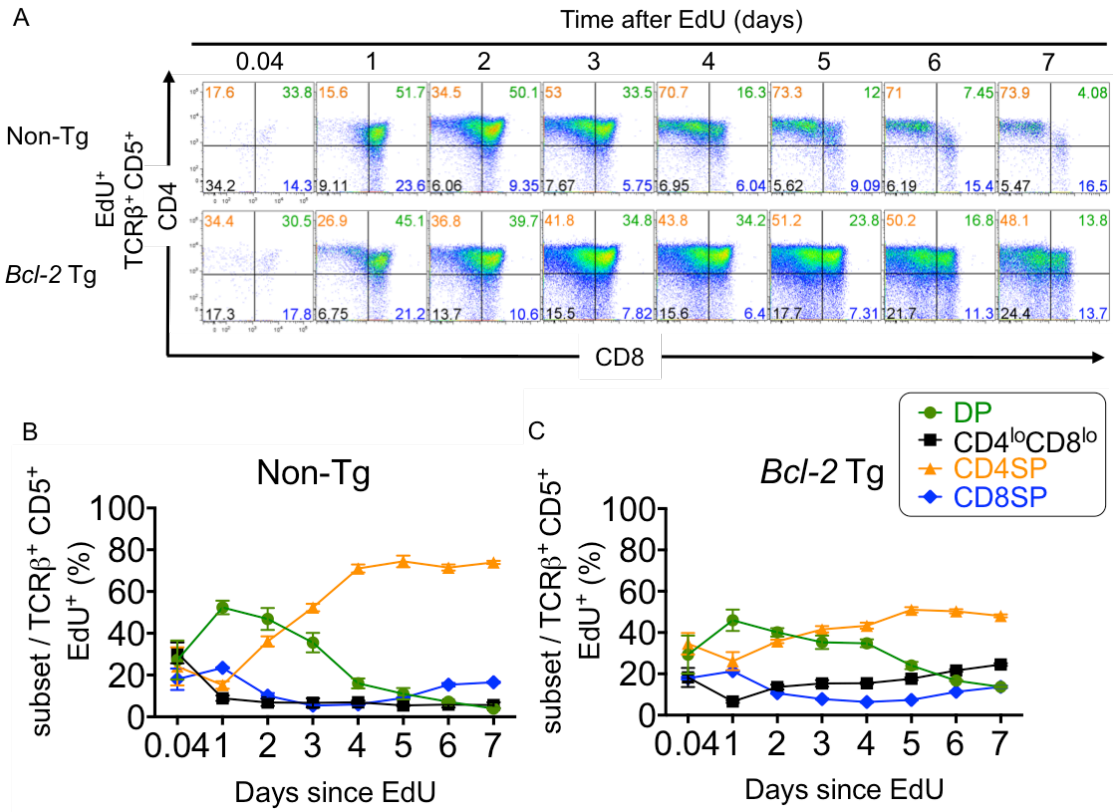

Figure 4.6. Attainment of non-DP phenotypes is common in TCRβ$^+$ CD5$^+$ thymocytes. As part of the time course experiment described in Fig. 4.1, (A) EdU$^+$ TCRβ$^+$ CD5$^+$ thymocytes were analysed for CD4/CD8 phenotype. (B) Summaries show the frequency of DP (green), CD4^{lo}CD8^{lo} (black), CD4SP (orange) and CD8SP (blue) subsets among EdU$^+$ TCRβ$^+$ CD5$^+$ thymocytes over time after EdU injection. Data were compiled from an experiment with a total of n = 3 mice per group, except n = 2 mice for 0.04 day in both genotypes and for 7 days after EdU in non-Tg mice. Symbols and error bars represent mean and SEM.

$CD5^+$ thymocytes than in $TCR\beta^-$ $CD5^-$ thymocytes. They are also consistent with reports that thymocytes progress to a CD4SP phenotype more rapidly than to a CD8SP phenotype (Lucas et al., 1993; Saini et al., 2010).

EdU^+ $TCR\beta^+$ $CD5^+$ thymocytes in *Bcl-2* Tg mice were also more heterogeneous than $TCR\beta^-$ $CD5^-$ counterparts. The frequency of CD4SP thymocytes increased gradually between 1 and 5 days after EdU injection, with the concomitant reduction of DP cell frequency during this interval (Fig. 4.6C). Although the frequency of $CD4^{lo}CD8^{lo}$ and CD8SP thymocytes remained relatively low throughout the time course in *Bcl-2* Tg mice, $CD4^{lo}CD8^{lo}$ cell frequency increased gradually over time, while the CD8SP cell frequency started to increase at day 5 after EdU injection (Fig. 4.6C). Considering EdU^+ $TCR\beta^+$ $CD5^+$ thymocytes, a contrast between genotypes was an increased $CD4^{lo}CD8^{lo}$ cell frequency in the *Bcl-2* Tg mice. Coreceptor dulling is a hallmark of the response to strong TCR signaling at the DP stage of thymocyte development (Daley et al., 2013; McCaughtry et al., 2008; McGargill and Hogquist, 1999; Swat et al., 1991). This effect is therefore probably due to the persistence in *Bcl-2* Tg mice of strongly TCR-signalled thymocytes that would normally undergo apoptosis in non-Tg mice.

iv) EdU^+ $TCR\beta^+$ $CD5^+$ thymocytes express more CD69 and Helios than EdU^+ $TCR\beta^-$ $CD5^-$ thymocytes

To extend the analysis above, the EdU^+ $TCR\beta^+$ $CD5^+$ and EdU^+ $TCR\beta^-$ $CD5^-$ thymocyte subsets were examined for expression of additional markers of TCR activation. CD69 is upregulated in thymocytes and T cells in response to TCR signaling (Testi et al., 1989) or type I interferon signaling (Shiow et al., 2006; Sun et al., 1998). Helios is a marker of strongly TCR-signalled thymocytes (Daley et al., 2013). In both non-Tg and *Bcl-2* Tg mice, the $TCR\beta^+$ $CD5^+$ subset had higher CD69 expression than the $TCR\beta^-$ $CD5^-$ subset throughout the time course after EdU injection (Fig. 4.7A). This suggests that thymocytes that attain a $TCR\beta^+$ $CD5^+$ phenotype are TCR-signalled whereas there is no evidence that the $TCR\beta^-$ $CD5^-$ thymocytes are TCR-signalled. Within the $TCR\beta^+$ $CD5^+$ subset of both non-Tg and *Bcl-2* Tg mice, the CD69 MFI decreased on day 5-7 after EdU injection, and a bimodal distribution of CD69 expression was observed at these later times after EdU (Fig. 4.7A). CD69 downregulation at later time points was expected based on the phenotype of mature SP cells: $Qa\text{-}2^{hi}CD62L^{hi}HSA^{lo}CD69^{lo}$ (Kishimoto and Sprent, 1997). CD69 downregulation may have a functional role in emigration of mature SP cells from the thymus (Shiow et al., 2006) 4-5 days after becoming single-positive thymocytes (McCaughtry et al., 2007). *Bcl-2* Tg expression subtly increased CD69 MFI on the $TCR\beta^+$ $CD5^+$ subset of EdU^+ thymocytes from 1 hour

to 3 days after EdU injection, in comparison to non-Tg mice (Fig. 4.7A).

In both non-Tg and *Bcl-2* Tg mice, Helios expression was consistently higher in the TCRβ$^+$ CD5$^+$ subset than in the TCRβ$^-$ CD5$^-$ subset throughout the time course after EdU injection (Fig. 4.7B). This provides further evidence that TCRβ$^+$ CD5$^+$ thymocytes are TCR-signalled, whereas TCRβ$^-$ CD5$^-$ thymocytes are TCR-unsignalled. Helios MFI in the TCRβ$^+$ CD5$^+$ subset was higher in *Bcl-2* Tg mice than in non-Tg mice, especially at 2 or more days after EdU injection, whereas Helios MFI in the TCRβ$^-$ CD5$^-$ subset was similar across the two genotypes (Fig. 4.7B). This suggests that *Bcl-2* transgene enhances the survival of Helios$^+$ thymocytes, as observed previously (Daley et al., 2013).

In summary, this section (4.2.1.1) provides evidence that TCRβ and CD5 co-expression identifies the TCR-signalled subset of nascent thymocytes, including thymocytes with non-DP phenotypes, in both wild-type and apoptosis-defective mice.

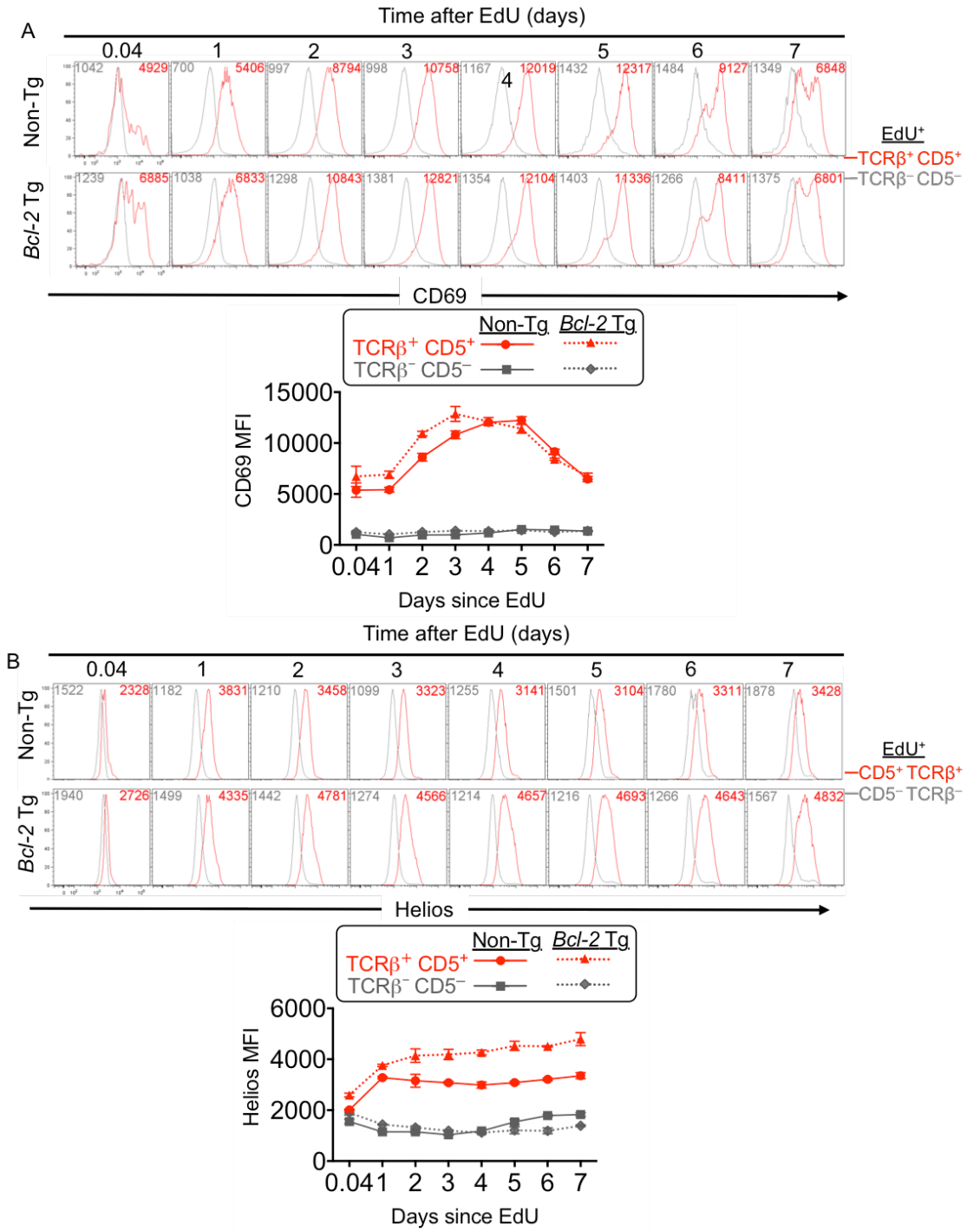
A
Time after EdU (days)
0.04
1
2
3
4
5
6
7
Non-Tg
Bcl-2 Tg
EdU+
TCRβ+ CD5+
TCRβ− CD5−
CD69
Non-Tg
Bcl-2 Tg
TCRβ+ CD5+
TCRβ− CD5−
CD69 MFI
15000
10000
5000
0
Days since EdU
B
Time after EdU (days)
Non-Tg
Bcl-2 Tg
EdU+
CD5+ TCRβ+
CD5− TCRβ−
Helios
Non-Tg
Bcl-2 Tg
TCRβ+ CD5+
TCRβ− CD5−
Helios MFI
6000
4000
2000
0
Days since EdU

Figure 4.7. The nascent TCRβ$^+$ CD5$^+$ thymocyte population expresses more CD69 and Helios than the nascent TCRβ$^-$ CD5$^-$ population. As part of the time course experiment described in Fig. 4.1, histograms show EdU$^+$ TCRβ$^+$ CD5$^+$ (red) and EdU$^+$ TCRβ$^-$ CD5$^-$ (grey) thymocytes analysed for CD69 (A) and Helios (B) over time after EdU injection. Numbers on histograms represent MFI of gated TCRβ$^+$ CD5$^+$ or TCRβ$^-$ CD5$^-$ events. Summaries show the MFIs of CD69 (A bottom) and Helios (B bottom) of EdU$^+$ TCRβ$^+$ CD5$^+$ (red) and EdU$^+$ TCRβ$^-$ CD5$^-$ (grey) of non-Tg mice (solid line) and *Bcl-2* Tg (dotted line). Data were compiled from an experiment with a total of n = 3 mice per group, except n = 2 mice per group for 0.04 day after EdU for non-Tg and *Bcl-2* Tg, and for 7 days after EdU in non-Tg mice. Symbols and error bars represent mean and SEM.

4.2.1.2 Characterisation of thymocytes expressing active caspase 3

To characterise thymocytes that are committed to apoptosis, this section analyses cells bound by an antibody specific for active caspase 3. Active caspase 3, one of the executioner caspases (Shi, 2002), has been reported to be the primary regulator of apoptosis via proteolytic inactivation of DFF45/ICAD (DNA fragmentation factor-45/inhibitor of caspase-activated DNase), which releases endonuclease active DFF40/CAD (caspase-activated DNase) (Wolf et al., 1999). DNA fragmentation was observed via agarose gel electrophoresis and ethidium bromide when pro-DFF40/CAD was incubated with rat liver nuclei and caspase 3 (Wolf et al., 1999).

i) Apoptosis-defective mice have fewer active caspase 3^+ thymocytes

To analyse thymocytes presumably committed to undergo apoptosis, active caspase 3^+ events were interrogated (Fig. 4.8A). Among all thymocytes, the mean active caspase 3^+ frequency was 0.46% in non-Tg mice (Fig. 4.8B). A 7-fold lower frequency was observed in *Bcl-2* Tg mice (Fig. 4.8B). This demonstrates that overexpression of anti-apoptotic Bcl-2 protein impairs the formation of active caspase 3^+ thymocytes. This is consistent with Bim-deficient HY^{CD4} male mice having greatly diminished active caspase 3^+ thymocyte frequencies compared to Bim-sufficient HY^{CD4} male mice (McCaughtry et al., 2008).

ii) Attainment of an active caspase 3^+ phenotype in thymocytes peaks at 3 days after DNA synthesis

To track the time interval during which thymocytes acquire an active caspase 3^+ phenotype after DNA synthesis, EdU^+ thymocytes were analysed for active caspase 3 expression in non-Tg and *Bcl-2* Tg mice (Fig. 4.9A). In non-Tg mice, the number of EdU^+ active caspase 3^+ thymocytes increased by 81-fold from 1 hour to 3 days after EdU injection, when it peaked at 1.6×10^5 (Fig. 4.9B). The EdU^+ active caspase 3^+ thymocytes then decreased by 19-fold between 3 and 5 days, and continued to decline over time (Fig. 4.9B). Overall, these findings suggest that thymocytes undergo apoptosis from 1 to 5 days after DNA synthesis, but thymocyte apoptosis peaks around 3 days after DNA synthesis.

In *Bcl-2* Tg mice, the number of EdU^+ active caspase 3^+ thymocytes also peaked at 3 days after EdU injection at 1.6×10^4 (Fig. 4.9B), 10-fold lower than non-Tg mice. The number of EdU^+ active caspase 3^+ thymocytes was similar from 3 to 6 days, as

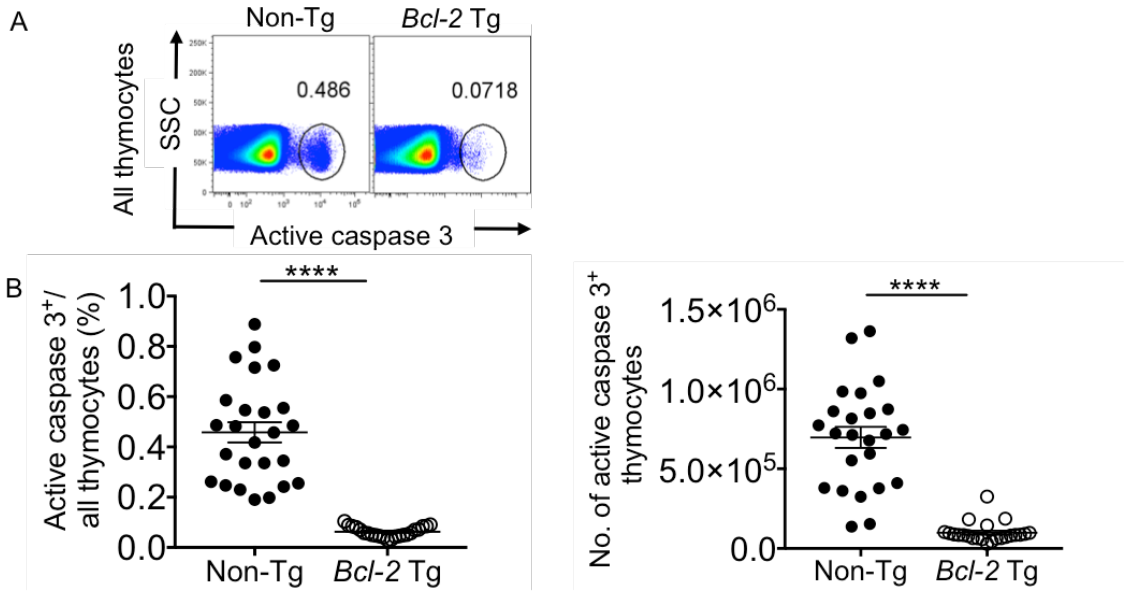

Figure 4.8. Decreased active caspase 3^+ thymocytes in mice overexpressing *Bcl-2* transgene within haemopoietic cells. (A) All thymocytes of non-Tg (n=25) and *Bcl-2* Tg (n = 23) mice were analysed for active caspase 3 expression. (B) Summaries show the frequency of active caspase 3^+ events among all thymocytes (left) and number of active caspase 3^+ thymocytes (right) in steady state. Data were compiled from one experiment, and were representative of four experiments. Symbols and error bars represent mean and SEM. Statistical analyses used unpaired Student's t-tests; P value symbol: **** <0.0001.

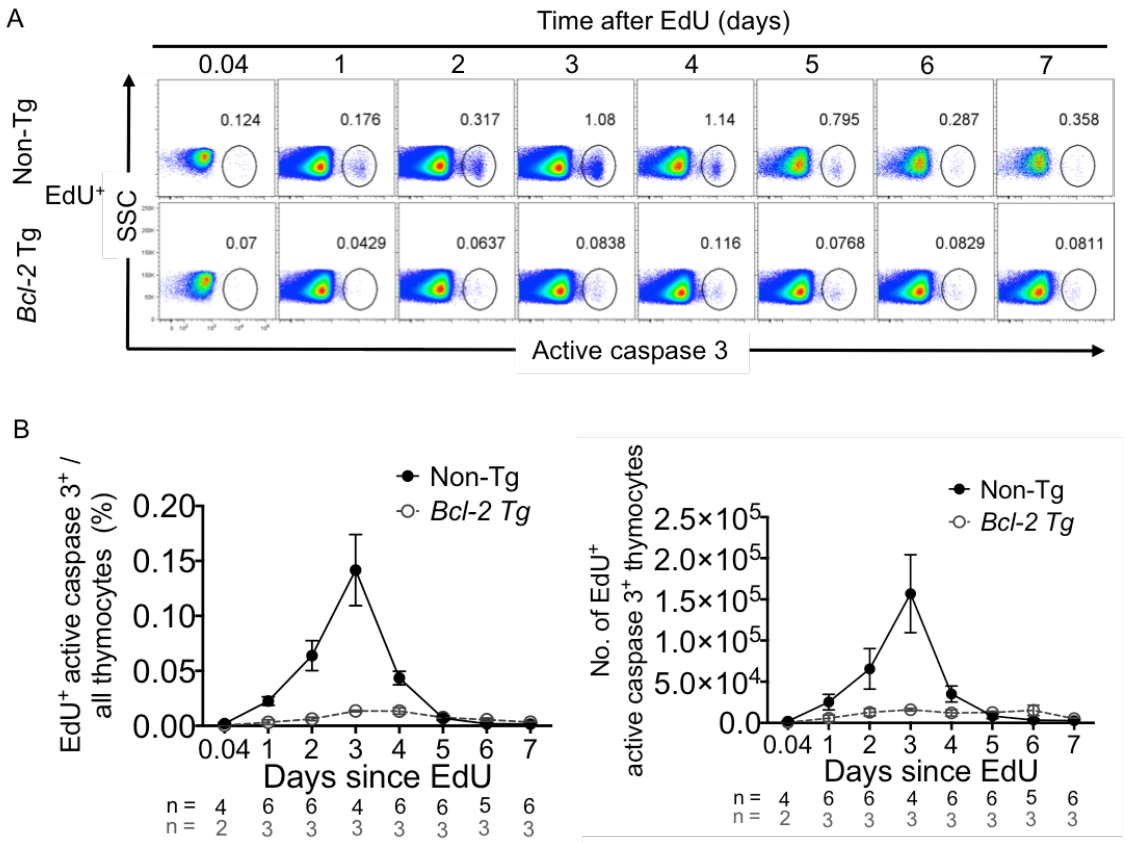

Figure 4.9. Active caspase 3$^+$ thymocyte formation peaks at day 3 after DNA synthesis. Non-Tg and *Bcl-2* Tg mice were injected with EdU from 1 hour (0.04d) to 7 days before flow cytometric analysis of thymocytes. (A) EdU$^+$ thymocytes were analysed for SSC/active caspase 3 over time after EdU injection. (B) Summaries show the frequency of EdU$^+$ active caspase 3$^+$ among all thymocytes (left) and absolute number of EdU$^+$ active caspase 3$^+$ thymocytes (right) in non-Tg (black solid line) and *Bcl-2* Tg (grey dotted line). Data were compiled from 2 independent experiments in non-Tg mice (n = 4-6 per group), and one experiment for *Bcl-2* Tg mice (n = 2-3 per group). Symbols and error bars represent mean and SEM.

opposed to a sharp decline between 3 to 5 days after EdU injection in non-Tg mice. EdU^+ active caspase 3^+ thymocytes decreased by 2.9–fold between 6 and 7 days after EdU injection in *Bcl-2* Tg mice (Fig. 4.9B). *Bcl-2* Tg mice had consistently fewer EdU^+ active caspase 3^+ thymocytes than non-Tg mice throughout the time course, indicating that *Bcl-2* transgene impairs the formation of nascent active caspase 3^+ thymocytes.

iii) Delineation of active caspase 3^+ thymocytes into $CD69^+$ $CD5^+$ and $CD69^-$ $CD5^-$ subsets

Active caspase 3^+ thymocytes from Nur77-GFP reporter mice were subdivided into $CD69^+$ $CD5^+$ and $CD69^-$ $CD5^-$ subsets, with high and low expression of GFP, respectively (Stritesky et al., 2013). The $CD69^+$ $CD5^+$ subset was a mixture of DP and CD4SP cells, whereas the $CD69^-$ $CD5^-$ subset was mostly DP cells. As these observations strongly suggest that the $CD69^+$ $CD5^+$ subset has undergone TCR-signalling but the $CD69^-$ $CD5^-$ subset has not, the authors concluded that the two active caspase 3^+ subsets are undergoing apoptosis by deletion and apoptosis by neglect, respectively (Stritesky et al., 2013). Among the active caspase 3^+ thymocytes in non-Tg mice, $CD69^-$ $CD5^-$ cells outnumbered $CD69^+$ $CD5^+$ cells by ~2-fold (Fig. 4.10A, B). This was not observed in *Bcl-2* Tg mice, in which the $CD69^+$ $CD5^+$ and $CD69^-$ $CD5^-$ subsets were approximately equal to each other in frequency (Fig. 4.10B). The absolute numbers of active caspase 3^+ thymocytes in both subsets defined by CD69 and CD5 were significantly higher in non-Tg mice than in *Bcl-2* Tg mice (Fig. 4.10B).

iv) Appearances of the $CD69^+$ $CD5^+$ and $CD69^-$ $CD5^-$ subsets of active caspase 3^+ thymocytes peak at a similar time after DNA synthesis

To track the appearance of apoptosis-committed thymocytes with TCR-signalled and TCR-unsignalled populations over time after DNA synthesis, the nascent EdU^+ active caspase 3^+ population was analysed for CD69 and CD5 (Fig. 4.11A). In non-Tg mice, $CD69^+$ $CD5^+$ cells made up <3% of EdU^+ active caspase 3^+ thymocytes at 1 hour after EdU injection, but this frequency increased sharply to ~40% at 1-2 days after EdU injection (Fig. 4.11B, left). This parameter decreased to 18.6% at 3 days after EdU injection, followed by a progressive increase between 4 and 7 days after EdU injection, reaching a second peak of ~50% at the day 7 time point (Fig. 4.11B, left). In absolute cell number terms, the data suggest that only ~70 EdU^+ active caspase 3^+ $CD69^+$ $CD5^+$ thymocytes were present in the thymus 1 hour after EdU injection, whereas 3.0×10^4 such cells were present at 2-3 days after EdU injection (Fig. 4.11B, right). The number

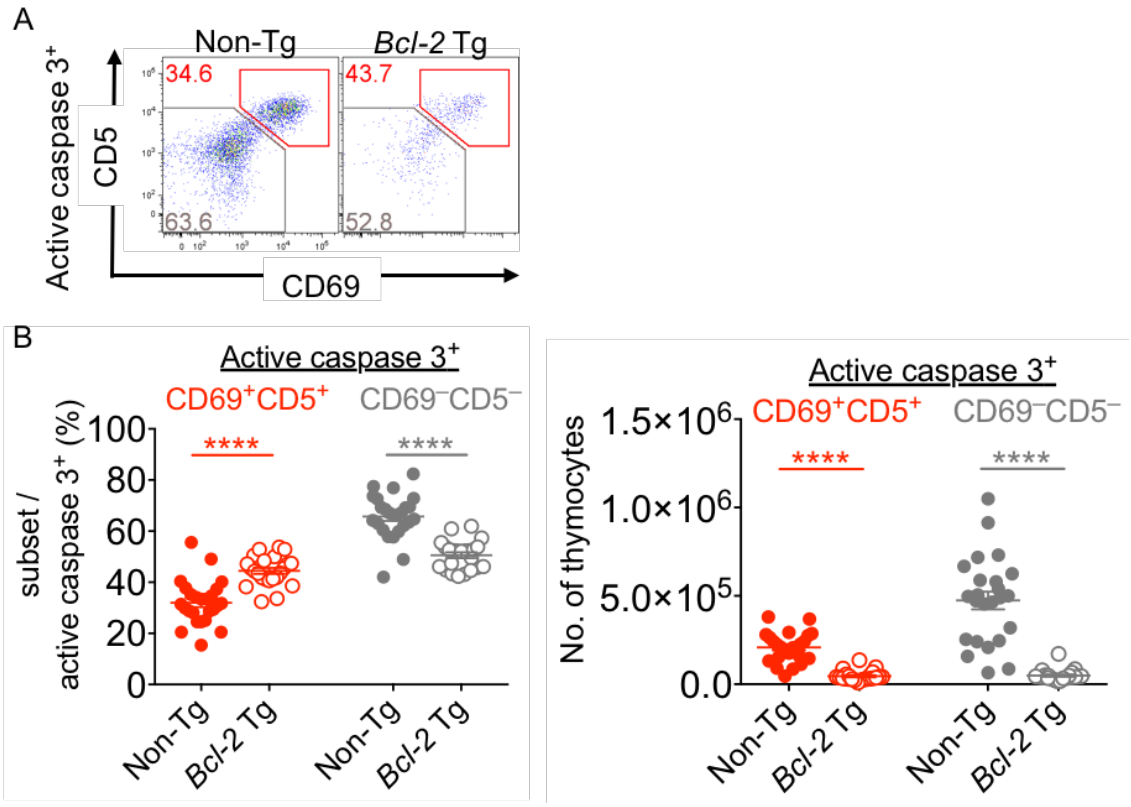

Figure 4.10. Delineation of active caspase 3$^+$ thymocytes into CD5$^+$ CD69$^+$ and CD5$^-$ CD69$^-$ subsets in steady state. (A) Active caspase 3$^+$ thymocytes were analysed for CD69/CD5 expression in non-Tg (n = 25) and *Bcl-2* Tg (n = 23) mice. (B) Summaries show the frequency of CD69$^+$CD5$^+$ (red) and CD69$^-$CD5$^-$ (grey) among active caspase 3$^+$ thymocytes (left), and the number of active caspase 3$^+$ thymocytes in each of the two subsets (right). Data were compiled from 1 experiment, and were representative of four experiments. Lines represent mean. Statistical analyses used unpaired Student's t-test; P value symbol: **** <0.0001.

decreased to fewer than 5.0×10^3 cells at 4-5 days after EdU injection, and fewer than 1.0×10^3 cells at 6-7 days after EdU injection (Fig. 4.11B, right). These data suggest that death by deletion peaks during the interval 2-3 days after DNA synthesis.

In non-Tg mice the number of the active caspase 3^+ $CD69^-$ $CD5^-$ thymocytes peaked at 1.3×10^5 cells 3 days after EdU injection, more than 3-fold higher than the number of these cells detected at 2 days after EdU injection (Fig. 4.11C, right). This suggests that death by neglect peaks at day 3 after DNA synthesis. The data also suggest that death by neglect is more synchronous than death by deletion.

In *Bcl-2* Tg mice, the frequency of $CD69^+$ $CD5^+$ cells within the active caspase 3^+ population was ~20% at 1 to 2 days after EdU injection, ~55% at 2 to 4 days, and declined progressively from 4 to 7 days after EdU injection to 25% (Fig. 4.11B, left). In *Bcl-2* Tg mice, the number of active caspase 3^+ $CD69^+$ $CD5^+$ thymocytes increased from ~200 at 1 hour after EdU injection to peak at 9×10^3 at 3 days after EdU injection (Fig. 4.11B, right). This number was maintained between 3 and 6 days after EdU, and declined only at 7 days after EdU injection (Fig. 4.11B, right). The number of active caspase 3^+ $CD69^-$ $CD5^-$ thymocytes increased from ~500 at 1 hour after EdU injection to 4.5×10^3 at 1 day after EdU injection, maintained at a similar number up to 6 days, and declined at 7 days after EdU injection (Fig. 4.11C, right).

Compared to non-Tg mice, *Bcl-2* Tg mice had fewer EdU^+ active caspase 3^+ thymocytes in both subsets between 1 to 4 days after EdU injection, but the reverse was true at 6 days after EdU injection (Fig. 4.11B, C, right). This suggests that *Bcl-2* transgene prolongs the life span of thymocytes before they undergo apoptosis by deletion or by neglect.

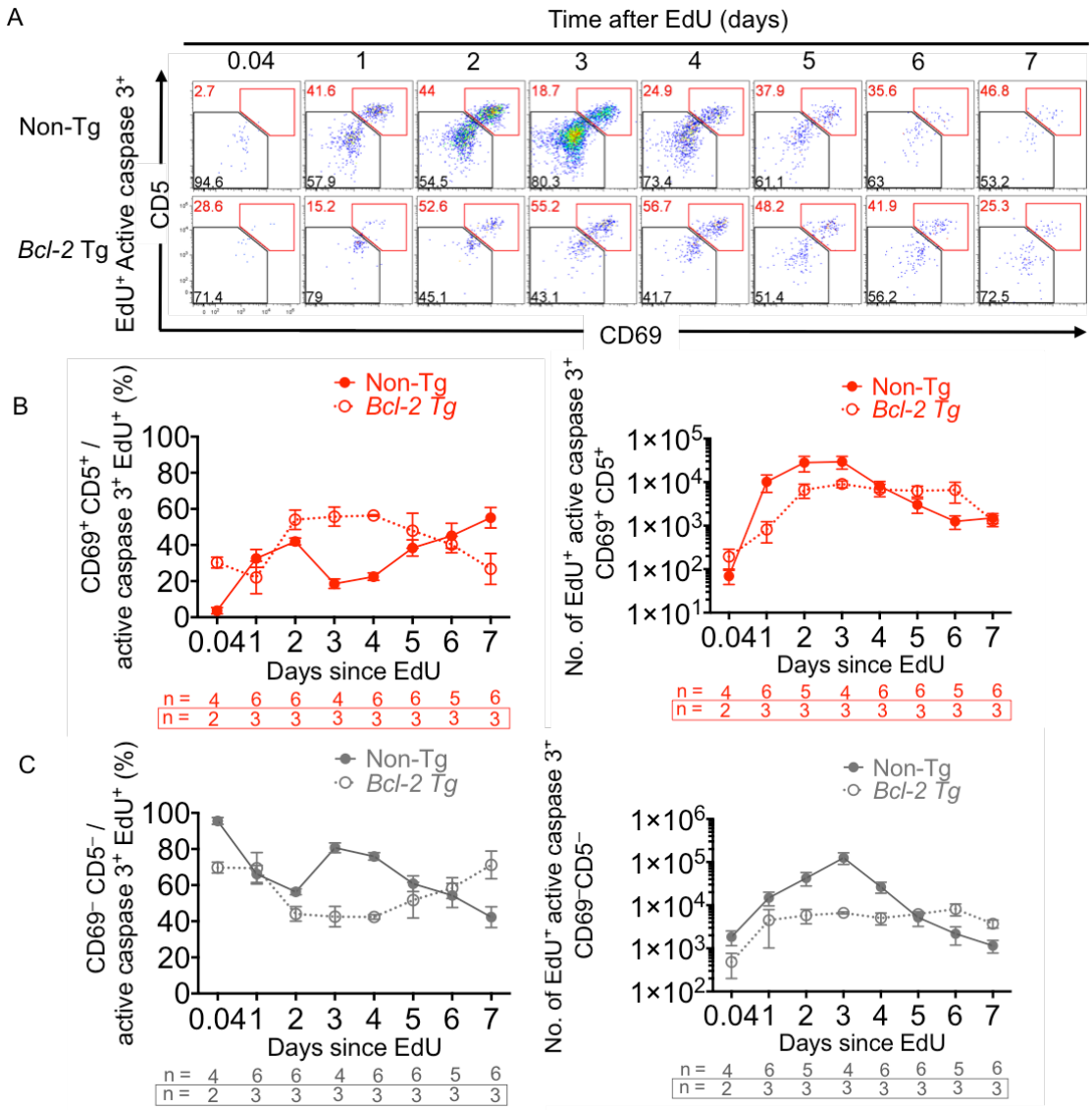

Figure 4.11. Appearance of active caspase 3$^+$ thymocyte subsets over time after DNA synthesis. In the EdU time course experiment described in Fig. 4.9, (A) EdU$^+$ active caspase 3$^+$ thymocytes were divided into CD69$^+$ CD5$^+$ (red) and CD69$^-$ CD5$^-$ (grey) subsets. (B) Summaries show the frequency of CD69$^+$ CD5$^+$ cells among active caspase 3$^+$ population (left), and the number of active caspase 3$^+$ CD69$^+$ CD5$^+$ thymocytes (right), in non-Tg (solid line) and *Bcl-2* Tg mice (dotted line). (C) Summaries show the frequency of CD69$^-$ CD5$^-$ cells among active caspase 3$^+$ population (left), and the number of active caspase 3$^+$ CD69$^-$ CD5$^-$ thymocytes (right). Data were compiled from two independent experiments in non-Tg mice (n = 4-6 per group), and one experiment for *Bcl-2* Tg mice (n = 2-3 per group). Symbols and error bars represent mean and SEM.

v) Within the EdU$^+$ active caspase 3$^+$ population, CD69$^-$ CD5$^-$ thymocytes commonly retain a DP phenotype, whereas CD69$^+$ CD5$^+$ thymocytes commonly attain non-DP phenotypes

To characterise phenotypes of TCR-signalled and TCR-unsignalled thymocytes committing to apoptosis over time, CD69$^-$ CD5$^-$ (Fig. 4.12A) and CD69$^+$ CD5$^+$ (Fig. 4.13A) subsets within the EdU$^+$ active caspase 3$^+$ population were analysed for CD4 and CD8 expression from 1 to 7 days after EdU injection. Data for the 1-hour time point after EdU injection was excluded as there were too few events to draw robust conclusions (Fig. 4.11A). The CD69$^-$ CD5$^-$ subset maintained a large proportion of DP cells (>60%) in both non-Tg (Fig. 4.12B) and *Bcl-2* Tg mice (Fig. 4.12C) throughout the time course. Each non-DP population constituted <20% of the CD69$^-$ CD5$^-$ subset throughout the time course in both non-Tg mice and *Bcl-2* Tg mice (Fig. 4.12B and C, respectively). These findings suggest that apoptotic thymocytes without a TCR-signal typically have a DP phenotype, consistent with the phenotype of thymocytes undergoing death by neglect (Stritesky et al., 2013).

The CD69$^+$ CD5$^+$ subset was more phenotypically heterogeneous than the CD69$^-$ CD5$^-$ subset. In non-Tg mice, among EdU$^+$ active caspase 3$^+$ CD69$^+$ CD5$^+$ thymocytes, the CD4SP frequency increased from 17% at 1 day to 62% at 5 days after EdU injection (Fig. 4.13B). In *Bcl-2* Tg mice, the CD4SP frequency was consistently the highest from 1 to 6 days after EdU injection, ranging from 36% to 48% (Fig. 4.13C). The rest of the non-CD4SP populations each constituted between 10% and 40% of the CD69$^+$ CD5$^+$ subset in both non-Tg mice and *Bcl-2* Tg mice (Fig. 4.13B and C, respectively). These data demonstrate that TCR-signalled apoptotic thymocytes are phenotypically heterogeneous compared to TCR-unsignalled apoptotic thymocytes, providing evidence that TCR-signalled thymocytes can undergo apoptosis at multiple stages of T cell development.

vi) CD69$^+$ CD5$^+$ thymocytes have higher TCRβ expression than CD69$^-$ CD5$^-$ thymocytes within the EdU$^+$ active caspase 3$^+$ population

As another measure of the maturity of CD69$^-$ CD5$^-$ and CD69$^+$ CD5$^+$ subsets within the EdU$^+$ active caspase 3$^+$ population, TCRβ expression was examined. TCRβ expression within the CD69$^-$ CD5$^-$ subset was consistently low throughout the time course, and was lower than TCRβ expression within the CD69$^+$ CD5$^+$ subset throughout the time course in both non-Tg and *Bcl-2* Tg mice (Fig. 4.14). In both non-Tg and *Bcl-2* Tg mice, TCRβ expression within the CD69$^+$ CD5$^+$ subset increased steadily throughout the time

course up to 6 days after EdU injection (Fig. 4.14B). The finding that CD69^{+} CD5^{+} thymocytes had low TCRβ expression at 1 day after EdU injection (Fig. 4.14B) excludes the possibility that these thymocytes incorporated EdU during pre-emigration proliferation (Pénit and Vasseur, 1997).

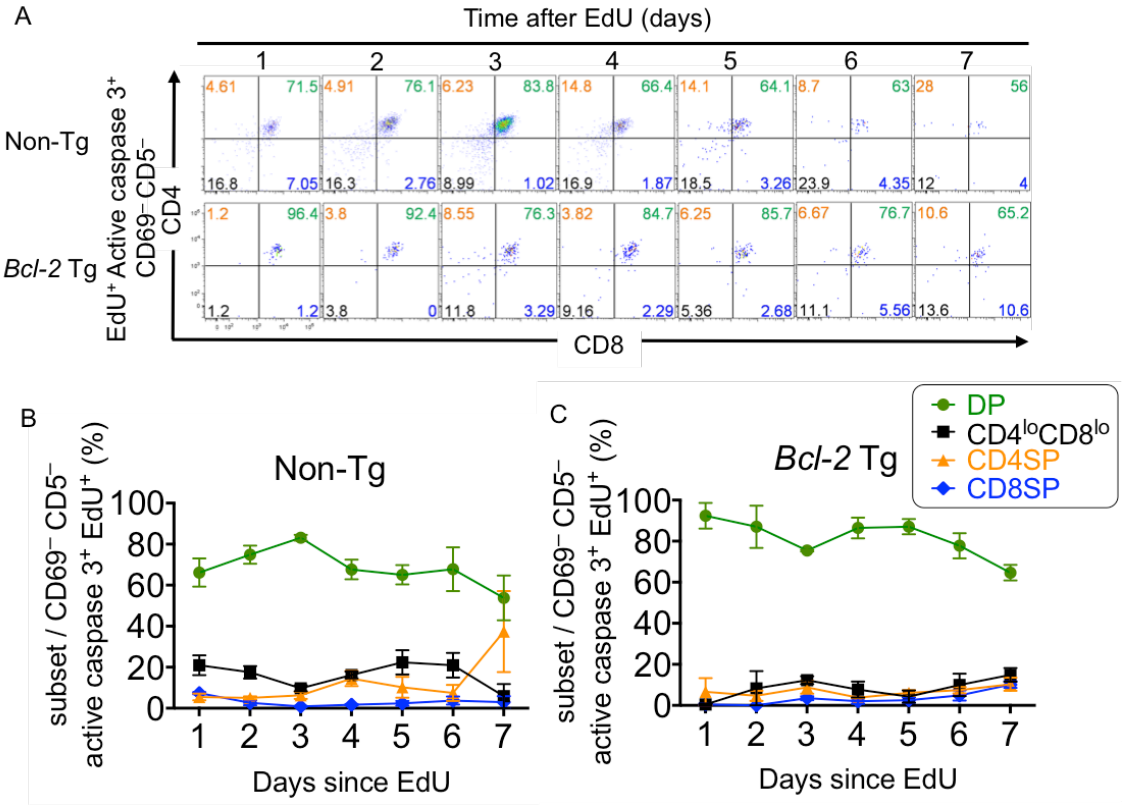

Figure 4.12. Retention of DP phenotype is common in active caspase 3^{+} CD69^{-} CD5^{-} thymocytes. In the EdU time course experiment described in Fig. 4.9, (A) EdU^{+} active caspase 3^{+} CD69^{-} CD5^{-} thymocytes were analysed for CD4/CD8 over time after EdU injection. (B) Summaries show the frequency of DP (green), CD4^{lo}CD8^{lo} (black), CD4SP (orange) and CD8SP (blue) subsets over time after EdU injection. Data were compiled from one experiment with a total of n = 3 mice per group, except n = 2 mice for 7 day after EdU in non-Tg mice. Symbols and error bars represent mean and SEM.

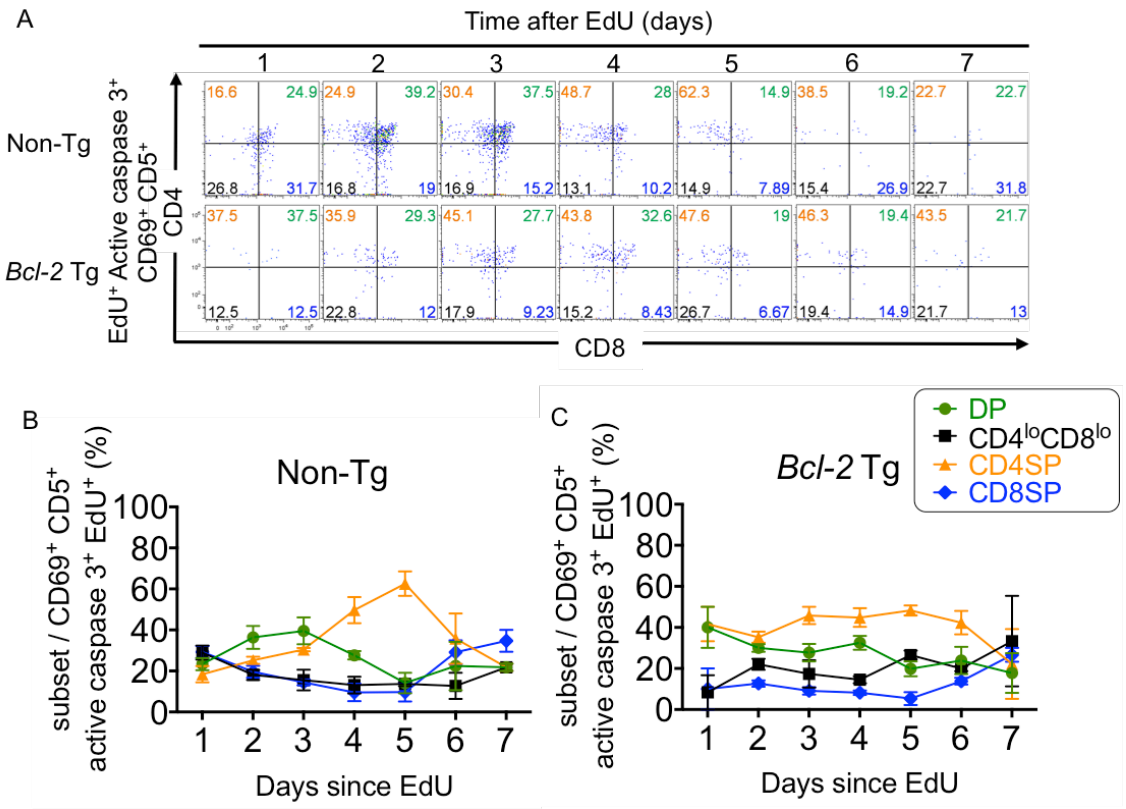

Figure 4.13. Attainment of non-DP phenotypes is common in active caspase 3$^+$ CD69$^+$ CD5$^+$ thymocytes. In the EdU time course experiment described in Fig. 4.9, (A) EdU$^+$ active caspase 3$^+$ CD69$^+$ CD5$^+$ thymocytes were analysed for CD4/CD8 over time after EdU injection. (B) Summaries show the frequency of DP (green), CD4^{lo}CD8^{lo} (black), CD4SP (orange) and CD8SP (blue) subsets over time after EdU injection. Data were compiled from one experiment with a total of n = 3 mice per group, except n = 2 mice for 1 day after EdU in *Bcl-2* Tg mice and 7 days after EdU injection in non-Tg mice. Symbols and error bars represent mean and SEM.

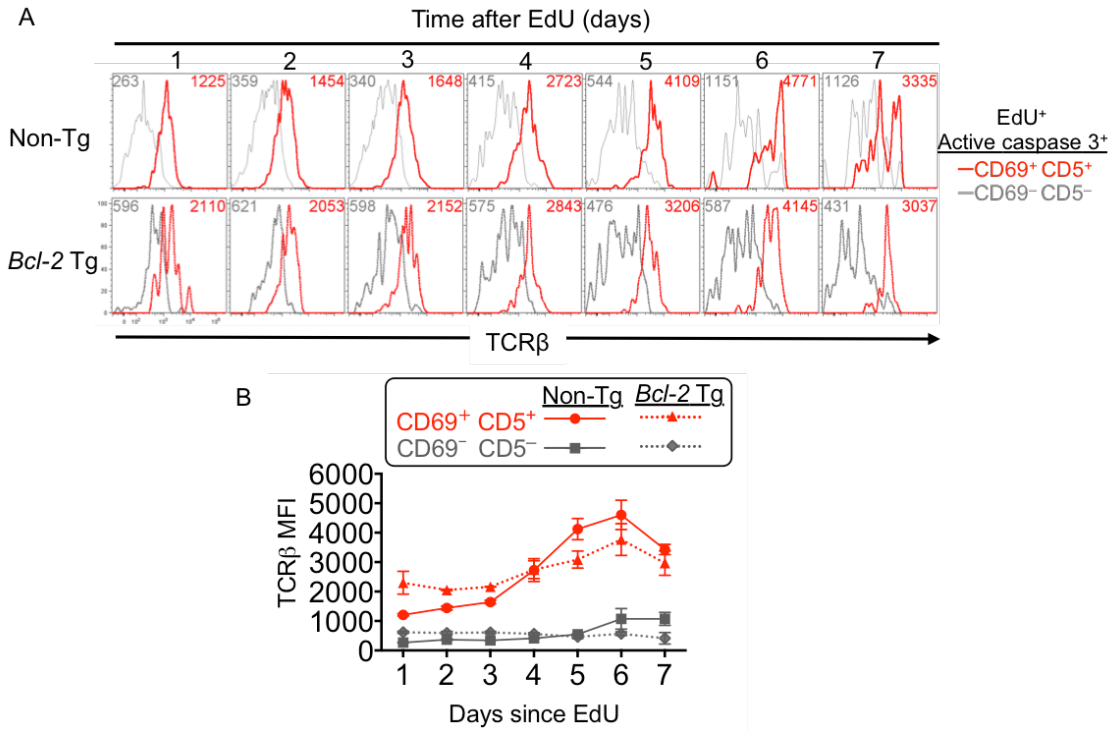

Figure 4.14. TCRβ expression is higher in CD69$^+$ CD5$^+$ thymocytes than CD69$^-$ CD5$^-$ thymocytes within the EdU$^+$ active caspase 3$^+$ population. In the EdU time course experiment described in Fig. 4.9, (A) CD69$^-$ CD5$^-$ (grey) and CD69$^+$ CD5$^+$ (red) subsets of EdU$^+$ active caspase 3$^+$ thymocytes were analysed for TCRβ expression, with numbers indicating the MFIs of TCRβ expression. (B) Summaries show the MFIs of TCRβ expression in the two subsets of EdU$^+$ active caspase 3$^+$ thymocytes. Data were compiled from one experiment with a total of n = 3 mice per group, except n = 2 mice for 1 day after EdU in *Bcl-2* Tg mice and 7 days after EdU injection in non-Tg mice. Symbols and error bars represent mean and SEM.

4.4.2 Contributions of MHCI and/or MHCII to TCR-signalling and apoptosis in the natural thymocyte repertoire

The aim of this chapter is to investigate the mechanism underlying the numerical imbalance between $CD4^+$ and $CD8^+$ T cells. This investigation requires a method to count thymocytes that initiate T cell development. The results above establish such a method by demonstrating that a $TCR\beta^+$ $CD5^+$ phenotype marks the TCR-signalled subset of nascent thymocytes labelled with EdU. The investigation also requires a method to count thymocytes that die between the initiation and completion of T cell development in the thymus. The results above suggest a method to estimate this variable, based on evidence that an active caspase 3^+ $CD69^+$ $CD5^+$ phenotype marks apoptosis-committed thymocytes that have received a TCR signal.

The results above also reveal similarities and differences between non-Tg and *Bcl-2* Tg mice. First, as in non-Tg mice, a $TCR\beta^+$ $CD5^+$ phenotype marks TCR-signalled thymocytes in *Bcl-2* Tg mice. Second, $Helios^+$ cells within the TCR-signalled population are normally susceptible to apoptosis in non-Tg mice but these cells persist (at least transiently) in the thymus of *Bcl-2* Tg mice, allowing them to be included in calculation of the TCR-signalled subset. Third, while consistent with perturbed apoptosis in *Bcl-2* Tg mice, the low number of active caspase 3^+ thymocytes in *Bcl-2* Tg mice limits the use of this marker in apoptosis-defective mice. Fourth, the time course suggested that *Bcl-2* transgene expression blunts thymocyte proliferation and prolongs thymocyte lifespan, especially in the TCR-unsignalled subset; however, the percentages and numbers of EdU^+ thymocytes in non-Tg and *Bcl-2* Tg mice were similar at 3 days after EdU injection. At this time point, a substantial fraction of the EdU^+ cohort had attained a $TCR\beta^+$ $CD5^+$ phenotype, establishing that 3 days is sufficient time to allow MHC-dependent TCR-signalling to be induced in nascent thymocytes. Finally, in non-Tg mice the EdU^+ thymocyte frequency dropped sharply between 3 and 4 days after EdU injection, indicating that the nascent thymocyte cohort shrinks markedly during this interval. For these reasons, in subsequent experiments thymocytes were analysed 3 days after EdU injection, and the non-Tg mice and *Bcl-2* Tg mice are analysed separately, providing related but distinct information on the requirements for each MHC class in inducing TCR signalling in thymocytes.

The section below investigates the fractions of the nascent natural thymocyte repertoire that require MHCI and/or MHCII (i) to perceive TCR-signalling or (ii) commit to apoptosis after receiving a TCR-signal. It concludes by using Helios and CCR7 to subdivide the TCR-signalled thymocyte cohorts into fractions that have received a

strong or weak TCR signal.

4.2.2.1 Role of MHC classes in inducing apoptosis-committed thymocytes

i) Similar frequencies of apoptosis-committed TCR-signalled thymocytes in the absence of MHCI or MHCII

The experiments below examined eight groups of mice: (1) wild-type (MHC-sufficient), (2) *B2m*$^{-/-}$ (absence of beta-2 microglobulin, also referred to as MHCI-deficient), (3) *H2-Aa*$^{-/-}$ (absence of histocompatibility 2, class II antigen A, alpha; also referred to as MHCII-deficient) and (4) *B2m*$^{-/-}$*H2-Aa*$^{-/-}$ (also referred to as MHC-deficient). Groups 5-8 were identical to groups 1-4, except that they carried the *Bcl-2* transgene. Some experiments included a ninth group consisting of *Tcra*$^{-/-}$ mice (lacking αβ TCR expression).

In steady state, the mean frequency of active caspase 3^{+} thymocytes was similar in the panel of non-Tg mice, except for *B2m*$^{-/-}$*H2-Aa*$^{-/-}$ mice, which had a small but statistically significant increase compared to wild-type mice (Fig. 4.15B). Within the panel of *Bcl-2* Tg mice, the mean frequency of active casapse 3^{+} thymocytes was similar across all groups, but it was ~4-fold lower than non-Tg mice (Fig. 4.15C). These data indicate that MHC expression does not markedly alter the frequency of apoptosis-committed thymocytes.

To confine the analysis to nascent thymocytes, the nine groups of mice were injected with EdU 3 days before analysis. Uninjected mice were analysed in parallel to ensure that detection of EdU^{+} thymocytes was specific (Fig. 4.16A). The frequency of EdU^{+} events among all thymocytes was similar across groups in non-Tg and *Bcl-2* Tg mice (Fig. 4.16B), suggesting that MHCI- and/or MHCII-deficiency does not markedly alter overall thymocyte turnover.

Among the EdU^{+} population in non-Tg mice, *B2m*$^{-/-}$*H2-Aa*$^{-/-}$ mice had a significantly higher mean frequency of active caspase 3^{+} thymocytes at 2.08% than wild-type mice at 1.06% (Fig. 4.17B, left). Although not statistically significant, *B2m*$^{-/-}$ and *H2-Aa*$^{-/-}$ mice had slightly higher active caspase 3^{+} frequencies compared to wild-type mice, both at 1.4% (Fig. 4.17B, left). These observations mirrored the results found in steady state within the panel of non-Tg mice (Fig. 4.15B, left). Among all thymocytes, the

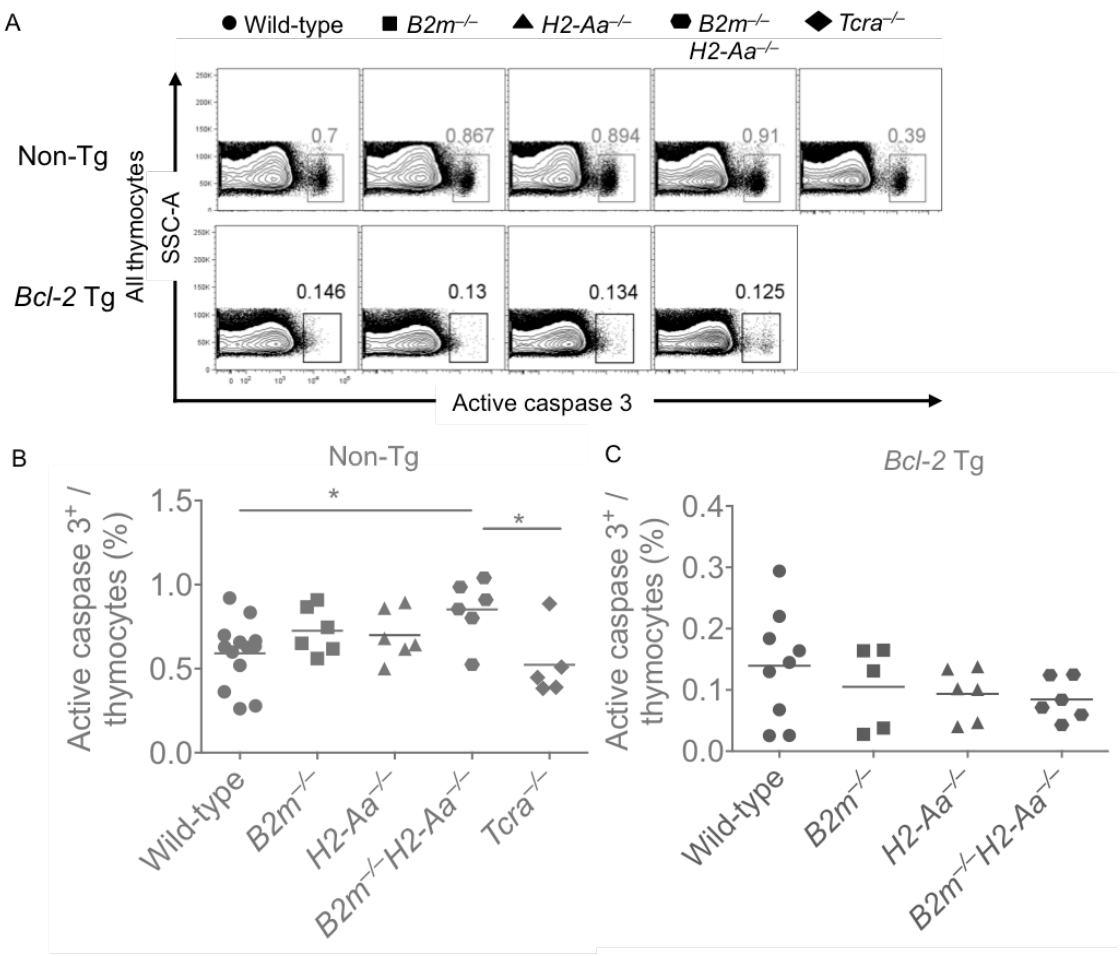

Figure 4.15. Normal active caspase 3$^+$ thymocyte frequency in the absence of MHCI or MHCII expression in steady state. (A) All thymocytes in non-Tg mice and *Bcl-2* Tg mice of the following groups: MHC wild-type, *B2m*$^{-/-}$ (MHCI$^{-/-}$), *H2-Aa*$^{-/-}$ (MHCII$^{-/-}$), *B2m*$^{-/-}$*H2-Aa*$^{-/-}$ and *Tcra*$^{-/-}$ were analysed for active caspase 3 expression. Summaries show the frequency of active caspase 3$^+$ events among all thymocytes in non-Tg mice (B) and *Bcl-2* Tg mice (C). Data were compiled from three independent experiments with a total of n = 5-13 mice per group; each symbol represents 1 mouse. Lines represent mean. Statistical analyses used 1-way ANOVA and Tukey's post-tests; P value symbol: * <0.05.

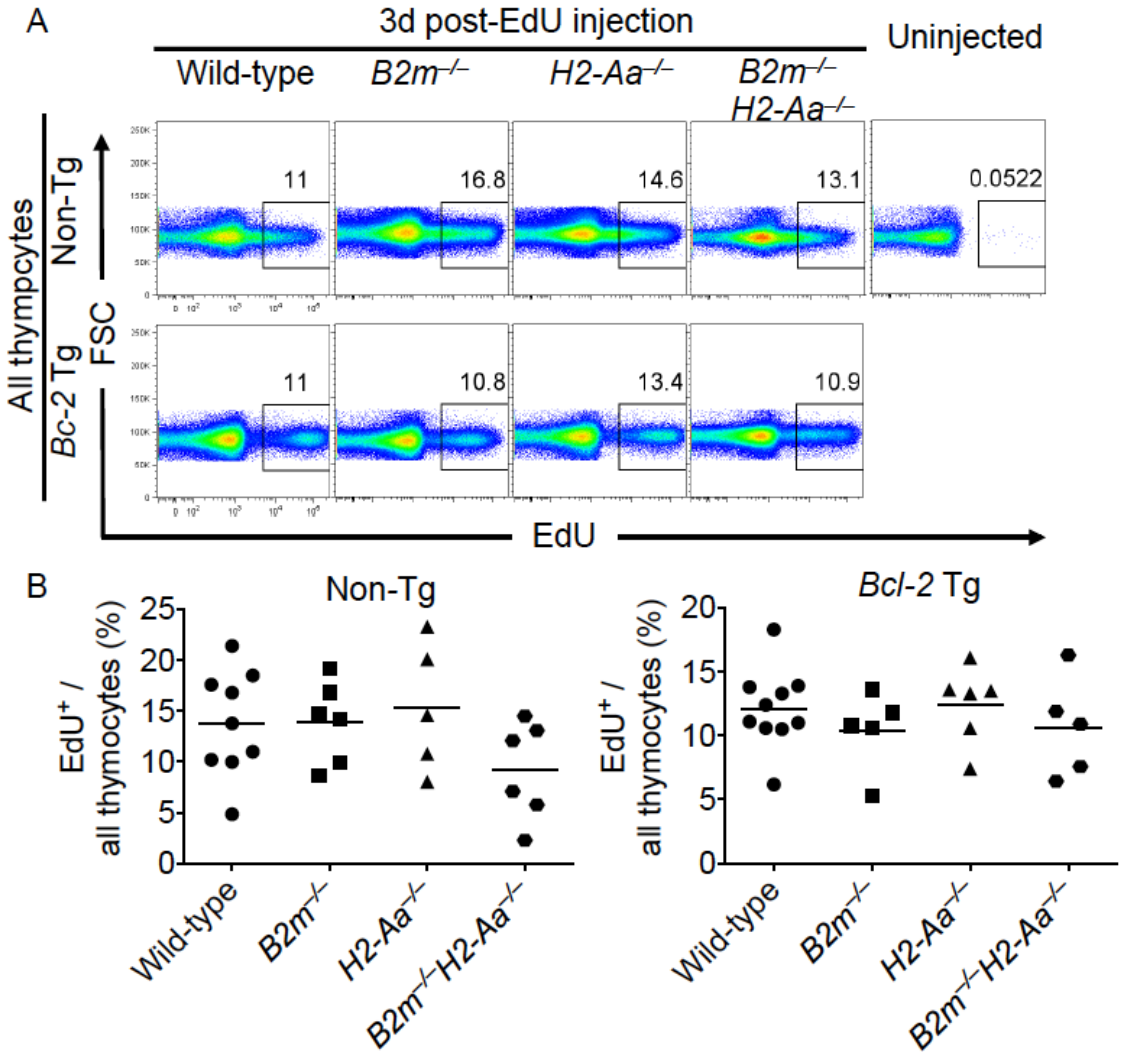

Figure 4.16. Absence of MHCI or MHCII expression does not obviously alter the turnover of nascent thymocytes. Nine groups of mice described in Fig. 4.15 were injected with EdU three days prior to flow cytometric analyses of thymocytes. (A) Representative FCS/EdU plots show all thymocytes with a gate for EdU^+ events, using the staining of samples from uninjected control mice to aid gate placement. (B) Summaries show the frequency of EdU^+ thymocytes for the indicated mouse genotypes; each symbol represents 1 mouse. A total of n = 5-10 mice per group compiled from three independent experiments. Lines represent mean. 1-way ANOVA and Tukey's post-tests revealed non-significant P values in all comparison groups.

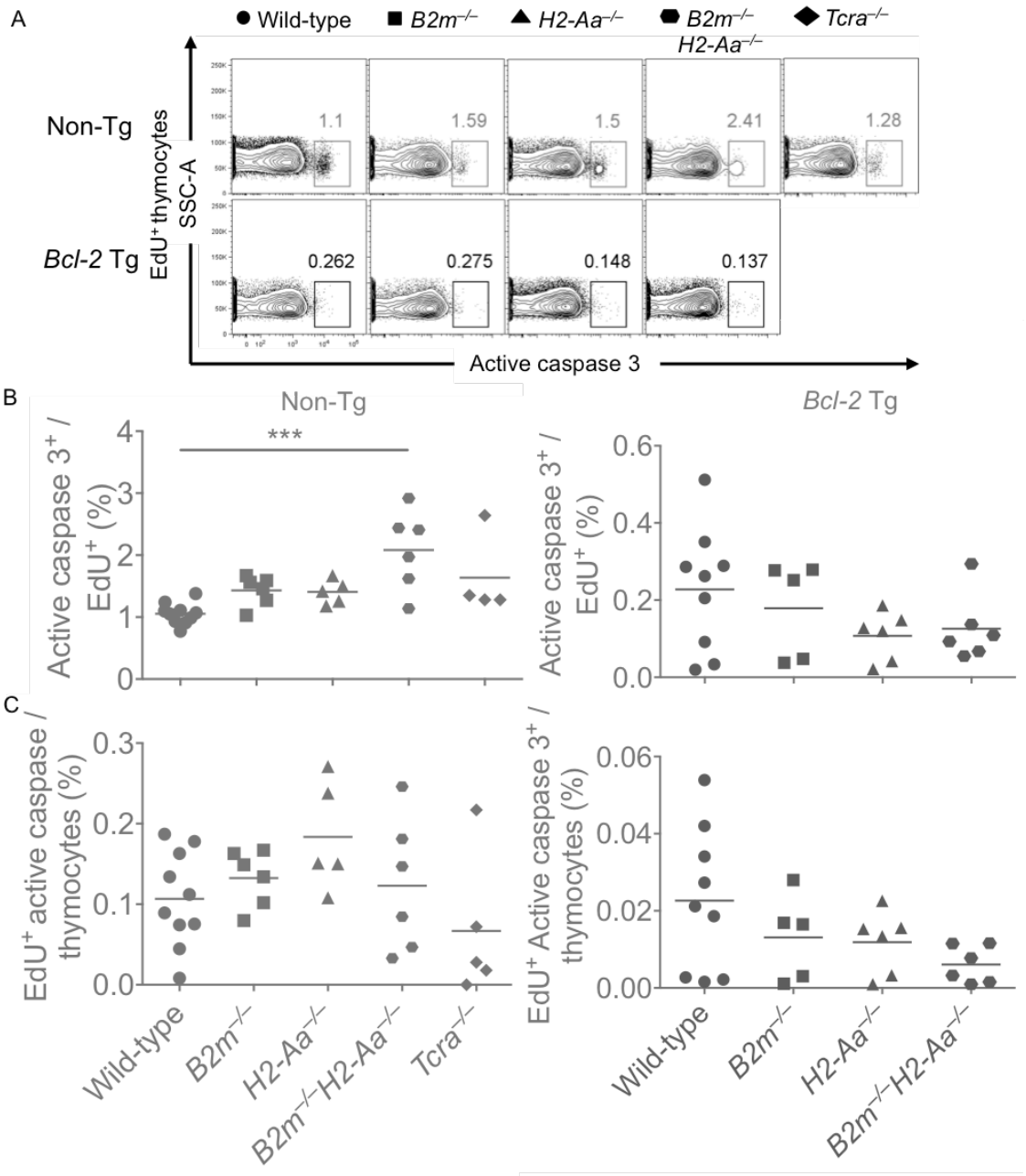

Figure 4.17. Normal formation of nascent active caspase 3$^+$ thymocytes in the absence of MHCI or MHCII expression. (A) EdU$^+$ thymocytes from Fig. 4.16 were analysed for active caspase 3$^+$ expression. Summaries show the frequency of (B) active caspase 3$^+$ events among EdU$^+$ thymocytes as gated in the representative plots, and (C) EdU$^+$ active caspase 3$^+$ among all thymocytes for the indicated mouse genotypes; each symbol represents 1 mouse, compiled from three independent experiments. Lines represent mean. (B, C) Statistical analyses used 1-way ANOVA and Tukey's post-tests; P value symbol: *** <0.001. (C) Non-significant in all comparison groups.

frequency of EdU$^+$ active caspase 3$^+$ cells in *B2m*$^{-/-}$ and *H2-Aa*$^{-/-}$ mice were also slightly higher than wild-type mice (Fig. 4.17C, left).

In *Bcl-2* Tg mice, the frequency of active caspase 3$^+$ cells among EdU$^+$ cells was similar across all groups (Fig. 4.17B, right), but it was 5 to 16-fold lower than observed in the panel of non-Tg mice (Fig. 4.17B, left). Consistent with the finding observed in steady state, overexpression of Bcl-2 anti-apoptotic molecule in mice inhibits the formation of active caspase 3$^+$ thymocytes at 3 days after EdU injection. Due to the low number of relevant events acquired, *Bcl-2* Tg mice were excluded from the subsequent analysis as robust conclusions could not be drawn. Overall, the phenotype and frequency of apoptosis-committed thymocytes within the nascent cohort were similar to the observations in steady state.

ii) MHC and αβ TCR expression are required for thymocytes to attain an active caspase 3/CD69/CD5$^+$ phenotype

In steady state, the mean CD69$^+$ CD5$^+$ cell frequency among active caspase 3$^+$ thymocytes was 16% in wild-type mice, whereas this parameter was <0.9% in *B2m*$^{-/-}$ *H2-Aa*$^{-/-}$ mice and *Tcra*$^{-/-}$ mice (Fig. 4.18B, left). A similar result was observed when the analysis was confined to EdU$^+$ thymocytes (Fig. 4.18C, left). The mean CD69$^-$ CD5$^-$ cell frequency among active caspase 3$^+$ thymocytes in steady state and in EdU$^+$ thymocytes was >98% in *B2m*$^{-/-}$*H2-Aa*$^{-/-}$ mice and *Tcra*$^{-/-}$ mice, compared to 81-85% in wild-type mice (Fig. 4.18D, E left). These data indicate that nearly all active caspase 3$^+$ CD69$^+$ CD5$^+$ thymocytes have received a signal that requires MHC and αβ TCR expression.

iii) Single deficiency of MHCI or MHCII reduces active caspase 3/CD69/CD5$^+$ thymocytes by similar amounts

B2m$^{-/-}$ mice and *H2-Aa*$^{-/-}$ mice were examined to test for a selective effect of MHCI or MHCII (Fig. 4.18A). In steady state, the CD69$^+$ CD5$^+$ cell frequency in the active caspase 3$^+$ population was 16.0% in wild-type, 9.4% in *B2m*$^{-/-}$ and 7.8% in *H2-Aa*$^{-/-}$ mice (Fig. 4.18B, left). Taking the wild-type measurement as 100%, there was a 41% and 51% reduction in this parameter in MHCI-deficient mice and MHCII-deficient mice, respectively. A similar trend was observed when the analysis was confined to EdU$^+$ thymocytes (Fig. 4.18C, left). There was no statistically significant difference in this parameter between *H2-Aa*$^{-/-}$ mice and *B2m*$^{-/-}$ mice in the steady state (Fig. 4.18B, left) or among EdU$^+$ thymocytes (Fig. 4.18C, left).

In steady state however, when the denominator is all thymocytes, the frequencies of active caspase 3^+ $CD69^+$ $CD5^+$ population in *B2m*$^{-/-}$ mice and *H2-Aa*$^{-/-}$ mice were not significantly different from wild-type mice (Fig. 4.18B, right). A similar result was found when the analysis was confined to EdU^+ thymocytes (Fig. 4.18C, right). This is due to the slightly higher frequencies of active caspase 3^+ thymocytes in *B2m*$^{-/-}$ mice and *H2-Aa*$^{-/-}$ mice compared to wild-type mice (Figs. 4.15B, 4.17B).

The frequency of $CD69^-$ $CD5^-$ cells among active caspase 3^+ thymocytes in steady state, and when confined to the EdU^+ population, was significantly increased in *B2m*$^{-/-}$ mice and *H2-Aa*$^{-/-}$ mice compared to wild-type mice (Fig. 4.18D, E, left). When the denominator is all thymocytes, the frequencies of active caspase 3^+ $CD69^-$ $CD5^-$ thymocytes in *B2m*$^{-/-}$ mice and *H2-Aa*$^{-/-}$ mice were not significantly different from wild-type mice (Fig. 4.18D, right), but appeared to be slightly higher than wild-type mice. A similar result was found when the analysis was confined to the EdU^+ thymocytes (Fig. 4.18E, right).

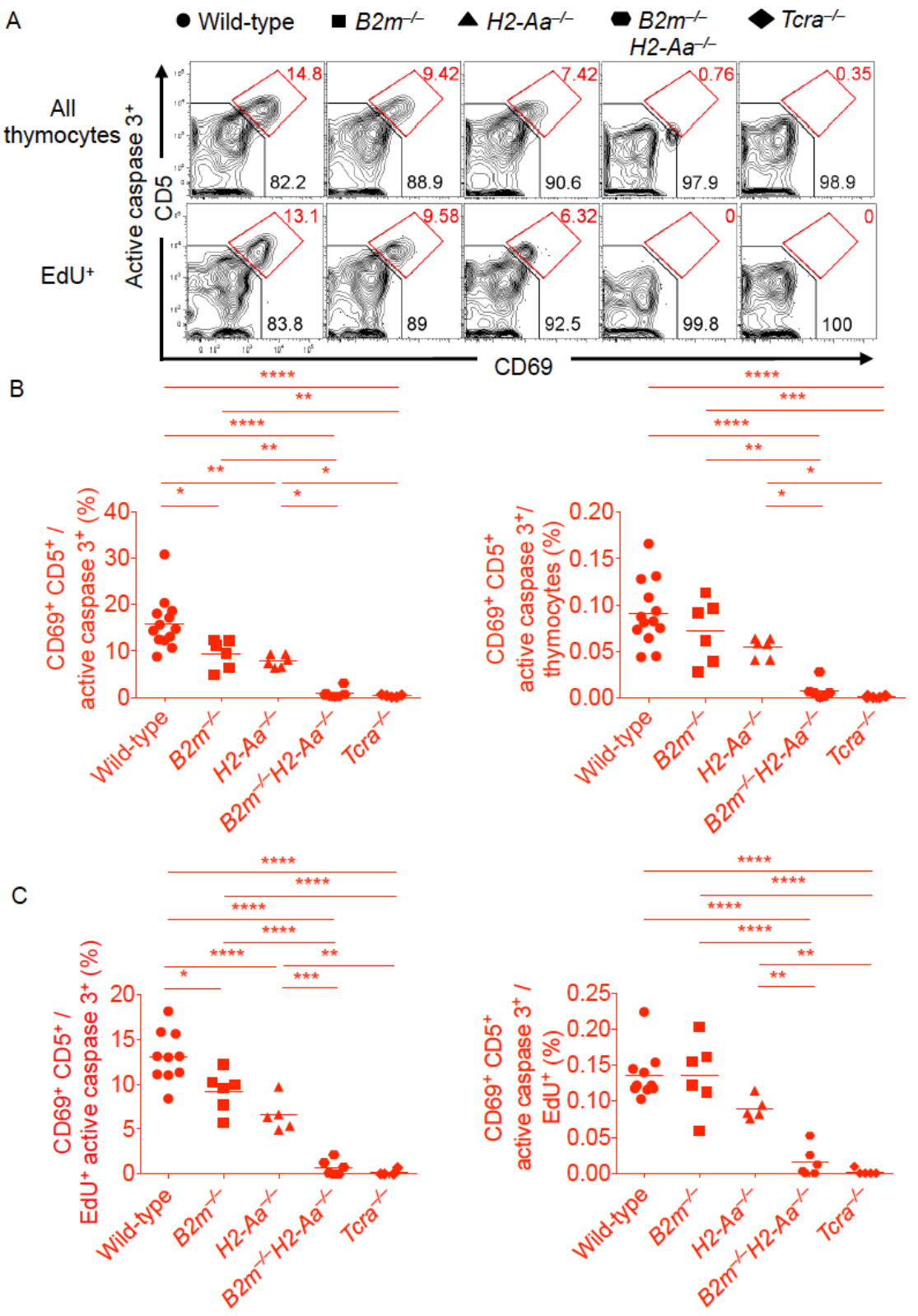
A
Wild-type
B2m−/−
H2-Aa−/−
B2m−/− H2-Aa−/−
Tcra−/−
All thymocytes
EdU+
Active caspase 3+
CD5
CD69
14.8
9.42
7.42
0.76
0.35
82.2
88.9
90.6
97.9
98.9
13.1
9.58
6.32
0
0
83.8
89
92.5
99.8
100
B
CD69+ CD5+ / active caspase 3+ (%)
CD69+ CD5+ active caspase 3+/ thymocytes (%)
C
CD69+ CD5+ / EdU+ active caspase 3+ (%)
CD69+ CD5+ active caspase 3+ / EdU+ (%)

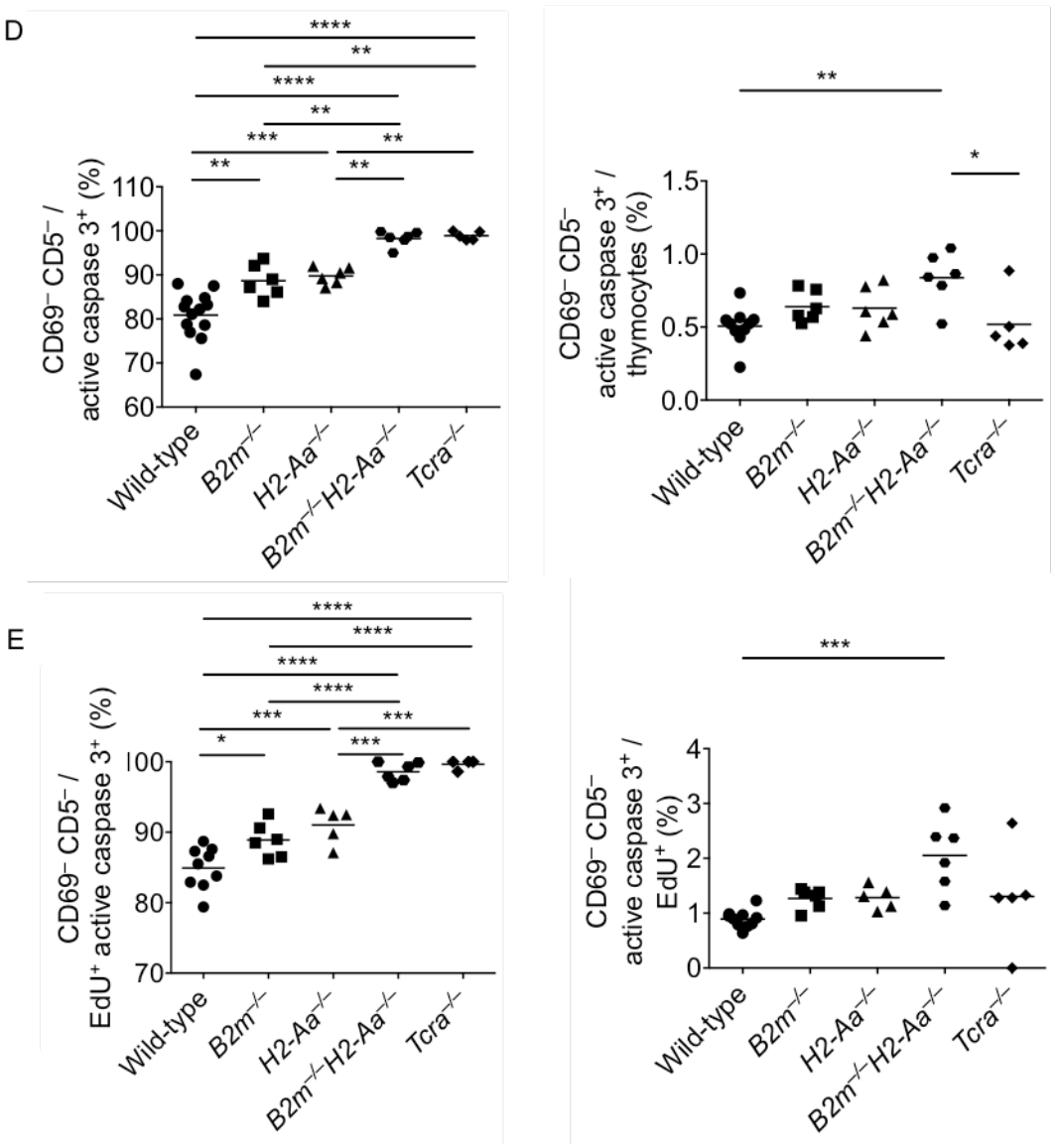

Figure 4.18. Roles for MHCI and/or MHCII in inducing CD69$^+$ CD5$^+$ and CD69$^-$ CD5$^-$ subsets of active caspase 3$^+$ thymocytes. Using the gating strategies shown in Figs. 4.16 and 4.17, (A) all (top) or EdU$^+$ (bottom) active caspase 3$^+$ thymocytes were analysed for CD69/CD5 expression. (B, C) Summaries show frequency of CD69$^+$ CD5$^+$ thymocytes in the active caspase 3$^+$ population in steady state (B, left) and in the EdU$^+$ active caspase 3$^+$ population (C, left); and frequency of CD69$^+$ CD5$^+$ active caspase 3$^+$ events among all thymocytes (B, right) or among EdU$^+$ thymocytes (C, right). (D, E) Summaries show frequency of CD69$^-$ CD5$^-$ thymocytes in the active caspase 3$^+$ population in steady state (D, left) and in the EdU$^+$ population (E, left); and frequency of CD69$^-$ CD5$^-$ active caspase 3$^+$ events among all thymocytes (D, right) or among EdU$^+$ thymocytes (E, right). Data were compiled from three independent experiments with a total of n = 5-10 mice per group. Each symbol represents 1 mouse and lines represent the group mean. Statistical analyses used 1-way ANOVA and Tukey's post-tests; P value symbols: **** <0.0001; *** <0.001; ** <0.01; * <0.05.

4.2.2.2 Effect of MHC expression on the induction of TCR-signalling in the natural thymocyte repertoire

The active caspase 3/CD69/CD5$^+$ approach (section 4.2.2.1) would be expected to capture only strongly TCR-signalled cells undergoing clonal deletion. This section examines the overall TCR signalling induction in nascent thymocytes, including weak TCR-signalling that facilitates naïve T cell development. It quantifies effects on this parameter caused by the absence of MHCI and/or MHCII expression.

i) No effect of single MHCI- or MHCII-deficiency on induction of TCR-signalled thymocytes in mice with normal apoptosis

Three days after EdU injection, EdU$^+$ thymocytes were interrogated for TCRβ^+ CD5$^+$ events as a means to enumerate TCR-signalled cells (Fig. 4.19A). In the panel of non-Tg mice (Fig. 4.19B), wild-type mice had the highest mean frequency of TCRβ^+ CD5$^+$ thymocytes at 17.3%. This parameter was reduced to <1% in *B2m*$^{-/-}$*H2-Aa*$^{-/-}$ double-deficient mice and *Tcra*$^{-/-}$ mice, demonstrating that formation of TCR-signalled cells depends largely on MHC and $\alpha\beta$ TCR expression. This parameter in *B2m*$^{-/-}$ mice (16.2%) and *H2-Aa*$^{-/-}$ mice (14.5%) was not significantly different from wild-type mice (Fig. 4.19B). Thus, in mice with normal apoptosis, there was no evidence that the absence of one MHC class alters the formation of TCRβ^+ CD5$^+$ thymocytes among the nascent cohorts 3 days after DNA synthesis.

ii) Inhibition of apoptosis reveals roles for MHCI and MHCII in inducing TCR-signalling in nascent thymocytes

In the panel of *Bcl-2* Tg mice (Fig. 4.19C), the mean frequency of TCRβ^+ CD5$^+$ thymocytes among the EdU$^+$ population was highest in wild-type mice at 22.1%, but was severely reduced to <1.5% in *B2m*$^{-/-}$*H2-Aa*$^{-/-}$ double-deficient mice. This indicates that most thymocytes within the natural TCR repertoire require β2-microglobulin or MHCII expression to receive a TCR signal, including when the thymocytes have impaired apoptosis. The same parameter was significantly reduced in *B2m*$^{-/-}$ mice (15.5%) and *H2-Aa*$^{-/-}$ (14.3%) mice, compared to wild-type mice (22.1%) (Fig. 4.19C). Taking the wild-type measurement as 100%, there was a 30% and 35% reduction in this parameter in MHCI-deficient mice and MHCII-deficient mice, respectively. As the frequency of TCR-signalled cells was decreased to a similar extent in the absence of MHCI and in the absence of MHCII compared to wild-type mice, similar fractions of the thymocyte repertoire require MHCI versus MHCII to receive a TCR signal. It is

noteworthy that the sum of TCR-signalled frequencies in the two groups expressing only one MHC class exceeds the measurement for wild-type mice.

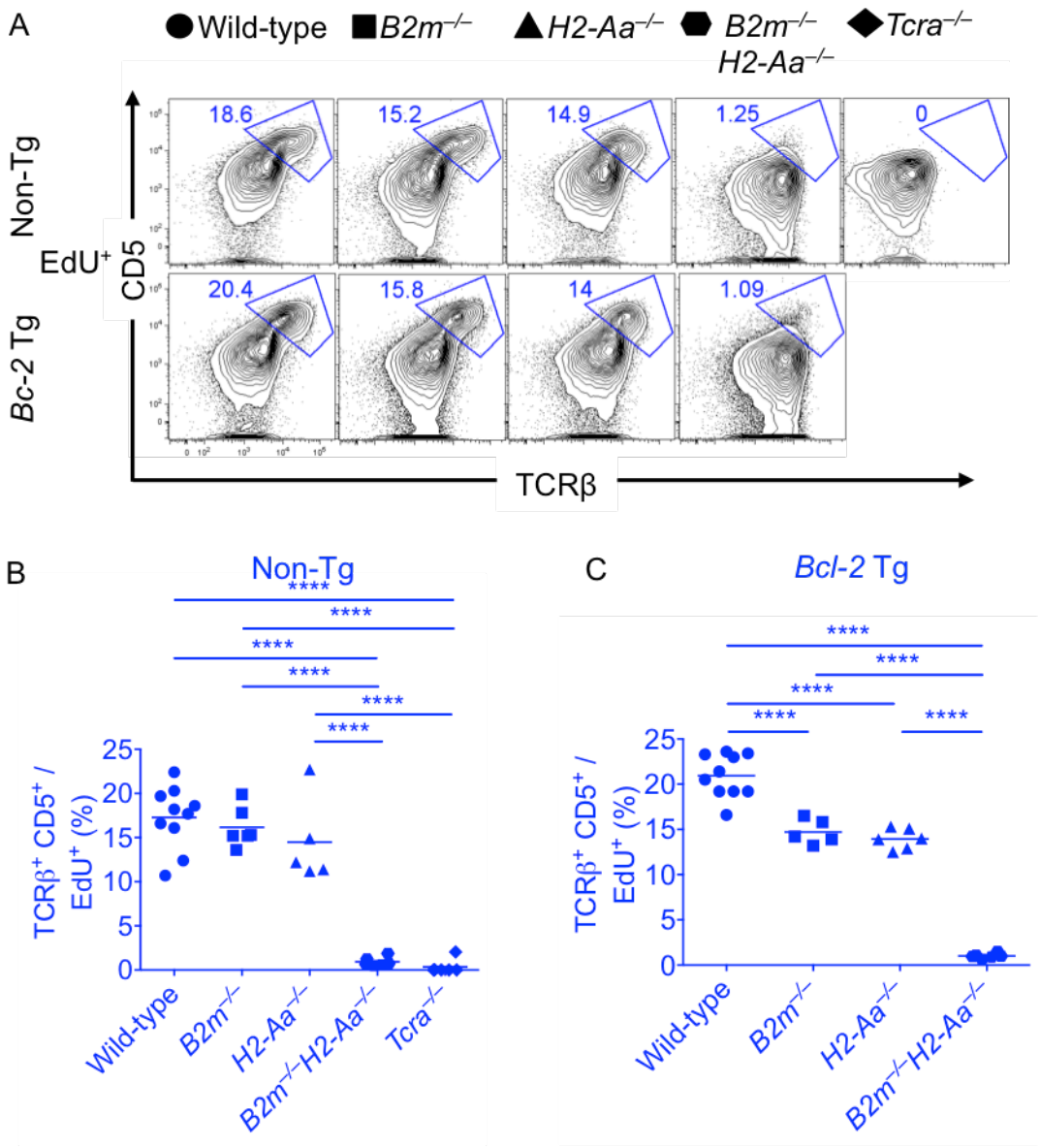

Figure 4.19. An apoptosis defect reveals that similar fractions of the natural thymocyte repertoire require MHCI versus MHCII to induce TCR-signalling. EdU^+ thymocytes gated in Fig. 4.16 were analysed for TCRβ and CD5 expression. Summaries show the frequency of $CD5^+$ $TCR\beta^+$ cells in non-Tg mice (B) and *Bcl-2* Tg mice (C). Data were compiled from three independent experiments, n = 5-10 mice per group. Lines represent mean. Statistical analyses used 1-way ANOVA and Tukey's post-tests; P value symbol: **** <0.0001.

4.2.2.3 Subdivision of nascent TCR-signalled thymocytes using Helios/CCR7 expression

As a TCRβ$^+$ CD5$^+$ phenotype marks the subset of nascent thymocytes that has received a TCR-signal, for brevity, the TCRβ$^+$ CD5$^+$ population is referred to as "TCR-signalled" in the results below. To subdivide the TCR-signalled population into strongly and weakly TCR-signalled subsets, Helios and CCR7 expression were examined. The subsets expressing Helios and/or CCR7 correspond to the populations analysed in Chapter 3. However, the Helios$^-$ CCR7$^-$ subset is different from the subset described in Chapter 3, because a TCR-signalled phenotype was a prerequisite for inclusion in the Helios$^-$ CCR7$^-$ population described below.

i) No decrease in Helios induction in apoptosis-intact mice lacking one MHC class

In the presence or absence of the *Bcl-2* transgene, *B2m*$^{-/-}$*H2-Aa*$^{-/-}$ double-deficient mice had a markedly diminished frequency of all four TCR-signalled Helios/CCR7 subsets (Fig. 4.20B, C), demonstrating that the populations of interest largely require MHC expression for their induction. In mice with normal apoptosis, the frequencies of TCR-signalled Helios$^-$ CCR7$^-$, Helios$^+$ CCR7$^-$ and Helios$^+$ CCR7$^+$ subsets among EdU$^+$ thymocytes in *B2m*$^{-/-}$ mice and *H2-Aa*$^{-/-}$ mice were not significantly different from wild-type mice (Fig. 4.20B). However, *H2-Aa*$^{-/-}$ mice had a significant decrease in Helios$^-$ CCR7$^+$ thymocytes compared to wild-type and *B2m*$^{-/-}$ mice (Fig. 4.20B). This was attributable to a marked reduction in CD4SP cells in *H2-Aa*$^{-/-}$ mice (Fig. 4.21B), consistent with the well-established requirement for MHCII in naïve CD4$^+$ T cell development. Reciprocally, few CD8SP cells were detected among TCR-signalled Helios$^-$ CCR7$^+$ cells in *B2m*$^{-/-}$ mice (Fig. 4.21B). Compared to *B2m*$^{-/-}$ mice, *H2-Aa*$^{-/-}$ mice had a small but statistically significant increase in the frequency of TCR-signalled Helios$^+$ CCR7$^-$ cells within the nascent thymocyte cohort (Fig. 4.20B).

ii) Apoptosis-defective mice reveal a greater requirement for MHCII than MHCI in Helios induction

Mice with defective apoptosis presented a different picture. The frequencies of TCR-signalled Helios$^-$ CCR7$^-$, Helios$^+$ CCR7$^+$ and Helios$^-$ CCR7$^+$ thymocytes were significantly lower in *B2m*$^{-/-}$ mice and *H2-Aa*$^{-/-}$ mice compared to wild-type mice; however, *B2m*$^{-/-}$ mice and *H2-Aa*$^{-/-}$ mice were not significantly different from each other in these parameters (Fig. 4.20C). Analysis of the TCR-signalled Helios$^-$ CCR7$^+$ cells for

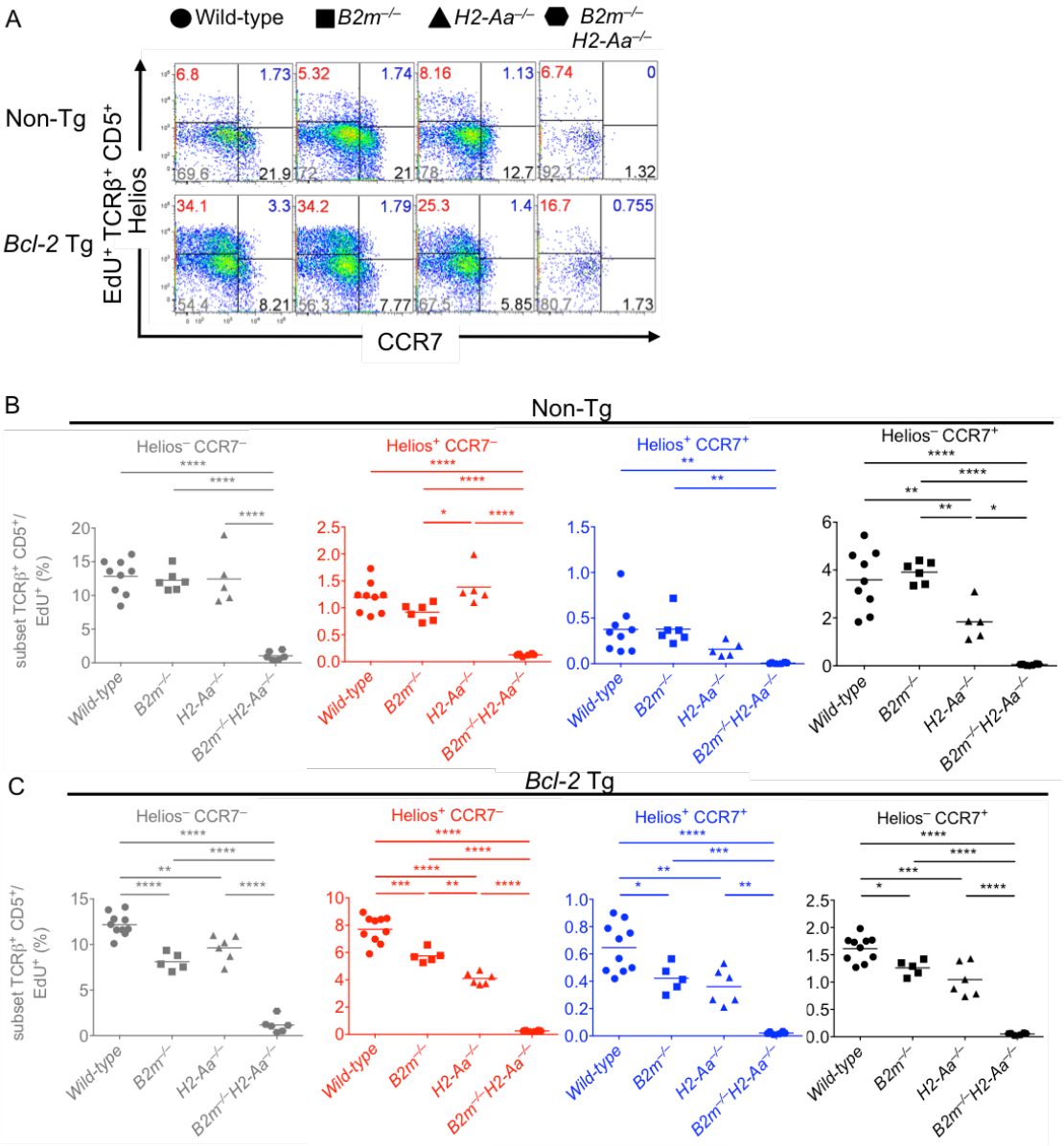

Figure 4.20. Quantification of requirements for MHC classes in nascent TCR-signalled thymocytes subdivided using Helios and CCR7 expression. (A) EdU$^+$ TCRβ$^+$ CD5$^+$ thymocytes gated in Fig. 4.19 were divided into four subpopulations using Helios/CCR7, consisting of Helios$^-$ CCR7$^-$ (grey), Helios$^+$ CCR7$^-$ (red), Helios$^+$ CCR7$^+$ (blue) and Helios$^-$ CCR7$^+$ (black). Summaries show the frequency of each of the four TCRβ$^+$ CD5$^+$ subsets, distinguished by Helios/CCR7 phenotype, among EdU$^+$ thymocytes in non-Tg mice (B) and *Bcl-2* Tg mice (C). Each symbol represents data from 1 mouse compiled from three independent experiments. Lines represent mean; statistical analyses used 1-way ANOVA and Tukey's post-tests. P value symbols: **** <0.0001; *** <0.001; ** <0.01; * <0.05.

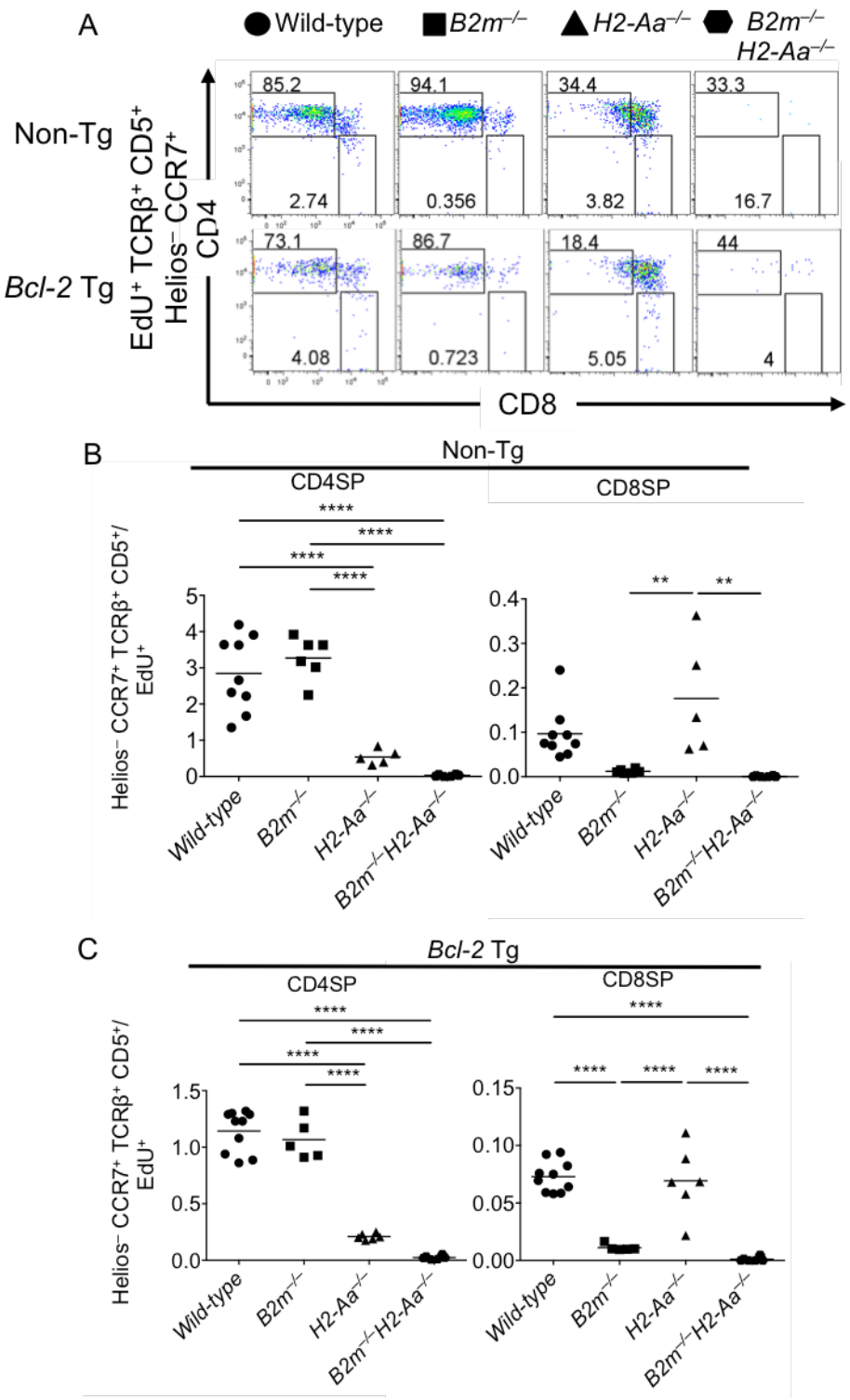

Figure 4.21. Quantification of nascent CD4SP and CD8SP thymocyte induction dependent on MHCI versus MHCII. (A) EdU$^+$ TCRβ$^+$ CD5$^+$ Helios$^-$ CCR7$^+$ thymocytes gated in Fig. 4.20 were analysed for CD4/CD8 expression and CD4SP and CD8SP subsets were quantified. Summaries show the frequency of the gated CD4SP or CD8SP thymocytes in non-Tg mice (B) and *Bcl-2* Tg mice (C). A total of n = 5-10 mice per group compiled from three independent experiments. Lines represent mean; statistical analyses used 1-way ANOVA and Tukey's post-tests. P value symbols: **** <0.0001; ** <0.01; * <0.05.

CD4 and CD8 expression revealed that *H2-Aa*$^{-/-}$ mice had marked reductions in CD4SP cells, whereas *B2m*$^{-/-}$ mice had reduced CD8SP cells, compared to wild-type mice (Fig. 4.21C), as expected.

The TCR-signalled Helios^{+} CCR7^{-} cell frequency in wild-type mice (7.7%) was significantly greater than *B2m*$^{-/-}$ mice (5.8%) and *H2-Aa*$^{-/-}$ mice (4.1%) (Fig. 4.20C). Interestingly, the difference between *H2-Aa*$^{-/-}$ mice and *B2m*$^{-/-}$ mice (4.1% versus 5.8%) was statistically significant (Fig. 4.20C). This finding reveals a greater requirement for MHCII than MHCI in Helios^{+} CCR7^{-} thymocyte induction.

4.2.3 Greater dependence of CD4^{lo}CD8^{lo} PD-1^{hi} thymocytes on MHCII than MHCI

The results above provide evidence that the induction of strongly TCR-signalled thymocytes depends to a greater extent on MHCII than on B2m-dependent ligands. To corroborate that conclusion, using an approach that does not rely on Helios labelling, the CD4^{lo}CD8^{lo} PD-1^{hi} thymocyte population was enumerated, since this population is thought to contain iIEL precursors (Mayans et al., 2014; McDonald et al., 2015; Pobezinsky et al., 2012). To exclude mature T cells, the analysis was confined to CD24^{+} FoxP3^{-} thymocytes, from which the CD4^{lo}CD8^{lo} population was gated as described in Chapter 3 (Fig. 3.12A). In non-Tg mice, analysis of the CD4^{lo}CD8^{lo} population revealed that the PD-1^{+} population consisted of a mixture of Helios^{intermediate} and Helios^{high} cells (Fig. 4.22A). However, in *Bcl-2* Tg mice, nearly all CD4^{lo}CD8^{lo} PD-1^{+} thymocytes were Helios^{high} (Fig. 4.22A).

In the non-Tg dataset, the frequency and number of CD24^{+} FoxP3^{-} CD4^{lo}CD8^{lo} PD-1^{hi} thymocytes in *B2m*$^{-/-}$, *H2-Aa*$^{-/-}$ and *B2m*$^{-/-}$*H2-Aa*$^{-/-}$ mice were similar to wild-type mice (Fig. 4.22B). However, when apoptosis was defective in *Bcl-2* Tg mice, the frequency of CD24^{+} FoxP3^{-} CD4^{lo}CD8^{lo} PD-1^{hi} thymocytes was significantly reduced in *H2-Aa*$^{-/-}$ and *B2m*$^{-/-}$*H2-Aa*$^{-/-}$ mice compared to wild-type mice (Fig. 4.22C). *B2m*$^{-/-}$ mice were not significantly different from wild-type mice on the *Bcl-2* Tg background (Fig. 4.22C). This finding provides additional evidence that the induction of strongly TCR-signalled thymocytes depends to a greater extent on MHCII than on MHCI, consistent with the findings using Helios-labelling. As above, this effect was detectable only when apoptosis was defective.

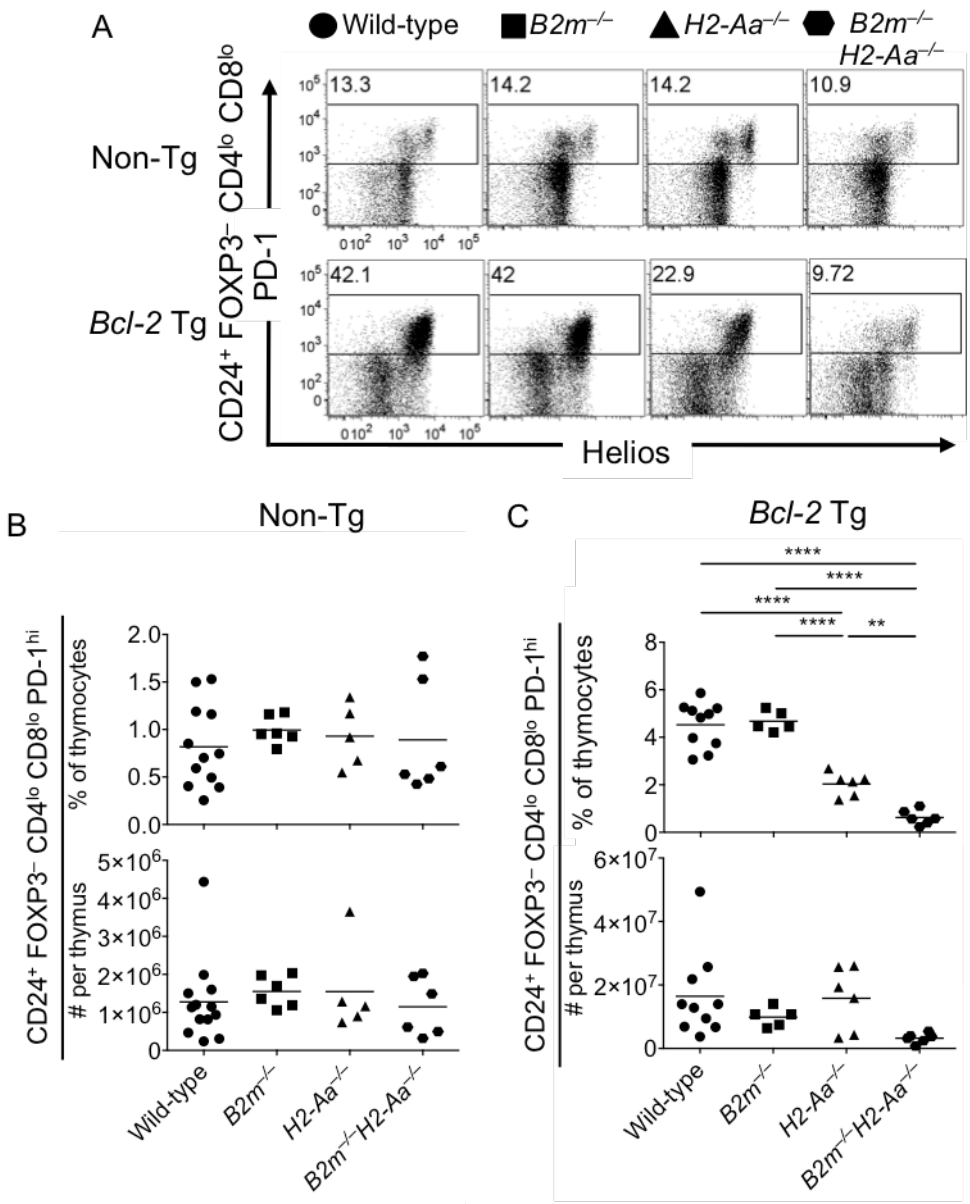

Figure 4.22. Greater dependence of CD4^{lo}CD8^{lo} PD-1^{hi} thymocytes on MHCII than MHCI. (A) Immature CD24^{+} FoxP3^{-} CD4^{lo}CD8^{lo} thymocytes in non-Tg mice and *Bcl-2* Tg mice of the following groups: MHC wild-type, *B2m*$^{-/-}$ (MHCI$^{-/-}$), *H2-Aa*$^{-/-}$ (MHCII$^{-/-}$) and *B2m*$^{-/-}$*H2-Aa*$^{-/-}$ were analysed for PD-1 expression. For reference to data above, dot plots show PD-1 versus Helios expression, although Helios expression is irrelevant to the placement of the PD-1^{+} gate. (B, C) Summaries show the frequency (top) and number (bottom) of CD24^{+} FoxP3^{-} CD4^{lo}CD8^{lo} PD-1^{hi} events among all thymocytes in non-Tg mice (B) and *Bcl-2* Tg mice (C). Data were compiled from the same three independent experiments described in Fig. 4.15, with a total of n = 5-12 mice per group. Lines represent mean. Statistical analyses used 1-way ANOVA and Tukey's post-tests; P value symbols: **** <0.0001; ** <0.01. Non-significant P values were obtained between all comparison groups in (B, bottom) and (C, bottom).

4.2.4 MHCI induces higher fraction of wave 2 cells than MHCI at steady state

The data above suggest that neither positive nor negative selection can explain the excess of $CD4^+$ over $CD8^+$ T cells. However, negative selection was measured within EdU^+ thymocytes at 3 days after EdU, a time when the cells analysed were probably mostly in the thymic cortex. It is therefore possible that negative selection of the $CD8^+$ T cells continues under the very different environment of wave 2, mainly in the medulla. If so, then negative selection at wave 2 may be mainly mediated by MHC I. While an analysis at 5 days after EdU injection is necessary to address this question, a preliminary analysis may be performed by looking at steady-state thymocytes. As most $Foxp3^+$ thymocytes are $Helios^+$, the analysis was performed on electronically gated $Foxp3^-$ thymocytes.

Mice with normal apoptosis are included for completeness, but those results are difficult to interpret because most thymocytes induced to express Helios are rapidly eliminated by apoptosis. The data of most interest come from the apoptosis-deficient *Bcl-2* Tg mice. On a *Bcl-2* Tg background, *H2Aa*$^{-/-}$ mice had a significantly lower frequency of $Helios^+$ $CCR7^-$ thymocytes than wild-type or *B2m*$^{-/-}$ mice (Fig. 4.23B), which replicates the observations above at day 3 after EdU pulse (Fig. 4.20) and reinforces the conclusion that MHCII makes a greater contribution than MHCI to negative selection at wave 1. Analysis of wave 2 revealed a different picture. On a *Bcl-2* Tg background, *B2m*$^{-/-}$ mice had a significantly lower frequency and number of $Helios^+$ $CCR7^+$ thymocytes than wild-type or *H2Aa*$^{-/-}$ mice (Fig. 4.23C). This suggests that MHCI may mediate the majority of negative selection at wave 2.

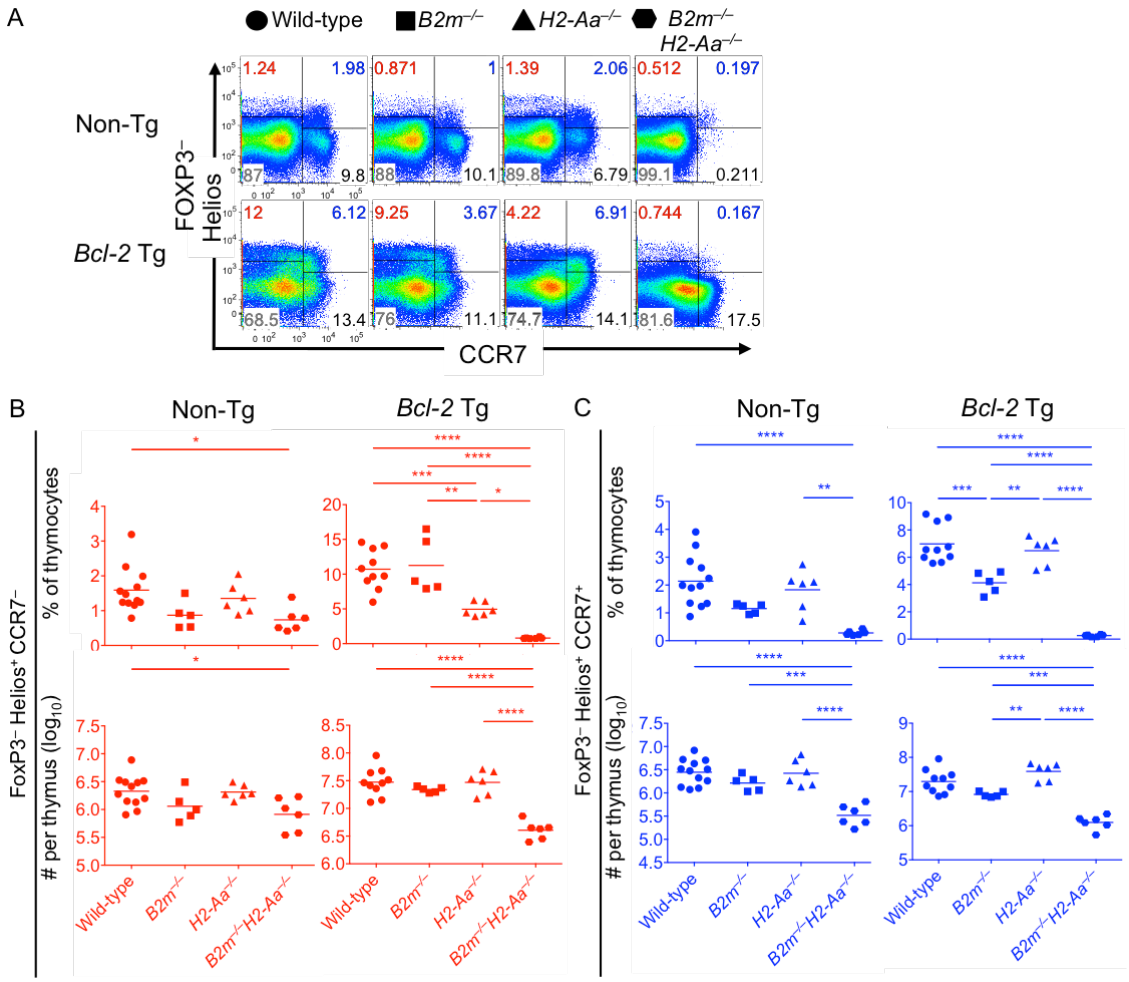

Figure 4.23. Quantification of requirements for MHC classes in Helios$^+$ CCR7$^-$ and Helios$^+$ CCR7$^+$ thymocytes at steady state. (A) FoxP3$^-$ thymocytes were divided into four subpopulations using Helios/CCR7, consisting of Helios$^-$ CCR7$^-$ (grey), Helios$^+$ CCR7$^-$ (red), Helios$^+$ CCR7$^+$ (blue) and Helios$^-$ CCR7$^+$ (black). Summaries show the frequency and number of (B) FoxP3$^-$ Helios$^+$ CCR7$^-$ thymocytes and (C) FoxP3$^-$ Helios$^+$ CCR7$^+$ thymocytes in non-Tg mice and *Bcl-2* Tg mice. Each symbol represents data from 1 mouse compiled from three independent experiments. Lines represent mean; statistical analyses used 1-way ANOVA and Tukey's post-tests. P value symbols: **** <0.0001; *** <0.001; ** <0.01; * <0.05.

4.3 Discussion

The mechanism underlying the numerical imbalance between $CD4^+$ and $CD8^+$ T cells is enigmatic**.** The findings above indicate that a similar number of MHCI-responsive and MHCII-responsive thymocytes initiate development. Analysis of active caspase 3/CD69/CD5 expression failed to uncover a difference in cell death between MHCI-responsive and MHCII-responsive cells after initiation of TCR-signalling**.** However, as $CD8^+$ T cell development takes twice as long as $CD4^+$ T cell development (Saini et al., 2010), an equivalent death rate would be expected to result in fewer $CD8^+$ T cells completing development. Two independent analytical methods provided evidence that MHCII makes a greater contribution to induction of strongly TCR-signalled thymocytes than MHCI.

To maintain a relatively constant number of thymocytes, cell loss via egress and death must be balanced by cell gain via ingress and mitosis. Ingress by itself constitutes a minor input, as the young adult mouse thymus contains ~1.5 x 10^8 thymocytes, but can accommodate only ~160 T-cell progenitors, and only ~10 niches are open to colonisation by circulating progenitors at any moment in time (Ziętara et al., 2015). Egress is a relatively minor output, as experiments blocking thymocyte egress using the FTY720 drug suggest that ~15% of SP cells (~2% of thymocytes) egress from the thymus per day (Sinclair et al., 2013). After repetitive administration of tritiated thymidine, the frequency of labelled thymocytes increases to 80-90% within 3 days, indicating that almost one-third of thymocytes arise by mitosis per day (Matsuyama et al., 1966). When thymic mass was substantially increased by transplantation of multiple thymuses under the skin, mitosis remained vigorous in each thymus graft, yet there was minimal impact on lymphocytes in peripheral lymphoid organs, demonstrating that most thymocytes die within the thymus (Matsuyama et al., 1966). Thus, thymocyte "turnover" is mainly governed by intra-thymic mitosis and cell death, with minor contributions by ingress and egress.

Thymocyte mitosis may be estimated by accumulation of EdU^+ thymocytes in the first 2 days after EdU injection, termed "A" in the schematic shown in Fig. 4.24. As the EdU^+ cell frequency among all thymocytes tended to be lower in *Bcl-2* Tg mice than in non-Tg mice at 1-2 days after EdU injection, *Bcl-2* transgene expression appears to decrease the magnitude of A (Fig. 4.24). Considering cell loss, *Bcl-2* Tg mice had a significantly lower frequency and number of active caspase 3^+ thymocytes than non-Tg mice. It is not clear that all apoptosis-committed thymocytes express active caspase 3, nor is it clear that non-Tg and *Bcl-2* Tg thymocytes express active caspase 3 for similar

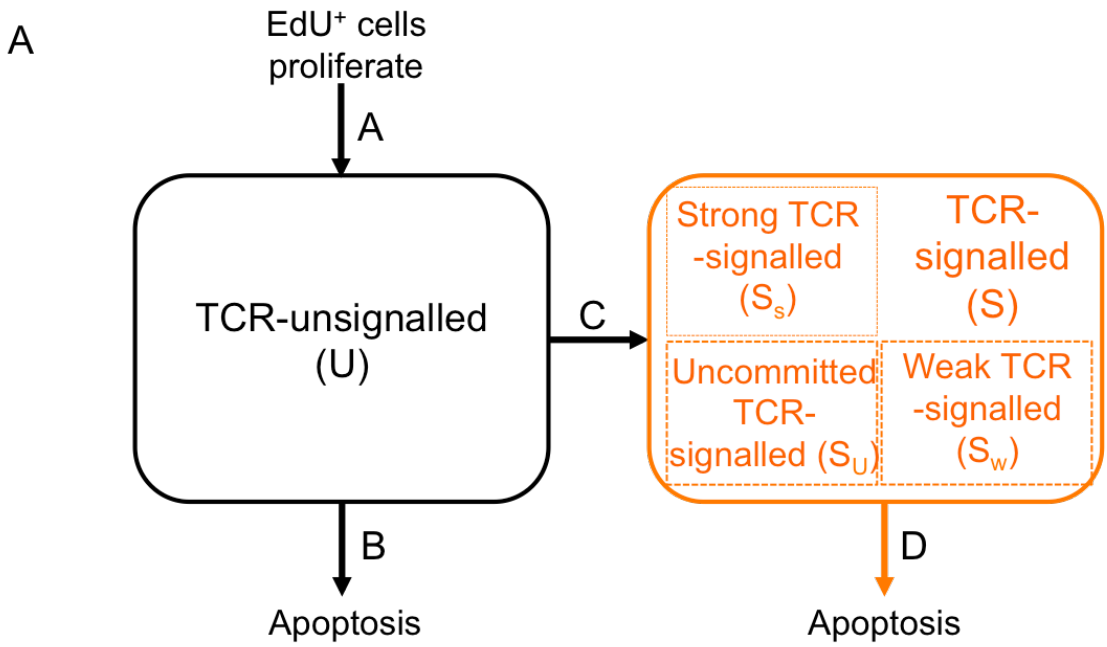

B

Definitions:

A ∝ EdU+ / thymocytes (%)

B ∝ active caspase 3+ CD69− CD5− / thymocytes (%)

C ∝ entering selection (the parameter of interest)

D ∝ active caspase 3+ CD69+ CD5+ / thymocytes (%)

U = TCRβ− CD5− / EdU+ thymocytes (%)

S = TCRβ+ CD5+ / EdU+ thymocytes (%)

S_s = Helios+ TCRβ+ CD5+ / EdU+ thymocytes (%)

S_U = Helios− CCR7− TCRβ+ CD5+ / EdU+ thymocytes (%)

S_W = Helios− CCR7+ TCRβ+ CD5+ / EdU+ thymocytes (%)

Figure 4.24. 2-compartment model of TCR-signalling and apoptosis within the nascent thymocytes during T cell development. (A) The schematic incorporates data from three analytical approaches: TCRβ/CD5, active caspase 3/CD69/CD5 and Helios/CCR7. The first compartment consists of TCR-unsignalled TCRβ$^-$CD5$^-$ cells, denoted "U". The TCR-signalled TCRβ$^+$ CD5$^+$ cells, denoted "S", form the second compartment. The input received by U as EdU$^+$ cells proliferate is denoted "A". Cells committed to apoptosis within U, measured as active caspase 3$^+$ CD69$^-$ CD5$^-$ thymocytes, are denoted "B". Transition of cells from U to S is denoted "C". Cells committed to apoptosis within S, measured as active caspase 3$^+$ CD69$^+$ CD5$^+$ thymocytes, are denoted "D". S is subdivided into Helios$^-$ CCR7$^-$ thymocytes that are uncommitted to selection (S_u), Helios$^+$ strongly TCR-signalled (S_s) and Helios$^-$ CCR7$^+$ weakly TCR-signalled (S_w). (B) Flow cytometric phenotypes of thymocytes analysed 3 days after a single EdU injection that were used to estimate variables within the 2-compartment scheme.

periods of time before disappearing. However, the diminished active caspase 3^+ thymocyte population in *Bcl-2* Tg mice is consistent with the hypothesis that *Bcl-2* transgene expression decreases cell death within the thymus. Together, these findings suggest that thymocyte "turnover" at equilibrium, defined as the rate of replacement of thymocyte loss by thymocyte mitosis, is decreased in *Bcl-2* Tg mice. This difference complicates the comparison of nascent thymocyte cohorts in non-Tg versus *Bcl-2* Tg mice. This issue may be avoided by considering the non-Tg and *Bcl-2* Tg datasets as separate bodies of information relevant to my research question.

To synthesise the data in this chapter, a 2-compartment model was conceived (Fig. 4.24). This model ignores thymocyte egress based on the following two sets of observations. After Zap70-dependent TCR-signalling is initiated, it takes DP thymocytes 2 and 4 days to progress to the CD4SP and CD8SP stages, respectively (Saini et al., 2010). From the beginning of the single-positive stage, it takes another 4-5 days for the nascent T cells to appear in the spleen (McCaughtry et al., 2007). As the experiments on mice lacking one or both MHC classes analysed thymocytes 3 days after *in vivo* proliferation, which precedes Zap70-dependent TCR-signalling, the nascent thymocyte cohorts examined were too immature to be influenced by egress.

Within the nascent cohort of EdU^+ thymocytes, the first compartment contains nascent TCR-**u**nsignalled cells, defined as $TCR\beta^-$ $CD5^-$, denoted "U" (Fig. 4.24). It is clear that most DNA-synthesising thymocytes belong to this compartment (Fig. 4.2). The second compartment contains TCR-**s**ignalled cells, defined as $TCR\beta^+$ $CD5^+$, denoted "S" (Fig. 4.24). Cell death within U is defined as the active caspase 3^+ $CD69^-$ $CD5^-$ population, denoted "B" in the model, and corresponds to death by neglect in the literature. Cell death within S is defined as the active caspase 3^+ $CD69^+$ $CD5^+$ population, denoted "D" in the model, and corresponds to death by clonal deletion in the literature. Similar estimates were obtained for B and D by analyzing all thymocytes or EdU^+ thymocytes. The parameter of interest, which describes progression from U to S, is denoted "C" (Fig. 4.24).

Among EdU^+ active caspase 3^+ cells in non-Tg mice, as $CD69^-$ $CD5^-$ thymocytes (~"B") outnumbered $CD69^+$ $CD5^+$ thymocytes (~"D") at all points in the time course, it may be inferred that apoptosis within the TCR-unsignalled pool, "B", exceeds apoptosis within the TCR-signalled pool, "D", consistent with published data (Stritesky et al., 2013; Surh and Sprent, 1994). The time course experiment also revealed that EdU^+ active caspase 3^+ $CD69^-$ $CD5^-$ thymocytes peak at 3 days after EdU injection, whereas EdU^+ active caspase 3^+ $CD69^+$ $CD5^+$ thymocytes are equally numerous at 2 and 3 days

after EdU injection (Fig. 4.11). With the caveat that some thymocytes undergoing clonal deletion may not attain an active caspase 3^+ phenotype, the data suggest that clonal deletion precedes, and coincides with, death by neglect during thymocyte development.

The 2-compartment model may help to distinguish requirements for the 2 major MHC classes in inducing T cell development in the thymus. At 3 days after EdU injection, the EdU^+ cell frequency among all thymocytes was similar across the non-Tg panel of mice (Fig. 4.16). This suggests that the input rate of thymocyte precursors (A) is similar within the non-Tg panel and not influenced by MHC. Considering cell death, the absence of both MHC classes clearly increased B and decreased D, relative to wild-type mice (Fig. 4.18). This is consistent with increased death by neglect and decreased death by clonal deletion in the absence of MHC molecules. The value of S was decreased by >90% in MHC-deficient mice compared to wild-type mice (Fig. 4.19). These findings show that thymocyte development in MHC-deficient mice is largely confined to the first compartment, whereby U receives input via A and gives output via B, with relatively little flow of thymocytes into S.

The groups lacking one MHC class had values for S and D that clearly exceeded the MHC-deficient group (Figs. 4.18, 19), indicating that expression of one MHC class was sufficient to restore a substantial flow of thymocytes into the second compartment, S. Relative to wild-type mice, there was no statistically significant decrease in the value of S in non-Tg mice lacking either MHC class (Fig. 4.19). This observation is discussed below, after the *Bcl-2* Tg dataset is considered.

In *Bcl-2* Tg mice, as in non-Tg mice, it is clear that the absence of both MHC classes markedly reduced S (Fig. 4.19), demonstrating that most thymocytes that attain a TCR-signalled phenotype require MHC to do so, even when apoptosis is defective. Unlike in non-Tg mice, however, the *Bcl-2* Tg dataset also revealed highly significant decreases in S in both groups lacking one MHC class (Fig. 4.19). As *Bcl-2* transgene markedly reduces the values of B and D (Fig. 4.10B), it is likely that B and D have little influence on the value of S in the *Bcl-2* Tg dataset. By diminishing B and D, *Bcl-2* transgene expression enables C to become the main determinant of S. Thus, when one MHC class is absent, it is postulated that the observed reduction in S is due to a significant reduction in C. These data provide evidence that each MHC class is required to induce significant fractions of the TCR-signalled cohort, and that those fractions are similar in size, representing 30-35% of the entire TCR-signalled cohort.

Further research is required to determine why the absence of one MHC class diminishes S in *Bcl-2* Tg mice but not in non-Tg mice. It is possible that the absence of one MHC class diminishes C to the same extent in non-Tg mice as in *Bcl-2* Tg mice, that is, by 30-35%. This explanation would predict that the absence of one MHC class fails to alter S in non-Tg mice because changes in B and/or D mask the effect of the reduction in C. Indeed, there is preliminary evidence that the absence of one MHC class alters B and D, relative to wild-type. Although not statistically significant, the groups lacking one MHC class tended to have higher values for B and lower values for D than the wild-type group (Fig. 4.18). Notably, increases in B and decreases in D would both tend to inflate the value of S in the model. Such inflationary effects may mask the deflationary effect of a decrease in C. Additional experiments, ideally performed as a time course, will be required to test this hypothesis.

It is inferred that MHCI- and MHCII-single deficiencies decrease S by decreasing C. Since MHCI- and MHCII-single deficiencies decreases S to a similar extent compared to wild-type mice (Fig. 4.19), this suggests that C is similar between MHCI- and MHCII-deficient mice. This indicates that a similar fraction of MHCI-responsive cells and MHCII-responsive cells register an initial TCR signal, and implies that the imbalance between the number of $CD4^+$ and $CD8^+$ T cells is not due to the initiation step. This is consistent with Sinclair et al.'s (2013) conclusion, as the maturation rates from DP1 to DP2 in MHCII-responsive cells was similar to MHCI-responsive cells.

The active caspase 3/CD69/$CD5^+$ population would be expected to contain strongly TCR-signalled cells committed to clonal deletion, D. MHC single deficiencies did significantly decrease a parameter similar to D, namely, the frequency of $CD69^+$ $CD5^+$ cells among active caspase 3^+ thymocytes (Fig. 4.18). This parameter was reduced in the absence of MHCI to a similar extent as in the absence of MHCII. There was no evidence that the frequency of apoptosis-committed cells was higher in the MHCI-responsive cohort than in the MHCII-responsive cohort. Given the evidence that equivalent numbers of MHCI-responsive cells and MHCII-responsive cells receive a TCR signal, and equivalent fractions of these TCR-signalled cohorts are committed to apoptosis at any moment in time, why do more $CD4^+$ T cells complete development? Consistent with previous studies, the data above demonstrate that it takes approximately twice as long for thymocytes to develop into $CD8^+$ T cells than $CD4^+$ T cells (Lucas et al., 1993; Saini et al., 2010). The longer interval required for completion of T cell development should ultimately result in higher death in the CD8 lineage and fewer $CD8^+$ T cells completing development, explaining why there are more $CD4^+$ T cells than $CD8^+$ T cells in the thymus. Alternatively, it is possible that MHCII may

induce the majority of wave 1 negative selection, whereas MHCI may induce majority of wave 2 negative selection, resulting in lower number of $CD8^+$ T cells than $CD4^+$ T cells in the thymus and periphery. This hypothesis is based on the evidence of decreased frequency of wave 1 cells only in MHCII-deficient mice but not in MHCI-deficient mice at steady state (Fig. 4.23B), and decreased steady-state frequency of wave 2 cells only in MHCI-deficient mice (Fig. 4.23C). Whether MHCI induces majority of wave 2 negative selection in nascent thymocyte cohort has yet to be confirmed by conducting experiments on day 5-post EdU injection, which is the optimal time point to assess wave 2 negative selection (Hu et al., 2016).

Sinclair et al. (2013) concluded that increased intrinsic susceptibility to apoptosis in MHCI-responsive cells at the DP2 stage gives rise to a higher death rate in MHCI-responsive cells than MHCII-responsive cells. The *in vivo* development of MHCI-restricted thymocytes was studied in the absence of MHCII on TECs. However, in these chimeras, recognition of wild-type MHCII molecules expressed on the surface of BM-derived cells may have induced deletion of thymocytes capable of developing into $CD8^+$ T cells. Indeed, in immunised chimeric mice lacking MHCII expression in epithelial cells, the presence of MHCII expression in BM-APCs reduced the number of MHCII-tetramer-binding $CD8^+$ T cells by 10-fold (Stadinski et al., 2011), suggesting that $MHCII^+$ BM-APCs are capable of deleting thymocytes with the potential to develop into $CD8^+$ T cells.

Sinclair et al. (2013) estimated cell death rate by subtracting the cells that progress to the subsequent stage (outflow) from the cells that enter a stage (inflow). This method of calculating cell death does not provide information on whether the thymocytes die due to too strong or too weak TCR-signalling. A $Helios^+$ phenotype marks thymocytes that have received a strong TCR signal, whereas a $Helios^-$ $CCR7^+$ phenotype marks thymocytes that have received a weak TCR signal (Daley et al., 2013). Helios and CCR7 thus allow S to be subdivided into a $Helios^-$ $CCR7^-$ **u**ncommitted subset (S_u), a $Helios^+$ **s**trongly TCR-signalled subset (S_s) and a **w**eakly TCR-signalled subset (S_w) (Fig. 4.24). The prolonged lifespan of $Helios^+$ thymocytes in *Bcl-2* Tg mice allows the enumeration of strongly TCR-signalled cells that would normally disappear due to apoptosis. Relative to wild-type mice, MHCI- and MHCII-single deficiencies decreased S_u and S_w to a similar extent. However, MHCII-deficiency diminished S_s by a greater magnitude than MHCI-deficiency (Fig. 4.20). This indicates that $Helios^+$ thymocyte induction depends more on MHCII than MHCI. This conclusion was corroborated by enumerating immature $CD24^+$ $FoxP3^-$ $CD4^{lo}CD8^{lo}$ $PD\text{-}1^{hi}$ "iIEL precursors" (Fig. 4.22) (Mayans et al., 2014; McDonald et al., 2015; Pobezinsky et al., 2012). These findings

suggest that the induction of strongly TCR-signalled thymocytes depends substantially more on MHCII than on MHCI.

Different mechanisms of cell death may operate in MHCI-responsive versus MHCII-responsive thymocytes. This hypothesis is based on the facts that although both cohorts have similar fractions of apoptosis-committed cells, the MHCII-responsive cohort has a greater fraction of Helios$^+$ strongly TCR-signalled cells. To date, the only well-appreciated mechanism of cell death in TCR-signalled thymocytes is clonal deletion due to TCR signaling above a certain threshold. The data suggest the existence of an additional mechanism of cell death, potentially induced in thymocytes with TCR signaling that is too weak. This putative cell death process is distinct from death by neglect because it occurs in cells expressing CD5 and TCRβ, i.e. TCR-signalled cells. This mechanism of cell death may be more common in MHCI-responsive thymocytes than in MHCII-responsive thymocytes. TNF-mediated cell death could be the distinct mechanism of cell death as CD8SP thymocytes were particularly sensitive to TNF-mediated cell death in the absence of NF-κB activation (Webb et al., 2016). NF-κB signaling, essential for late stages of thymocyte maturation in the thymus, protects against TNF-mediated cell death (Xing et al., 2016). Alternatively, clonal deletion may be the only mechanism of cell death in TCR-signalled thymocytes, but MHCI-responsive thymocytes are able to undergo clonal deletion as a consequence of TCR-signalling under the threshold for Helios upregulation.

The conclusion that strong TCR-signalling is more dependent on MHCII than MHCI fits well with the difference in coupling of Lck (signal-initiating kinase) to CD4 or CD8 coreceptor (Stepanek et al., 2014). Lck is crucial for TCR-signalling because it phosphorylates the intracellular domains of TCRζ and CD3 molecules early after TCR engagement by MHC, and also phosphorylates Zap70 later in T cell activation (Straus and Weiss, 1992; Straus and Weiss, 1993). The increased coupling of Lck to CD4 coreceptors compared to CD8 coreceptors lowers the deletion threshold for MHCII-responsive cells compared to MHCI-responsive cells (Stepanek et al., 2014). When MHCI-restricted OT-I thymocytes bind to OVA-derived altered peptide ligands (APL) Q4R7 or T4, OT-I cells expressing a variant CD8 molecule bearing CD4's intracellular domain (CD8.4) are deleted whereas wild-type OT-I cells with CD8's intracellular domain are positively selected. Furthermore, by visualising the detachment of monomeric pMHC complexes from TCR transgenic thymocytes, it was shown that a positive selecting pMHCI ligand (T4) and a deleting pMHCII ligand (3K) have similar on-cell dwell times (i.e. 1.3s). These observations suggest that MHCII-responsive thymocytes may be more likely to upregulate Helios than MHCI-responsive thymocytes

due to CD4's capacity to interact with MHCII and to CD4's greater capacity to recruit Lck to engaged TCRs, explaining why MHCII makes a greater contribution than MHCI to Helios induction, especially in $CCR7^{-}$ thymocytes.

It is also possible that the difference in proportions of $Helios^{+}$ thymocytes stems from differences in the self-antigen repertoires presented to thymocytes by MHCII versus MHCI. Macroautophagy is an endogenous antigen processing pathway that promotes MHCII presentation (Dengjel et al., 2005). Macroautophagy was detected in 70% of cTECs, 5-10% of mTECs and <1% of thymic DCs in mice (Nedjic et al., 2008). However, another group detected macroautophagy in human epithelial cells, DCs and B cells (Schmid et al., 2007). TECs with an inactivated autophagy-related gene (Atg) 5 have defective macroautophagy and defective development of certain MHCII-restricted TCR transgenic T cells, showing that macroautophagy is essential for thymic $CD4^{+}$ T cell positive selection (Nedjic et al., 2008). Macroautophagy was also shown to be important in inducing $CD4^{+}$ T cell clonal deletion in some but not all TCR transgenic models (Aichinger et al., 2013). Recent data suggests that MHCI-restricted antigen presentation is less dependent on macroautophagy, as the absence of Atg5 and Atg7 autophagy factors increased MHCI surface levels due to decreased endocytosis and degradation of MHCI (Loi et al., 2016). The absence of Atg-dependent MHCI internalisation enhanced virus-specific $CD8^{+}$ T cell responses (Loi et al., 2016). Although further research is required, macroautophagy may diversify the self-antigen repertoire presented by MHCII but not MHCI, increasing the scope for the induction of strong TCR interactions required for $Helios^{+}$ thymocyte induction.

Since it has often been mentioned in this thesis that Helios expression reports the "strength" of TCR signaling in thymocytes, it is pertinent to ask "What is the difference between a "weak" TCR signal and a "strong" one?" Real-time observation of living thymocytes in thymic slices has revealed that the average duration of interaction between a thymocyte and an APC is 4 minutes in positive selecting conditions versus 1 hour in negative selecting conditions (Melichar et al., 2013). However, real-time observation of peptide/MHC monomers in solution with live T cells has revealed that the duration of a monomeric TCR:peptide/MHC interaction that leads to negative selection can be much shorter in duration (>0.2 s for MHCII-responsive TCRs and >0.9 s for MHCI-restricted TCRs) (Stepanek et al., 2014). At an intermediate level between these extremes of interaction times, intracellular signaling proteins are modified, for example phosphorylated or dephosphorylated, within seconds of TCR engagement. While there are still many unknowns about the mechanisms underlying TCR signaling, it is likely that TCR signaling outcomes depend on the longevity of the "TCR

signalosome", which includes the TCR, CD3, coreceptors, kinases (Lck, Zap70) and adapter proteins (LAT, SLP76). The CD4 and CD8 coreceptors are thought to contribute to the longevity of the TCR signalosome in two ways: by binding to MHC with their extracellular domain and by bringing Lck close to the TCR/CD3 complex with their intracellular domain, allowing Lck to phosphorylate TCR/CD3 and Zap70 (Straus and Weiss, 1992; Straus and Weiss, 1993). Although the affinity of CD8 for MHCI (K^d= 50-200μM) (Merwe and Davis, 2003) is much higher than the affinity of CD4 for MHCII (K^d= 2.5mM) (Jönsson et al., 2016), it is unclear whether or how this difference impacts the multifactorial process of T cell activation. Furthermore, more CD4 coreceptors are loaded with Lck compared to CD8 (Stepanek et al., 2014). Data presented in this thesis provides the new insight that MHCII makes a greater contribution than MHCI to Helios induction in $CCR7^-$ thymocytes, whereas MHCI may make a greater contribution than MHCII to Helios induction in $CCR7^+$ thymocytes. This suggests that there is a differential and stage-dependent contribution of MHCI vs MHCII to the induction of $Helios^+$ thymocytes.

It could be argued that the EdU^+ thymocytes analysed in this present study may contain a small fraction of dividing SP cells instead of dividing DN-DP cells. To exclude this possibility, EdU^+ $CD24^+$ gate was used to mark the immature thymocytes, thereby excluding the DNA-synthesising SP cells that are $CD24^-$ (Chapter 3). Furthermore, at 1h post-EdU injection, almost all (97-99%) recently EdU^+ cells were $TCR\beta^-$ $CD5^-$, suggesting they had not received a TCR signal (Figs. 4.2 and 4.3). This shows that almost all the DNA-synthesising cells are at the DN-DP transition (the largest proliferative phase), instead of dividing SP cells.

A weakness arises if one tries to measure negative selection, i.e. apoptotic deletion and agonist selection, by comparing apoptosis-sufficient mice with apoptosis-deficient mice. This is because the denominators may not be constant. In other words, the EdU^+ population may differ in composition. For this reason, this study did not compare directly the data from apoptosis-sufficient mice with apoptosis-deficient mice. Rather, it considered the results obtained from non-Tg and *Bcl-2* Tg mice as two separate sets of data. What is clear is that apoptosis defects prolong the lifespan of strongly TCR-signalled $Helios^+$ thymocytes. This allows apoptosis-defective mice to be used to quantify the change in negative selection caused by defects in MHC molecules or APC types.

A weakness arises if one tries to measure negative selection, i.e. apoptotic deletion and agonist selection, by comparing apoptosis-sufficient mice with apoptosis-deficient

mice. This is because the denominators may not be constant. In other words, the EdU^+ population may differ in both size and composition. However, the EdU^+ thymocyte frequency is similar across all MHC genotypes in both non-Tg mice and in apoptosis defective *Bcl-2* Tg mice (Fig. 4.16), ruling out the possibility that the EdU^+ size in non-Tg and *Bcl-2* Tg mice are different. Furthermore, this study did not compare directly the data from apoptosis-sufficient mice with apoptosis-deficient mice, but consider the results obtained from non-Tg and *Bcl-2* Tg mice as two separate sets of data. What is clear is that apoptosis defects prolong the lifespan of strongly TCR-signalled $Helios^+$ thymocytes compared to apoptosis-sufficient mice, allowing the quantification of negative selection mediated by defects in MHC molecules or APC types to be possible when mice are defective in apoptosis.

In summary, similar frequencies of TCR-signalled apoptotic cells were detected in mice expressing only one MHC class. However, as $CD8^+$ T cell development takes longer than $CD4^+$ T cell development, similar rates of apoptosis at any moment in time would be expected to result in fewer $CD8^+$ T cells completing development, explaining why $CD4^+$ T cells outnumber $CD8^+$ T cells. Analysis of apoptosis-defective mice revealed that MHCI induces TCR signalling in a similar fraction of thymocytes as MHCII, but MHCII makes a greater contribution to induction of strongly TCR-signalled thymocytes than MHCI, particularly at the $CCR7^-$ stage.

CHAPTER 5

A comparison of TCR repertoires positively or negatively selected in the absence or presence of one or both MHC classes

5.1 Introduction

In chapter 4, the frequency of TCR-signalled cells ("S") in nascent thymocyte cohorts was measured. When apoptosis is defective, wild-type mice had a greater frequency of TCR-signalled thymocytes than MHCI-deficient mice or MHCII-deficient mice, indicating that portions of the thymocyte repertoire require either MHCI or MHCII to receive a TCR signal. Mice lacking both MHCI and MHCII had very few TCR-signalled cells. Notably, the individual frequency of TCR-signalled thymocytes in MHCI-deficient mice and MHCII-deficient mice summed to a value 35% greater than the frequency of thymocytes in mice bearing both MHCI and MHCII. The 35% difference may be explained by two hypotheses: (1) interclonal competition between MHCI-responsive and MHCII-responsive thymocytes for access to a limited number of APCs or (2) existence of MHC class cross-reactive thymocytes that can receive a TCR signal from both MHCI and MHCII.

Regarding the former hypothesis, many thymic APC types such as cTECs, mTECs, DCs and B cells, express both MHCI and MHCII. When all these APC types express only one class of MHC, thymocytes that can only interact with the absent MHC class may fail to compete against thymocytes that can interact with the expressed MHC class. Relaxation of this interclonal competition for access to APCs, together with the constant number of APCs, may allow a greater proportion of thymocytes to interact with the expressed MHC class to derive a TCR signal. This interpretation was favoured by Sinclair et al. (2013).

The MHC class cross-reactivity hypothesis posits that a substantial proportion of TCRs are capable of binding to both MHCI and MHCII. As MHCI-deficiency decreased the production of TCR signalled thymocytes by 30% in apoptosis-defective mice, the inference was that 30% of the TCR-signalled repertoire in wild-type mice requires MHCI to derive a TCR signal. Following this logic, 35% of the TCR-signalled repertoire in wild-type mice requires MHCII. The MHC class cross-reactivity hypothesis postulates that the remainder of the TCR signalled cohort in wild-type mice (100 – 30 – 35 = 35%) expresses TCRs that are capable of deriving a TCR signal from either MHCI or MHCII. The hypothesis further predicts that, in mice lacking one MHC class, at least half of the TCR-signalled repertoire is MHC class cross-reactive (i.e. 35 / 70 = 50% of the TCR-signalled repertoire in MHCI-deficient mice and 35 / 65 = 54% in MHCII-deficient mice).

Consistent with the latter hypothesis, some TCRs are capable of binding to both MHCI and MHCII. Thymocytes expressing the YAe62.8 TCR are deleted in wild-type mice,

positively selected into $CD4^+$ T cells in mice that express only one self-peptide/MHCII complex (Ep/H2-A^b) and positively selected into $CD8^+$ T cells in mice lacking MHCII expression (*H2-Ab1*$^{-/-}$)(Huseby et al., 2005). YAe62.8 TCR-expressing thymocytes undergo death by neglect in mice lacking MHCII and MHCI expression (*H2-Ab1*$^{-/-}$*B2m*$^{-/-}$) (Huseby et al., 2005). Evidence that this phenomenon occurs in polyclonal T cells was established by immunising mice with recombinant vaccinia virus engineered to express a peptide, 3K, that is "foreign" to B6 mice. At 7-10 days after the immunisation, the number of $CD8^+$ T cells capable of binding to 3K/H2-A^b (peptide/MHCII) tetramers were enumerated. Wild-type mice, and mice lacking both B2m and MHCII, had very few $CD8^+$ T cells capable of binding to the tetramers. In contrast, MHCII-deficient mice were found to have at least 10-fold more tetramer-binding $CD8^+$ T cells (Stadinski et al., 2011). This suggests that MHCII normally deletes some T cells with the capacity to develop into $CD8^+$ T cells. In a recent study, out of a panel of 19 TCRs ascertained to drive deletion in B6 mice, approximately one-third were responsive to both MHCI and MHCII (McDonald et al., 2015). Of 12 TCRs that were expressed in thymocytes *in vivo*, 11 drove deletion at the $CCR7^-$ stage and one drove deletion at the $CCR7^+$ stage (McDonald et al., 2015). These observations suggest that MHC class cross-reactive TCRs facilitate deletion in the wild-type thymus, predominantly at the $CCR7^-$ stage of development. MHC class cross-reactivity has also been observed in humans, whereby virus specific $CD8^+$ T cells can cross-recognise HLA DR4 (class II molecules) (Rist et al., 2009).

The vast TCR diversity in polyclonal T cells makes TCR repertoire analysis challenging. Fixing the TCR β chain reduces TCR diversity and enables TCR repertoire analysis via sequencing of TCRα chains (Sant'Angelo et al., 1998) This approach can be used to analyse T cell selection in response to the natural self-antigen repertoire and has advanced our understanding of T cell development. For instance, a specific TCRα chain sequence was identified as a molecular marker for positive selection (Sant'Angelo et al., 1998). The TCR repertoires of T-reg and conventional $CD4^+$ T cells were found to be distinct yet with significant overlap (Hsieh et al., 2004; Pacholczyk et al., 2006; Wong et al., 2007). This strategy was used to profile $CD4^+$ T conventional and T-reg TCR repertoires in mice lacking MHCII expression in BM-APCs, in mice with reduced MHCII expression in mature mTECs, and in mice lacking Aire. It was concluded $MHCII^+$ BM-APCs and Aire have distinct and cooperative roles in establishing central T cell tolerance via clonal deletion and T-reg selection (Perry et al., 2014). This strategy was also used to reveal that Aire directs T cells expressing prostate-reactive TCRs into the T-reg cell lineage (Malchow et al., 2016) and to reveal that T-reg TCRs that recognise a peptide from the self-antigen, myelin oligodendrocyte

glycoprotein, have much higher TCR affinity than non-T-reg cells that recognise the same self-antigen (Kieback et al., 2016).

To test the two hypotheses to explain why the individual values of TCR-signalled cells (S) in MHCI-deficient mice and MHCII-deficient mice summed to a value 35% greater than the frequency of TCR-signaled cells in mice with both MHC classes, deep sequencing of the TCRα chain repertoire was performed on samples from mice expressing a transgenic TCRβ chain (62b-Tg) (Stadinski et al., 2011) derived from the YAe62.8 TCR (Huseby et al., 2005). Data analysis was performed using the VDJtools software package, which was designed to standardise the analysis and reporting of TCR sequencing data (Shugay et al., 2015).

5.2 Results

5.2.1 Genotype, age and gender of mice and the T cell subsets used for TCR sequencing

To define TCR clonotypes that derive a TCR signal in the presence or absence of either MHC class, 62b-Tg thymocytes and/or splenocytes were sorted from wild-type, *B2m*$^{-/-}$, *H2-Aa*$^{-/-}$ and *B2m*$^{-/-}$*H2-Aa*$^{-/-}$ mice which all carried the 62b transgene (Stadinski et al., 2011). Each of these 4 groups comprised male and female mice (Fig. 5.1). The average age of mice ranged from 7 to 11 weeks, with a slightly higher average age in *B2m*$^{-/-}$ mice and *H2-Aa*$^{-/-}$ mice compared to the rest of the groups (Fig. 5.1).

For wild-type mice, three thymocyte subsets were sorted, namely, wave 1 (W1), CD4SP and CD8SP (Fig. 5.2). The W1 thymocyte subset had the phenotype of DN (CD4^{lo}CD8^{lo}) PD-1^{hi} CCR7^{-} (Fig. 5.2A), based on evidence that coreceptor dulling and PD-1 induction identify thymocytes that receive a strong TCR signal at the CCR7^{-} stage (Daley et al., 2013). A CCR7^{-} gate was set because CCR7 is a thymocyte maturation marker and the least mature thymocytes that have received a strong TCR signal were the population of interest for sorting. Thymocytes also attain a CD4^{lo}CD8^{lo} PD-1^{hi} CCR7^{-} phenotype during agonist selection into small intestinal IEL (McDonald et al., 2015). Although the term “W1” is used in this chapter, the sorted CD4^{lo}CD8^{lo} PD-1^{hi} CCR7^{-} cells might represent only a portion of the Wave 1 population. Thus, an alternative description for W1 is “cells that have survived deletion at Wave 1 and progressed to the next stage of agonist selection into IEL”.

The mature thymic CD4SP and CD8SP subsets were sorted by gating the non-DN population into CD4SP and CD8SP subsets, from which CCR7^{+} cells were sorted (Fig. 5.2B). The CCR7^{+} gate was used because the most mature of the newly formed thymocytes were the population of interest for sorting (Cowan et al., 2016). W1 and CD4SP were sorted from *B2m*$^{-/-}$ mice, while W1 and CD8SP were sorted from *H2-Aa*$^{-/-}$ mice. From *B2m*$^{-/-}$*H2-Aa*$^{-/-}$ mice, W1, CD4SP and CD8SP thymocyte subsets were sorted, as well as TCRβ^{+} B220^{-} splenocytes (Fig. 5.2C). TCRβ^{+} B220^{-} splenocytes were sorted to i) identify TCRs in the periphery to examine whether peripheral MHC-independent TCRs were similar to thymic MHC-independent TCRs and ii) to serve as a back up TCR data in the case of very few thymic TCRs obtained in the absence of MHC molecules.

In all cases, the number of cells sorted per cell type from each mouse was capped at 50,000. However, there were four samples with fewer than 50,000 sorted cells: one CD4SP sample from the wild-type group, one W1 sample from the *B2m*$^{-/-}$ group and two samples (CD4SP and CD8SP subsets) from *B2m*$^{-/-}$*H2-Aa*$^{-/-}$ mice (Fig. 5.3). Due to the failure to reliably obtain 50,000 cells in each thymocyte subset from *B2m*$^{-/-}$*H2-Aa*$^{-/-}$ mice, two *Bcl-2* Tg *B2m*$^{-/-}$*H2-Aa*$^{-/-}$ mice were used (Fig. 5.3) based on the assumption that expression of the Bcl-2 transgene would increase the number of T cells available. Indeed, this assumption was correct as 50,000 cells were obtained in *Bcl-2* Tg *B2m*$^{-/-}$ *H2-Aa*$^{-/-}$ mice.

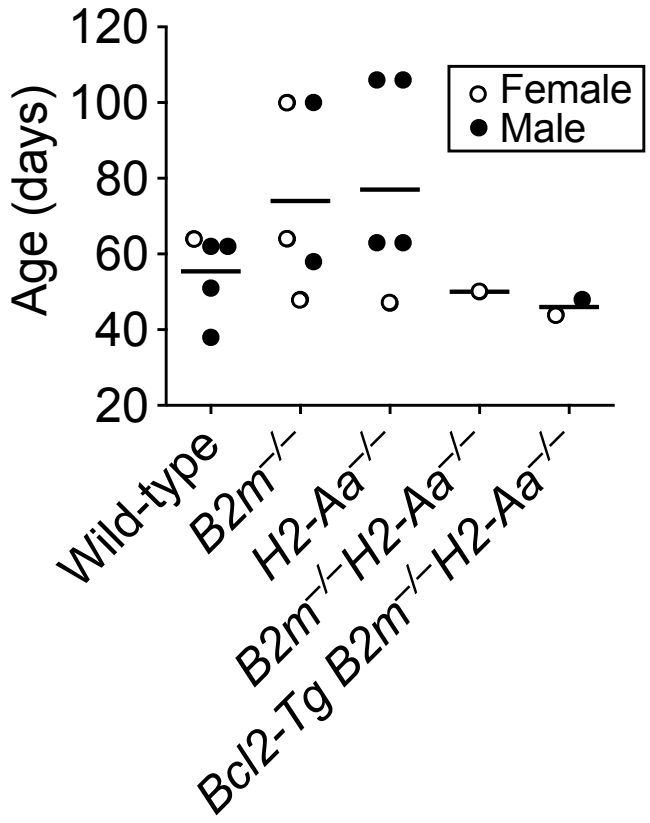

Figure 5.1. Genotype, age and gender of mice used for TCR sequencing. Graph shows the age and gender of mice examined in the following groups: wild-type (n=5), *B2m*$^{-/-}$ (n=5), *H2-Aa*$^{-/-}$ (n=5), *B2m*$^{-/-}$*H2-Aa*$^{-/-}$ (n=1), *Bcl-2* Tg *B2m*$^{-/-}$*H2-Aa*$^{-/-}$ (n=2), comprising a total of 18 mice used in TCR sequencing analysis. Each symbol represents an individual mouse.

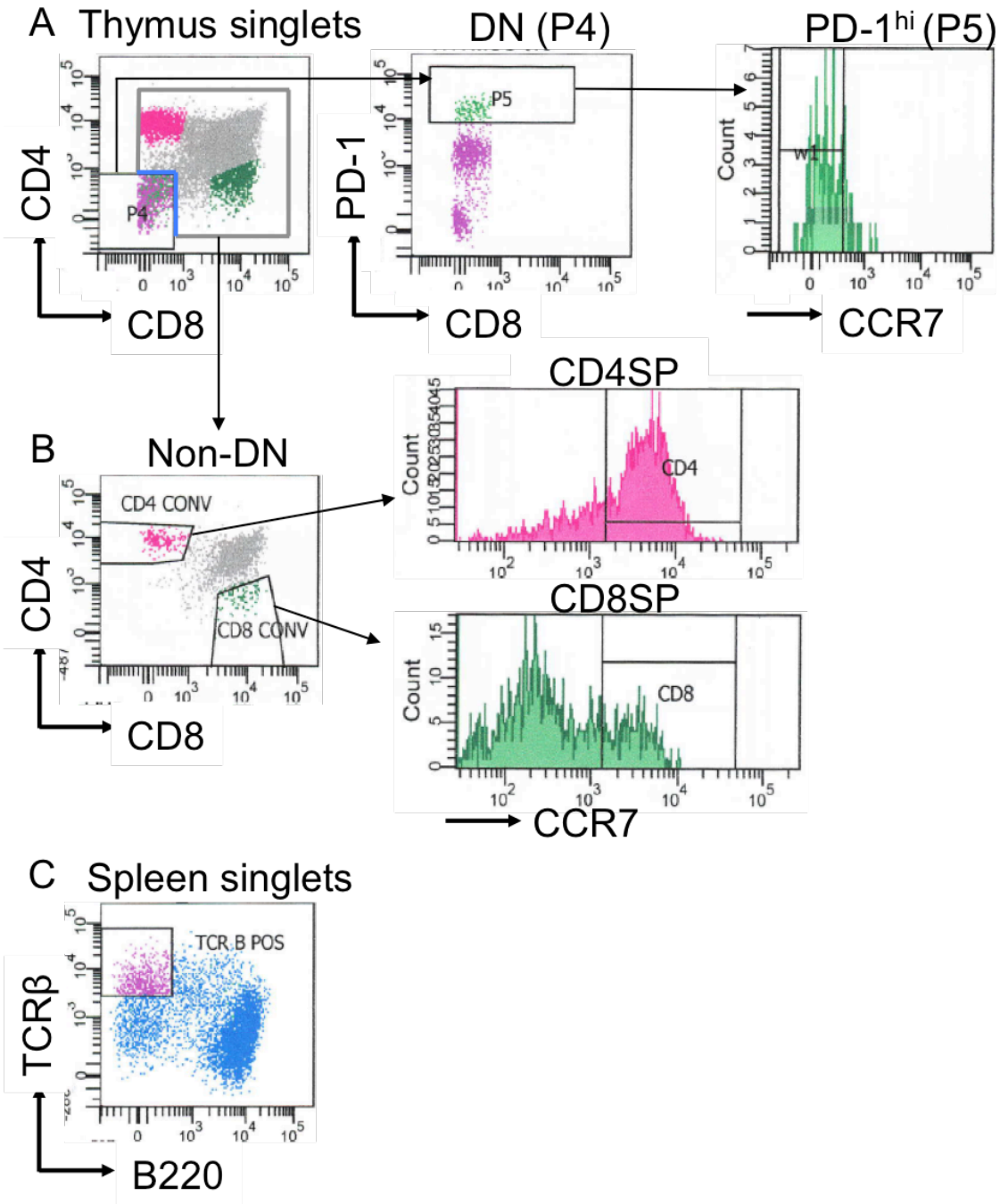

Figure 5.2. Cell sorting strategy to define thymocyte and splenocyte subsets for TCR sequencing. Thymus was harvested from WT, *B2m*$^{-/-}$, *H2-Aa*$^{-/-}$ and *B2m*$^{-/-}$*H2-Aa*$^{-/-}$ mice and spleen harvested from *B2m*$^{-/-}$*H2-Aa*$^{-/-}$ mice. After doublet exclusion, (A) W1 thymocytes were identified as CD4^{-}CD8^{-} PD-1^{hi} CCR7^{-} and (B) CD4SP and CD8SP subsets were non-DN, CD4^{+} CCR7^{+} or CD8^{+} CCR7^{+} cells. (C) After excluding doublets, splenocytes were gated for TCRβ^{+} B220^{-} population. A total of 50,000 cells were sorted for each subset or until the sample was exhausted.

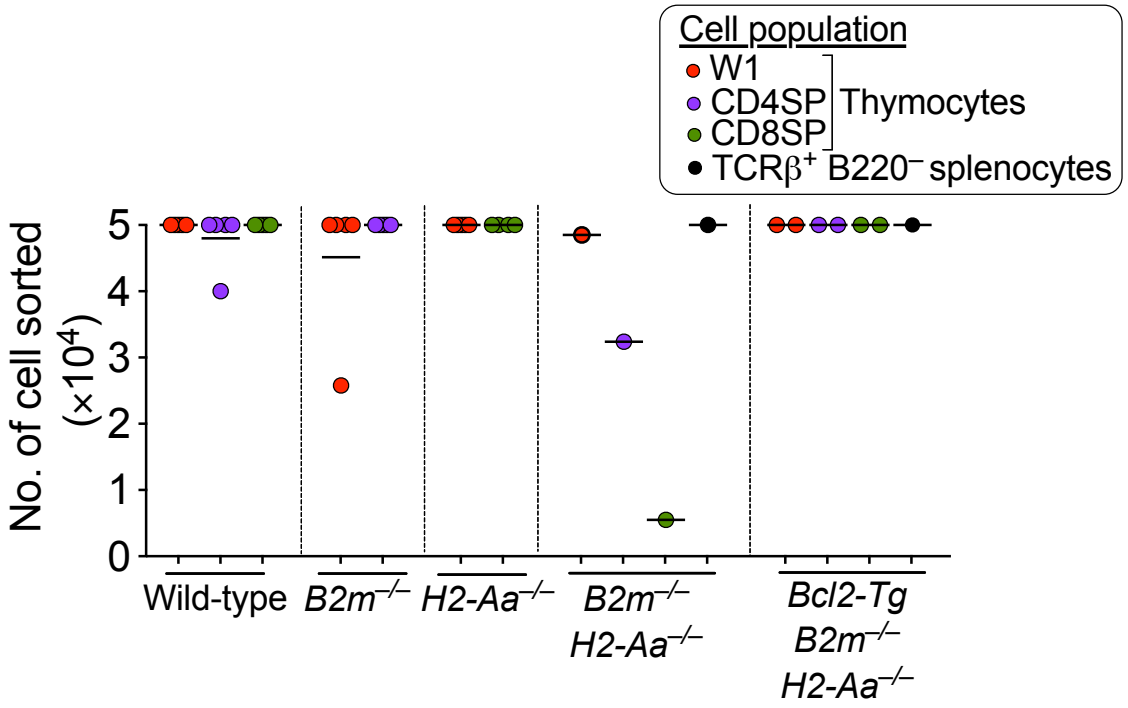

Figure 5.3. Number of T cells sorted per sample. Graph shows the number of cells sorted for each of the 45 samples described in Figs. 5.1-5.2. Each symbol represents an individual sample.

5.2.2 Preparation and sequencing of TCRα chain libraries

After cell sorting, RNA was extracted and reverse transcription performed to obtain cDNA (Fig. 5.4A). PCR was performed using a pool of 14 forward primers complementary to TCRα chain V (TRAV) segments and one reverse primer complementary to the TCRα chain constant (TRAC) region (Dash et al., 2011) (Fig. 5.4A) (Table 2.3, Chapter 2). Each forward and reverse primer contains a 5' adapter sequence, which was used as a target in a second PCR amplification (also known as indexing PCR), for the addition of sample-specific "barcodes" plus P5/P7 sequences to facilitate binding of amplicons to the Illumina flowcell (Bourlat et al., 2016). Gel electrophoresis of a representative sample following the first PCR demonstrated a prominent band at ~300bp, similar to a positive control thymocyte subset (Fig. 5.4B). This suggested that the first PCR amplifying TCRα chain transcripts was successful.

Before and after the second PCR, the PCR products were processed using the Agencourt AMPure XP purification system. In this step, the DNA amplicons were immobilised with magnetic beads (Beckman Coulter) while the unincorporated dNTPs, primers, primer dimers and salts were removed (Fig. 2.4, Chapter 2). Gel electrophoresis after the indexing PCR demonstrated two distinct bands at 380 and 400 bp, with the latter band being more prominent. This is consistent with successful incorporation of sequencing adaptors and sample-specific barcodes during the second PCR (Fig. 5.4C).

The size and the concentration of the purified and indexed PCR amplicons in each sample were determined by PerkinElmer LabChip® GX high-resolution electrophoretic separation. Four bands between 300 and 700bp were detected in each of the sorted W1, CD4SP and CD8SP samples (Fig. 5.4D). In each sample, the concentration of PCR amplicons ranging from 380 to 610 bp were summed to facilitate their dilution to a final concentration of 2 nM per sample (section 2.3.6.7). Finally, equivalent volumes of all 45 samples were pooled in a single tube for paired-end sequencing-by-synthesis using reversible terminator dye nucleotides on an Illumina MiSeq machine (2 x 250 cycles) (Bentley et al., 2008; Kozich et al., 2013) (Fig. 5.4A).

5.2.3 Processing raw sequencing reads for TCRα chains into TCR nucleotypes

PANDAseq (PAired-eND Assembler for Illumina sequences) software was used to assemble TCRα chain Illumina paired-end sequence reads (forward read (read 1) and reverse read (read 2)) into a single sequence (Masella et al., 2012). PANDAseq determines the amount of overlap between read 1 and read 2, and constructs a consensus sequence by correcting uncalled bases and mismatches in the overlapping region based on the read quality (quality score assigned to the assembled sequence) (Masella et al., 2012).

MiTCR (V-(D)-J mapping software) was used to convert the assembled sequencing reads into TCR "nucleotypes". A TCR nucleotype is a unique nucleotide sequence that MiTCR aligns to V and J segments of the *Tcra* locus. MiTCR also reports the read count of each TCR nucleotype within each sample (Bolotin et al., 2013) (Fig. 5.5). MiTCR uses the conserved cysteine (C) residue to mark the N-terminal residue of the CDR3, and Phenylalanine (F) or Tryptophan (W) to mark the C-terminal residue of the CDR3. Since multiple TCR nucleotypes could encode the same amino acid sequence (Miles et al., 2011), the term TCR "clonotype" denotes a unique combination of CDR3 amino acid sequence (CDR3α) and V segment of TCRα chain (TRAV).

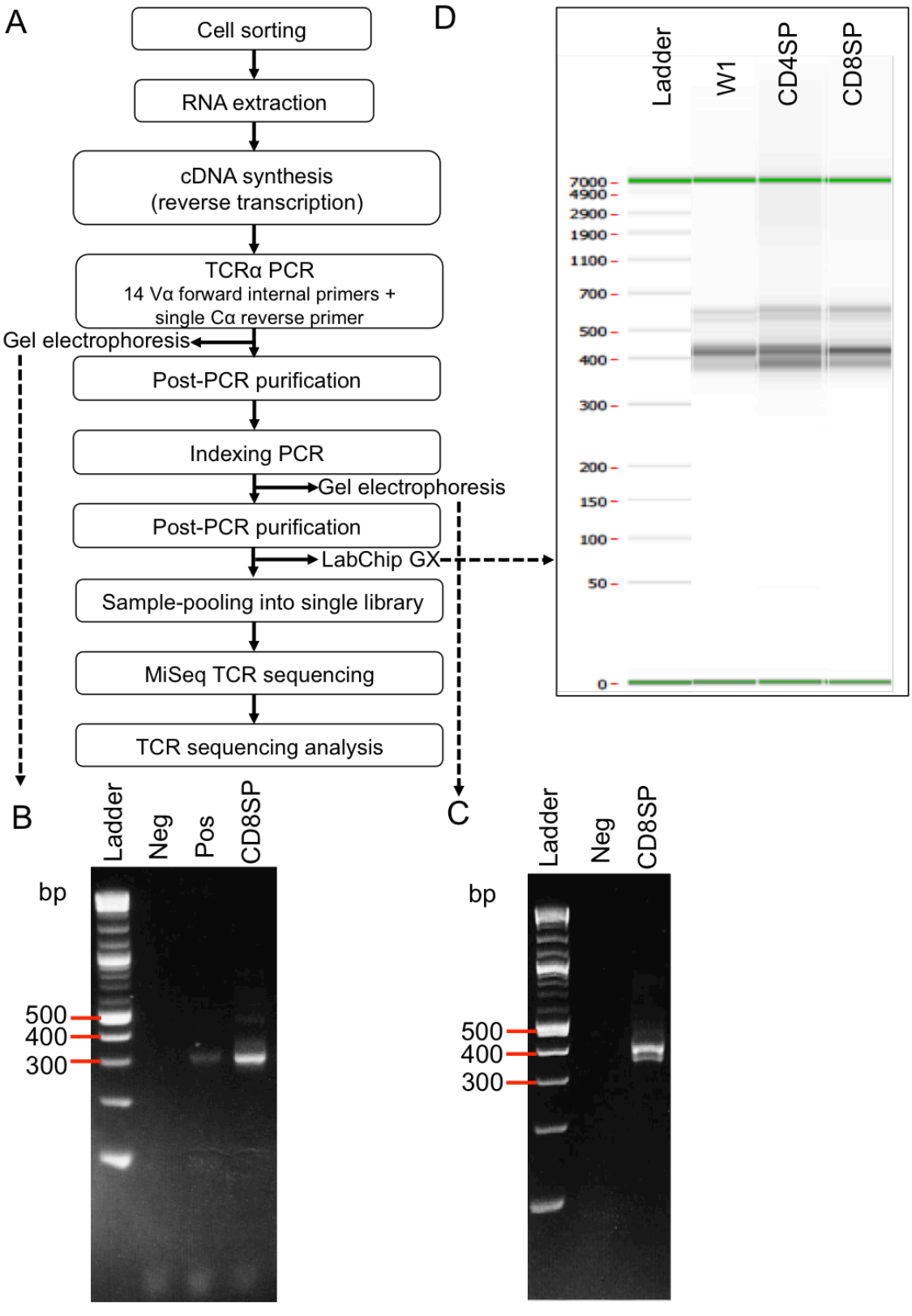
A
Cell sorting
RNA extraction
cDNA synthesis
(reverse transcription)
TCRα PCR
14 Vα forward internal primers +
single Cα reverse primer
Gel electrophoresis
Post-PCR purification
Indexing PCR
Gel electrophoresis
Post-PCR purification
LabChip GX
Sample-pooling into single library
MiSeq TCR sequencing
TCR sequencing analysis
D
Ladder
W1
CD4SP
CD8SP
7000
4900
2900
1900
1100
700
500
400
300
200
150
100
50
0
B
Ladder
Neg
Pos
CD8SP
bp
500
400
300
C
Ladder
Neg
CD8SP
bp
500
400
300

Figure 5.4. Strategy for TCRα chain amplification and sequencing. (A) Overview of the TCRα chain amplification and sequencing. After cell sorting as described in Fig. 5.2, RNA of the sorted cells was extracted for cDNA synthesis. TCRα chain was first PCR amplified using 14 Vα forward internal primers and one Cα reverse primer. Each primer contains a 5' overhang adapter sequence, which allows the binding of index adapter primers (containing P5/P7 sequencing adaptors, unique 8bp-index sequence and sequence complementary to the 5' overhang adaptor sequence) (Fig. 2.2, Chapter 2) during the indexing (second) PCR. The indexing PCR was performed to add sequencing adapters and sample-specific indices to the amplicons. Agarose gel electrophoresis and purification of PCR products were performed after the first and second PCRs. After purification of the indexed PCR products, samples were analysed by PerkinElmer LabChip® GX to perform high-resolution electrophoretic separations, to determine the concentration and size of the final PCR amplicons. After diluting all samples to a concentration of 2 nM, equal volumes of each sample were pooled into a single library for TCR deep sequencing. (B) Gel electrophoresis of the first PCR amplicons. (Left to right) DNA ladder, negative control (without cDNA template but with nuclease free water), positive control containing cDNA of unsorted mouse thymocytes and CD8SP thymocyte subset of a wild-type mouse. (C) Gel electrophoresis of indexed PCR amplicons. (Left to right) DNA ladder, negative control (without cDNA template but with nuclease free water), CD8SP sample from a wild-type mouse. (D) Gel appearance of the indexed TCRα amplicon from sorted W1, CD4SP and CD8SP sorted thymocyte subsets from a wild-type mouse as performed by LabChip® GX.

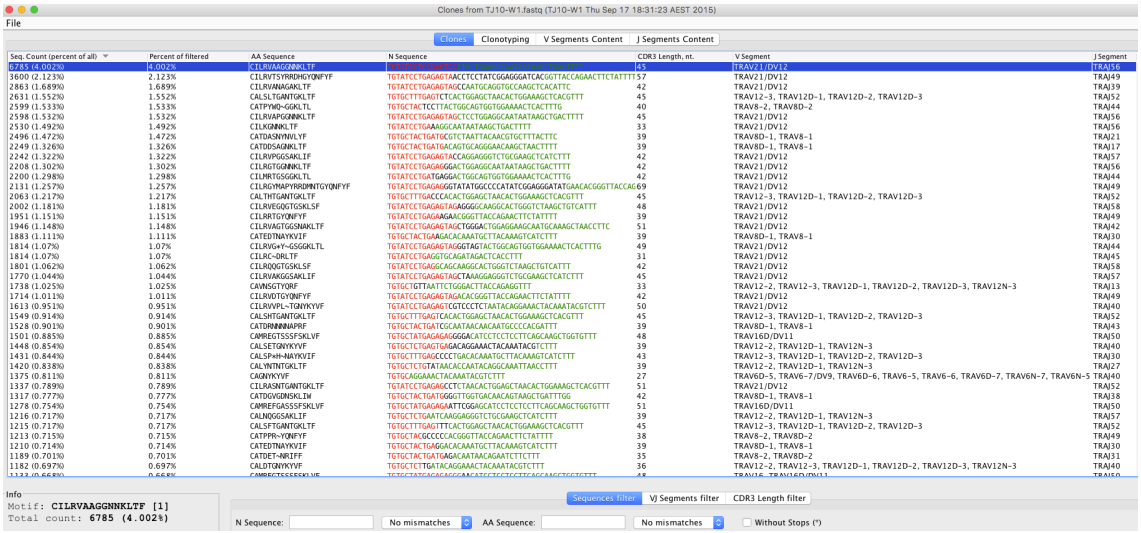

Figure 5.5. Ascertainment and counting of TCRα chain sequence reads by MiTCR software. Diagram of MiTCR interface shows (left to right column) the number of sequencing reads of each TCR nucleotype and the percentage of this nucleotype in a sample (equal to the number of sequencing reads for each TCR nucleotype divided by the total number of sequencing reads per sample), CDR3α amino acid sequence, CDR3α nucleotide sequence, the number of nucleotides encoding the CDR3α, the list of possible V segments and J segment for each TCR nucleotype.

5.2.4 Count and diversity of TCR nucleotypes

TCR sequencing data were analysed using VDJtools software (Shugay et al., 2015). This required data to be converted from MiTCR format into VDJtools format. As VDJtools accepts only one TRAV segment per TCR nucleotype, for each TCR nucleotype only the TRAV segment listed first by MiTCR was retained in the datasets used for VDJtools analysis. The basic information on the TCR nucleotypes in each sample was obtained using *CalcBasicStats* routine. Across the groups defined by MHC genotype and T cell subset, the mean number of sequencing reads (i.e. "count" in VDJtools) ranged from 1.4×10^5 to 3.5×10^5 (Fig. 5.6A). The mean of number of TCR nucleotypes (i.e. "diversity" in VDJtools) ranged from 101 to 994 (Fig. 5.6B). CD4SP and CD8SP samples tended to have more TCR nucleotypes than the W1 samples, except for Non-Tg and *Bcl2*-Tg *B2m*$^{-/-}$*H2-Aa*$^{-/-}$ mice (Fig. 5.6B). A W1 sample in the *H2-Aa*$^{-/-}$ group had the lowest number of sequencing reads (Fig. 5.6A) and also the lowest number of nucleotypes (Fig. 5.6B). The number of nucleotypes per sample correlated with the number of sequencing reads per sample (Fig. 5.6C). This suggests that the estimation of TCR nucleotype diversity in each sample was limited by the number of sequencing reads obtained.

5.2.5 Pre-processing of the TCR nucleotypes

Prior to assignment of TCR clonotype for subsequent analysis, the VDJtools *Correct* routine was used to merge low-abundance nucleotypes into higher-abundance nucleotypes with a similar nucleotide sequence. The maximum number of nucleotide mismatches allowed between merged sequences was 2. The maximum fold-difference in read frequency allowed between the low-abundance sequence and high-abundance sequence was 0.05. After the VDJtools *Correct* routine was performed, the mean frequency of nucleotypes retained, relative to pre-processing, was >97%. Some samples in *B2m*$^{-/-}$*H2-Aa*$^{-/-}$ and *Bcl-2* Tg *B2m*$^{-/-}$*H2-Aa*$^{-/-}$ groups had as low as 91% of clonotypes retained (Fig. 5.7A).

The VDJtools *FilterNonFunctional* routine was then used to remove sequences containing a stop codon or a frameshift in the putative TCRα sequence. Across all cell subsets and mouse groups, a mean of ~75% of nucleotypes were functional (Fig. 5.7B). In mature T cells, non-functional TCRα chain sequences are transcribed from the *Tcra* locus situated on the homologous chromosome, which was rearranged during thymocyte development but failed to encode a functional protein.

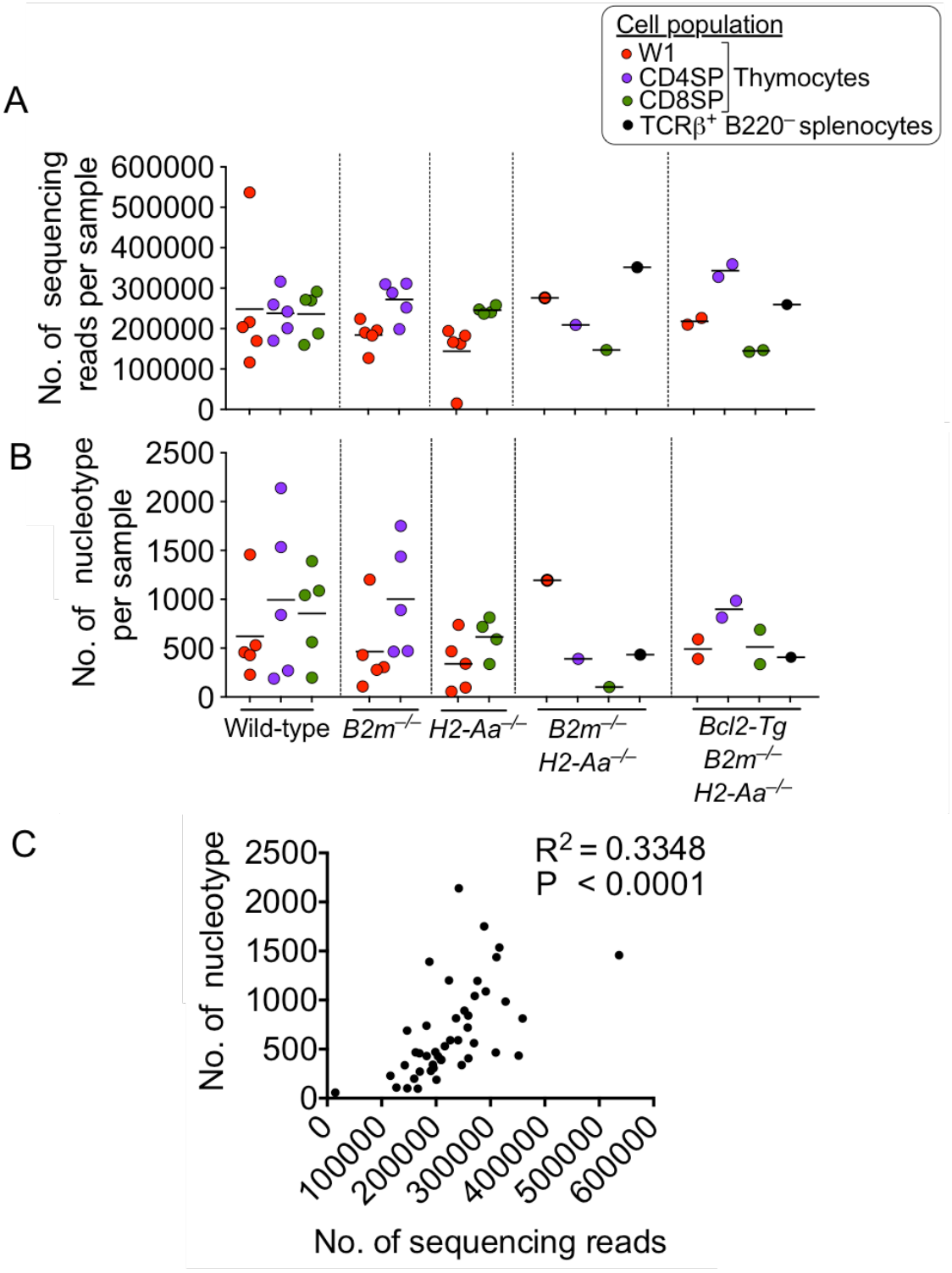

Figure 5.6. Count and diversity of TCR nucleotypes. For the 45 samples described in Figs. 5.1-5.3, graphs show (A) number of sequencing reads (i.e. count), (B) number of TCR nucleotypes (i.e. diversity) and (c) XY plot for the count and diversity of each sample. The r^2 and two-tailed P values were calculated from the Pearson correlation coefficient by GraphPad Prism. Each symbol represents a sample. Data were analysed using VDJtools *CalcBasicStats* routines.

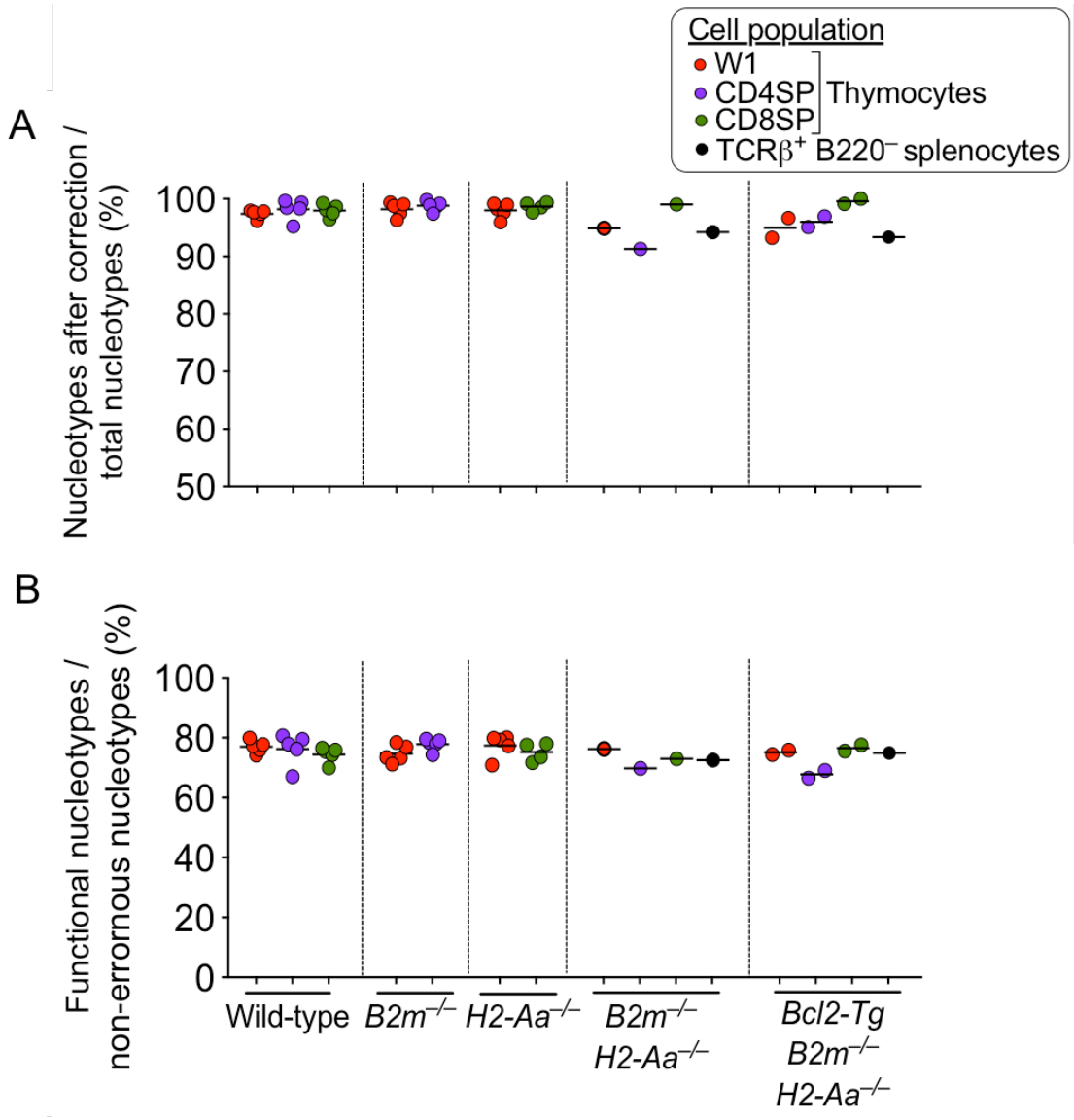

Figure 5.7. Erroneous nucleotype correction and non-functional nucleotype filtering. For the 45 samples described in Figs. 5.1-5.3, graphs show the frequency of (A) TCR nucleotypes retained after correction and (B) functional nucleotypes after filtering the non-functional clonotypes. Each symbol represents a sample. Data were analysed using VDJtools *Correct* and *FilterNonFunctional* routines.

5.2.6 Unsupervised hierarchical clustering of TCR clonotypes

Unless stated otherwise, analyses were performed based on data collapsed by "TCR clonotype", which was defined as a unique combination of CDR3α amino acid sequence and TRAV segment. To gain an overview of the TCR sequencing data, VDJtools *CalcPairwiseDistances* and *ClusterSamples* routines were used to generate a multidimensional scaling (MDS) plot on which all samples were represented (Fig. 5.8). The MDS plot was generated based on the default setting in VDJtools (the "F" metric). In this metric, the distance between a pair of samples is calculated as $-\log_{10}$ of the geometric mean of the frequencies of TCR clonotypes that were present in both samples in the pair (Shugay et al., 2015) (section 2.3.7.3 for formula). For example, two samples in which 10% of sequences encode shared TCR clonotypes would be placed 1 unit apart. Two samples in which 1% of sequences encode shared TCR clonotypes would be placed 2 units apart.

In the wild-type dataset, W1, CD4SP and CD8SP repertoires formed three distinct clusters (Fig. 5.8, green symbols). This suggests the W1 repertoire and both positively selected CD4SP and CD8SP repertoires are all distinct from each other in wild-type mice. W1 and CD4SP repertoires in *B2m*$^{-/-}$ (orange) mice formed two distinct clusters, while W1 and CD8SP repertoires in *H2-Aa*$^{-/-}$ (blue) mice were also separated from each other (Fig. 5.8).

In *B2m*$^{-/-}$*H2-Aa*$^{-/-}$ (pink) and *Bcl-2* Tg *B2m*$^{-/-}$*H2-Aa*$^{-/-}$ (turquoise) mice, W1 repertoires were clustered together (Fig. 5.8). CD4SP and CD8SP repertoires from *B2m*$^{-/-}$*H2-Aa*$^{-/-}$ and *Bcl-2* Tg *B2m*$^{-/-}$*H2-Aa*$^{-/-}$ mice formed a single cluster that was separate from W1 repertoires (Fig. 5.8). The two TCRβ^{+} B220^{-} splenocyte samples from *B2m*$^{-/-}$*H2-Aa*$^{-/-}$ and *Bcl-2* Tg *B2m*$^{-/-}$*H2-Aa*$^{-/-}$ mice fell between the W1 cluster and the CD4SP/CD8SP cluster from the same mice (Fig. 5.8). Since the TCR repertoires between *B2m*$^{-/-}$*H2-Aa*$^{-/-}$ and *Bcl-2* Tg *B2m*$^{-/-}$*H2-Aa*$^{-/-}$ mice were similar in all cell subsets analysed, *B2m*$^{-/-}$*H2-Aa*$^{-/-}$ and *Bcl-2* Tg *B2m*$^{-/-}$*H2-Aa*$^{-/-}$ mice are collectively called "*B2m*$^{-/-}$*H2-Aa*$^{-/-}$" mice below.

W1 repertoires in wild-type, *B2m*$^{-/-}$ and *H2-Aa*$^{-/-}$ mice were broadly clustered together, but were distinct from the W1 repertoires in *B2m*$^{-/-}$*H2-Aa*$^{-/-}$ mice (Fig. 5.8). However, there was a *H2-Aa*$^{-/-}$ W1 sample identified with an asterisk that was far from the rest of W1 samples and located at the centre of the plot. This particular sample also had the lowest number of sequencing reads and nucleotypes (Fig. 5.6).

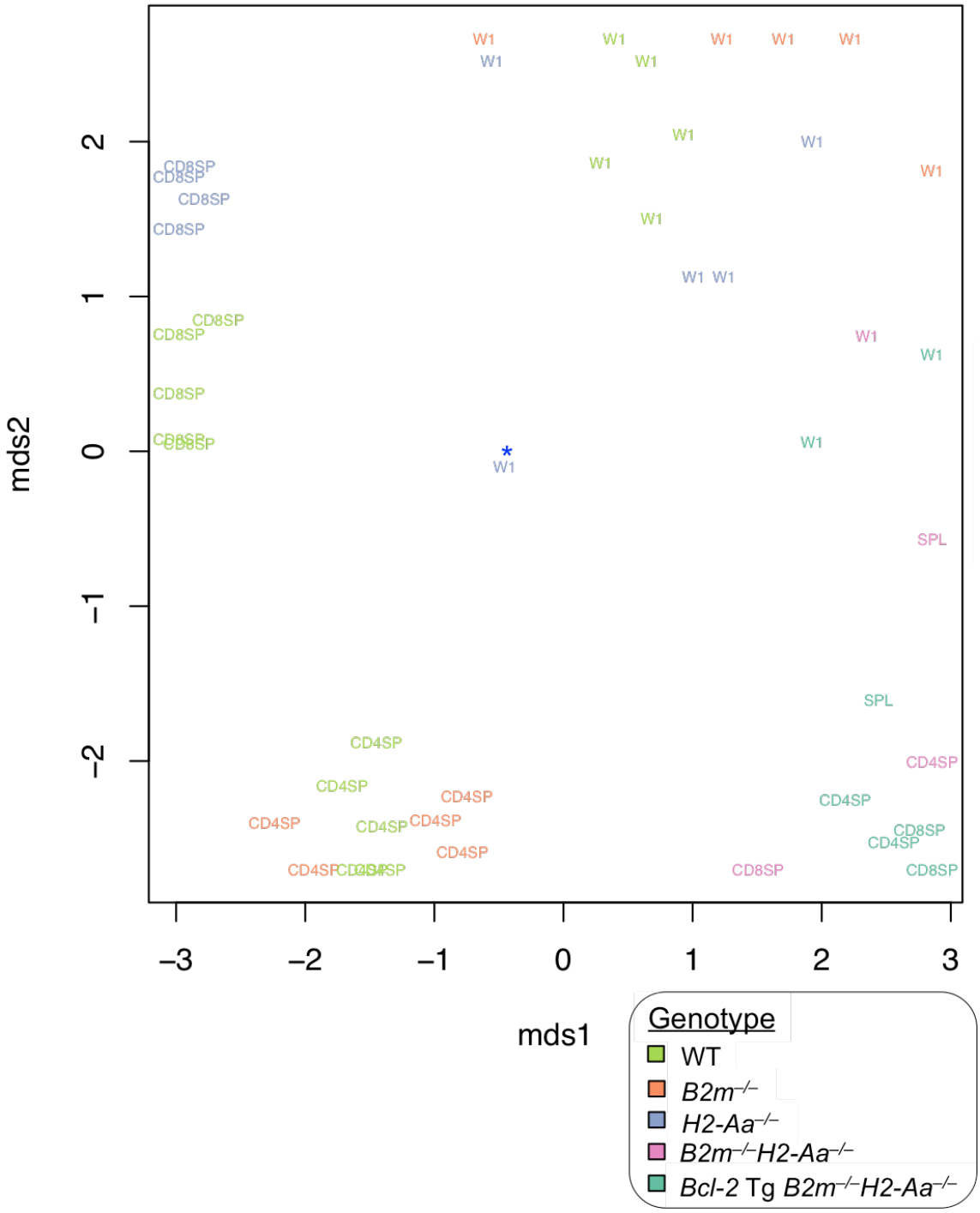

Figure 5.8. Unsupervised clustering of TCR repertoires of different cell subsets across different mouse genotypes. For the 45 samples described in Figs. 5.1-5.3, the multidimensional scaling (MDS) plot shows the distance between TCR repertoires (i.e. samples) on a two-dimensional plane computed by *CalcPairwiseDistances* and *ClusterSamples* routines in VDJtools. The distances between samples were calculated based on F pairwise similarity metric. In this and subsequent analyses, a TCR clonotype was defined as a TCRα sequence, or family of TCRα nucleotypes, that encodes a unique combination of CDR3 amino acid sequence and V segment (specified by the code "-i aaV" in VDJtools). *Sample with lowest number of sequencing reads and nucleotypes.

The CD4SP repertoires in *B2m*$^{-/-}$ mice and wild-type mice were co-clustered (Fig. 5.8). By contrast, the wild-type CD8SP cluster was adjacent to, but detectably removed from the *H2-Aa*$^{-/-}$ CD8SP cluster. CD4SP/CD8SP repertoires in *B2m*$^{-/-}$*H2-Aa*$^{-/-}$ mice did not cluster with either CD4SP or CD8SP repertoires in mice expressing one or other MHC class (Fig. 5.8).

5.2.7 MHC class cross-reactive TCRs are not common in the Wave 1 TCR repertoire

5.2.7.1 Sharing of TCR clonotypes within and across boundaries of cell type and MHC genotype

As the number of TCR clonotypes per sample varied from 44 to 1654 across the 45 samples (Fig. 5.9), this variation could affect estimates of the extent of TCR sharing between any pair of samples. To hold constant the number of clonotypes per sample, VDJtools *SelectTop* routine was used to select the 200* TCR clonotypes with the most sequencing reads in each sample. VDJtools *TrackClonotypes* routine was then used to investigate TCR sharing between pairs of samples**. The data are presented as heatmaps with individual samples arranged in the same order on the *x*- and *y*-axes, forming a grid. Darker squares on the grid indicate higher numbers of shared TCR clonotypes in the 2 samples whose column or row intersect at that square.

5.2.7.1.1 TCR clonotype sharing within MHC genotype boundaries

i) Distinct W1, CD4SP and CD8SP TCR repertoires in wild-type mice

In the wild-type dataset derived from 5 mice, each pair of W1 samples shared between 8 and 26 TCR clonotypes (Fig. 5.10A). CD4SP sample pairs showed slightly more overlap, between 9 and 41 shared TCR clonotypes, while CD8SP sample pairs shared 21-49 TCR clonotypes (Fig. 5.10A). TCR clonotype sharing between CD4SP and CD8SP was detectable, albeit at a lower level, with up to 10 shared TCR clonotypes per pair (Fig. 5.10A). The lowest level of TCR clonotype sharing was detected between W1 and the CD4SP or CD8SP subsets. Here, the only overlaps detected were <8 TCR clonotypes in a particular W1 sample (#5) and one CD4SP sample (#23) plus one

*Some samples contained <200 TCR clonotypes. These are indicated by asterisks.
**This analysis (Fig. 5.13) was also performed on the samples containing all TCR clonotypes (not just the top 200 clonotypes). The results were consistent with the analysis reported and no additional conclusions were drawn.

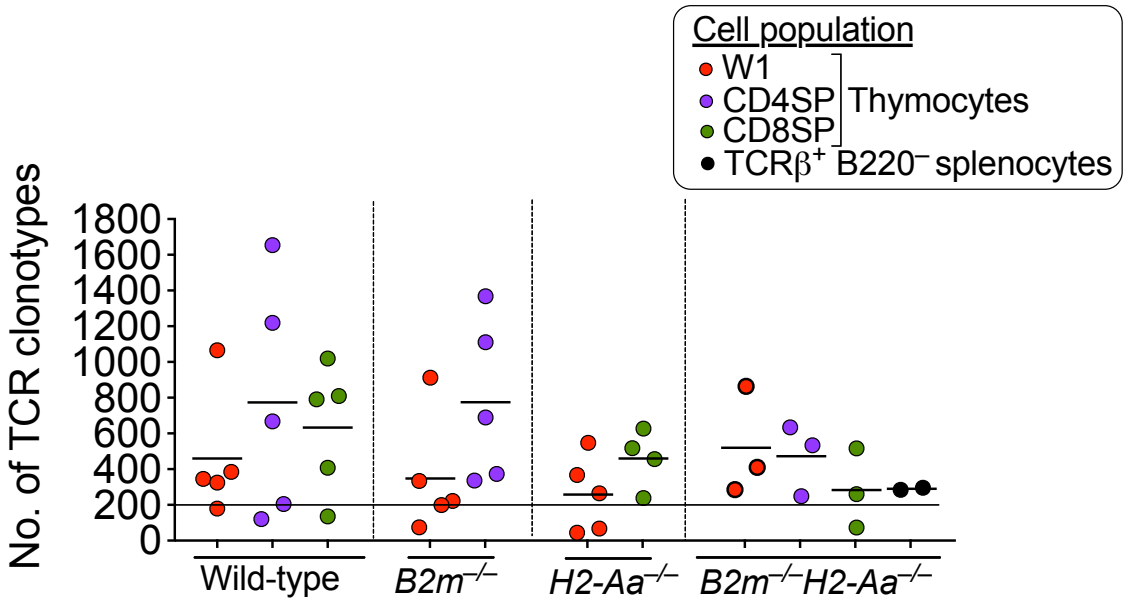

Figure 5.9. The number of TCR clonotypes varies across all sequencing samples. Graph shows the number of TCR clonotypes detected in each of the 45 samples described in Figs. 5.1-5.3. Short lines represent group means. Samples below the long line have <200 TCR clonotypes.

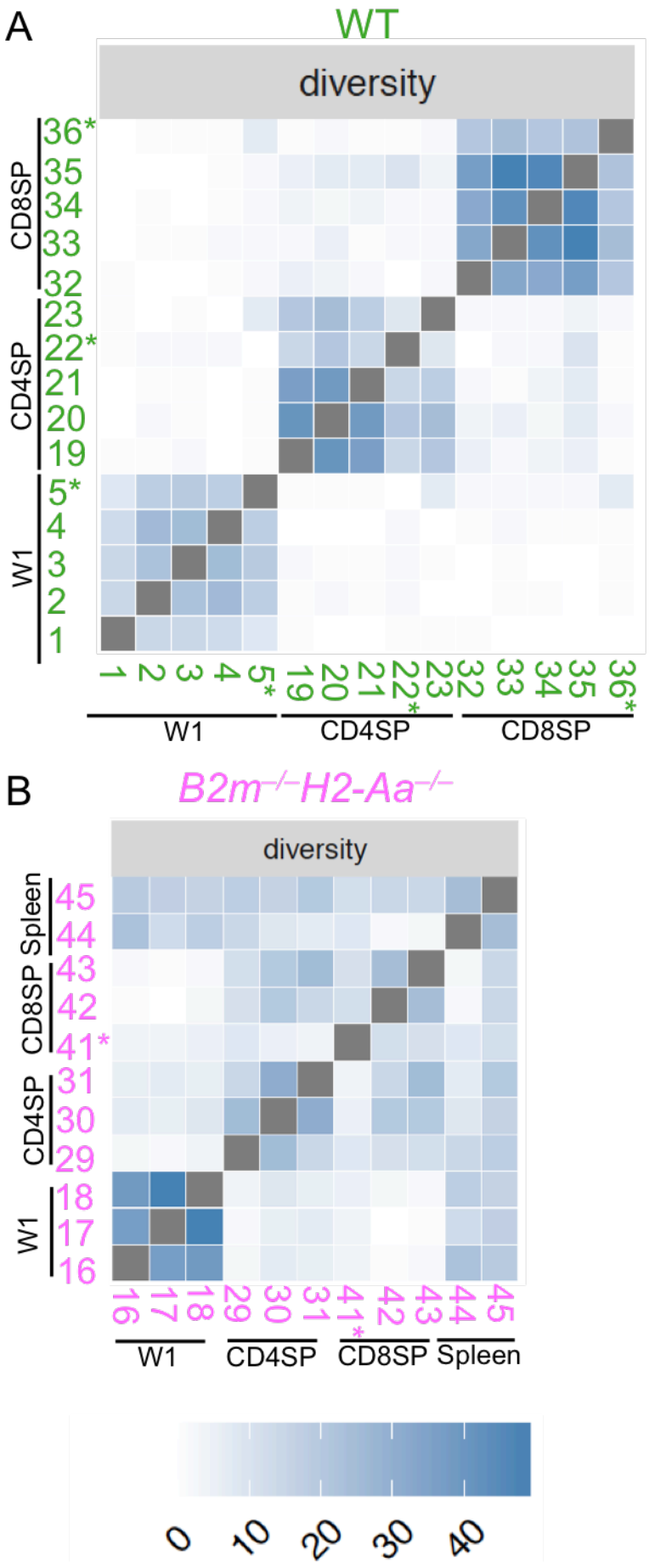
A
WT
diversity
CD8SP
CD4SP
W1
36*
35
34
33
32
23
22*
21
20
19
5*
4
3
2
1
1 2 3 4 5* 19 20 21 22* 23 32 33 34 35 36*
W1
CD4SP
CD8SP
B
B2m−/−H2-Aa−/−
diversity
Spleen
CD8SP
CD4SP
W1
45
44
43
42
41*
31
30
29
18
17
16
16 17 18 29 30 31 41* 42 43 44 45
W1
CD4SP
CD8SP
Spleen
0
10
20
30
40

Figure 5.10. The delineation between CD4SP and CD8SP TCR repertoires observed in wild-type mice requires MHC expression. VDJtools *SelectTop* routine was used to identify the 200 most abundant TCR clonotypes in each W1, CD4SP, CD8SP and/or TCRβ^{+} B220^{-} splenocyte sample of (A) wild-type mice (n = 5) and (B) *B2m*$^{-/-}$*H2-Aa*$^{-/-}$ mice (n = 2-3). VDJtools *TrackClonotypes* routine was used to generate heatmaps that indicate the number of shared TCR clonotypes (ranging from 0 to 50, see key at bottom) in pairs of samples denoted on the axes: W1, CD4SP, CD8SP thymocytes or TCRβ^{+} B220^{-} splenocytes. Numbers in green and pink indicate an arbitrary sample identifier (1-45 for the entire dataset). * indicates sample with <200 total TCR clonotypes. *Sample #5, 179 TCR clonotypes; *#22, 120 TCR clonotypes; *#36, 135 TCR clonotypes; *#41, 73 TCR clonotypes.

clonotypes in a particular W1 sample (#5) and one CD4SP sample (#23) plus one CD8SP sample (#36) (Fig. 5.10A). This suggests that in wild-type mice there is a sharp delineation between the W1 TCR repertoire and the other 2 TCR repertoires examined. The CD4SP and CD8SP TCR repertoires are also distinguishable from each other.

ii) Mice lacking MHC expression have a "fused" CD4SP/CD8SP TCR repertoire that remains distinct from the W1 repertoire

In the *B2m*$^{-/-}$*H2-Aa*$^{-/-}$ dataset derived from 3 mice, the highest level of TCR clonotype sharing was observed in W1 samples (35-50 shared TCR clonotypes per pair), while CD4SP, CD8SP and TCRβ^{+} B220^{-} splenocytes each had 15 to 31, 11 to 24, and 24 shared TCR clonotypes per pair, respectively (Fig. 5.10B). TCR clonotypes in W1 samples were less commonly shared with CD4SP and CD8SP samples (<10 per pair) (Fig. 5.10B). This indicates that the W1 TCR repertoire is distinguishable from CD4SP and CD8SP repertoires in mice lacking MHC expression (Fig. 5.10B).

In contrast to the wild-type dataset, there was a significant level of TCR clonotype sharing between CD4SP and CD8SP samples in the *B2m*$^{-/-}$*H2-Aa*$^{-/-}$ dataset (4 to 25 TCR clonotypes per pair) (Fig. 5.10B). This level of TCR clonotype sharing, across the so-called CD4SP/CD8SP cell type "boundary", was similar to the level observed when comparing pairs of samples within each cell type. These data show that the delineation between CD4SP and CD8SP TCR repertoires observed in wild-type mice requires MHC expression.

The TCRβ^{+} B220^{-} splenocyte TCR repertoire overlapped with that of CD4SP and CD8SP thymocytes (2 to 20 shared TCR clonotypes per pair) in the *B2m*$^{-/-}$*H2-Aa*$^{-/-}$ dataset (Fig. 5.10B). The W1 TCR repertoire overlapped more with the TCRβ^{+} B220^{-} splenocyte TCR repertoire (13 to 23 per pair) than with CD4SP or CD8SP thymocyte repertoires (<10 per pair) (Fig. 5.10B).

iii) Distinct W1 and CD4SP TCR repertoires in *B2m*$^{-/-}$ mice

In the *B2m*$^{-/-}$ dataset derived from 5 mice, 5 to 11 TCR clonotypes were shared per pair of W1 samples (Fig. 5.11A). CD4SP sample pairs showed more overlap, with 16 to 35 shared TCR clonotypes (Fig. 5.11A). W1 samples generally did not share TCR clonotypes with CD4SP samples, except for one W1 sample (#7) and one CD4SP sample (#25) (Fig. 5.11A). This suggests that W1 and CD4SP TCR repertoires remain distinct in mice lacking MHCI expression.

iv) Distinct W1 and CD8SP TCR repertoires in *H2-Aa*$^{-/-}$ mice

In the *H2-Aa*$^{-/-}$ dataset derived from 4 to 5 mice, 23 to 33 TCR clonotypes were shared per pair of W1 samples, except for two samples #11 and #15 with lower TCR clonotype sharing (<16 per pair) (Fig. 5.11B). Within the CD8SP samples, 13 to 30 shared TCR clonotypes per pair were observed (Fig. 5.11B). W1 samples did not share TCR clonotypes with CD8SP samples (Fig. 5.11B). This suggests that W1 and CD8SP TCR repertoires remain distinct in the absence of MHCII expression.

5.2.7.1.2 TCR clonotype sharing within cell type boundaries

i) Elevated TCR clonotype sharing in W1 sample pairs involving wild-type and *H2-Aa*$^{-/-}$ mice

Within the W1 dataset, the extent of TCR clonotype sharing across MHC genotype "boundaries" was greatest when comparing WT with *H2-Aa*$^{-/-}$ mice (up to 25 TCR clonotypes per pair), exceeding the levels observed when comparing WT with *B2m*$^{-/-}$ mice (up to 12 shared TCRs per pair) (Fig. 5.12A). This observation suggests the W1 repertoire in wild-type mice is enriched in TCRs responsive to MHC class I.

TCR clonotype sharing was very low when comparing W1 samples from wild-type mice with *B2m*$^{-/-}$*H2-Aa*$^{-/-}$ mice (<5 per pair) (Fig. 5.12A). More TCR sharing was detected when comparing W1 samples from mice lacking a single MHC class with *B2m*$^{-/-}$*H2-Aa*$^{-/-}$ mice (up to 9 per pair for both comparisons) (Fig. 5.12A). This observation suggests that deficiency of one MHC class may increase the appearance of MHC-independent TCRs in the W1 TCR repertoire.

ii) The wild-type CD4SP TCR repertoire remains intact in *B2m*$^{-/-}$ mice, but is profoundly altered in *B2m*$^{-/-}$*H2-Aa*$^{-/-}$ mice

Within the CD4SP dataset, all wild-type mice shared TCR clonotypes with all *B2m*$^{-/-}$ mice. Wild-type samples #19-21 shared a higher number of TCR clonotypes with all *B2m*$^{-/-}$ mice (up to 37 per pair) (Fig. 5.12B). This suggests that the wild-type CD4SP TCR repertoire remains intact in the absence of MHCI. However, CD4SP samples from *B2m*$^{-/-}$*H2-Aa*$^{-/-}$ mice exhibited little TCR clonotype sharing with CD4SP samples from wild-type or *B2m*$^{-/-}$ mice (Fig. 5.12B). This data provides no evidence that the absence

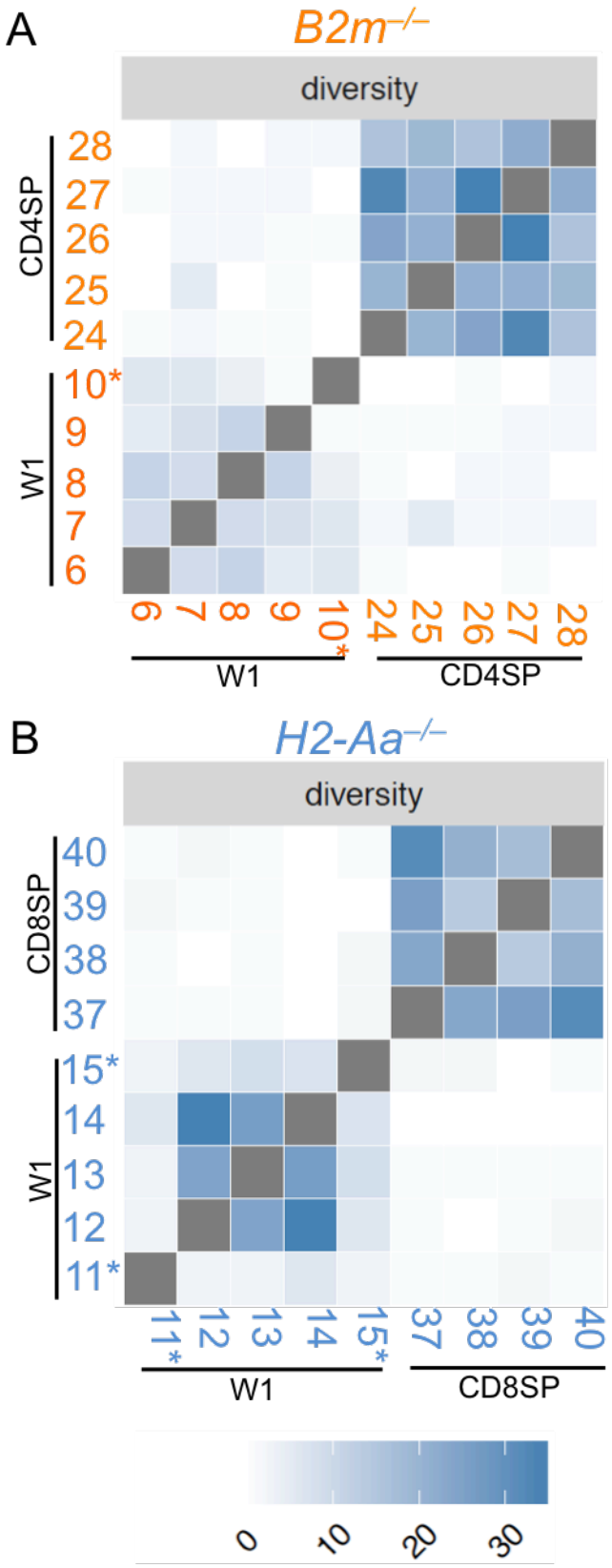
A
B2m−/−
diversity
CD4SP
28
27
26
25
24
W1
10*
9
8
7
6
6 7 8 9 10* 24 25 26 27 28
W1
CD4SP
B
H2-Aa−/−
diversity
CD8SP
40
39
38
37
W1
15*
14
13
12
11*
11* 12 13 14 15* 37 38 39 40
W1
CD8SP
0
10
20
30

Figure 5.11. The delineation between W1 and CD4SP or CD8SP TCR repertoires remains intact in mice expressing only 1 MHC class. VDJtools *SelectTop* routine was used to identify the 200 most abundant TCR clonotypes in each W1, CD4SP or CD8SP thymocyte sample of (A) *B2m*$^{-/-}$ mice (n = 5) and (B) *H2-Aa*$^{-/-}$ mice (n = 4-5). VDJtools *TrackClonotypes* routine was used to generate heatmaps that indicate the number of shared TCR clonotypes (ranging from 0 to 35, see key at bottom) in pairs of samples denoted on the axes: W1, CD4SP or CD8SP thymocytes. Numbers in orange and blue indicate an arbitrary sample identifier (1-45 for the entire dataset). * indicates sample with <200 total TCR clonotypes. *Sample #10, 74 TCR clonotypes; *#11, 44 TCR clonotypes; *#15, 68 TCR clonotypes.

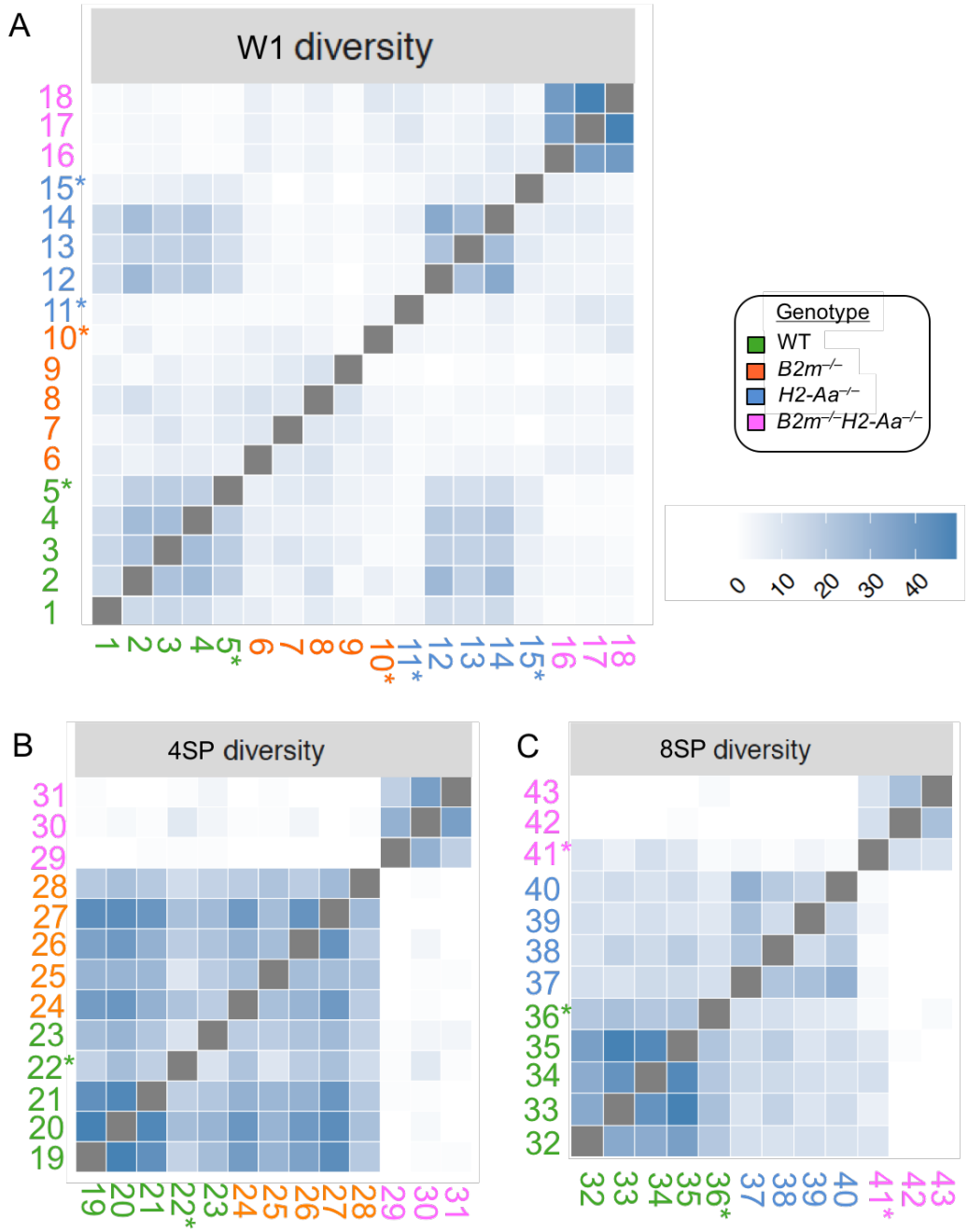

Figure 5.12. Wild-type W1, CD4SP and CD8SP TCR repertoire remains largely intact in and/or *H2-Aa*$^{-/-}$ mice, but is altered in *B2m*$^{-/-}$*H2-Aa*$^{-/-}$ mice. VDJtools *SelectTop* routine was used to identify the 200 most abundant TCR clonotypes in the samples described in Figs. 5.1-5.3. VDJtools *TrackClonotypes* routine was used to generate heatmaps that indicate the number of shared TCR clonotypes (ranging from 0 to 50, see key at top right) in pairs of samples denoted on the axes: thymocyte samples of each MHC genotype. Numbers indicate an arbitrary sample identifier (1-45 for the entire dataset). * indicates sample with <200 total TCR clonotypes. *Sample #5, 179 TCR clonotypes; #10, 74 TCR clonotypes; *#11, 44 TCR clonotypes; *#15, 68 TCR clonotypes; *#22, 120 TCR clonotypes; *#36, 135 TCR clonotypes; *#41, 73 TCR clonotypes.

of MHCI expression alters the CD4SP TCR repertoire, whereas the additional absence of MHCII is sufficient to markedly alter the CD4SP TCR repertoire.

iii) The wild-type CD8SP TCR repertoire remains largely intact in *H2-Aa*$^{-/-}$ mice, but appears to be altered in *B2m*$^{-/-}$*H2-Aa*$^{-/-}$ mice

Within the CD8SP dataset, TCR clonotype sharing was detected between all wild-type mice and all *H2-Aa*$^{-/-}$ mice (8 to 17 TCR clonotypes per pair) (Fig. 5.12C). This suggests that the wild-type CD8SP TCR repertoire remains largely intact in *H2-Aa*$^{-/-}$ mice. Two out of three *B2m*$^{-/-}$*H2-Aa*$^{-/-}$ CD8SP samples did not share TCR clonotypes with CD8 samples in wild-type or *H2-Aa*$^{-/-}$ mice (Fig. 5.12C). However, one *B2m*$^{-/-}$*H2-Aa*$^{-/-}$ CD8SP sample (#41) shared TCR clonotypes with nearly all wild-type samples (up to 12 per pair) (Fig. 5.12C). This data provides no obvious evidence that the absence of MHCII expression alters the CD8SP TCR repertoire. With the caveat that 1 out of 3 *B2m*$^{-/-}$*H2-Aa*$^{-/-}$ CD8SP samples generated different results, it appears that the additional absence of both MHCI and MHCII is sufficient to markedly alter the CD8SP TCR repertoire.

5.2.7.1.3 TCR clonotype sharing across MHC genotype and cell type boundaries

To look for unexpected examples of TCR clonotype sharing, a comparison was performed that included all possible pairs derived from the 45 samples, filtered to contain only the top 200 TCR clonotypes in each sample. This procedure has the potential to reveal TCR clonotype sharing across both types of boundary: MHC genotype and cell type. Such putative TCR clonotype sharing would have been missed by the analysis described above.

In Fig. 5.13, the 45 samples are arranged in the same order on the *x*- and *y*-axes. There is a trend for TCR sharing, indicated by darker shading, to occur in square blocks along the diagonal (Fig. 5.13). There are 2 large square blocks of darker shading: the first is delimited by CD4SP samples from WT and *B2m*$^{-/-}$ mice and the second by CD8SP samples from WT and *H2-Aa*$^{-/-}$ mice (Fig. 5.13). While the CD4SP block is relatively homogenous, the CD8SP block may be divided into quadrants, in a pattern consistent with greater TCR sharing within MHC genotypes than across MHC genotypes (Fig. 5.13). Other blocks of darker shading fall along the diagonal, due to the grouping of samples according to cell type and MHC genotype. W1 samples from *B2m*$^{-/-}$ mice provide an exception to this trend, because these samples exhibit a

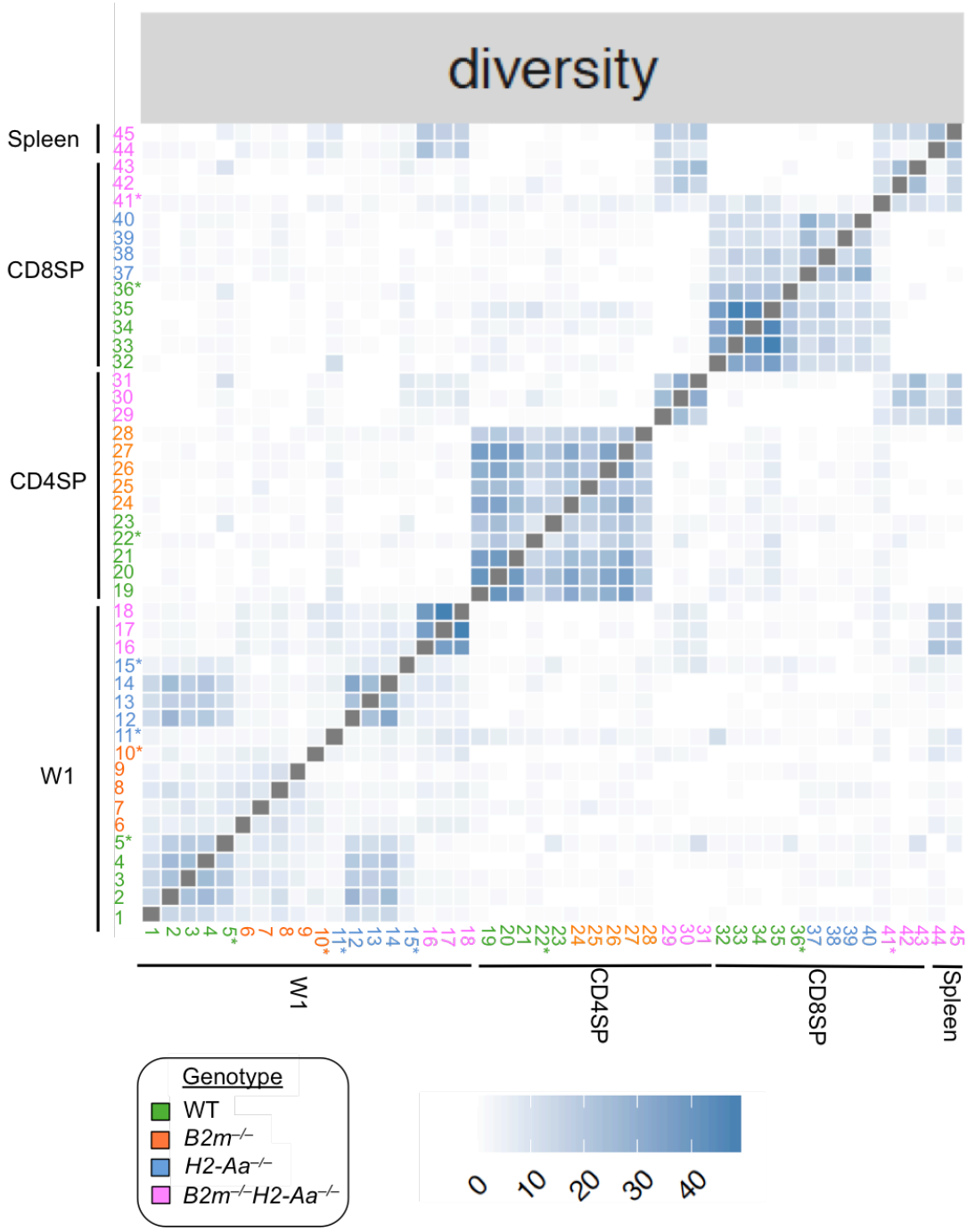

Figure 5.13. TCR clonotype sharing across both types of boundary: MHC genotype and cell type. Considering only the 200 most abundant TCR clonotypes in the 45 samples described in Figs. 5.1-5.3, VDJtools *TrackClonotypes* routine was used to generate heatmaps that indicate the number of shared TCR clonotypes (ranging from 0 to 50, see key at top right) in pairs of samples denoted on the axes: thymocyte samples of each cell type and MHC genotype. Numbers indicate an arbitrary sample identifier (1-45 for the entire dataset). * indicates sample with <200 total TCR clonotypes. *Sample #5, 179 TCR clonotypes; #10, 74 TCR clonotypes; *#11, 44 TCR clonotypes; *#15, 68 TCR clonotypes; *#22, 120 TCR clonotypes; *#36, 135 TCR clonotypes; *#41, 73 TCR clonotypes.

somewhat lower level of TCR sharing (Fig. 5.11A and 5.13). In areas outside the diagonal, several blocks of darker shading correspond to examples of TCR sharing described above. First, W1 samples from WT mice overlap with W1 samples from *H2-Aa*$^{-/-}$ mice. Second, in the *B2m*$^{-/-}$*H2-Aa*$^{-/-}$ dataset, there is TCR sharing between each thymocyte subset and TCRβ^+ B220$^-$ splenocytes and also between the CD4SP and CD8SP samples (Fig. 5.13). Third, a low level of TCR sharing is detectable between CD8SP samples from WT mice and CD4SP samples from WT or *B2m*$^{-/-}$ mice. This contrasts with W1 samples from WT mice, which did not overlap with either CD4SP or CD8SP samples, as described above (Fig. 5.10A).

There is one other noteworthy area of darker shading. A significant amount of TCR sharing was detected between a particular CD8SP sample (#41) from a *B2m*$^{-/-}$*H2-Aa*$^{-/-}$ mouse and many other samples, including the W1, CD4SP and CD8SP cell types and all MHC genotypes (Fig. 5.13). As it shares TCR clonotypes with a wide range of samples across both cell type and MHC genotype boundaries, sample 41 is an outlier in this dataset. It is possible that sample #41 was contaminated with material from another sample at some stage preceding the indexing (second) PCR.

5.2.7.2 TCR clonotype sharing in W1 samples across MHC genotype boundaries fails to identify MHC class cross-reactive TCRs

One limitation of the analysis above is that it was confined to the top 200 TCR clonotypes from each sample. To search for MHC class cross-reactive TCRs across the entire dataset, the data were reanalysed. The input files for this analysis had been pre-processed with the VDJtools *Correct* routine to merge low-abundance nucleotypes with high-abundance nucleotypes that differed in a maximum of 2 nucleotides, as described (section 5.2.5). They had also been processed with the VDJtools *FilterNonFunctional* routine to remove sequences that could not encode a functional TCRα chain, as described (section 5.2.5). Based on evidence that MHC class cross-reactive TCRs are commonly deleted at the CCR7$^-$ stage of thymocyte development (McDonald et al., 2015), the analysis focussed on the W1 samples, which were sorted based on their CCR7$^-$ CD4^{lo}CD8^{lo} PD-1$^+$ phenotype.

W1 samples within each MHC genotype were pooled to form a single virtual sample using the VDJtools *PoolSamples* routine. The frequency of each TCR in the virtual sample was calculated as the number of reads encoding that TCR divided by the cumulative number of reads in all samples within that group. The VDJtools *OverlapPair* routine was then used to determine the number and percentage of shared TCRs and

reads between each pair of virtual samples. A summary of the results is presented in Table 5.1.

The wild-type W1 repertoire shared more TCR clonotypes with the *B2m*$^{-/-}$ and *H2-Aa*$^{-/-}$ W1 repertoires (12.0% and 11.1% of wild-type W1 TCRs, respectively) than with the *B2m*$^{-/-}$*H2-Aa*$^{-/-}$ W1 repertoire (2.5% of wild-type W1 TCRs) (Table 5.1). The *B2m*$^{-/-}$*H2-Aa*$^{-/-}$ W1 repertoire shared a low percentage of TCR clonotypes with the wild-type, *B2m*$^{-/-}$ and *H2-Aa*$^{-/-}$ W1 repertoires (4.1%, 6.2 and 7.3% of *B2m*$^{-/-}$*H2-Aa*$^{-/-}$ W1 TCRs, respectively). However, this low frequency of clonotypes contributed a large percentage of reads (29.0% to 48.5%) in the *B2m*$^{-/-}$*H2-Aa*$^{-/-}$ W1 samples (Table 5.1).

The level of TCR sharing between W1 samples from *B2m*$^{-/-}$ and *H2-Aa*$^{-/-}$ mice was 3.3% of TCR clonotypes and 6.7% of reads in the *B2m*$^{-/-}$ W1 dataset (Table 5.1). This level of TCR sharing was not greater than that observed between *B2m*$^{-/-}$ and the *B2m*$^{-/-}$*H2-Aa*$^{-/-}$ W1 repertoires (4.7% of TCR clonotypes and 9.8% reads, calculated as a percentage of the *B2m*$^{-/-}$ W1 dataset) (Table 5.1). Similarly, the level of TCR sharing between W1 samples from *B2m*$^{-/-}$ and *H2-Aa*$^{-/-}$ mice contributes to only 5.0% of TCR clonotypes and 8.9% of reads in *H2-Aa*$^{-/-}$ mice, which was smaller than the TCR sharing observed between *H2-Aa*$^{-/-}$ and the *B2m*$^{-/-}$*H2-Aa*$^{-/-}$ repertoire (8.3% of TCR clonotypes and 10.0% reads, calculated as a percentage of the *H2-Aa*$^{-/-}$ W1 dataset) (Table 5.1). The lower amount of TCR sharing between *B2m*$^{-/-}$ and *H2-Aa*$^{-/-}$ mice compared to the TCR sharing between each of these single MHC class-deficient repertoires and *B2m*$^{-/-}$*H2-Aa*$^{-/-}$ repertoire provides no support for the MHC class cross-reactivity hypothesis.

To visualise TCR sharing in the virtual W1 samples described in Table 5.1, scatterplots generated by the VDJtools *OverlapPair* routine are shown (Fig. 5.14). The clonotype scatterplot shows the abundance of only the overlapping clonotypes, with each clonotype represented by a circle. The size of the circle is scaled to the geometric mean of clonotype frequency in a pair of virtual samples. The axes represent $\log_{10}$ clonotype frequencies in each W1 virtual sample (i.e. MHC genotype). The horizontal red histogram represents the frequency distribution of the overlapping TCR clonotypes in the virtual sample represented on the x-axis, whereas the horizontal grey histogram shows the frequency distribution of all TCRs (both non-overlapping and overlapping) in the virtual sample represented on the x-axis (Shugay et al., 2015). A single TCR clonotype (red arrows, Fig. 5.14) contributed ~18% of the reads in the *B2m*$^{-/-}$*H2-Aa*$^{-/-}$ dataset, exceeding the peak TCR clonotype in the other datasets by ~10-fold. This partially explains why a low number of shared TCR clonotypes contributed a large

percentage of reads in the *B2m*$^{-/-}$*H2-Aa*$^{-/-}$ W1 sample.

Table 5.1. W1 TCR clonotype sharing. After pre-processing of the TCR sequencing data as described in section 5.2.5, W1 samples within each of the four MHC genotypes were pooled to form a "virtual" sample for each MHC genotype using the VDJtools *PoolSamples* routine. The percentage of overlapping wave 1 TCR clonotypes between any two MHC genotypes was determined by taking the number of overlapping wave 1 TCRs (the numerator) divided by the number of total TCRs (i.e. overlapping and non-overlapping) in one MHC genotype (the denominator), multiplied by 100. The frequency of overlapping reads was calculated in the same way, except that the numerator and denominator values were sequencing reads instead of TCR clonotypes. To summarise, the first approach ignores TCR clonotype abundance whereas the second approach takes TCR clonotype abundance into account.

			W1 TCR repertoire (numerator)							
W1 TCR repertoire (denominator)	# TCRs	# reads	**Wild-type**		***B2m*$^{-/-}$**		***H2-Aa*$^{-/-}$**		***B2m*$^{-/-}$*H2-Aa*$^{-/-}$**	
			% TCRs	% reads	% TCRs	% reads	% TCRs	% reads	% TCRs	% reads
Wild-type	1933	1006374	*100.0*	*100.0*	12.0	23.4	11.1	27.1	2.5	5.7
***B2m*$^{-/-}$**	1584	754727	14.6	27.7	*100.0*	*100.0*	3.3	6.7	4.7	9.8
***H2-Aa*$^{-/-}$**	1063	601878	20.1	38.9	5.0	8.9	*100.0*	*100.0*	8.3	10.0
***B2m*$^{-/-}$*H2-Aa*$^{-/-}$**	1203	635584	4.1	29.0	6.2	37.1	7.3	48.5	*100.0*	*100.0*

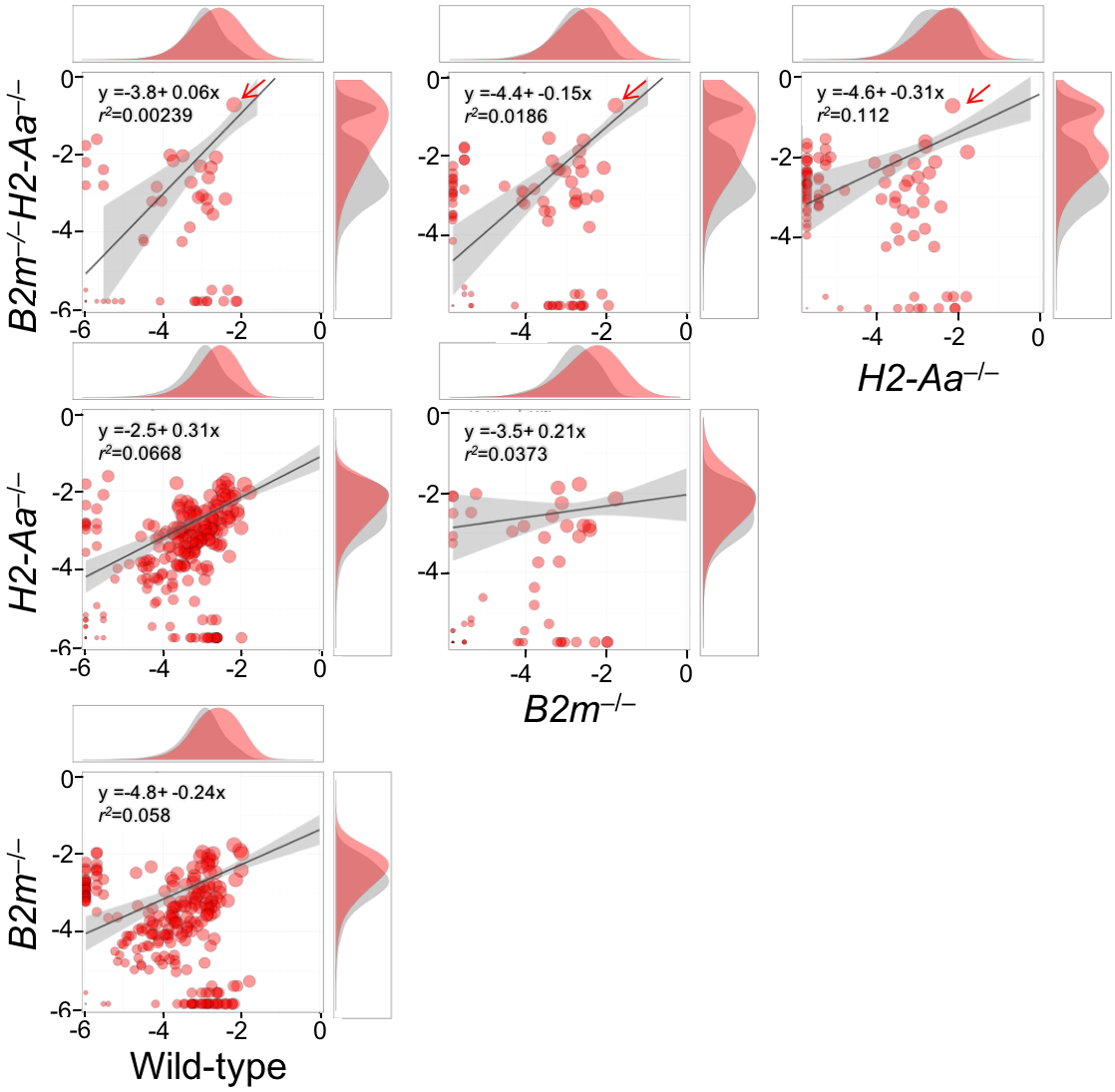

Figure 5.14. Visualisation of overlapping wave 1 TCRs between MHC genotypes. Each pair of virtual W1 samples described in Table 5.1 was compared using the VDJtools *OverlapPair* routine. Scatterplots show the abundance (log_{10} clonotype frequencies) of the overlapping clonotypes between one MHC genotype on x-axis and another MHC genotype on y-axis. Each circle represents an overlapping TCR clonotype. The size of the circle is scaled to the geometric mean of clonotype frequency in the pair of samples. Horizontal red histogram represents the frequency distribution of the overlapping TCR clonotypes in the virtual sample represented on the x-axis, whereas the horizontal grey histogram shows the frequency distribution of all TCRs (both non-overlapping and overlapping) in the virtual sample represented on the x-axis. The vertical histograms show corresponding distributions for the virtual sample on the y-axis. Red arrows indicate a single TCR clonotype that contributed to ~18% of the reads in the *B2m*$^{-/-}$*H2-Aa*$^{-/-}$ dataset.

5.2.8 TRAV and TRAJ usage bias associated with MHC genotypes and cell types

5.2.8.1 TRAV usage biases are related to MHC genotype and cell type

A recent study revealed associations between MHC alleles and TRAV segment usage in humans (Sharon et al., 2016). This suggests that regions encoded by the TRAV segment, likely the CDR1 and CDR2 loops that primarily interact with MHC molecules themselves (Rudolph et al., 2006), impose a bias on MHC recognition and T cell development. Both TRAV (to a lesser extent) and TRAJ genes encode parts of the CDR3α region, which commonly interacts with the peptide within the antigen-binding cleft of MHC molecules (Rossjohn et al., 2015). To examine whether the clustering of the samples in Fig. 5.8 was mainly based on TRAV or TRAJ segment usage, the TRAV and TRAJ segment usage profiles of all samples were analysed using the VDJtools *CalcSegmentUsage* routine.

Most TCRα sequences mapped to five TRAV segments (in order from top to bottom on the heatmap in Fig. 5.15): TRAV16D/DV11, TRAV8D-1, TRAV12-3, TRAV21/DV12 and TRAV12-2. Summaries show the percentage of reads per sample that mapped to each of these five TRAV segments (Fig. 5.16).

In the wild-type dataset, TRAV12-3 was detected more frequently in W1 samples than in CD4SP samples (Fig. 5.16A). In *B2m*$^{-/-}$ mice the frequency of TRAV12-3 usage was similar in W1 and CD4SP samples, and was lower compared to W1 samples in wild-type mice (Fig. 5.16A). TRAV12-3 usage in W1 samples from *H2-Aa*$^{-/-}$ mice exceeded its usage in W1 samples from wild-type mice (Fig. 5.16A). These data show that the relative enrichment of TCRs using TRAV12-3 in W1 samples requires B2m.

TRAV16D/DV11 had a similar pattern of B2m-dependent enrichment in W1 samples. TRAV16D/DV11 was used more commonly in W1 samples than in CD4SP samples in wild-type mice, but not in *B2m*$^{-/-}$ mice (Fig. 5.16B). TRAV16D/DV11 was also highly expressed in CD8SP samples in wild-type mice (Fig. 5.16B). These findings suggest that, at least when paired with the YAe62.8 TCRβ chain, the products of the TRAV12-3 and TRAV16D/DV11 gene segments favour TCR interactions with B2m-dependent ligand(s).

TRAV21/DV12 was commonly detected in W1 and CD4SP samples from wild-type and *B2m*$^{-/-}$ mice; however, it was detected less commonly in W1 samples from *H2-Aa*$^{-/-}$

mice (Fig. 5.16C). These data suggest that TRAV21/DV12 expression favours TCR interactions with MHCII.

TRAV8D-1 was used ~3.5 times more commonly in W1 samples from *B2m*$^{-/-}$ mice (mean = 20.2% of reads) compared to wild-type (5.4%) and *H2-Aa*$^{-/-}$ mice (5.9%) (Fig. 5.16D). It is conceivable that TRAV8D-1 favours interaction with MHCII (present in MHCI-deficient mice), with this effect most obvious in the absence of B2m expression.

TRAV12-2 usage was relatively homogenous in samples from MHC-expressing mice, with group means ranging from 18 to 38% (Fig. 5.16E). At least considering the usage of the five TRAV gene segments shown in the summaries, the MHC double-deficient W1, CD4SP and CD8SP samples were not obviously different from the samples from MHC single deficient- and MHC wild-type mice (Fig. 5.16).

Using the wild-type W1 dataset as a reference point, TRAV12-3 and TRAV16D/DV11 segments were depleted in W1 from *B2m*$^{-/-}$ mice (Figs. 5.16A, B), while TRAV21/DV12 was depleted in W1 from *H2-Aa*$^{-/-}$ mice (Fig. 5.16C). The depletion of these TRAV segments in a single MHC-deficient W1 dataset suggests that these TRAV segments facilitate strong TCR-MHC interactions with the "absent" MHC class.

In summary, the TRAV usage bias associated with particular MHC genotypes and cell types supports the role of CDR1 and CDR2 loops in MHC recognition and in thymocyte fate.

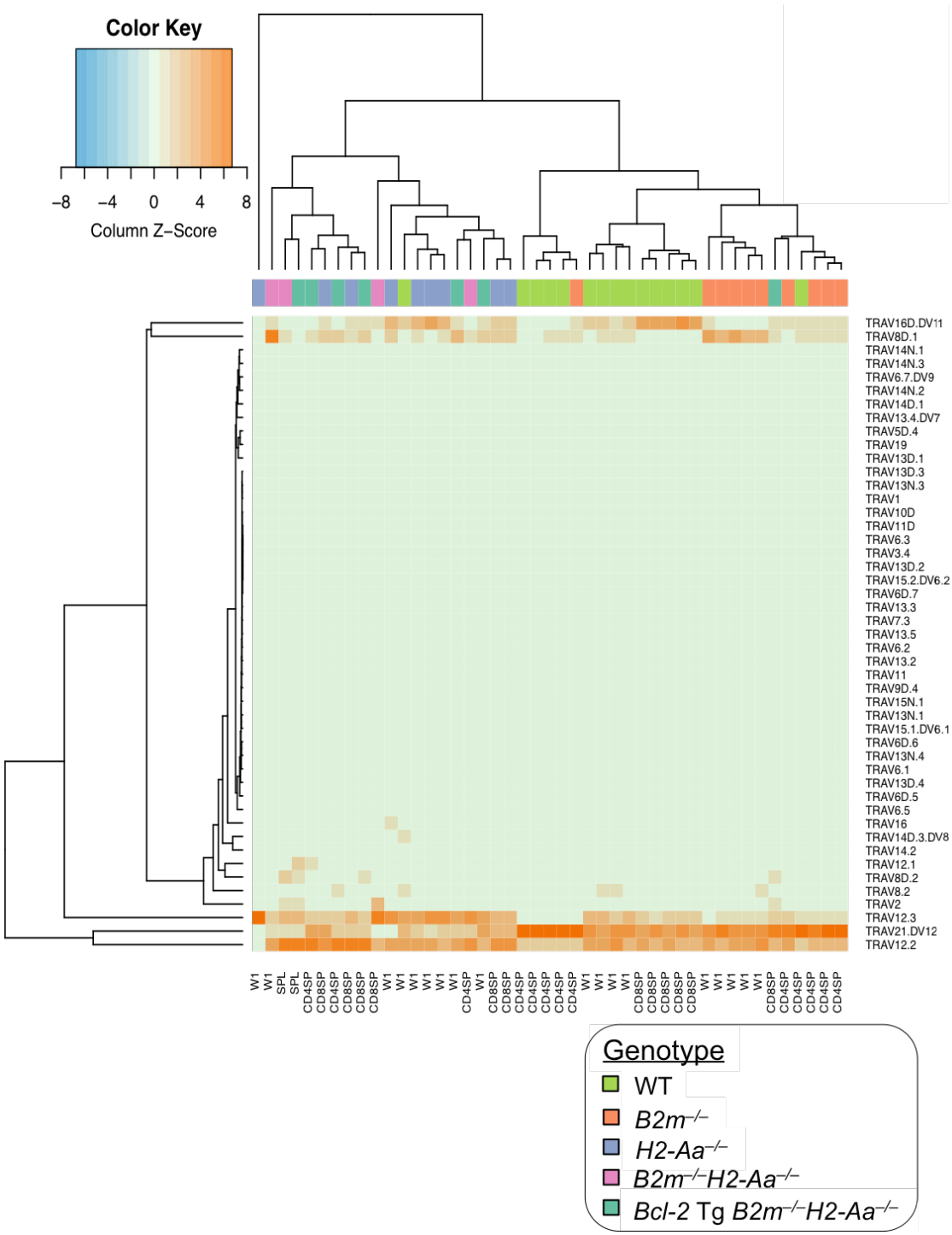

Figure 5.15. TRAV segment usage varies with MHC genotypes and cell types. The 45 TCR sequencing datasets described in Figs. 5.1-5.3 were clustered based on the Euclidean distance between the TRAV segment usage (or frequency) vectors (ie. the frequency of associated reads in each V segment present in samples). Data were analysed using VDJtools *CalcSegmentUsage* routine. Weighted V profile was used. Z-score on heatmap: 0, the score is identical to the mean score (green); positive value, the score is above the mean, ie., highly expressed (orange); and negative value, the score is below the mean (blue).

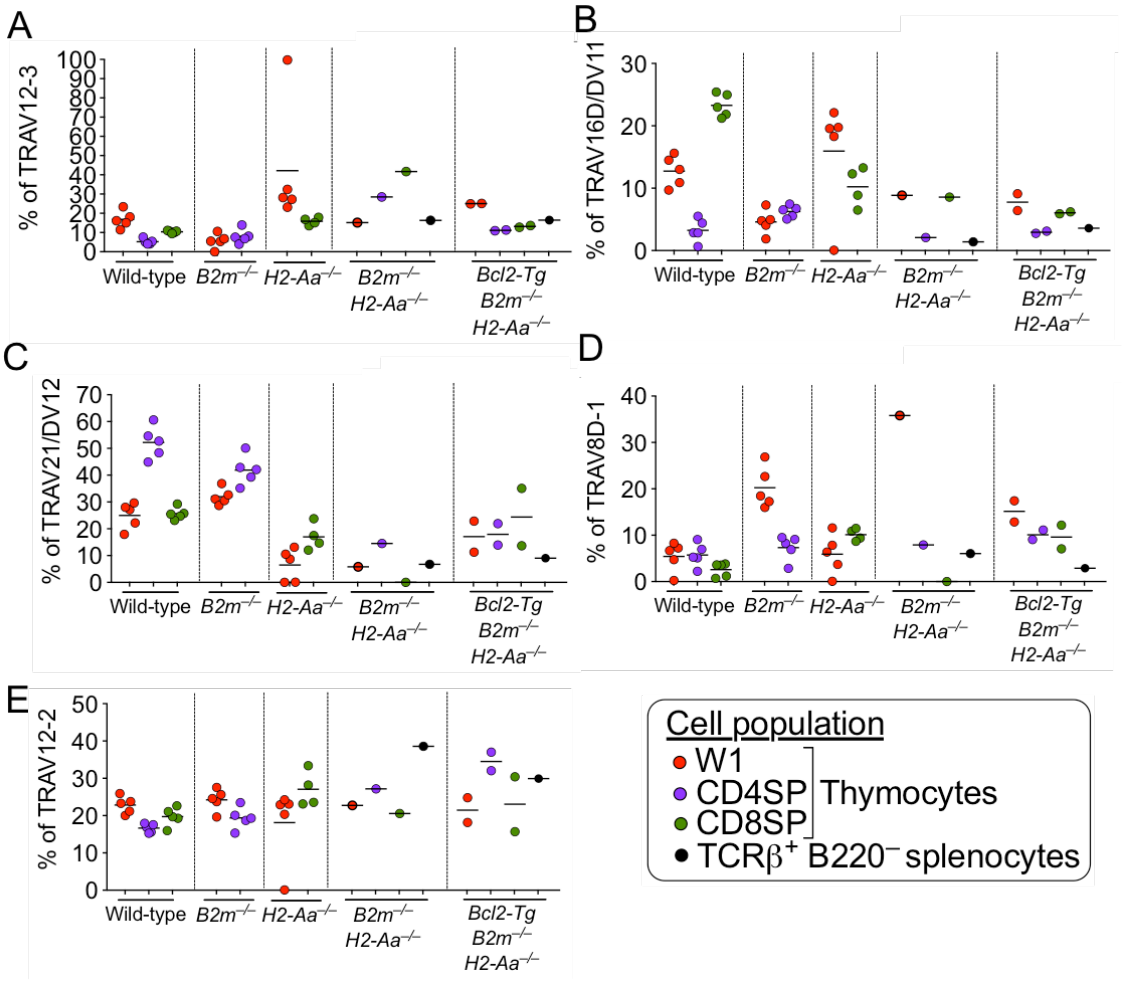

Figure 5.16. Enrichment of TRAV segments supporting interclonal competition hypothesis. Summaries show the frequency for each of the five highly used TRAV segments in Fig. 5.15, namely (A) TRAV12-3, (B) TRAV16D/DV11, (C) TRAV21/DV12, (D) TRAV8D-1 and (E) TRAV12-2 in the 45 TCR sequencing datasets described in Figs. 5.1-5.3.

5.2.8.2 Enrichment of TRAV usage in MHC single-deficiency provides evidence supporting the interclonal competition hypothesis

A ~4-fold enrichment of TRAV8D-1 usage was observed in the *B2m*$^{-/-}$ W1 dataset compared to the wild-type W1 dataset (Fig. 5.16D). This type of enrichment may arise from 2 non-mutually exclusive effects. First, enrichment may arise due to the depletion of TRAV segments that facilitate TCR-MHC interactions with the "absent" MHC class. Removal of these TCRs “non-specifically” increases the frequency of those TCRs capable of interacting with the “present” MHC class. Second, in theory, enrichment may arise due to the relaxation of interclonal competition as postulated above. Because thymocytes bearing TCRs that can only interact with the absent MHC class are rendered uncompetitive, competition between remaining thymocytes may be altered. This could increase the probability of productive interactions by TCRs using certain TRAV segments; in other words, the absence of one MHC class may cause a “specific” enrichment of certain TRAV segments over others. TRAV21/DV12 and TRAV12-2 segments were used similarly in wild-type and *B2m*$^{-/-}$ W1 datasets (Fig. 5.16C, E). Therefore, the ~4-fold TRAV8D-1 enrichment in the *B2m*$^{-/-}$ W1 dataset seems consistent with a “specific” rather than a “non-specific” enrichment.

It is notable that TRAV8D-1 also showed a ~4-fold enrichment in CD8SP samples from *H2-Aa*$^{-/-}$ mice (mean = 10.1%) compared to wild-type mice (mean = 2.6%) (Fig. 5.16D). TRAV12-3 and TRAV12-2 were found at similar and substantial frequencies in CD8SP samples from *H2-Aa*$^{-/-}$ mice and wild-type mice (Fig. 5.16A, E). This finding suggests that TCRs that use TRAV8D-1 have an above-average capacity to interact with MHCI. In summary, the disproportionate enrichment of certain TRAV segments in mice lacking one MHC class provides preliminary evidence consistent with the interclonal competition hypothesis.

5.2.8.3 No evidence of decrease in W1 cells in the absence of one or both MHC classes

In mice with normal apoptosis, CD4^{lo}CD8^{lo} PD-1^{+} thymocytes, i.e. W1-phenotype cells, are equally abundant in the presence or absence of MHC expression (Fig. 4.22). To test whether this is also the case when the mice express the Yae62β transgene, the frequency of sorted W1 cells among all thymocytes across MHC genotypes was determined (Fig. 5.17). Among all thymocytes, the frequency of W1 cells in *B2m*$^{-/-}$ mice and *H2-Aa*$^{-/-}$ mice (mean = 0.29% and 0.34%, respectively) was not statistically different to the wild-type mice (mean = 0.27%). W1 cells were also detected at a similar

frequency in the three *B2m*$^{-/-}$*H2-Aa*$^{-/-}$ mice examined (Fig. 5.17). This suggests that thymocytes with the potential to enter Wave 1, but fail to do so because their TCRs bind to the "absent" MHC class, are replaced by other thymocytes that "fill the niche".

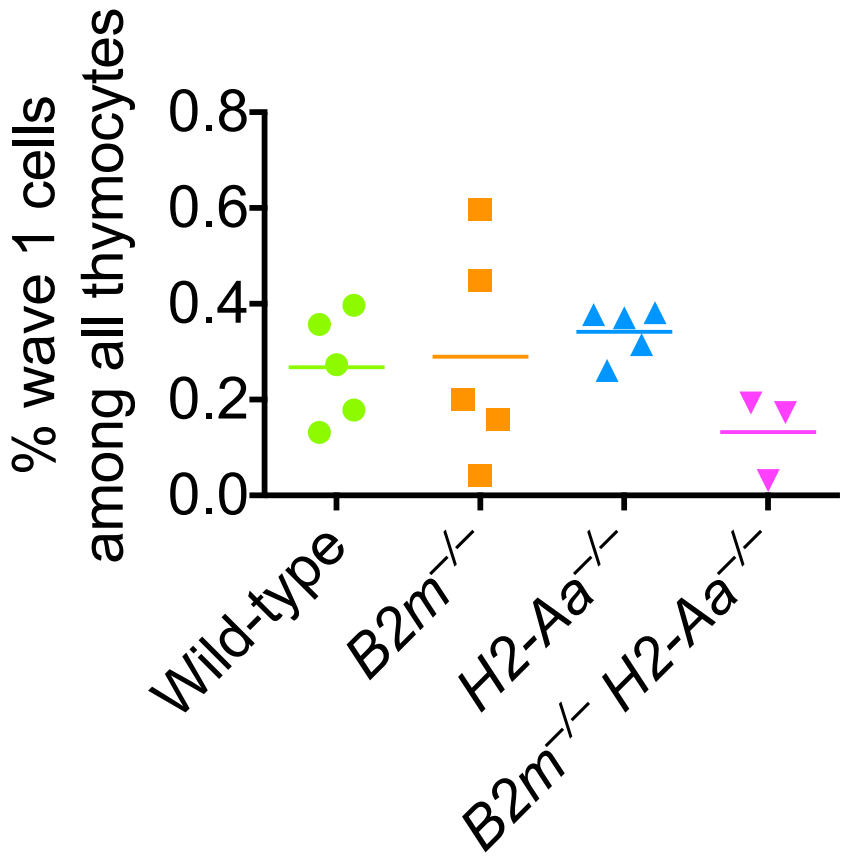

Figure 5.17: Frequency of wave 1 cells in single MHC-deficient mice is similar to MHC wild-type mice. Graphs show the frequency of sorted wave 1 cells with CCR7^{-} CD4^{lo}CD8^{lo} PD-1^{hi} phenotype (Fig. 5.2) among all thymocytes across wild-type (n=5), *H2-Aa*$^{-/-}$ (n=5), *B2m*$^{-/-}$ (n=5) and *H2-Aa*$^{-/-}$*B2m*$^{-/-}$ (n=3) mice. Non-significant P values were obtained between all comparison groups using 1-way ANOVA with Tukey's post-tests.

5.2.8.4 TRAJ usage biases related to the presence or absence of any MHC molecules

Analysis of TRAJ segments revealed a very different pattern. There were two clusters (Fig. 5.18). The first cluster (in red box) contained all samples from *H2-Aa*$^{-/-}$*B2m*$^{-/-}$ mice, plus two W1 *H2-Aa*$^{-/-}$ samples, which had low numbers of nucleotypes (Fig. 5.6B). The second cluster (in blue box) contained samples from mice with one or both MHC classes (i.e. wild-type, *B2m*$^{-/-}$ and *H2-Aa*$^{-/-}$ mice).

Cluster 1 samples commonly used TRAJ18, 21, 24, 15, 5, 12, 23, 9, 7, 4, 2, 30 and 26, as highlighted in pink on the right of the heatmap (Fig. 5.18). These TRAJ segments were expressed at the highest levels (45.8 to 51.6% cumulative percentage of reads) in all cell subsets of *H2-Aa*$^{-/-}$*B2m*$^{-/-}$ mice (Fig. 19A). These segments were used much less frequently (~3% to 15.6%) in samples from mice expressing at least one MHC class (Fig. 5.19A) as indicated by the decreased density of orange boxes in Cluster 2 samples on the heatmap (Fig. 5.18).

Cluster 2 samples commonly used TRAJ43, 32, 44, 39, 31, 53, 57, 34, 37, 45, 42, 50, 52, 58 and 56 highlighted in blue on the right of the heatmap (Fig. 5.18). These segments were commonly used in samples from mice expressing one or both MHC classes, ranging from 42.75% to 82.6% cumulative percentage of reads (Fig. 5.19B). These segments were used less frequently (19.1% to 28.8%) in samples from mice lacking both MHC classes (Figs. 5.18, 5.19B). As TRAJ segments encode part of the CDR3α loop, this suggests that the CDR3α loops of MHC-independent TCRs have different features from the TCRs that engage MHC ligands.

The remaining TRAJ segments (TRAJ11, 6, 13, 28, 16, 35, 38, 27, 22, 17, 33, 40, 49 and 48) highlighted in white on the right of the heatmap (Fig. 5.18) were expressed relatively homogenously across MHC genotypes (14.5% to 28.7%), except for W1 *H2-Aa*$^{-/-}$ samples (41.8%) (Fig. 5.19C).

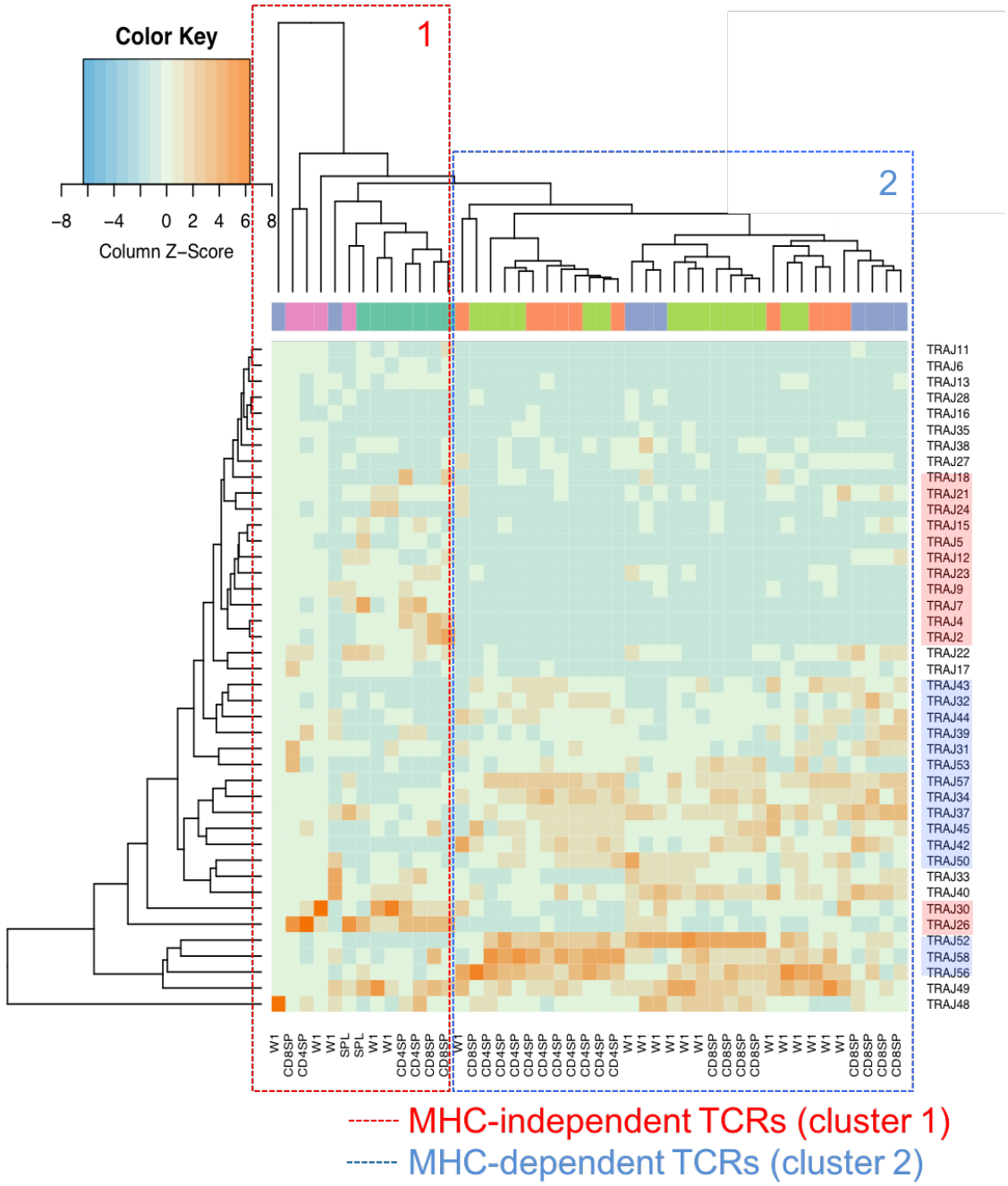

Figure 5.18. TRAJ segment usage varies with the presence or absence of any MHC molecules. The 45 TCR sequencing datasets described in Figs. 5.1-5.3 were clustered based on the Euclidean distance between the TRAJ segment usage (or frequency) vectors (ie. the frequency of associated reads in each J segment present in samples). Two clusters were formed based on TRAV usage. Cluster 1, indicated by dotted red box, comprising the *H2-Aa*$^{-/-}$*B2m*$^{-/-}$ samples that commonly use TRAJ segments highlighted in pink. Cluster 2 (blue dotted box) consists of the MHC-dependent TCRs from samples expressing one or both classes of MHC, with commonly used TRAJ segments highlighted in blue. Data were analysed using VDJtools *CalcSegmentUsage* routine. Weighted J profile was used. Z-score on heatmap: 0, the score is identical to the mean score (green); positive value, the score is above the mean (orange); and negative value, the score is below the mean (blue).

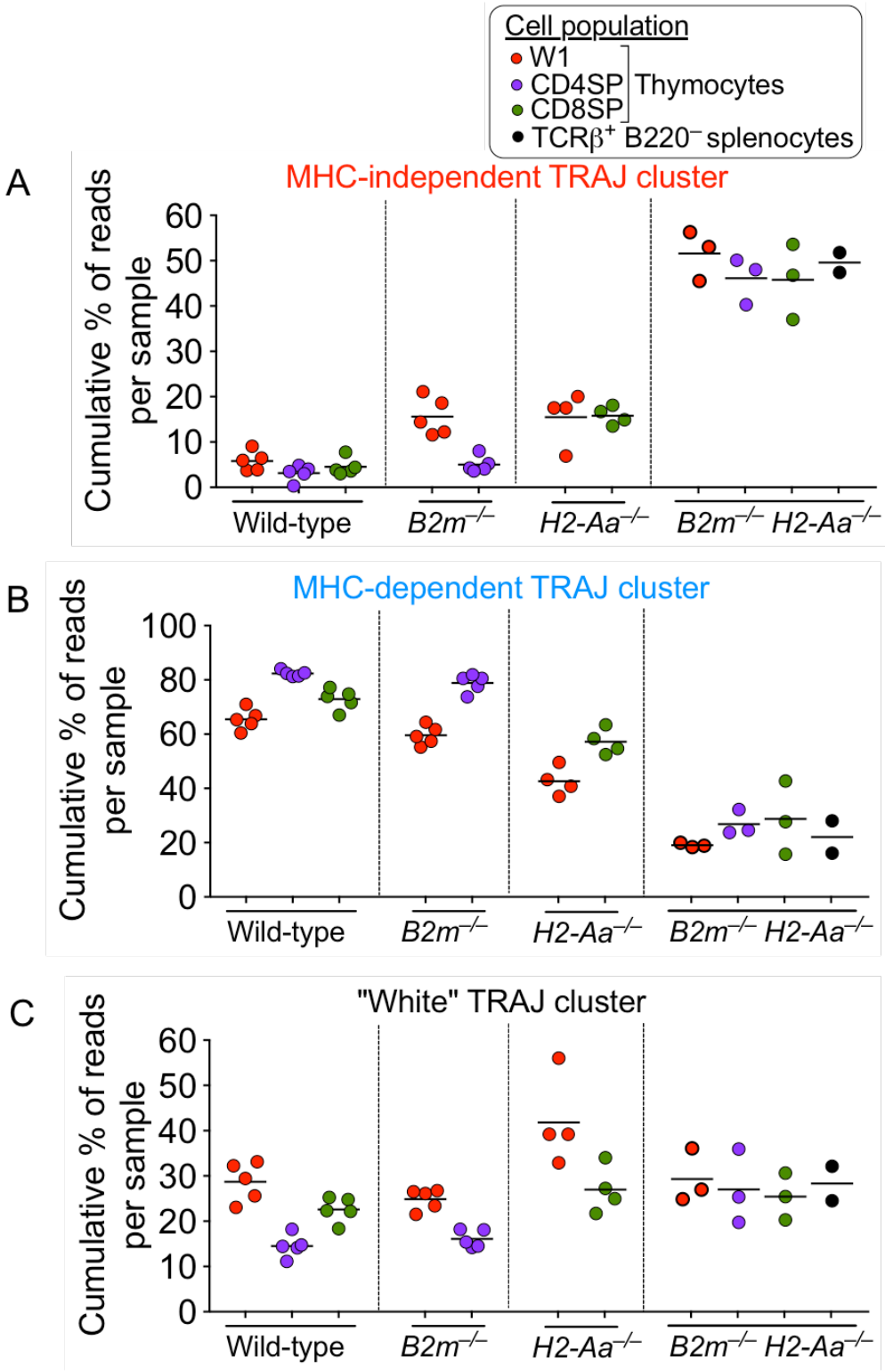

Figure 5.19. Commonly used TRAJ segments in presence or absence of any MHC molecules. Graphs show the cumulative percentage of reads per sample of TRAJ cluster commonly used (analysed in Fig. 5.18) (A) in the absence of MHC molecules (TRAJ18, 21, 24, 15, 5, 12, 23, 9, 7, 4, 2, 30 and 26), (B) in the presence of one or both classes of MHC (TRAJ43, 32, 44, 39, 31, 53, 57, 34, 37, 45, 42, 50, 52, 58 and 56), and (C) regardless of the presence or absence of MHC molecules (TRAJ11, 6, 13, 28, 16, 35, 38, 27, 22, 17, 33, 40, 49 and 48) across TCR sequencing datasets derived from the 45 samples described in Figs. 5.1-5.3.

5.2.9 CDR3α amino acids profile analysis

TRAV usage thus appears to vary in a manner modulated by both cell type and MHC genotype. In addition, the so-called MHC-independent TCRs, which stimulate T cell development in Yae62β transgenic mice lacking B2m and MHCII expression, were enriched in CDR3α loops encoded by a distinct set of TRAJ genes. This section aims to identify factor(s) that distinguish the TRAJ genes that were highly used in *H2-Aa*$^{-/-}$ *B2m*$^{-/-}$ samples from the TRAJ genes used in the other T cell samples. Analysis was performed using the VDJtools *CalcCdrAAProfile* routine, which measures the chemical and physical properties of amino acids (Table 5.2) in CDR3α loops detected in each of the 45 samples.

Table 5.2. Chemical and physical properties of amino acids in CDR3α analysis. Modified from Shugay et al. (2015).

Physical properties	Description	Reference
Count	Total number amino acids	-
Volume	Sum of each amino acid volume Number of polar amino acids	(Pommié et al., 2004; Zamyatnin, 1972)
Polarity	Total number of polar amino acids	(Pommié et al., 2004)
Hydropathy	Sum of each amino acid hydrophobic index according to Kyte-Doolittle scale	(Kyte and Doolittle, 1982; Pommié et al., 2004)
Disorder	Intrinsic structural disorder is defined as proteins that lack a well-defined conformation under native conditions. A disorder- producing amino acid has a positive value weighted by the SVM	(Dunker et al., 2008; Hansen et al., 2006; Weathers et al., 2004)
Strength	Number of amino acids that most inter-residue contacts (i.e. capacity of amino acid to interact with other amino acid measured using the Miyazawa-Jernigan (M-J) matrix	(Miyazawa and Jernigan, 1996)

Each CDR3α amino acid sequence is divided into 2 or 3 subregions based on whether the residues are encoded by V, VJ or J segments of the *Tcra* locus. The reason that some CDR3 amino acids sequences have only 2 subregions is because the V and J gene segments are sometimes joined at the break between codons so that no amino acid is encoded by nucleotides at the VJ junction. VJ amino acids are amino acids that are partly encoded by a nucleotide derived from a V and/or J gene segment, or are completely encoded by non-templated nucleotides. Conserved residues in the CDR3 amino acid sequence (cysteine (C) at the N-terminus and F (phenylalanine) or W (tryptophan) at the C-terminus) are excluded from this analysis. To avoid skewing of the results by highly abundant TCRs, as observed in Fig. 5.14 above, the following analyses used the "unweighted" option, in which the VDJtools *CalcCdrAAProfile* routine ignores read count for each nucleotype.

5.2.9.1 Relatively homogenous CDR3α amino acid count, volume and polarity across the dataset

The average number of amino acids ("count" or length) per CDR3α subregion of each nucleotype shows that the J subregion is the longest, contributing a mean of 7.7 - 8.5 amino acids, whereas the V and VJ subregions together contribute 3 - 4 amino acids (Fig. 5.20). The average lengths of CD4SP and CD8SP CDR3α loops were slightly longer than W1 CDR3α loops (8.5 versus 8 in the J subregion), except for the *H2-Aa*$^{-/-}$ group, in which CD8SP and W1 CDR3α loops were similar in length (~8 amino acids in the J subregion) (Fig. 5.20). Regardless of cell type, CDR3α loops in *H2-Aa*$^{-/-}$*B2m*$^{-/-}$ samples were at the short end of the range observed in MHC-expressing mice (e.g. ~8 amino acids in the J subregion).

There are common 20 amino acids used for amino acid physical or chemical property analyses: A (alanine), C (cysteine), D (aspartate), E (glutamate), F (phenylalanine), G (glycine), H (histidine), I (isoleucine), K (lysine), L (leucine), M (methionine), N (asparagine), P (proline), Q (glutamine), R (arginine), S (serine), T (threonine), V (valine), W (tryptophan) and Y (tyrosine). Five classes of amino acid volume were defined based on the amino acid volumes in angstrom^3 (Å^3) (Zamyatnin, 1972): very small (60 - 90Å^3; G, A, S); small (108 - 117Å^3; C, D, P, N, T); medium (138 - 154Å^3; E, V, Q, H); large (162 - 174Å^3; M, I, L, K, R); and very large (189 - 228Å^3; F, Y, W). The average sum of amino acid volumes per nucleotype in all three CDR3α subregions (Fig. 5.21) followed a pattern similar to that observed for "count" Fig. 5.20), as expected, because the main determinant of "volume" is likely to be the number of amino acids present.

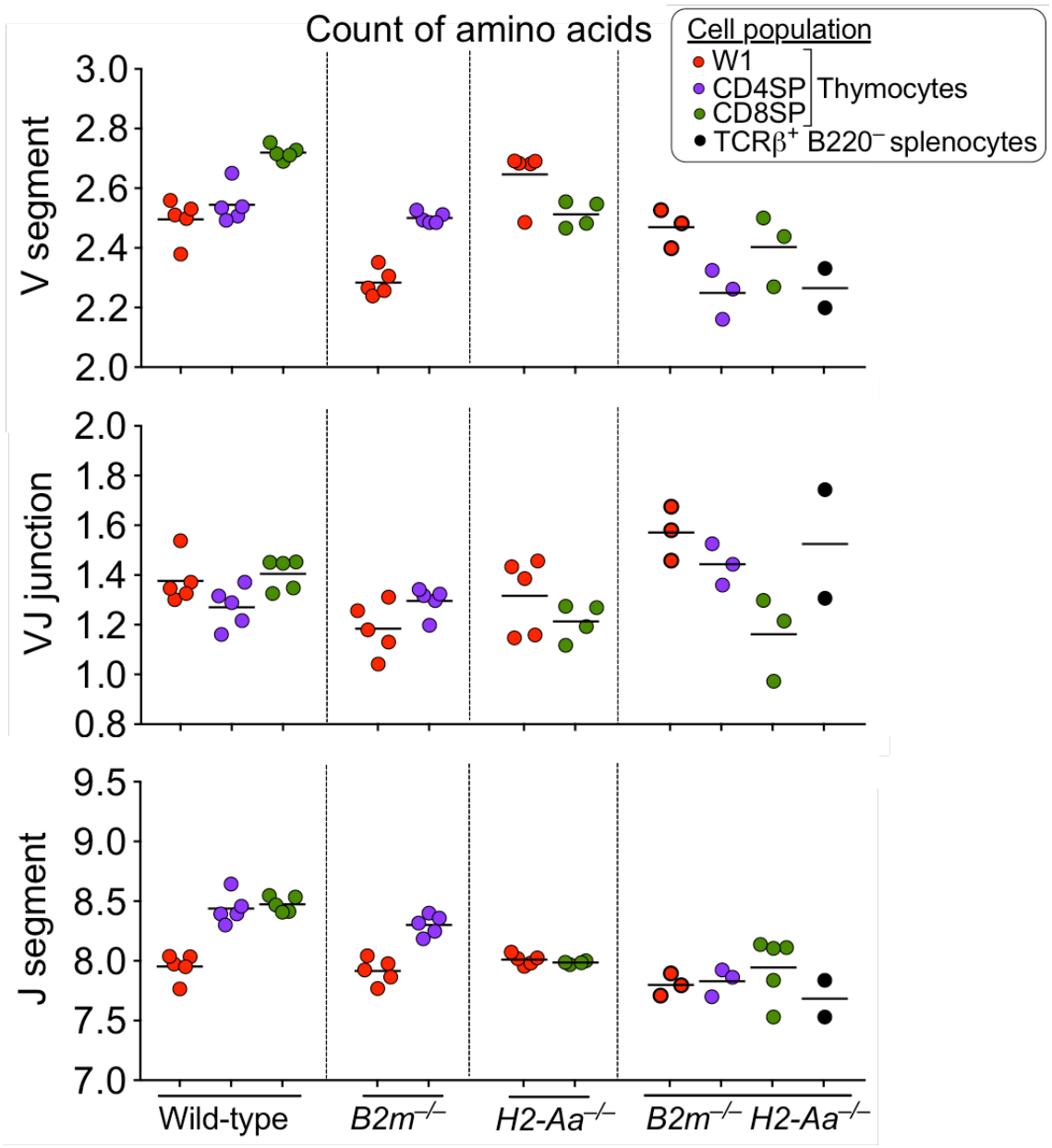

Figure 5.20. Count (or number) of amino acids in each subregion of CDR3α loops. Graphs show the average number of amino acids in the V, VJ and J subregions of the CDR3α loops (top to bottom) per nucleotype for each sample. Each circle represents a TCR sequencing dataset derived from 1 of the 45 samples described in Figs. 5.1-5.3. Lines represent group means. Data were analysed using VDJtools *CalcCdrAAProfile* routine set to "unweighted", i.e. ignoring TCR nucleotype frequency.

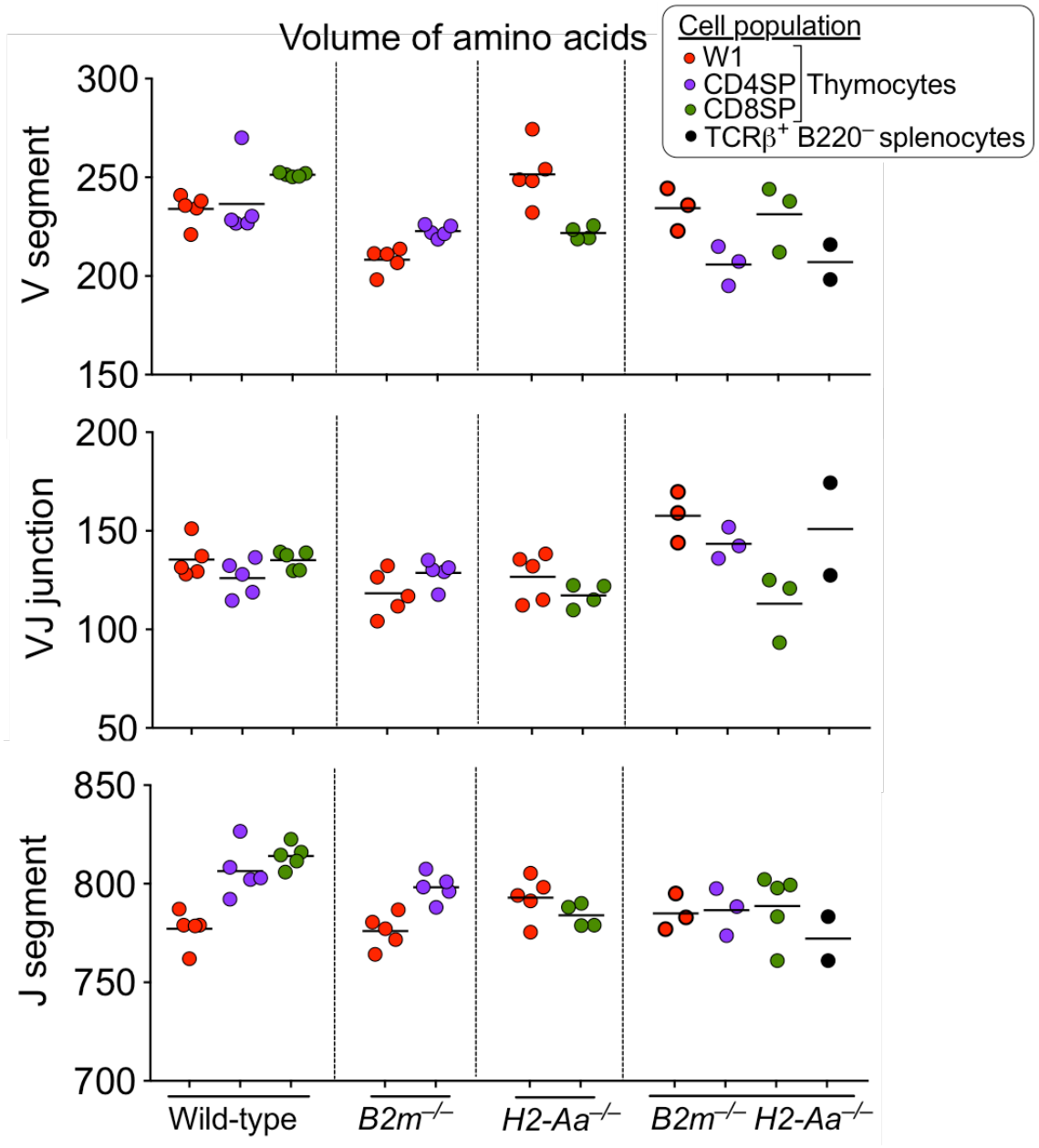

Figure 5.21. Volume of amino acids in the subregions of CDR3α loops is similar to the profile of "count". Graphs show the average sum of volume of amino acids, measured in units of $Å^3$, in the V, VJ and J subregions of the CDR3α loops per nucleotype for each sample. Each circle represents a TCR sequencing dataset derived from 1 of the 45 samples described in Figs. 5.1-5.3. Lines represent group means. Data were analysed using VDJtools *CalcCdrAAProfile* routine, unweighted by TCR nucleotype frequency.

Polar amino acids include all the five charged (H, K, R, D, E) and five uncharged amino acids (T, S, Q, N and Y), whereas the remaining 10 amino acids are non-polar amino acids with aliphatic side chains (A, V, I, L); sulfur-containing side chains (C, M); or F, W, P and G (Pommié et al., 2004). In the V region of CDR3α loops, the average number of polar amino acids per nucleotype was higher in all cells subsets in wild-type mice and W1 samples in *H2-Aa*$^{-/-}$ mice compared to the rest of the mouse genotypes (Fig. 2.22). The polarity measurements for VJ and J subregions of CDR3α loops were relatively homogenous across the dataset (Fig. 2.22).

5.2.9.2 Distinctive "hydropathy", "strength" and "disorder" CDR3α measurements in *H2-Aa*$^{-/-}$*B2m*$^{-/-}$ samples

Hydropathy measurements are based on the average sum of hydropathy index of each amino acid per nucleotype. Hydropathy index for 20 amino acids are designated by Kyte and Doolittle (Kyte and Doolittle, 1982). Amino acids I, V, L, F, C, M, A, W are classified into hydrophobic (synonymous with hydropathic) as they have hydrophathy index of ≥ 1.8, except for W with -0.9. Hydrophilic amino acids include N, D, Q, E, K, R, are defined as amino acids with < -3.3 hydropathy index, whereas neutral amino acids G, T, S, Y, P, H have hydropathy index < 1.8 but > -3.3 (Pommié et al., 2004) (Table 5.3). *H2-Aa*$^{-/-}$*B2m*$^{-/-}$ samples had highest hydropathy measurements compared to the rest of the MHC mouse genotypes, particularly in the CDR3α J subregion and to a lesser extent in the V subregion (Fig. 5.23).

Intrinsic disorder refers to amino acid sequences that lack a well-defined conformation and are thus thought to be more flexible or mobile under native conditions (Hansen et al., 2006). Disorder of the amino acids are determined by *support vector machine* (SVM) vector weights for 20 amino acids (Weathers et al., 2004). SVM was first trained to recognise disordered protein based on amino acid sequences by feeding the machine with ordered and disordered proteins (training dataset) and each amino acid in the protein was translated into the vector. After training the SVM, the machine's accuracy was calculated based on the ability of SVM to accurately recognise disordered protein in a testing dataset. Disorder-producing amino acids include K, P, G, N, Q, S, E, D, M and R (yellow), all associated with a positive value and are bias towards hydrophilic amino acids (Fig. 5.24) (Hansen et al., 2006; Weathers et al., 2004). Order-producing amino acids include V, H, F, I, L, C, W and Y (blue), all associated with a negative value and are bias towards hydrophobic amino acids (Fig. 5.24). Neutral amino acids include A and T (red), associated with values close to zero. In each TCR nucleotype, VDJtools *CalcCdrAAProfile* routine annotates

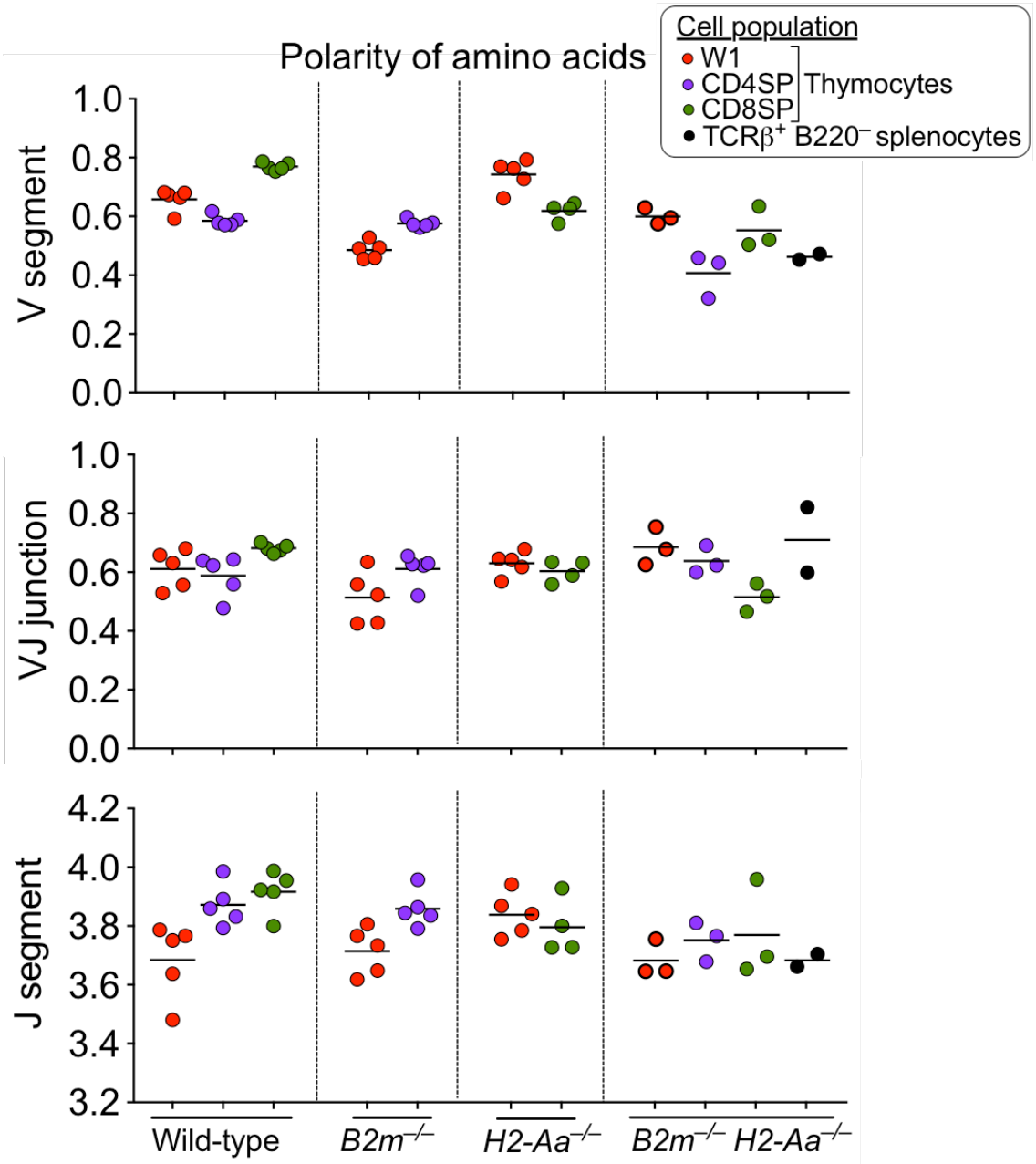

Figure 5.22. Polarity of amino acids in the subregions of CDR3α loops. Graphs show the average number of polar amino acids (D, E, H, K, R, N, Q, S, T, Y) in the V, VJ and J subregions of the CDR3α loops for each sample. Each circle represents a TCR sequencing dataset derived from 1 of the 45 samples described in Figs. 5.1-5.3. Lines represent group means. Data were analysed using VDJtools *CalcCdrAAProfile* routine, unweighted by TCR nucleotype frequency.

Table 5.3. Three hydropathy classes of amino acids. Table shows the most hydrophobic amino acid (left) to most hydrophilic amino acid (right). Hydropathy (hydrophobicity) index of each amino acid is designated according to the Kyte-Doolittle scale. Hydrophobic amino acids (blue) include A (alanine), C (cysteine), I (isoleucine), L (leucine), M (methionine), F (phenylalanine), W (tryptophan) and V (valine), with ≥ 1.8 hydropathy index, except for W with -0.9 as it involves in the hydrophobic core of the structural domains. Neutral amino acids (red) include G (glycine), H (histidine), P (proline), S (serine), T (threonine) and Y (tyrosine) with hydropathy index < 1.8 but > -3.3. Hydropholic amino acids (yellow) include R (arginine), N (asparagine), D (aspartate), Q (glutamine), E (glutamate) and K (lysine) with hydropathy index < 3.3. Diagram is modified from Pommié, et al. (2004).

I	V	L	F	C	M	A	W (1)	G	T	S	Y	P	H	N	D	Q	E	K	R
4.5	4.2	3.8	2.8	2.5	1.9	1.8	-0.9	-0.4	-0.7	-0.8	-1.3	-1.6	-3.2	-3.5	-3.5	-3.5	-3.5	-3.9	-4.5
HYDROPHOBIC								NEUTRAL						HYDROPHILIC					

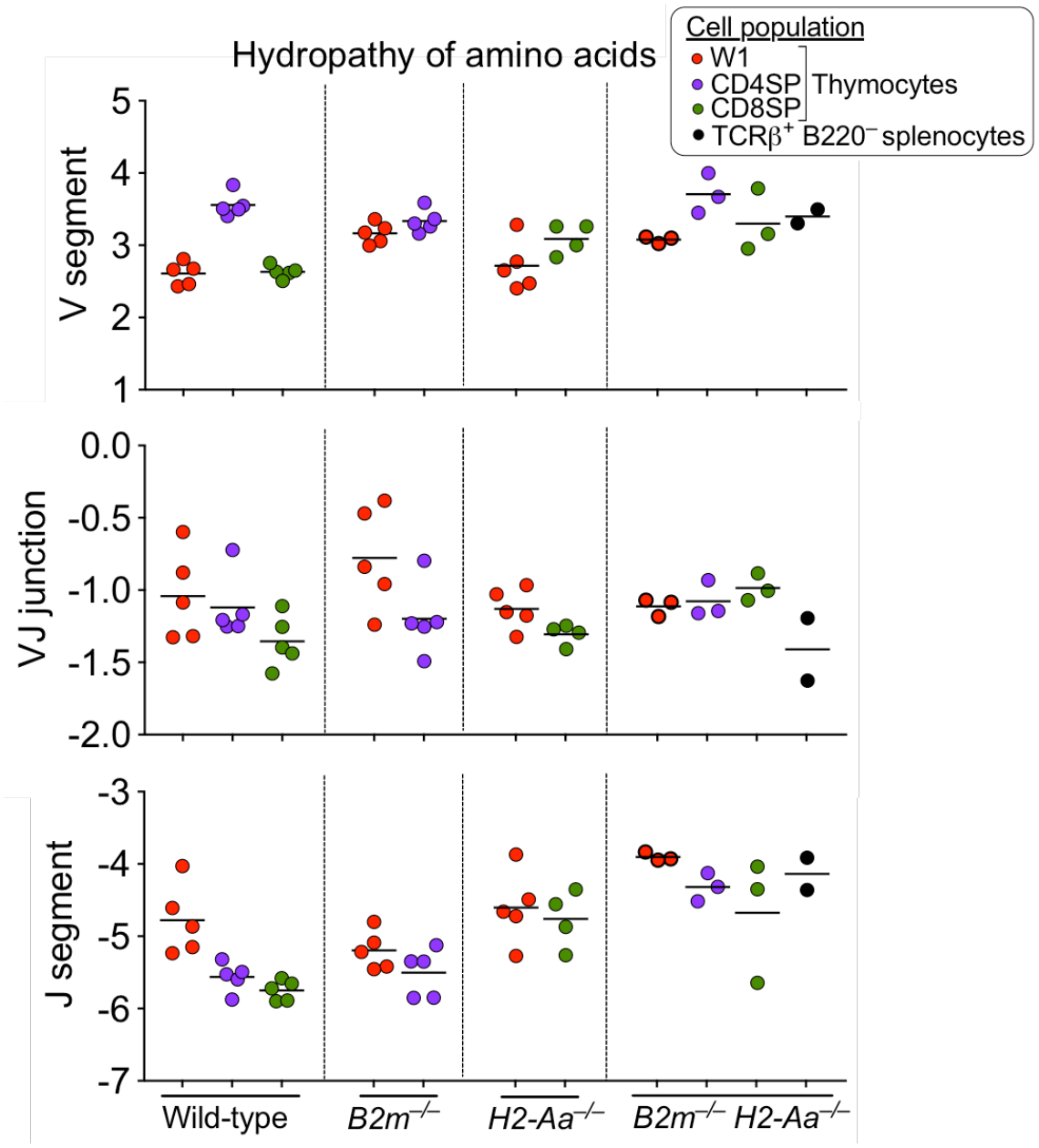

Figure 5.23. *H2-Aa*$^{-/-}$*B2m*$^{-/-}$ samples exhibit high amino acid "hydropathy" in the J subregion of CDR3α loops. Graphs show the average sum of hydropathy index of amino acids (Table 5.3) per nucleotype for each sample in V, VJ and J subregions of CDR3α (top to bottom). Each circle represents a TCR sequencing dataset derived from 1 of the 45 samples described in Figs. 5.1-5.3. Lines represent group means. Data were analysed using VDJtools *CalcCdrAAProfile* routine set to "unweighted", i.e. ignoring TCR nucleotype frequency.

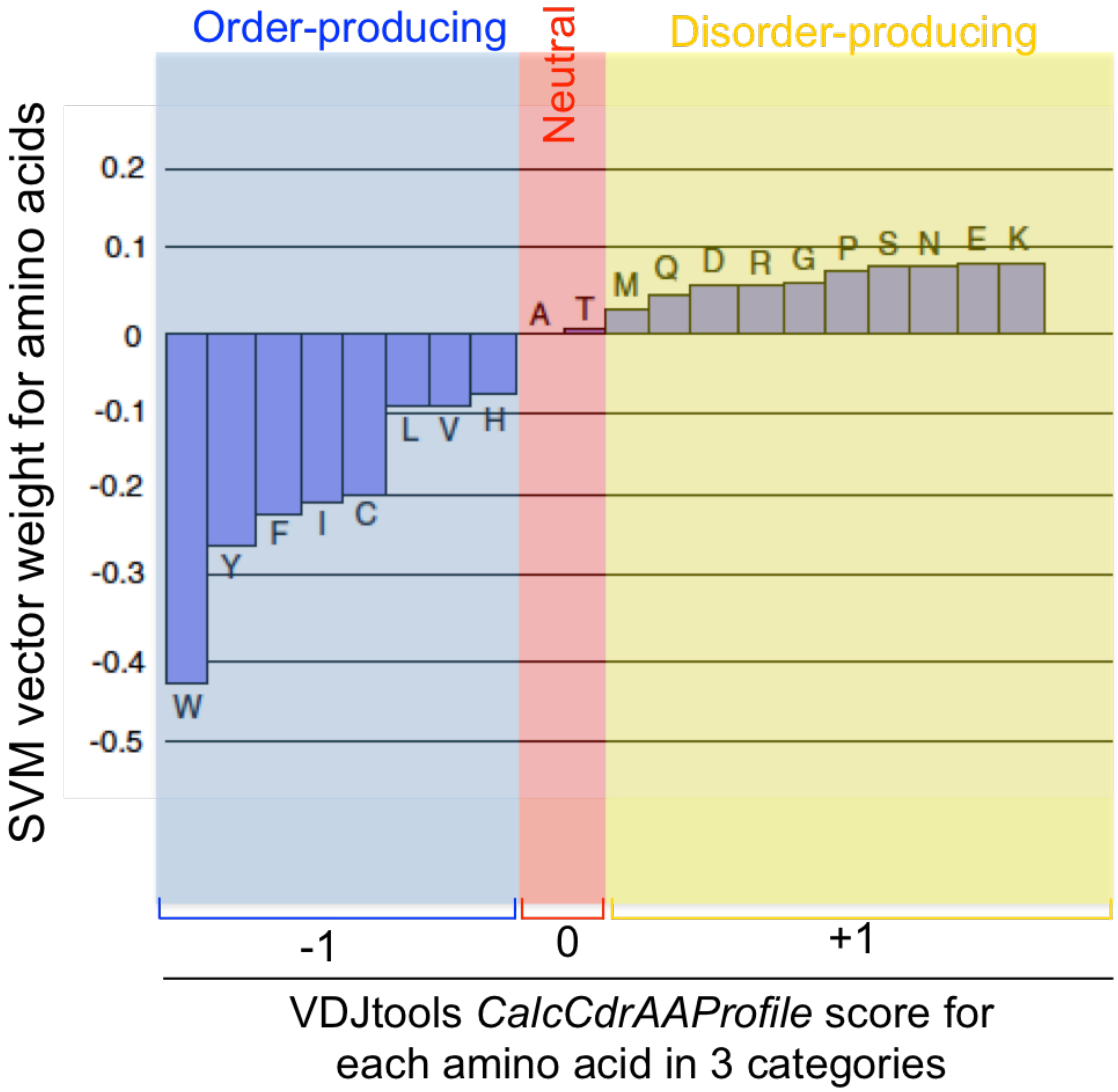

Figure 5.24. Disorder-producing, neutral and order-producing amino acids. Disorder of amino acids is based on vector weights for the 20 amino acids by support vector machine (SVM) (Weathers et al., 2004). In the VDJtools *CalcCdrAAProfile* routine, each of the disorder-producing amino acids (mostly hydrophilic) including K, P, G, N, Q, S, E, D, M and R (yellow), is assigned a value of +1 (positive 1). Each of the order-producing amino acids (mostly hydrophobic) including V, H, F, I, L, C, W and Y (blue), is assigned a value of –1 (negative 1). Each of the neutral amino acids including A and T (red), is assigned a value of 0. Modified from Weathers et al. (2004).

each disorder-producing amino acid as “+1”, each neutral amino acid as “0” and each order-producing amino acid as “-1”, and sum up these values as the “disorder” measurements. The more positive the value is, the higher the intrinsic structural disorder of the TCR is. The average sum of amino acid “disorder” per nucleotype for each sample in *H2-Aa*$^{-/-}$*B2m*$^{-/-}$ samples in the J subregion and to a lesser extent in the V subregion of CDR3α loops was lowest compared to the rest of the MHC-expressing samples (Fig. 5.25). “Disorder” measurements were generally lower in W1 samples than in CD4SP and/or CD8SP samples in the J subregion across all MHC genotypes (Fig. 5.25).

“Strength” refers to the capacity of amino acids to interact with other amino acids and is measured using the M-J matrix, conceived by Miyazawa and Jernigan (Miyazawa and Jernigan, 1996). VDJtools counts the occurrences of the 8 amino acids found to have the most inter-residue attraction, which are L, F, I, M, V, W, C and Y, in each nucleotype (Miyazawa and Jernigan, 1996). Almost all of these amino acid residues are hydrophobic. “Strength” measurements tended to be higher in *H2-Aa*$^{-/-}$*B2m*$^{-/-}$ samples in the CDR3α J subregion, but not in the V or VJ subregions (Fig. 5.26). This trend is consistent with the hydropathy mesurements above (Fig. 5.25).

In short, these findings indicate that samples that lack both classes of MHC exhibit high hydropathy and strength but low disorder in the J subregion of CDR3α in comparison to samples from mice expressing one or both classes of MHC.

5.2.9.3 Hydropathy analysis of J subregion of CDR3α loops

i) Hydrophobic amino acids are enriched in wave 1 cells of MHC-dependent and MHC-independent TCRs

Stadinski et al. (2016) recently reported that self-reactive TCRs may be characterised by hydrophobic (which is synonymous with hydropathic) residues in the CDR3 of the TCRβ chain. This section examined whether the strongly TCR-signalled W1 TCRs also exhibit high hydropathy in the CDR3α J subregion. The hydropathy at individual amino acid level was determined by dividing the average hydropathy value in each sample with the average number (or count) of amino acids in each sample, all within the J subregion, analysed by VDJtools *CalcCdrAAProfile* routine.

Wild-type samples were directly compared to *H2-Aa*$^{-/-}$*B2m*$^{-/-}$ samples as these two genotypes had all three W1, CD4SP and CD8SP cell subsets. When the data were stratified by cell type, W1 samples had significantly higher hydropathy measurements

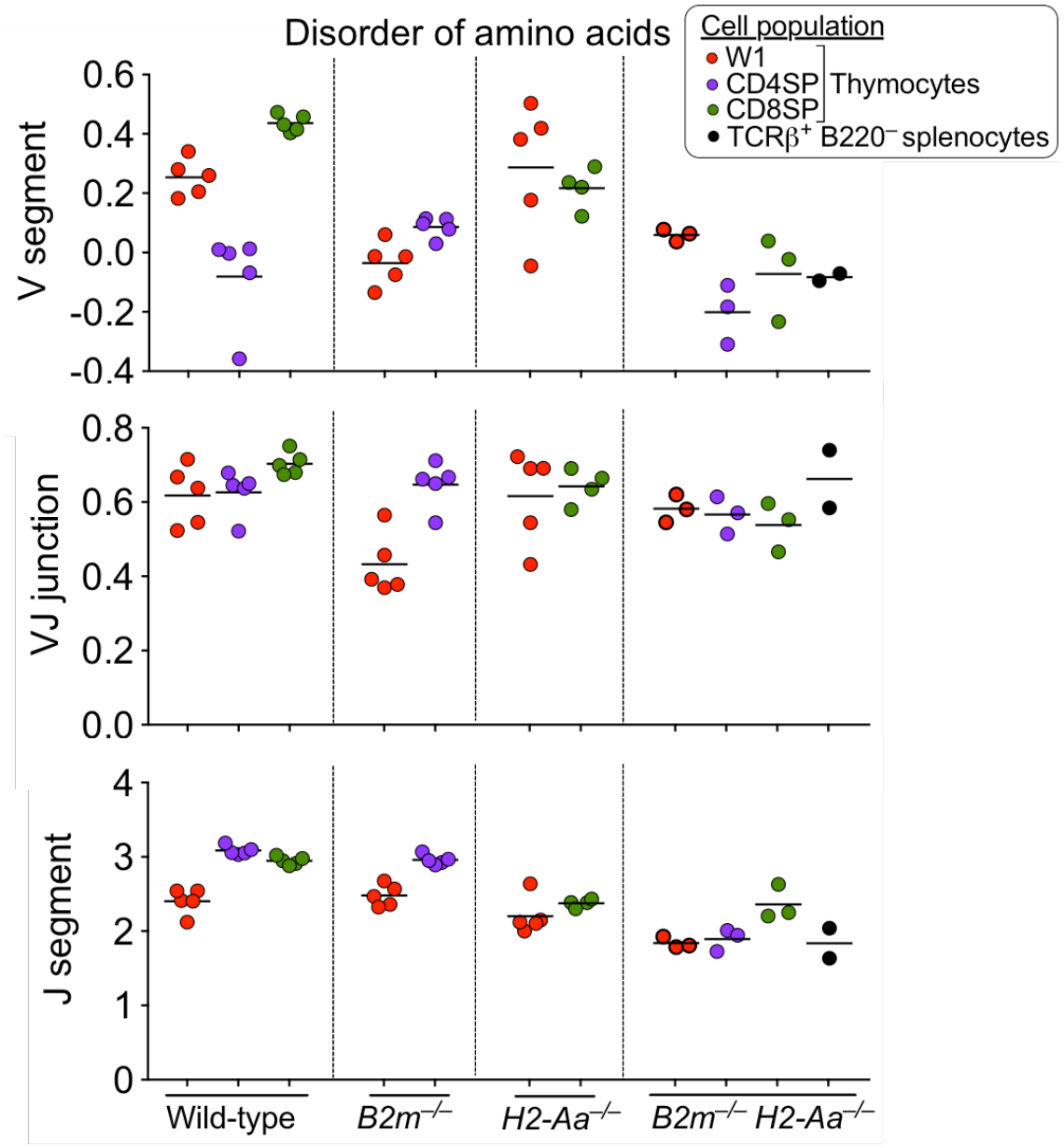

Figure 5.25. *H2-Aa*$^{-/-}$*B2m*$^{-/-}$ samples exhibit low amino acid "disorder" profile in the J subregion of CDR3α loops. Graphs show the average sum of disorder values of amino acids per nucleotype for each sample in V, VJ and J subregions of CDR3α, according to the VDJtools annotation for disorder-producing, neutral and order-producing amino acids described in Fig. 5.24. Each circle represents a TCR sequencing dataset derived from 1 of the 45 samples described in Figs. 5.1-5.3. Lines represent group means. Data were analysed using VDJtools *CalcCdrAAProfile* routine set to "unweighted", i.e. ignoring TCR nucleotype frequency.

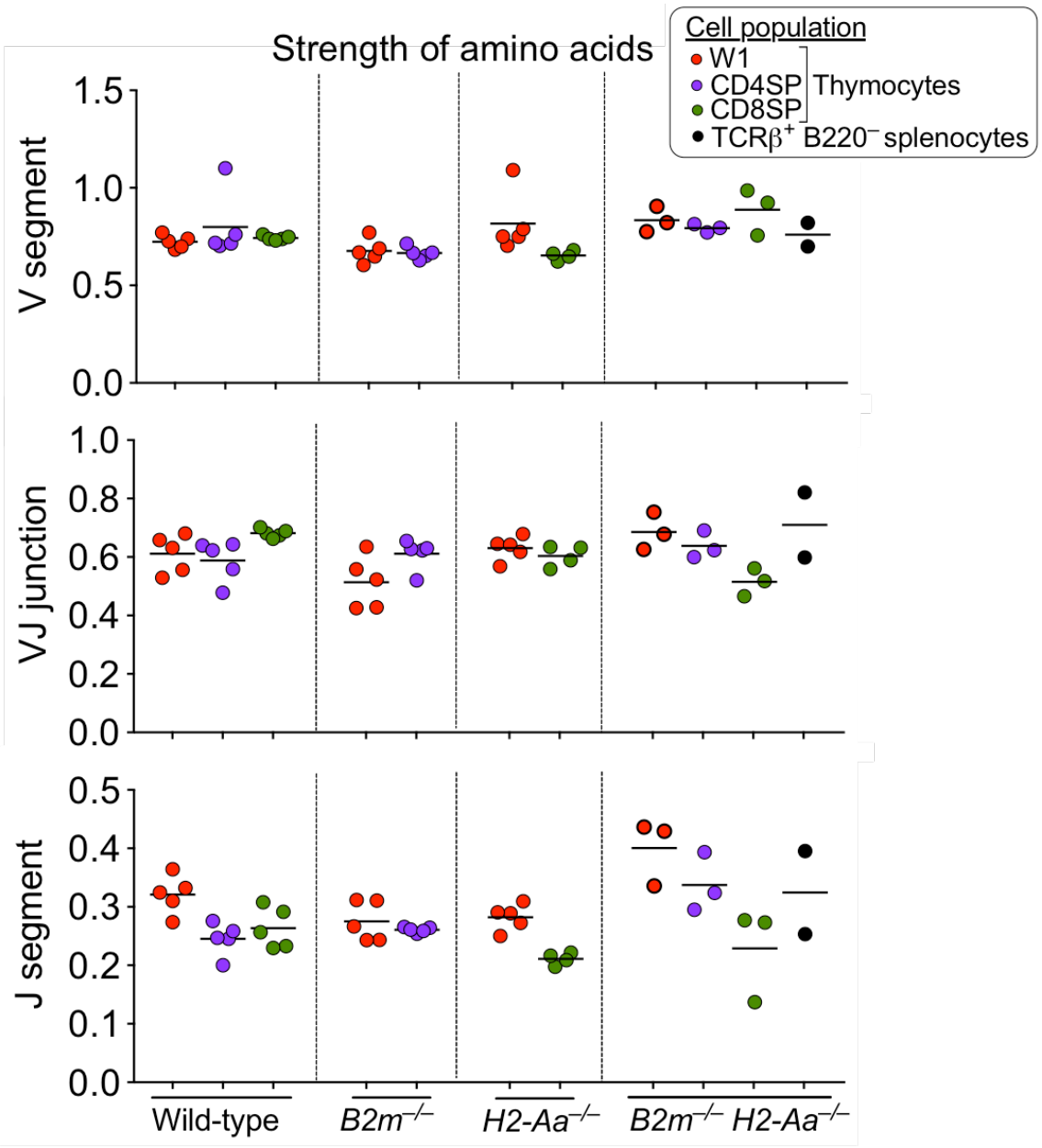

Figure 5.26. *H2-Aa*$^{-/-}$*B2m*$^{-/-}$ samples demonstrate high amino acid "strength" measurements in the J subregion of CDR3α loops. "Strength" measurement is the average number of occurrences of the amino acids L, F, I, M, V, W, C and Y per nucleotype. Graphs show the average "strength" measurements for each sample in V, VJ and J subregions of CDR3α. Each circle represents a TCR sequencing dataset derived from 1 of the 45 samples described in Figs. 5.1-5.3. Lines represent group means. Data were analysed using VDJtools *CalcCdrAAProfile* routine set to "unweighted", i.e. ignoring TCR nucleotype frequency.

at the individual amino acid level than the positively selected CD8SP (Fig. 5.27). This result suggests that both MHC-dependent and MHC-independent strongly signalled W1 TCRs, may be characterised by the increased presence of hydrophobic residues in the CDR3 of TCRα chain.

Notably, CD8SP samples in *H2-Aa*$^{-/-}$ mice had significantly greater hydropathy measurements than CD8SP samples from wild-type mice (Fig. 5.28). This finding suggests that MHCII expression impinges on, and possibly decreases the self-reactivity of, the CD8^{+} T cell TCR repertoire. A caveat of this finding, however, is that the Yae62 TCRβ chain may be unusual because it is capable of binding to both the MHCII molecule, H2-A^{b}, and the MHCI molecule, H2-K^{b} (Huseby et al., 2005; Yin et al., 2011). This cross-reactivity may increase the impact of MHCII expression in Yae62 TCRβ transgenic mice compared to mice with a fully diverse CD8^{+} T cell repertoire.

ii) MHC-independent TCRs have increased usage of hydrophobic residues in the J subregion of CDR3α

When the data were stratified by MHC genotype, ignoring cell type information, *H2-Aa*$^{-/-}$*B2m*$^{-/-}$ samples exhibit significantly higher hydropathy per amino acid in the J subregion of the CDR3α compared to wild-type mice (Fig. 5.29). This indicates that MHC-independent TCRs are characterised by increased usage of hydrophobic residues in the J subregion of CDR3 TCRα chain, which is also consistent with the finding above (Fig. 5.23).

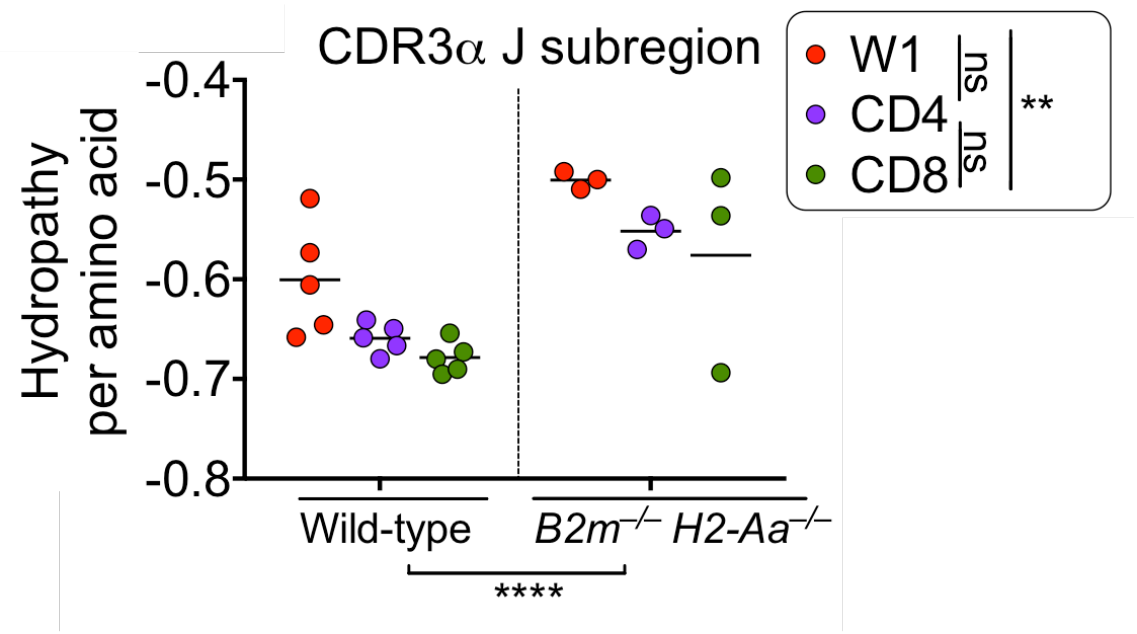

Figure 5.27. Wave 1 TCRs have increased hydropathy per amino acid in the CDR3α J subregion. Graphs show the average hydropathy per amino acid in the J subregion of CDR3 TCRα chain determined by dividing the average hydropathy value in each sample with the average number (or count) of amino acids in each sample. Each circle represents a sample from wave 1, CD4SP and CD8SP thymocytes subsets of wild-type mice (n=5) and *H2-Aa*$^{-/-}$*B2m*$^{-/-}$ wild-type mice (n=3). Lines represent group means. Data were analysed using VDJtools *CalcCdrAAProfile* routine, unweighted by TCR nucleotype frequency. 2-way ANOVA and Tukey's post-tests; P values are shown with symbols: ns, non-significant; ** <0.01; **** <0.0001 (between MHC genotype).

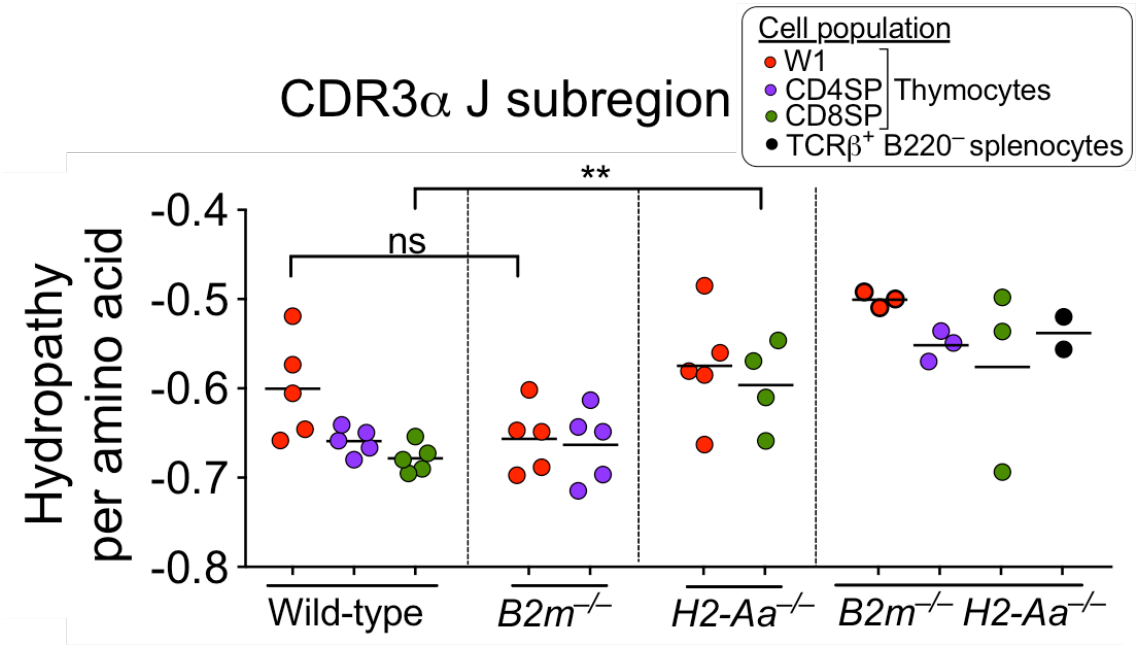

Figure 5.28. MHCII-deficient CD8SP TCRs have higher hydropathy per amino acid in the CDR3α J subregion than wild-type CD8SP TCRs. Graphs show the average hydropathy per amino acid in the J subregion of CDR3 TCRα chain for individual samples. Each circle represents a sample from wave 1, CD4SP and CD8SP thymocytes subsets and/or TCRβ^{+} B220^{-} splenocyte subset across four MHC genotypes described in Fig. 5.23. Lines represent group means. Data were analysed using VDJtools *CalcCdrAAProfile* routine, unweighted by TCR nucleotype frequency. Statistical analysis used unpaired Student's t-tests. P value symbols: ns, non-significant; ** <0.01.

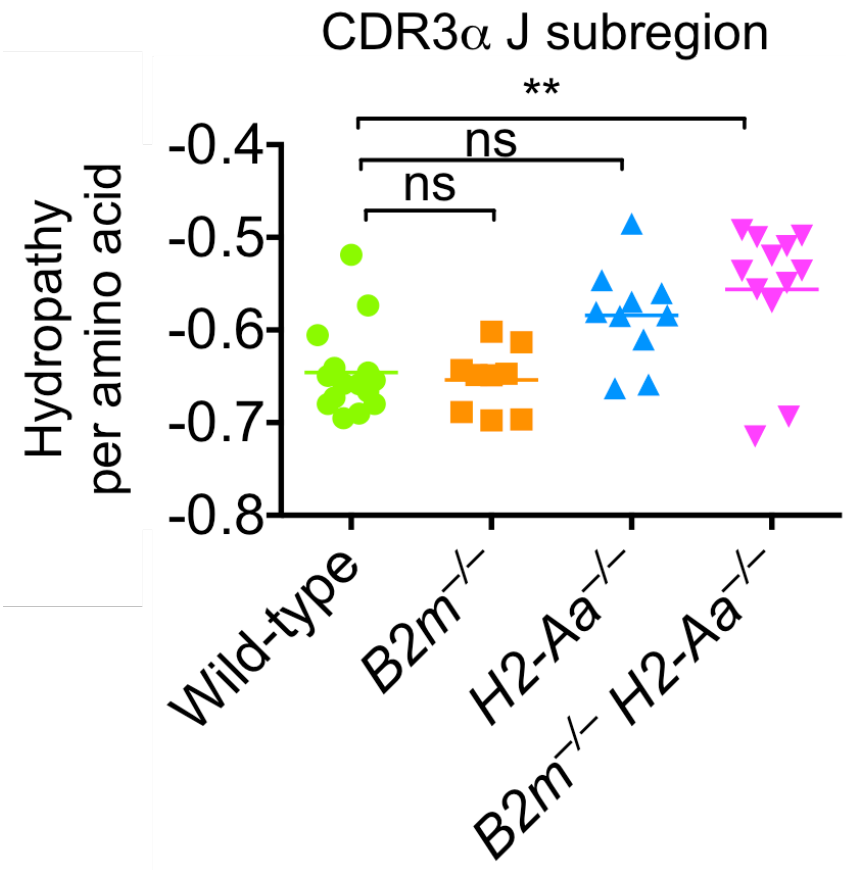

Figure 5.29. MHC-independent TCRs have increased hydropathy per amino acid in the CDR3α J subregion. Graphs show the average hydropathy per amino acid in the J subregion of CDR3 TCRα chain for each sample. Each symbol represents a sample from one of the four MHC genotypes described in Fig. 5.28, ignoring T cell subsets (i.e. wave 1, CD4SP and CD8SP thymocytes subsets and/or TCRβ^{+} B220^{-} splenocyte subset). Lines represent group means. Data were analysed using VDJtools *CalcCdrAAProfile* routine, unweighted by TCR nucleotype frequency. Statistical analysis used unpaired Student's t-tests. P value symbols: ns, non-significant; ** <0.01.

5.2.10 Visualisation of CDR3 amino acid sequences for MHC-independent and MHC-dependent TCRs by IceLogo

To investigate which amino acids are enriched within the CDR3α of MHC-independent TCRs, and their positioning within the CDR3α, IceLogo software was used. IceLogo provides a visual and intuitive comparison of two datasets containing peptide sequences of a defined length. Icelogo first calculates from a reference dataset the occurrences (mean and standard deviation) of each amino acid at each position in the sequence by repetitive random sub-sampling of the data. Icelogo repeats this procedure in the experimental dataset and displays any amino acid with significantly different frequencies in the reference and experimental datasets (p-value <0.05 as determined by a *t*-test). The height of an individual amino acid symbol reflects the difference in frequencies in the 2 datasets at that position in the sequence; symbols above the *x*-axis indicate enrichment in the experimental dataset; symbols below indicate enrichment in the reference dataset (Colaert et al., 2009; Maddelein et al., 2015).

Datasets were compiled containing CDR3α sequences of 12, 13, 14, 15 or 16 amino acids, inclusive of the conserved residues in the CDR3 amino acid sequence (C at the N-terminus and F or W at the C-terminus). These numbers cover the CDR3α lengths most commonly observed in the datasets (Fig. 5.30). All TCR samples (i.e., W1, CD4 and CD8SP thymocyte samples and TCRβ$^+$ B220$^-$ splenocyte samples) of *H2-Aa*$^{-/-}$ *B2m*$^{-/-}$ mice were pooled using VDJtools *PoolSamples* routine to form the MHC-independent TCR dataset. W1, CD4 and CD8SP TCRs from wild-type mice were pooled to form the MHC-dependent TCR dataset.

Unlike “disorder” and “strength”, the “hydropathy” of amino acids can be estimated in an objective manner (Pommie et al., 2004) as 20 amino acids are classified into hydrophobic (synonymous with hydropathic), neutral and hydrophilic categories (Pommié et al., 2004) (Table 5.3). At position 3, hydrophobic amino acids L (leucine) and V (valine) were enriched in the MHC-independent dataset (Fig. 5.31). As TRAV12-1, TRAV12-2 and TRAV12-3 encode an “L” at position 3, this is probably due to these TRAV segments being commonly used in *H2-Aa*$^{-/-}$*B2m*$^{-/-}$ samples. Enrichment of “V” at position 3 may be due to the “V” at position 3 encoded by TRAV2, which was detected only in *H2-Aa*$^{-/-}$*B2m*$^{-/-}$ samples. On the other hand, hydrophobic A (alanine) was enriched in the reference dataset at position 3 (Fig. 5.31). This is probably due to TRAV14, TRAV19 and TRAV5D encoding “A” at position 3 of CDR3α sequences in wild-type samples.

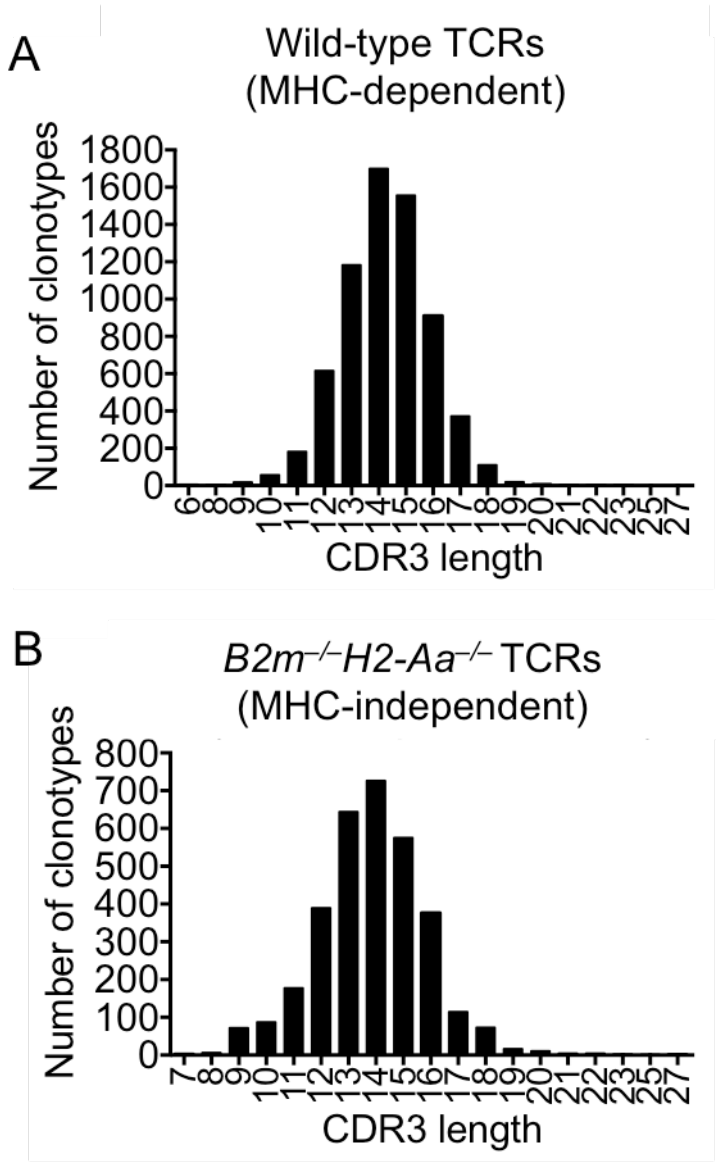

Figure 30. MHC-dependent and MHC-independent TCRs peaked at 12 to 16 amino acid residues in CDR3α length. TCRs from W1, CD4 and CD8SP thymocyte subsets and TCRβ$^+$ B220$^-$ splenocyte subset of *H2-Aa*$^{-/-}$*B2m*$^{-/-}$ mice were pooled using VDJtools *PoolSamples* routine, forming the MHC-independent TCRs. W1, CD4 and CD8SP TCRs from wild-type mice were pooled to form MHC-dependent TCRs. Graphs show the number of clonotypes found in every CDR3α length detected in (A) wild-type TCRs and (B) *B2m*$^{-/-}$*H2-Aa*$^{-/-}$ TCRs.

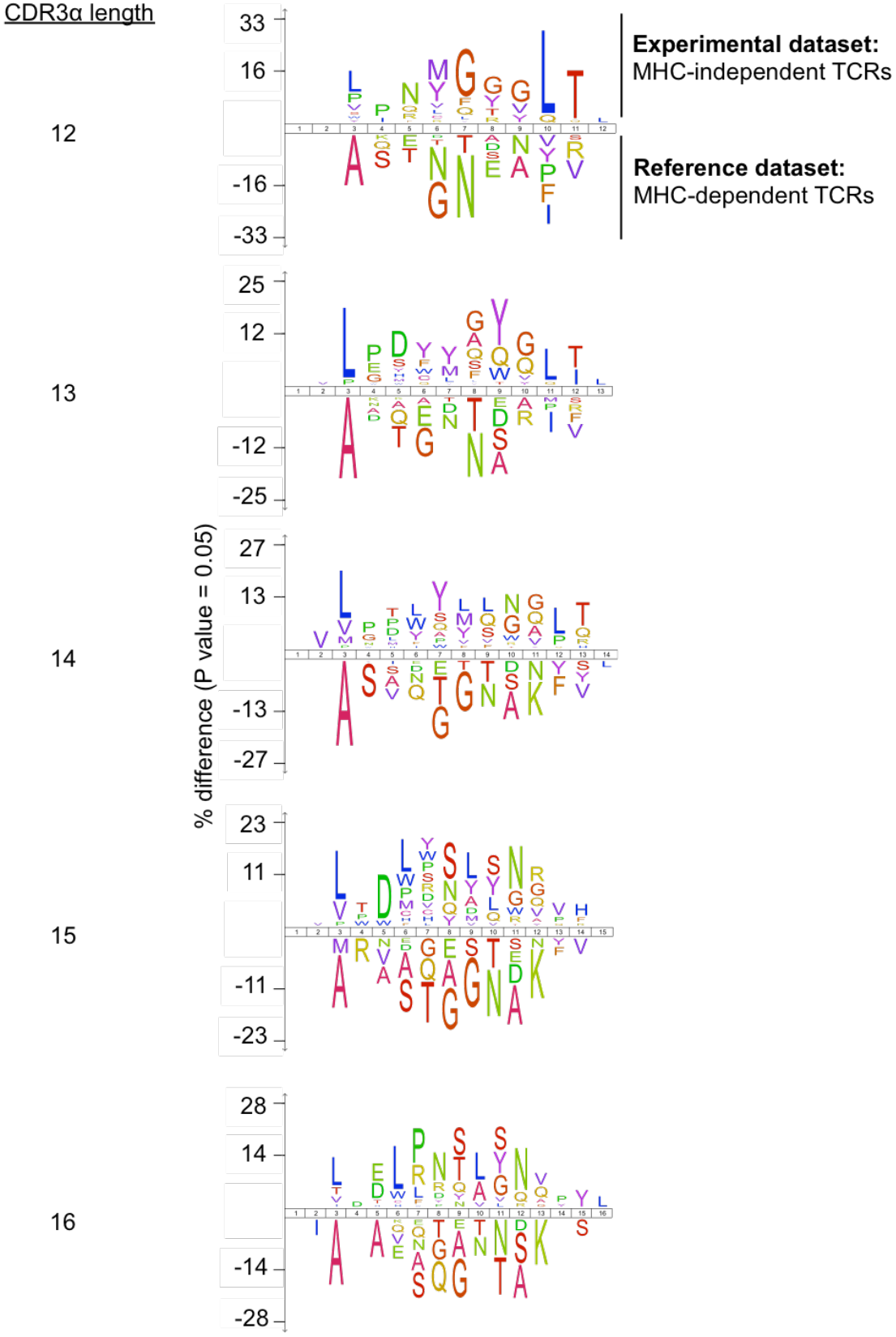
CDR3α length
12
13
14
15
16
% difference (P value = 0.05)
33
16
-16
-33
25
12
-12
-25
27
13
-13
-27
23
11
-11
-23
28
14
-14
-28
Experimental dataset:
MHC-independent TCRs
Reference dataset:
MHC-dependent TCRs

Figure 31. Hydrophobic amino acid residues (L, W, V) are enriched at positions 3, and 6, 7, 9, 10 (J subregion) of the CDR3α in MHC-independent TCRs. IceLogos generated from the *B2m*$^{-/-}$*H2-Aa*$^{-/-}$ MHC-independent TCRs (experimental set, above x-axis) and the wild-type MHC-dependent TCRs (reference set, below x-axis), both with CDR3α length of 12, 13, 14, 15 and 16 amino acid residues. IceLogo showed only the significant difference in frequency of each amino acid at every position ($P < 0.05$) in the experimental set (denoted as positive frequency) and the reference set (denoted as positive frequency). Positive frequency represents the high abundance amino acids in the experimental set over reference set, whereas negative frequency shows the low abundance amino acids in the experimental set over reference set. The size of an amino acid reflects the difference in the frequency of an amino acid in the experimental and its percentage in the reference set.

All enrichments observed at positions >3 are attributable to the tendency for MHC-dependent and MHC-independent TCRs to use different TRAJ genes. In the MHC-independent TCRs, hydrophobic residues W (tryptophan) and/or L were consistently enriched at position 6 and/or 7 in all CDR3 lengths analysed (Fig. 5.31). Hydrophobic residues L, V and/or W were consistently enriched in MHC-independent TCRs at positions 9 and/or 10 (Fig. 5.31). These findings suggest that hydrophobic residues are enriched in the J subregion of CDR3α in MHC-independent TCRs. However, hydrophilic residues Q (glutamine), R (arginine), D (aspartate) or N (asparagine) were commonly enriched at positions 9 and 10 in the MHC-independent TCRs. By contrast, in the MHC-dependent TCR reference dataset, the neutral amino acids (G (glycine) or T) and hydrophilic amino acids (N, D, E (glutamate) or Q) were enriched at positions 6 to 10 (Fig. 5.31).

5.3 Discussion

To investigate why the individual frequency of TCR-signalled cells in MHCI-deficient mice and MHCII-deficient mice sum to 35% greater than the frequency of TCR-signalled cells in mice bearing both MHCI and MHCII, TCR repertoire sequencing was performed. The overlap in TCR usage between MHCI-deficient and MHCII-deficient mice did not exceed the overlap between either of these datasets and the dataset from mice lacking both classes of MHC. Thus, the data provide no support for the MHC class cross-reactivity hypothesis. Differences in TRAV usage associated with particular MHC genotypes and/or cell types suggest that the TRAV-encoded portions of the TCR bias MHC recognition and thymocyte fate. Increased usage of certain TRAV segments in mice lacking one MHC class is consistent with the interclonal competition hypothesis to explain the "35% difference". Interestingly, mice lacking both MHC classes exhibit "fusion" of CD4SP and CD8SP TCR repertoires, a distinctive TRAJ segment usage profile and enrichment of hydrophobic amino acids in the J subregion of CDR3α loops.

TCRα chain sequencing was performed on sorted T cells from mice with a fixed Yae62β (TCRβ) chain. The negatively selected wave 1 TCR repertoire was distinct from the positively selected CD4SP and CD8SP TCRs in the presence of one or both MHC classes, based on the following evidence. First, wave 1 TCR repertoire formed a distinct cluster from CD4SP and CD8SP TCR repertoires using unsupervised clustering (Fig. 5.8). Second, certain TRAV segments were detected more frequently in wave 1 samples than in positively selected CD4SP or CD8SP samples (Fig. 5.16). Third, there was little overlap in TCR clonotypes between W1 samples and either CD4SP or CD8SP samples (Figs. 5.10, 5.11). Fourth, the strongly TCR-signalled wave 1 TCRs in wild-type and MHC-double deficient mice are enriched for hydrophobic amino acids in the J subregion of CDR3α loops as compared to positively selected CD8SP (Fig. 5.27, Table 6.1). Wave 1 TCRs were also somewhat distinct from CD4SP/CD8SP TCRs in mice lacking both classes of MHC (Fig. 5.10B). It is concluded that MHC expression is not necessary for a difference to be observed in the TCR repertoires that provoke positive versus negative selection.

The TRAV segment encodes the CDR1α and CDR2α loops, which commonly interact with the MHC portion of peptide/MHC complexes (Rossjohn et al., 2015; Rudolph et al., 2006). When paired with the YAe62β chain, TRAV21/DV12 appears to favour TCR interactions with MHCII as it is enriched in CD4SP TCRs of wild-type and *B2m*$^{-/-}$ mice (Fig. 5.16). TRAV16/DV11 and TRAV8D-1 appear to favour TCR interactions with MHCI as these TRAV segments are highly expressed in CD8SP cells (Fig. 5.16). A

recent study showed that expression of TRAV and TRBV gene segments is significantly associated with polymorphisms in MHC genes whereas expression of TRDV and TRGV genes is not (Sharon et al., 2016). The effect of TRAV segment on CD4 versus CD8 lineage choice is consistent with $CD4^+$ and $CD8^+$ T cells having different TRBV segment usage (Klarenbeek et al., 2015). Similarly, the two closely related germline-derived Vα3.1 (encoded by TRAV9-2) and Vα3.2 (encoded by TRAV9D-2) (Bosc and Lefranc, 2003) segments bias selection into CD4 and CD8 subsets, respectively (Sim et al., 1996). Three mutations created in Vα3.1 gene were sufficient to bias selection from CD4 towards the CD8 subset (Sim et al., 1996). In addition, TRAV12-2 gene encoding CDR1α was found to be highly expressed in human $CD8^+$ T cell TCRs that bind to ELA:HLA-A*0201 (peptide:MHCI). This is due to the TRAV12-2 germline-encoded of CDR1α loop of TCR dominating the recognition of residues on MHC surface and bound peptide (Cole et al., 2009). The observed associations between TRAV usage, MHC genotype and cell type indicate that TRAV usage influences MHC recognition.

Germline-encoded amino acids in the CDR2β play a role in controlling positive selection. Substitution of alanine into the CDR2 region of a transgenic TCRβ chain was sufficient to reduce the frequency and number of mature CD4SP and CD8SP thymocytes and peripheral T cells (Scott-Browne et al., 2009). The present findings suggest that CDR1 and CDR2 loops could also have a role in negative selection as evident by the enrichment of TRAV usage in wave 1 cells. TRAV12-3 usage was enriched in wave 1 samples in a B2m-dependent manner (Fig. 5.16). The enrichment of certain TRAV segments in negatively selected wave 1 cells may be due to the role of CDR1 and CDR2 loops in self-antigen-binding. Amino acids in the CDR1 can alter antigen-binding even when they do not interact at the TCR-pMHC interface. For example, the affinity of the J809.B5 TCR for 3K-IA^b is reduced by 260-fold by an alanine substitution at the CDR1 αY31 residue (aY31A) (Stadinski et al., 2014). Another study revealed that two TCRs with identical TCRβ chains and an identical CDR3 amino acid sequence in the TCRα chain, but a different TRAV segment, had different antigen-binding properties (Lee et al., 2012). The findings of TRAV usage enrichment associated with particular MHC genotypes and/or cell types suggest that portions of the TCR encoded by TRAV segments can bias thymocyte fate.

Compared to wild-type wave 1 samples, TRAV8D-1 usage was increased by 3.5-fold in *B2m*$^{-/-}$ wave 1 samples, versus 1.1-fold for TRAV12-2 and 1.28-fold for TRAV21/DV12 (Fig. 5.16). This “preferential” increase suggests that thymocytes bearing TCRs using TRAV8D-1 compete more effectively for APCs when the APCs cannot express B2m

compared to when the APCs can express B2m. This provides preliminary evidence supporting the interclonal competition hypothesis as an explanation for the "35% difference" described above.

No evidence was found to support the MHC class cross-reactivity hypothesis. The percentage of negatively selected wave 1 TCRs shared between MHCI-deficient mice and MHCII-deficient mice was not greater than the percentage shared between either of these groups and the group lacking MHC expression (Table 5.1). This result was surprising because it was recently shown that TCRs that induce clonal deletion are often MHC class cross-reactive (McDonald et al., 2015). The Yae62β transgenic mice used in this thesis would be expected to provide an ideal setting to detect MHC class cross-reactive TCRs. This is because the Yae62 TCRβ chain is known to be capable of binding to the α1 chain of H2-K^b (MHCI) and the α chain of H2-A^b (MHCII) (Yin et al., 2011). To explain the apparent discrepancy, it is possible that the wave 1 cells sorted here may represent only a small portion of the true wave 1 TCR repertoire. The sorting strategy may only capture a subset of thymocytes that have survived deletion at wave 1 and progressed to the next stage of IEL differentiation. It is possible that MHC class cross-reactive TCRs are deleted at the DP stage, explaining the failure to detect MHC class cross-reactive TCRs in this thesis. MHC class cross-reactive TCRs may be detected if the apoptosis-defective *Bcl-2* Tg mice are used. This is because the apoptosis defect might enable cells bearing MHC class cross-reactive TCRs to survive long enough to attain the $CD4^{lo}CD8^{lo}$ PD-1^{hi} phenotype used for wave 1 cell sorting.

Unlike samples from mice expressing at least one MHC class, the CD4SP and CD8SP TCR repertoires of *B2m*$^{-/-}$*H2Aa*$^{-/-}$ mice were clustered together (Fig. 5.8). CD4SP TCR clonotypes commonly overlapped with CD8SP TCR clonotypes in *B2m*$^{-/-}$*H2Aa*$^{-/-}$ mice (Fig. 5.13). These findings indicate that MHC expression is required for the CD4SP and CD8SP TCR repertoires to be distinct from each other. TCRs in *B2m*$^{-/-}$*H2Aa*$^{-/-}$ mice and wild-type mice are referred to as MHC-independent and MHC-dependent TCRs, respectively, hereon. The "fusion" of CD4SP and CD8SP TCR repertoires in mice lacking both MHC classes suggests that MHC expression is required for coreceptors to affect T cell selection. Although the αβT cells that develop in mice lacking both CD4 and CD8 coreceptors and both MHC molecules (referred to as Quad-deficient mice) have been described, there was no report of "fusion" of CD4SP and CD8SP TCR repertoires in Quad-deficient mice (Van Laethem et al., 2007; Van Laethem et al., 2013). It was concluded that coreceptor-free Lck (Lck that is not bound to a coreceptor) promotes thymic selection of MHC-independent TCRs, as opposed to the coreceptor-associated Lck that promotes thymic selection of MHC-restricted TCRs (Van Laethem

et al., 2013). The observed CD4SP and CD8SP TCR repertoire "fusion" is consistent with the hypothesis that coreceptors have a key role in the CD4/CD8 lineage decision.

The MHC-independent TCR repertoire has a distinctive TRAJ segment usage profile compared to TCR repertoires in mice expressing one or both MHC classes (Figs. 5.18, 5.19). CDR3 loops are predominantly encoded by the TRAJ segment and form the region that commonly binds to the peptide portion of peptide-MHC complexes. MHC-independent αβTCRs are thought to interact with ligands in a manner resembling antibody-antigen interactions (Tikhonova et al., 2012). CDR3α sequences are required for the interaction of one MHC-independent TCR with glycosylation-dependent conformational epitopes on the self-protein, CD155 (Tikhonova et al., 2012). This recognition is in contrast to the MHC-dependent TCRs recognising peptide-MHC complexes, potentially explaining why MHC-independent TCRs have a unique TRAJ segment usage.

The MHC-independent TCR repertoire is enriched in hydrophobic amino acids in the J subregion of CDR3α loops (Figs. 5.23, 5.28, 5.29). In particular, the enrichment of hydrophobic amino acid residues (tryptophan (W), leucine (L) and valine (V)) was commonly found at positions 6, 7 and 9, 10 of CDR3α regardless of the CDR3α length analysed (Fig. 5.31). The presence of hydrophobic amino acid residues at position 6 and 7 in CDR3β was found to increase the self-reactivity of T cells (Stadinski et al., 2016). This is also consistent with enrichment of hydrophobic amino acids in negatively selected wave 1 TCRs in MHC-dependent and MHC-independent TCRs (Fig. 5.27). Structural analyses indicate that the CDR3 loops of both α and β chains fold into the interior of the TCR heterodimer (Rossjohn et al., 2015). It is conceivable that hydrophobic amino acids in the CDR3 loops help to stabilise the TCR heterodimer itself as well as stabilise the interaction between the TCR and its ligand in the negatively selected wave 1 TCRs and MHC-independent TCRs. In folded proteins, hydrophobic residues tend to occupy the interior of the molecule, away from the surrounding water. Although the MHC-independent or -dependent TCR-ligand interface is composed of multiple proteins, the entire assembly might be considered as a unit that is stabilised by a hydrophobic interior consisting of the CDR3α and CDR3β loops. The potential role of high amino acid hydrophobicity in the CDR3α J subregion of MHC-independent TCRs in stabilising the TCR-ligand interaction is supported by the low intrinsic structural disorder (stable protein under native condition) within the same region (Fig. 5.26). This is consistent with previous literature reporting that hydrophobic amino acids promote structure order (Hansen et al., 2006; Uversky et al., 2000).

Based on surface plasmon resonance measurements, the MHC-independent αβTCR (B12A) and its ligand CD155 have a K^d of 230 nM (=0.23μM) (Tikhonova et al., 2012), as opposed to the 6-60μM reported for αβTCRs and peptide-MHC complexes in mice (Margulies, 1997; Matsui et al., 1991; Naeher et al., 2007). The smaller the K^d value (i.e. nM versus μM), the greater the binding affinity. So, the MHC-independent interaction is 26- to 260-fold higher in affinity than typical MHC-dependent interactions in mice. In humans however, it has been reported that MHC-dependent TCRs could have a wide range of binding affinities between TCR peptide-MHC (K^d of 1μM-500μM) (Bridgeman et al., 2012; Cole et al., 2007). The affinity threshold that discriminates positive versus negative selecting ligands in MHCI-restricted TCRs (T1, S14, and OT-1 TCR) is ~6 μM K^d (Naeher et al., 2007). The high "strength" (i.e. high capacity of amino acid-amino acid interaction) (Fig. 5.26) that is closely associated with hydrophobic amino acids (Miyazawa and Jernigan, 1996), and the high hydrophobicity in CDR3α J subregion of MHC-independent TCRs, may contribute to the high binding affinity of MHC-independent TCR with its ligand. Why might a high affinity MHC-independent interaction (~230 nM) not result in strong TCR signalling and clonal deletion? A simple explanation is that coreceptors contribute less, or not at all, to MHC-independent TCR-ligand interactions compared to MHC-dependent TCR-pMHC interactions. Without coreceptors, a greater intrinsic affinity between TCR and ligand may be required to induce equivalent TCR clustering at the cell surface and signalling inside the T cell (Taylor et al., 2017). Assuming that high affinity MHC-independent interaction (~230 nM) induces positive selection, an even higher affinity may be required for negative selection in MHC-independent TCRs.

One potential weakness of this experimental system is that each TCRβ transgenic cell that was TCR-sequenced could potentially express two TCRα chains. As dual-TCRα expressing cells can be found in the thymus and in the periphery (Hale and Fink, 2010; Simmons et al., 2012), some of the TCRα sequences detected were very likely to be from dual-TCR expressing T cells. However, the fact that TCR sharing was more common within than across cell-type boundaries indicates a clear association between TCR sequence and cell fate. Since sequences from dual-TCR expressing T cells would be expected to decrease the strength of this association, the actual association is probably stronger than what is reflected in the data.

In summary, this study did not find evidence of MHC class cross-reactive TCRs within the wave 1 repertoire, but did provide evidence supporting the interclonal competition hypothesis. The MHC class cross-reactive TCR hypothesis cannot be excluded, however, because it is possible that the sorting strategy used here captured only a

portion of the true wave 1 TCR repertoire.

CHAPTER 6

General discussion

6.1 The partition of two waves of thymic negative selection

Thymocytes that receive strong TCR signalling undergo negative selection (which encompasses clonal deletion or agonist selection) at either the immature $CCR7^{-}$ or DP stage (wave 1), or the mature $CCR7^{+}$ or SP stage (wave 2). The thymic negative selection mechanisms examined in this thesis and previous studies, focusing on the roles of thymic APC types ($MHCII^{+}$ BM-APCs and $Aire^{+}$ mTECs) and MHC molecules are depicted in Fig. 6.1. The characteristics of MHC-dependent and MHC-independent TCR selection investigated in this study are discussed below (Table 6.1).

In wave 1 $CCR7^{-}$ (or DP) negative selection, presumably in the thymic cortex (Kurd and Robey, 2016; McCaughtry et al., 2008), wave 1 cells are characterised by the dulling of CD4 and CD8 coreceptors ($CD4^{lo}CD8^{lo}$) and PD-1 upregulation (Daley et al., 2013; McCaughtry et al., 2008). The strongly TCR-signalled thymocytes undergo one of two processes. Firstly, they may undergo wave 1 clonal deletion, which accounts for more than half of all negative selection (Daley et al., 2013; Sinclair et al., 2013; Stritesky et al., 2013). This occurs at 1-2 days after proliferation during the DN-DP transition (Hu et al., 2016). Alternatively, wave 1 thymocytes that do not undergo clonal deletion at the $CCR7^{-}$ stage become $CD4^{lo}CD8^{lo}$ $PD\text{-}1^{hi}$ iIEL thymic precursors and may eventually differentiate into $TCR\alpha\beta^{+}$ $CD8\alpha\alpha^{+}$ iIEL in the periphery (McDonald et al., 2014; Pobezinsky et al., 2012) (Fig. 6.1). This is based on the evidence that thymocytes that survived superantigen-mediated clonal deletion (Pobezinsky et al., 2012) or survived negative selection by thymic self-ligands (e.g., Bcl-xL Tg thymocytes), exhibiting $CD4^{lo}CD8^{lo}$ $PD\text{-}1^{hi}$ phenotype, differentiate into $CD8\alpha\alpha^{+}$ iIELs in the gut (Gangadharan et al., 2006; Leishman et al., 2002; McDonald et al., 2014). Direct evidence that $Helios^{+}$ $CCR7^{-}$ thymocytes give rise to iIELs in the periphery remains lacking. This could be tested by generating $Helios^{GFP}$ mice, sorting GFP^{+} $CCR7^{-}$ thymocytes, injecting them into recipient mice and detecting the presence or absence of GFP^{+} cells in the small intestine of the recipient mice.

Some wave 1 negatively selected thymocytes have been reported to be MHC class cross-reactive (McDonald et al., 2015), although this study fails to provide evidence of MHC class cross-reactive TCRs within the wave 1 cells as discussed in Chapter 5. This study demonstrates a requirement for $MHCII^{+}$ BM-APCs in mediating stringent wave 1 negative selection (clonal deletion and iIEL thymic precursors) to establish central tolerance. Wave 1 negative selection was found to be more dependent on MHCII than MHCI, although this effect was evident only in apoptosis-defective mice (Fig. 6.1).

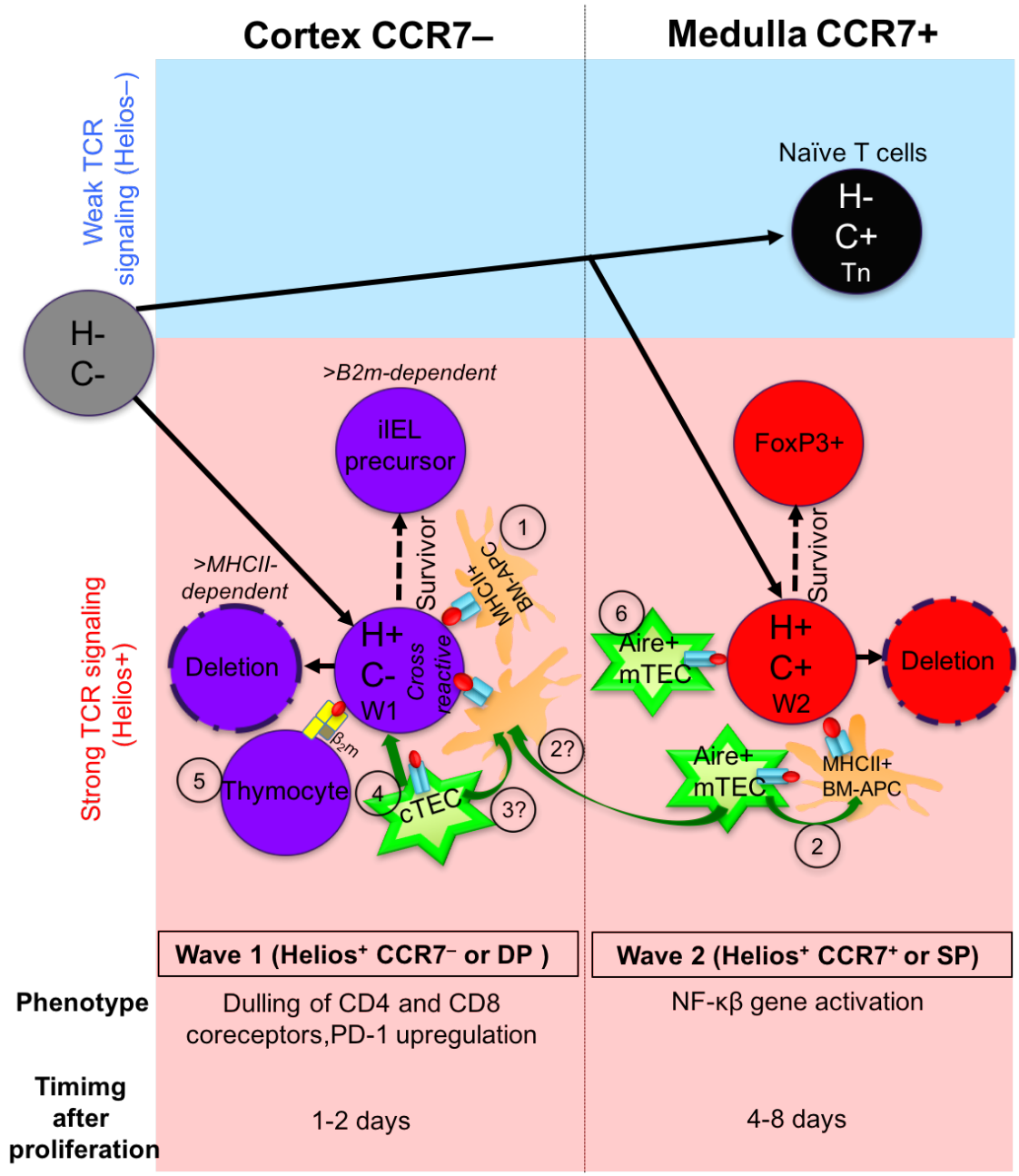

Figure 6.1. Thymic negative selection mechanisms. Pre-selection thymocytes have a Helios^{-} CCR7^{-} phenotype. Thymocytes that receive a strong TCR signal upregulate Helios. Helios+ thymocytes at CCR7^{-} (similar to DP) or CCR7^{+} (similar to SP) stages of development are characterised as undergoing "wave 1" and "wave 2" negative selection, respectively. Timecourse experiments revealed that, on average, thymocytes enter wave 1 approximately 2 days after they proliferate during beta selection. Wave 1 is presumed to occur in the thymic cortex. Wave 1 thymocytes exhibit a phenotype of coreceptor dulling and PD-1 upregulation. The present study demonstrates that MHCII^{+} BM-APCs are required for wave 1 negative selection (mechanism 1). Within mechanism 1 in wave 1, it is possible that some self-antigens are handed over from cTECs to MHCII^{+} BM-APCs (mechanism 3?), or self-antigens are derived from the

bloodstream. Other antigen-presenting mechanisms that may contribute to wave 1 include direct presentation by cTECs (mechanism 4) and B2m-dependent presentation by thymocytes or other BM-APCs (mechanism 5). A substantial proportion of wave 1 thymocytes are thought to be MHC class cross-reactive. Most of the wave 1 thymocytes undergo clonal deletion (apoptosis), in which MHCII-responsive thymocytes may die quicker than MHCI-responsive thymocytes, but some wave 1 cells that survived a strong TCR signal in the thymic cortex differentiate into $CD4^{-}CD8\beta^{-}$ iIEL thymic precursors, which predominantly recognise B2m-dependent ligands. Wave 2 negative selection occurs 4-8 days after thymocyte proliferation, and presumably occurs in the thymic medulla. This study shows that tissue-specific antigens can either require handover from TECs to $MHCII^{+}$ BM-APCs to induce negative selection (mechanism 2). Although speculative, if migratory DCs that acquire self-antigens derived from mTECs (Koble and Kyewski, 2009) transport them into the cortex, this may provide an explanation for how Aire, which is expressed within mTECs (Heino et al., 1999), contributes to wave 1 in the cortex (mechanism 2?). Tissue-specific antigens expressed within mTECs may also be directly presented to thymocytes by mTECs (mechanism 6). Strong TCR signalling drives concurrent pro-apoptotic and pro-survival signals in wave 2 thymocytes, resulting in medullary clonal deletion and $FoxP3^{+}$ T-reg cell differentiation, respectively. Pre-selection thymocytes that receive a weak TCR signal in the cortex and in the medulla are allowed to mature into $Helios^{-}$ $CCR7^{+}$ naïve T cells that emigrate to the periphery, a process termed "positive selection" in this thesis. H, Helios; C, CCR7; Tn, naïve T cells; W1, wave 1 negatively selected thymocytes; W2, wave 2 negatively selected thymocytes; iIEL, intestine intraepithelial lymphocyte; $FoxP3^{+}$, T-regulatory cells.

However, the $CD4^{lo}CD8^{lo}$ PD-1^{hi} iIEL thymic precursors in apoptosis-intact mice appear to commonly express TCRs that bind to B2m-dependent ligands (Fig. 6.1). Since TCR cross-reactivity could contribute to autoimmunity, in part due to the structural similarity between foreign and self-peptides (Li et al., 2005), wave 1 may be important in eliminating the cross-reactive TCRs via clonal deletion (McDonald et al., 2015). Wave 1 negative selection takes place before the distinct process of T-reg selection occurs in wave 2 (Fig. 6.1). If these cross-reactive cells are allowed to mature into T-reg cells that recognise multiple pMHC complexes, it may result in excessive immune suppression in the periphery.

Wave 2 negative selection at the $CCR7^{+}$ (or SP) stage presumably occurs in the thymic medulla (Kurd and Robey, 2016). The strongly TCR-signalled thymocytes either undergo wave 2 clonal deletion, accounting for a minority of negative selection (Daley et al., 2013; McDonald et al., 2015) or differentiate into thymic $FoxP3^{+}$ T-reg cells (Cowan et al., 2013; Hu et al., 2016) (Fig. 6.1). Our group recently delineated two bottlenecks at which wave 2 cells either undergo deletion or progress to the next stage of T-reg differentiation: Card11 signalling regulates the first bottleneck and IL-2 signalling regulates the second (Hu et al., 2017). Wave 2 cells are phenotypically distinct from wave 1 cells. Wave 2 cells induce Card11/NF-κβ gene activation that opposes Bim-mediated apoptosis (Daley et al., 2013). Wave 2 cells form 4-8 days after DN-DP proliferation versus 0-2 days for wave 1 cells (Hu et al., 2016). The thymus may have evolved to make T-reg selecting self-antigens accessible only to wave 2 thymocytes, in part due the supportive medullary environment facilitating T-reg selection (discussed in section 6.3). This is consistent with recent evidence of the requirement for Aire in shaping the T-reg TCR repertoire (Malchow et al., 2016; Perry et al., 2014; Yang et al., 2015). This study provided preliminary evidence that Aire is required for normal induction of negative selection at wave 2, although confirmation of this point awaits analysis at 5 days after EdU injection instead of 3 days.

Several groups have detected a clear overlap in the TCR repertoires of naïve $CD4^{+}$ T cells and T-reg cells (Hsieh et al., 2004; Pacholczyk et al., 2006; Wong et al., 2007). How can this observation be reconciled with the hypothesis that strongly TCR-signalled wave 2 cells either undergo deletion or differentiate into T-reg cells? It is hypothesised that not all medullary self-antigens are scanned by each medullary thymocyte. Consequently, a self-reactive thymocyte can emerge from the thymus “ignorant” of the self-antigen to which it binds. It was recently shown that the probability of a self-reactive T cell becoming an “ignorant” naïve T cell increases as the number of thymic APCs that express the self-antigen decreases (Malhotra et al., 2016). Thus, the

observation that overlap exists between naïve CD4 and T-reg TCR repertoires can be explained by the concept of “ignorance”.

It is also important to consider the TCR repertoire of thymocytes that are deleted at wave 2. The TCR repertoire of thymocytes that are deleted at wave 2 has yet to be examined directly. However, preliminary evidence that Aire-deficiency diminishes wave 2 (this thesis) suggests that TCRs that are normally deleted at wave 2 may enter the naïve $CD4^+$ repertoire in *Aire*$^{-/-}$ mice. The TCR repertoire of $CD4^+$ $Foxp3^-$ T cells in the prostate of *Aire*$^{-/-}$ mice overlapped substantially with the T-reg TCR repertoire in *Aire*$^{+/+}$ mice (Malchow et al., 2016). A smaller number of TCRs expressed by $CD4^+$ $Foxp3^-$ T cells in the prostate of *Aire*$^{-/-}$ mice were never found in *Aire*$^{+/+}$ mice. These latter TCRs may correspond to TCRs that are deleted at wave 2 in wild-type mice (Malchow et al., 2016). Taken together, the available data suggest that a defect in wave 2 caused by Aire-deficiency alters the peripheral TCR repertoire mainly by allowing T-reg TCRs, and not “deletable” TCRs, into the $CD4^+$ $Foxp3^-$ pool. To explain this, we hypothesise that wave 2 deletes TCRs with an affinity for self-antigen that is too low for T-reg selection (Daley et al., 2017; Hu et al., 2017). TCRs that are normally deleted at wave 2 may have an affinity for self-antigen that is too weak for the T cell to be activated in the periphery, explaining why they are uncompetitive at infiltrating the prostate. On the other hand, TCRs that normally drive T-reg selection have very high affinity for self-antigen and are highly competitive at infiltrating the prostate.

This study applied two analytical approaches to quantify wave 1 negative selection at the immature $CCR7^-$ stage: (1) The $Helios^+$ $CCR7^-$ approach devised by our group and (2) the $CD4^{lo}CD8^{lo}$ PD-1^{hi} iIEL thymic precursor approach (Mayans et al., 2014; McDonald et al., 2015; McDonald et al., 2014; Pobezinsky et al., 2012). Second approach was applied to check whether the conclusions based on analysis of Helios/CCR7 were supported.

In addition, this study used the $TCR\beta^+$ $CD5^+$ approach to quantify all TCR-signalled thymocytes, EdU to label the newly proliferating thymocytes, and TCR/antigen transgenic model systems, all dependent on flow cytometry and/or TCR sequencing methods, to investigate the contributions of thymic APCs and MHC molecules to thymic negative selection, particularly at the immature stage.

6.2 Comparisons of two approaches to analyse wave 1 negative selection

The Helios^{+} CCR7$^{–}$ wave 1 approach characterises thymocytes that have received strong TCR signalling at an early CCR7$^{–}$ maturation stage (Daley et al., 2013; Hu et al., 2016). Unlike the of the TCRβ/CD5 gating approach which was straightforward because *B2m$^{–/–}$ and Tcra$^{–/–}$* mice were available as gating controls, the cutoff for Helios staining in the Helios^{+} CCR7$^{–}$ gate was more subjective, but was always placed above the outer edge of the main CCR7$^{–}$ population detected in apoptosis-sufficient mice. Similarly, the cutoff for Helios staining in the Helios^{+} CCR7^{+} gate was placed just above the outer edge of the main CCR7$^{–}$ population from apoptosis-sufficient mice. Helios^{+} CCR7$^{–}$ thymocytes exhibit the phenotype of coreceptor dulling (CD4^{lo}CD8^{lo}) and PD-1 upregulation in superantigen reactive thymocytes and in apoptosis-defective mice (Daley et al., 2013; Hu et al., 2016), similar to the phenotype of TCRβ^{hi} CD4^{lo}CD8^{lo} PD-1^{hi} iIEL thymic precursors in the second approach to analyse wave 1 negative selection. This phenotype of coreceptor-dulling is similar that of DP thymocytes undergoing negative selection *in vitro* (Page et al., 1993; Swat et al., 1991; Vasquez et al., 1992) or *in vivo* (McCaughtry et al., 2008; Pobezinsky et al., 2012).
The CD4^{lo}CD8^{lo} PD-1^{hi} iIEL thymic precursors have also received strong TCR signalling as evident by the upregulation of Nur77, Bim, Helios and increased active caspase 3 (McDonald et al., 2015; McDonald et al., 2014; Pobezinsky et al., 2012). TCRs that induce CD4^{lo}CD8^{lo} PD-1^{hi} thymocytes also commonly facilitate clonal deletion at the CCR7$^{–}$ stage (McDonald et al., 2015).

In this study, the Helios^{+} CCR7$^{–}$ approach analyses nascent thymocyte cohorts, whereas the CD4^{lo}CD8^{lo} PD-1^{hi} approach analyses thymocytes in steady state. This present study reveals that the formation of both the TCRβ^{+} CD5^{+} Helios^{+} CCR7$^{–}$ thymocytes (in normal and apoptosis-defective mice), and the CD4^{lo}CD8^{lo} PD-1^{hi} iIEL thymic precursors (in apoptosis-defective mice) requires MHC molecules. This is consistent with the drastic impairment of Helios^{+} CCR7$^{–}$ and CD4^{lo}CD8^{lo} PD-1^{hi} CD69^{+} thymocyte populations in the absence of both MHC classes (Hu et al., 2016; McDonald et al., 2015).

The potential differences between the two wave 1 approaches is that the Helios^{+} CCR7$^{–}$ approach contains strongly TCR-signalled DP cells that are deleted quickly before acquiring the CD4^{lo}CD8^{lo} phenotype and thus encompassing DP and CD4^{lo}CD8^{lo} thymocytes undergoing negative selection. In the CD4^{lo}CD8^{lo} PD-1^{hi} iIEL thymic precursor approach, only CD4^{lo}CD8^{lo} thymocytes, constituting a portion of true Helios^{+} CCR7$^{–}$ wave 1 cells, that survived longer are captured, but not the DP cells that

undergo apoptosis quickly. In short, the $CD4^{lo}CD8^{lo}$ $PD\text{-}1^{hi}$ iIEL thymic precursors probably represent a more mature subset of wave 1 cells that survived the initial period of strong TCR signalling. This difference could provide an explanation as to why $CD4^{lo}CD8^{lo}$ $PD\text{-}1^{hi}$ thymic iIEL precursors are not decreased in the absence of MHCI, but $Helios^{+}$ $CCR7^{-}$ cells are decreased. This difference could also explain why TCRα chain sequencing results fail to provide evidence of MHC class cross-reactive TCRs within wave 1 cells ($CD4^{lo}CD8^{lo}$ $PD\text{-}1^{hi}$ $CCR7^{-}$) sorted in apoptosis-intact mice with a fixed TCRβ chain (Chapter 5). Future TCRα sequencing experiments in apoptosis-defective mice with a fixed TCRβ chains across all four MHC genotypes (i.e. MHC single- or double-deficient mice and wild-type mice) could be performed to re-examine whether MHC class cross-reactive TCRs are enriched within wave 1 cells. The use of apoptosis-defective mice will also allow parallel comparisons of data between the quantitative and sequencing approaches in examining the contributions of MHC molecules to thymic selection.

6.3 Requirement for $MHCII^{+}$ BM-APCs in inducing wave 1 negative selection

The role of thymic APCs (i.e. DCs, $MHCII^{+}$ BM-APCs, Aire, mTECs) in clonal deletion has been inferred by an increase of CD4SP frequency, or number, in mice with defective APCs (Hinterberger et al., 2010; Liston et al., 2004a; Liston et al., 2008; Malhotra et al., 2016; Ohnmacht et al., 2009; van Meerwijk et al., 1997). The limitations of this approach are the inability to provide direct estimation of strongly TCR-signalled thymocytes undergoing negative selection, and the lack of information about the stage at which clonal deletion occurs. By contrast, the Helios/CCR7 approach provides not only direct quantification of strongly and weakly TCR-signalled thymocytes, but also quantifies negative selection at immature $CCR7^{-}$ and mature $CCR7^{+}$ developmental stages.

Studies in a monoclonal thymocyte repertoire

This study provides evidence that $MHCII^{+}$ BM-APCs are required to mediate strongly TCR-signalled $Helios^{+}$ $CCR7^{-}$ wave 1 negative selection in monoclonal and polyclonal thymocyte repertoires. In the insHEL x 3A9 and thyroHEL x 3A9 transgenic models, the HEL self-antigens are not derived from the BM-APCs, but rely on an antigen handover mechanism to induce negative selection (Fig. 6.1). Introducing a defect in BM-APCs changes thymocyte fate, by abolishing clonal deletion altogether in insHEL, or by shifting clonal deletion from the $CCR7^{-}$ to the $CCR7^{+}$ stage in thyroHEL. These findings

highlight the crucial role of MHCII$^+$ BM-APCs in mediating stringent wave 1 negative selection.

The role of an antigen handover mechanism in mediating negative selection has recently been appreciated, although this study did not define the stage at which antigen handover leads to clonal deletion (Perry et al., 2014). It remains unclear why self-antigens that are expressed by mTECs are required to be presented by BM-APCs, but Klein et al. (2014) proposed that antigen handover mechanisms to adjacent BM-APCs may increase the antigen presentation area in a mosaic fashion, in which antigen presentation by mTECs alone could not perform. Alternatively, this present study hypotheses that antigen handover mechanism may serve as a back-up mechanism to induce central tolerance if antigen expressing-mTECs are defective in antigen presentation. This speculation is based on the case of thyroHEL in which central tolerance can be established by the antigen expressing-mTECs, although tolerance appears more robust when the antigen handover mechanism is functional.

Defective antigen handover can change the strength of TCR signalling, the maturation stage at which thymocytes encounter self-antigens and the fate of thymocytes. Defective antigen handover abrogates negative selection altogether in insHEL, causing the strongly TCR-signalled thymocytes to be weakly TCR-signalled and positively selected into Helios$^-$ CCR7$^+$ or CD4SP naïve T cells. Defective antigen handover shifts negative selection from wave 1 CCR7$^-$ stage towards wave 2 CCR7$^+$ stage in thyroHEL, whereby thymocytes are able to mature into CCR7$^+$ thymocytes and upregulate OX40, a hallmark of wave 2 negative selection (Daley et al., 2013). This is accompanied by an increase in FoxP3$^+$ T-reg differentiation in the thyroHEL, instead of being deleted at wave 1.

The change of thymocyte fate from wave 1 negative selection to wave 2 FoxP3$^+$ T-reg differentiation in thyroHEL when antigen handover mechanism is defective is consistent with evidence that T-reg selection occurs at wave 2 (Hu et al., 2016). FoxP3$^+$ T-regs were known to express high levels of Helios (Thornton et al., 2010). The thymic medulla is necessary to support FoxP3$^+$ CD25$^+$ CCR7$^+$ T-reg differentiation (Cowan et al., 2015; Hsieh et al., 2012). The facilitation of T-reg selection in medullary wave 2 negative selection may be due to the importance of NF-κB transcription factor (RELB) in supporting mTEC differentiation as the absence of RELB impairs thymic T-reg selection (Cowan et al., 2013). The RELB-mediating mTEC differentiation allows the mTECs to express and present diverse TSAs that are dependent on Aire or Fezf2 (Takaba et al., 2015), providing a diverse array of self-antigens to induce T-reg

differentiation at the CCR7^{+} stage.

The partial impairment of clonal deletion accompanied by an increase in T-reg differentiation in thyroHEL has been observed in an *Ins2*^{eGFP} model (Malhotra et al., 2016). The authors associate low thymic expression of self-antigens with partial clonal deletion and enhanced T-reg differentiation as a mechanism to establish polyclonal CD4^{+} T central tolerance (Malhotra et al., 2016). This study provides the new insight that partial impairment of clonal deletion accompanied by enhancement of T-reg differentiation could also be attributed to the maturation stages in which thymocytes encounter self-antigens. These observations also highlight how the immune system evolved to maintain central tolerance by enhancing the T-reg selection when clonal deletion is incomplete.

The 3A9 transgenic/HEL system shows that the antigen handover mechanism for antigen presentation is effective at inducing central tolerance in a large number of thymocytes. The mechanism may be even more efficient in a physiological setting with natural thymocyte and self-antigen repertoires. In the thymus, lowering the number of TCR^{3A9} thymocytes increases Helios induction in the remaining TCR^{3A9} thymocytes by the insHEL antigen (Daley et al., 2013). This suggests that the antigen handover mechanism is partially overwhelmed by the high number of self-reactive thymocytes in the 3A9 transgenic/HEL system. Thus, the antigen handover mechanism could be even more effective at inducing central tolerance in physiological settings.

Studies in the polyclonal thymocyte repertoire

MHCII-deficiency within BM-APCs leads to ~42% reduction in negative selection at wave 1, based on Helios^{+} CCR7^{-} approach, analysed on a synchronised cohort of nascent thymocytes. DCs play a role in cortical clonal deletion as thymocytes are arrested and signalled adjacent to DCs *in situ* even when the antigen is also available to cTECs (Melichar et al., 2013). A more efficient endocytic pathway in DCs compared to cTECs might explain this difference. cTECs are five times less efficient than DCs at presenting peptide to T hybridoma cells, and are >100 times less efficient than DCs at processing a protein into peptide and presenting it to T hybridomas (Klein et al., 2001). Immunofluoresent microscopy observations show that apoptotic HY^{cd4} DP thymocytes tend to be associated with DCs in the thymic cortex despite the cTECs also expressing the relevant self-antigen (McCaughtry et al., 2008). The frequency of apoptotic DP thymocytes was reduced when CD11c^{+} DCs were absent (McCaughtry et al., 2008). It is interesting that DCs play an essential role in wave 1 negative selection, considering

the low abundance DCs (or BM-derived cells) within the thymic cortex (Barclay and Mayrhofer, 1981; Le Borgne et al., 2009; McCaughtry et al., 2008) compared to the thymic medulla. It is noteworthy that ~50% of wave 1 cells does not require the well-described negative selecting APC types, $MHCII^+$ BM-APCs or Aire. cTECs may directly present self-antigen to mediate wave 1 deletion (Fig. 6.1) as K14-driven HYp expression (only expressed in cTECs) was sufficient to induce coreceptor dulling and PD-1 expression, hallmarks of wave 1 negative selection, in HY^{cd4} thymocytes (McCaughtry et al., 2008). Therefore, the data suggest that the traditional view that cTECs are ineffective at inducing negative selection should perhaps be revisited. Furthermore, two photon imaging on thymic slice revealed that direct presentation of self-antigen OVA by OT-I Tg thymocytes to OT-I Tg DP thymocytes in the thymc cortex resulted in strong TCR signaling (increased and persistant $Ca2^+$ signaling) (Melichar et al., 2015). This indicates that B2m-dependent direct presentation by thymocytes themselves to other thymocytes could induce negative selection at DP stage (Fig. 6.1) (Melichar et al., 2015).

Apoptosis-defective mice (i.e. *Bcl-2* Tg or $Bim^{-/-}$) are useful in enumerating the strongly TCR-signalled negatively selected thymocytes. Defective apoptosis prolongs the survival of strongly TCR-signalled cells that would otherwise have been phagocytosed rapidly by macrophages (Dzhagalov et al., 2013) or died. Nevertheless, one potential limitation of using apoptosis defective mice is that the presence of undeleted thymocytes could interfere with the access of newly formed thymocytes to the APC network. Due to increased competition from “undeleted” thymocytes, assays that use apoptosis-defective mice might underestimate the true scale of negative selection (and positive selection).

6.4 Preliminary evidence: Requirement for Aire in wave 2 negative selection

This present study reveals that Aire plays a role in wave 2 ($Helios^+$ $CCR7^+$) negative selection as evident by the ~50% reduction in wave 2 polyclonal thymocytes in the absence of Aire. This is consistent with the requirement for Aire in mediating the negative selection (clonal deletion) of self-reactive CD4SP monoclonal thymocytes in RIP-mOVA and insHEL models (Anderson et al., 2005; Liston et al., 2003). Aire is important in ectopic expression of TSAs in mTECs (Anderson et al., 2002), which suggests that the $Aire^+$ mTECs, serving as a thymic APC, have a role in mediating wave 2 negative selection. However, a previous study based on the deletion of Aire-dependent IRBP-specific CD4SP polyclonal thymocytes suggests that Aire-dependent

deletion not only relies on the role of Aire in TSA expression in the mTECs, but also requires antigen handover to BM-APCs to induce negative selection (Taniguchi et al., 2012). Similarly, another study shows that although that Aire is not required for transcription of RIP-OVA^{hi} in mTECs, Aire is required for RIP-OVA^{hi}-dependent deletion of OT-II CD4SP thymocytes (Hubert et al., 2011). The authors concluded that Aire is required to regulate the transfer of self-antigen from mTECs to DCs to induce central tolerance.

Several other functions of Aire in the thymic medulla, in addition to its promotion of TSA expression in mTECs, are reviewed (Anderson and Su, 2016). For instance, Aire may regulate T cell negative selection by a TSA-independent mechanism since the transcript levels of membrane-bound OVA neo-self-antigen are barely affected in the absence of Aire, although deletion of OT-II thymocytes is Aire-dependent (Anderson et al., 2005). Aire may also enhance self-tolerance by promoting apoptosis of mTECs as Aire-deficiency results in an increase in MHCII^{hi} mTEC number, potentially promoting cross presentation and phagocytosis of the TSAs by thymic APCs (Gray et al., 2007). Aire has a role in proper localisation or migration of BM-APCs in the thymic medulla (Lei et al., 2011). Aire has been reported to maintain thymic organisation and mTEC morphology as Aire-deficiency alters the complexity of cell shape in mTECs and their distribution (Yano et al., 2008), and has role in late-stage of mTEC differentiation (Wang et al., 2012).

Aire also has a role in regulating non-mTECs. Aire-expressing thymic B cells are reported to have an immunoregulatory function in promoting central tolerance (Yamano et al., 2015). This present study did not measure FoxP3^{+} Helios^{+} CCR7^{+} thymic T-regs in the absence of Aire, as the day 3 post-EdU time point may have been early to detect wave 2 T-reg thymocytes. But, it is possible that Aire plays a role in promoting thymic T-reg differentiation. This is because Aire-deficiency decreases the number of CD4^{+} T-reg cells in neonatal mice (Yang et al., 2015) and decreases the Aire-dependent prostate-antigen specific thymic T-regs in adult mice (Malchow et al., 2013). Also, low abundance T-reg clones are reported to be more Aire-dependent than the high abundance T-reg clones (Perry et al., 2014). Recently, Aire has been suggested to prevent autoimmunity by directing self-reactive cells into the T-reg cell lineage, as the conventional T cell TCR clonotypes infiltrating target lesions in the periphery of *Aire*$^{-/-}$ mice are found to be the same TCR clonotypes expressed in FoxP3^{+} T-reg cells in *Aire*$^{+/+}$ mice (Malchow et al., 2016). All these functions of Aire may explain its role in wave 2 negative selection.

6.5 Contributions of MHC molecules to T cell signalling provide preliminary support for the interclonal competition hypothesis

After discussing the cellular interaction between thymic APCs and thymocytes, this section emphasises the contribution of MHC molecules to thymic selection. The EdU^+ $TCR\beta^+CD5^+$ analytical approach was used to quantify all TCR-signalled cells (strong or weak) in nascent thymocyte cohorts. $TCR\beta^+CD5^+$ thymocyte formation relies on MHC-dependent mechanisms. In apoptosis-defective mice, MHCI induces TCR signalling in a similar fraction of thymocytes as MHCII. However, both wave 1 analytical approaches: (1) $Helios^+$ $CCR7^-$ and (2) $CD4^{lo}CD8^{lo}$ $PD\text{-}1^{hi}$ iIEL thymic precursors, find that induction of strongly TCR-signalled thymocytes at the $CCR7^-$ stage is more dependent on MHCII than MHCI, in apoptosis-defective mice.

A previous study proposed the existence of intraclonal competition for peptide-MHC complexes to explain the correlation between the low clonal frequency and high efficiency of thymic T-reg selection in mice (Bautista et al., 2009). This present study provides a new but preliminary concept regarding interclonal competition between MHCI-responsive and MHCII-responsive thymocytes, to explain why the combined fractions of TCR-signalled cells induced by MHCI (in MHCII-deficient mice) and by MHCII (in MHCI-deficient mice) are not equal to, but 35% greater than the fraction of TCR-signalled cells induced in wild-type mice. This unequal sum of TCR-signalled thymocytes induced by MHCI and by MHCII is similar to Sinclair et al.'s (2013) observation in TetZap70 mice. The evidence for interclonal competition stems from the enrichment of certain TRAV segments in single MHC-deficient mice in comparison to wild-type mice. For instance, MHCI-responsive thymocytes may have less competition for MHCI molecules on APCs in MHCII-deficient mice, compared to the higher competition between MHCI-responsive and MHCII-responsive thymocytes for MHCI molecules on APCs in wild-type mice. Future experiment could be performed to verify this finding by transferring carboxyfluorescein succinimidyl ester (CFSE)-labelled MHCI-restricted OT-I Tg (CD45.1) and cell trace violet (CTV)-labelled MHCII-restricted OT-II Tg thymocytes (CD45.1), via intrathymic injection, into mice (CD45.2) with either both MHC classes or with a single MHC class. Positive selection of $CFSE^+$ OT-I Tg T cells in the presence of both MHC classes could be compared to positive selection of $CFSE^+$ OT-I Tg T cells in the absence of a single MHC class (MHCII-deficient mice). Similarly, positive selection of CTV^+ OT-II Tg T cells in the presence of both MHC classes could be compared to positive selection of CTV^+ OT-II Tg T cells in the absence of a single MHC class (MHCI-deficient). If the hypothesis is correct, more $CFSE^+$ OT-I or CTV^+ OT-II Tg thymocytes will be found to undergo positive selection in

MHCII-deficient mice and MHCI-deficient mice, respectively, compared to wild-type mice.

6.6 The $CD4^{lo}CD8^{lo}$ PD-1^{hi} $CCR7^{-}$ TCR repertoire appears to be enriched in TCRs that recognise B2m-dependent ligands

In the periphery, there is a requirement for B2m-dependent classical K^b or D^b (polymorphic) and/or non-classical (non-polymorphic) MHCI molecules in iIEL development (Das et al., 2000; Fujiura et al., 1996; Gapin et al., 1999; Leishman et al., 2002; Mayans et al., 2014; Park et al., 1999; Pobezinsky et al., 2012). A recent study revealed IEL TCRs can recognise classical MHCI or as yet uncharacterised B2m-dependent ligand(s) (Mayans et al., 2014). Some iIEL-inducing ligands are TAP-independent, indicating that iIELs recognise antigens that are distinct from the MHCI-restricted conventional $CD8^+$ T cells (Fujiura et al., 1996; Mayans et al., 2014; Park et al., 1999).

In the thymus, this present study demonstrates that the development of $CD4^{lo}CD8^{lo}$ PD-1^{hi} iIEL thymic precursors in apoptosis-defective mice is MHC-dependent. Substantial $CD4^{lo}CD8^{lo}$ PD-1^{hi} iIEL populations were detectable in apoptosis-defective mice lacking one MHC class, indicating that either MHCI or MHCII is sufficient for the induction of these cells. The BM chimera experiments reported above demonstrate a role for $MHCII^+$ BM-APCs in inducing $CD4^{lo}CD8^{lo}$ PD-1^{hi} iIEL thymic precursors in apoptosis-defective mice with or without B2m expression in the thymic epithelium. Although apoptosis defects "artificially" expand the $CD4^{lo}CD8^{lo}$ PD-1^{hi} population, this enables the capacity of the APC network to induce these cells to be measured. The data show that MHCII expression on BM-APCs is required for the normal induction of $CD4^{lo}CD8^{lo}$ PD-1^{hi} iIEL thymic precursors.

Despite the ability of $CD4^{lo}CD8^{lo}$ PD-1^{hi} iIEL thymic precursors to recognise B2m- and/or MHCII-dependent ligands, this present study provides new insight that $CD4^{lo}CD8^{lo}$ PD-1^{hi} $CCR7^{-}$ iIEL thymic precursors are enriched for B2m-dependent ligands in apoptosis-intact mice (Fig. 6.1). This is evident by the higher TCR overlapping between wild-type mice and *H2-Aa*$^{-/-}$ (TCR signalling induced by MHCI) than the TCR overlapping between the wild-type and *B2m*$^{-/-}$ (TCR signalling induced by MHCII) in the $CD4^{lo}CD8^{lo}$ PD-1^{hi} $CCR7^{-}$ wave 1 subset. It is hypothesised that, within wave 1, MHCII-responsive thymocytes die faster than MHCI-responsive

thymocytes. This can explain why the wave 1 cells that were sorted and sequenced more commonly expressed MHCI-responsive TCRs.

Since *Bcl-2* Tg expression enables more MHCII-responsive $CD4^{lo}CD8^{lo}$ $PD\text{-}1^{hi}$ $CCR7^{-}$ thymocytes to survive long enough to downregulate both coreceptors, the hypothesis that MHCII-responsive iIEL thymic precursors are short-lived could be tested by comparing the sorted $CD4^{lo}CD8^{lo}$ $PD\text{-}1^{hi}$ $CCR7^{-}$ thymocytes in *Bcl-2* Tg $B2m^{-/-}$ mice and *Bcl-2* Tg wild-type mice. If this hypothesis is correct, a higher TCR overlapping between these two groups of mice within $CD4^{lo}CD8^{lo}$ $PD\text{-}1^{hi}$ $CCR7^{-}$ thymocytes would be expected in comparison to non-Tg $B2m^{-/-}$ mice and non-Tg wild-type mice.

6.7 The distinctions between MHC-independent and MHC-dependent αβTCR repertoires

At the TCR clonal level in Yae62β transgenic mice, this present study has shed light on the distinctive characteristics of MHC-independent αβTCRs (derived from mice deficient in both MHC classes) versus MHC-dependent αβTCRs (derived from mice with single or both MHC classes) (Table 6.1). First, the thymic MHC-independent CD4SP and CD8SP TCR repertoires are indistinguishable from each other, as opposed to the highly distinguishable thymic MHC-dependent CD4SP and CD8SP TCR repertoires. This finding supports the theory that coreceptor-independent signalling promotes MHC-independent TCRs, whereas coreceptor-dependent signalling promotes MHC-dependent TCRs (Tikhonova et al., 2012; Van Laethem et al., 2007; Van Laethem et al., 2013). Second, MHC-independent TCRs have a distinctive TRAJ segment usage profile. Third, MHC-independent TCRs are enriched with high hydrophobic amino acids in the CDR3α J subregion, revealing the role of CDR3α, mainly encoded by the J segment, in the development of MHC-independent TCRs.

Among MHC-dependent TCRs, this study shows that the usage of TRAV segments, encoding the CDR1 and CDR2 of TCRα chains, is biased according to the MHC genotypes and cell types (Table 6.1). This suggests that CDR1α and CDR2α impose biases in MHC restriction (MHCI- or MHCII-restriction) and the selection fate of thymocytes (positive or negative selection). These findings support the theory that MHC restriction is imposed by the conserved interaction between the germline-encoded TCR sequences (CDR1 and CDR2 loops) and MHC, thereby eliminating TCRs that are unable to recognise MHC (Feng et al., 2007; Garcia, 2012; Garcia et al.,

2009; Marrack et al., 2008; Scott-Browne et al., 2009). In short, this study supports both MHC restriction theories: (1) the coreceptor-dependent signalling theory and (2) the germline-encoded TCR sequences theory.

Table 6.1 Characteristics of MHC-independent TCR repertoire versus MHC-dependent TCR repertoire

		Cell types	
MHC genotype	**Characteristics**	**Wave 1 negative selection**	**Positive selection (CD4SP and CD8SP)**
MHC-dependent TCRs (wild-type mice)	**Clustering of positively selected SP TCRs**	–	Distinguishable CD4SP and CD8SP TCR repertoires
	TRAV segment usage	Unique enrichment associated with MHC genotypes (wild-type, *B2m*$^{-/-}$ or *H2Aa*$^{-/-}$ mice) and cell types	
	Hydrophobicity within CDR3 J subregion	W1 > CD4SP/CD8SP	
MHC-independent TCRs (*B2m*$^{-/-}$ *H2Aa*$^{-/-}$ mice)	**Clustering of positively selected SP TCRs**	–	Indistinguishable CD4SP and CD8SP TCR repertoires
	TRAJ segment usage	Unique enrichment compared to wild-type, *B2m*$^{-/-}$ or *H2Aa*$^{-/-}$ mice	
	Hydrophobicity within CDR3 J subregion between cell subsets	W1 > CD4SP/CD8SP	
	Hydrophobicity within CDR3 J subregion between MHC genotype	Higher hydrophobicity compared to MHC-dependent TCRs	
	Binding affinity	Higher than MHC-dependent TCRs	

6.8 Remarks on EdU^{+} Helios/CCR7 approach

This study shows that the EdU^{+} Helios/CCR7 approach appears to be a more sensitive approach in detecting thymocytes undergoing wave 1 CCR7^{-} negative selection than the CD4^{lo}CD8^{lo} PD-1^{hi} approach. This is evident by a slight defect (~20%) in wave 1 Helios^{+} CCR7^{-} cells could be detected in Aire-deficiency but no impairment is observed by using a CD4^{lo}CD8^{lo} PD-1^{hi} approach. Similarly, MHCI-deficiency significantly reduces wave 1 Helios^{+} CCR7^{-} thymocytes but it does not reduce CD4^{lo}CD8^{lo} PD-1^{hi} thymocytes. However, this discrepancy could also be due to the fact that the former approach analyses nascent thymocyte cohorts, whereas the latter approach analyses thymocytes in steady state. Ideally, nascent thymocyte cohorts should be analysed with both approaches for an objective comparison of sensitivity in detecting negatively selected thymocytes at the CCR7^{-} stage. Importantly, the two approaches generally produce consistent conclusions. For instance, both clearly demonstrate that MHCII^{+} BM-APCs are required to induce CCR7^{-} wave 1 negative selection.

The potential caveat of analysing EdU^{+} Helios/CCR7 thymocytes on day 3 post-EdU injection is that this time point may not be optimal in detecting wave 2 Helios^{+} CCR7^{+} thymocytes, which peak at day 5, but are detectable between day 4 and day 8 (Hu et al., 2016). However, wave 2 cells could be detected as early as day 3, and a few BrdU^{+} thymocytes were found in the thymic medulla 3 days post injection (Penit, 1986). The fact that Aire deficiency significantly impaired wave 2 thymocytes strongly suggests that wave 2 cells are detectable 3 days post-EdU injection, although it may not be sensitive enough to detect wave 2 cells that are subtly affected due to defective thymic APCs or deficiencies in single MHC class in mice. On the other hand, the inability to detect the impairment of wave 2 cells either by depriving MHCII^{+} BM-APCs or single MHC class, may not exclude the qualitative thymocyte repertoire changes in wave 2 thymocytes. This is because wave 2 thymocytes might be confounded by wave 1 escapees that fail to undergo wave 1 negative selection, upregulate CCR7, and enter wave 2 negative selection. This explanation is evident by the finding in thyroHEL in which MHCII-deficiency within BM-APCs could delay negative selection from wave 1 to wave 2. To overcome this potential caveat, mice could be analysed at day 5 post-EdU injection to confirm the role of MHCII^{+} BM-APCs, MHCI or MHCII in inducing wave 2 negative selection.

6.9 Concluding remarks

This study provides new insights into thymic negative selection mechanisms, especially on the roles of thymic APCs and MHC molecules in mediating thymic negative selection. $MHCII^+$ BM-APCs are required to induce ~42% wave 1 $CCR7^-$ negative selection. Ablation of $MHCII^+$ BM-APCs either abrogated negative selection completely or delayed negative selection from wave 1 to wave 2. Preliminary evidence suggests that Aire induces wave 2 $CCR7^+$ negative selection, suggesting that different APC types are required for thymic negative selection at distinct developmental stages. MHCI induces a similar fraction of TCR-signalled thymocytes as MHCII, but MHCII induces more negative selection, at least as measured by Helios expression. The enrichment of TRAV usage associated with MHC genotypes and cell types provides evidence supporting the interclonal competition hypothesis between MHCI-responsive and MHCII-responsive thymocytes to access limited APCs. TRAV segment usage, encoding CDR1 and CDR2, is sufficient to impose bias in CD4/CD8 lineage commitment and in thymic (positive or negative) selection fate. The $CD4^{lo}CD8^{lo}$ $PD\text{-}1^{hi}$ $CCR7^-$ wave 1 cells, constituting the iIEL thymic precursors, are enriched for B2m-dependent ligands in apoptosis-intact mice. The negatively selected $CD4^{lo}CD8^{lo}$ $PD\text{-}1^{hi}$ $CCR7^-$ wave 1 cells are enriched with hydrophobic amino acids in the CDR3α J subregion. Finally, MHC-independent TCRs are distinct from the MHC-dependent TCRs, in that the former have indistinguishable CD4SP and CD8SP TCR repertoires, use a distinct set of TRAJ segments and are enriched with hydrophobic amino acid residues in the CDR3α J subregion.

References

Ahn, S., Lee, G., Yang, S.J., Lee, D., Lee, S., Shin, H.S., Kim, M.C., Lee, K.N., Palmer, D.C., Theoret, M.R.*, et al.* (2008). TSCOT+ Thymic Epithelial Cell-Mediated Sensitive CD4 Tolerance by Direct Presentation. PLoS Biol *6*, e191.

Aichinger, M., Wu, C., Nedjic, J., and Klein, L. (2013). Macroautophagy substrates are loaded onto MHC class II of medullary thymic epithelial cells for central tolerance. The Journal of Experimental Medicine *210*, 287-300.

Akkaraju, S., Ho, W.Y., Leong, D., Canaan, K., Davis, M.M., and Goodnow, C.C. (1997). A Range of CD4 T Cell Tolerance: Partial Inactivation to Organ-Specific Antigen Allows Nondestructive Thyroiditis or Insulitis. Immunity *7*, 255-271.

Anderson, M.S., and Su, M.A. (2016). AIRE expands: new roles in immune tolerance and beyond. Nat Rev Immunol *16*, 247-258.

Anderson, M.S., Venanzi, E.S., Chen, Z., Berzins, S.P., Benoist, C., and Mathis, D. (2005). The Cellular Mechanism of Aire Control of T Cell Tolerance. Immunity *23*, 227-239.

Anderson, M.S., Venanzi, E.S., Klein, L., Chen, Z., Berzins, S.P., Turley, S.J., von Boehmer, H., Bronson, R., Dierich, A., Benoist, C., and Mathis, D. (2002). Projection of an Immunological Self Shadow Within the Thymus by the Aire Protein. Science *298*, 1395-1401.

Apostolou, I., Sarukhan, A., Klein, L., and von Boehmer, H. (2002). Origin of regulatory T cells with known specificity for antigen. Nature Immunology *3*, 756-763.

Artyomov, M.N., Lis, M., Devadas, S., Davis, M.M., and Chakraborty, A.K. (2010). CD4 and CD8 binding to MHC molecules primarily acts to enhance Lck delivery. Proceedings of the National Academy of Sciences of the United States of America *107*, 16916-16921.

Aschenbrenner, K., D'Cruz, L.M., Vollmann, E.H., Hinterberger, M., Emmerich, J., Swee, L.K., Rolink, A., and Klein, L. (2007). Selection of Foxp3+ regulatory T cells specific for self antigen expressed and presented by Aire+ medullary thymic epithelial cells. Nat Immunol *8*, 351-358.

Atibalentja, D.F., Byersdorfer, C.A., and Unanue, E.R. (2009). Thymus-Blood Protein Interactions Are Highly Effective in Negative Selection and Regulatory T Cell Induction. The Journal of Immunology *183*, 7909-7918.

Attaf, M., Huseby, E., and Sewell, A.K. (2015). αβ T cell receptors as predictors of health and disease. Cell Mol Immunol *12*, 391-399.

Azzam, H.S., Grinberg, A., Lui, K., Shen, H., Shores, E.W., and Love, P.E. (1998). CD5 Expression Is Developmentally Regulated By T Cell Receptor (TCR) Signals and TCR Avidity. The Journal of Experimental Medicine *188*, 2301-2311.

Baba, T., Nakamoto, Y., and Mukaida, N. (2009). Crucial Contribution of Thymic Sirpα+ Conventional Dendritic Cells to Central Tolerance against Blood-Borne Antigens in a CCR2-Dependent Manner. The Journal of Immunology *183*, 3053-3063.

Baldwin, K.K., Trenchak, B.P., Altman, J.D., and Davis3, M.M. (1999). Negative Selection of T Cells Occurs Throughout Thymic Development. The Journal of Immunology *163*, 689-698.

Baldwin, T.A., and Hogquist, K.A. (2007). Transcriptional Analysis of Clonal Deletion In Vivo. The Journal of Immunology *179*, 837.

Baldwin, T.A., Sandau, M.M., Jameson, S.C., and Hogquist, K.A. (2005). The timing of TCR alpha expression critically influences T cell development and selection. J Exp Med *202*, 111-121.

Barclay, A.N., and Mayrhofer, G. (1981). Bone marrow origin of Ia-positive cells in the medulla rat thymus. The Journal of experimental medicine *153*, 1666-1671.

Bautista, J.L., Lio, C.-W.J., Lathrop, S.K., Forbush, K., Liang, Y., Luo, J., Rudensky, A.Y., and Hsieh, C.-S. (2009). Intraclonal competition limits the fate determination of regulatory T cells in the thymus. Nat Immunol *10*, 610-617.

Bentley, D.R., Balasubramanian, S., Swerdlow, H.P., Smith, G.P., Milton, J., Brown, C.G., Hall, K.P., Evers, D.J., Barnes, C.L., Bignell, H.R.*, et al.* (2008). Accurate whole human genome sequencing using reversible terminator chemistry. Nature *456*, 53-59.

Berzins, S.P., McNab, F.W., Jones, C.M., Smyth, M.J., and Godfrey, D.I. (2006). Long-Term Retention of Mature NK1.1+ NKT Cells in the Thymus. The Journal of Immunology *176*, 4059-4065.

Bijlmakers, M.J.E., Neefjes, J.J., Wojcik-Jacobs, E.H.M., and Ploegh, H.L. (1993). The assembly of H2-Kb class I molecules translated in vitro requires oxidized glutathione and peptide. European Journal of Immunology *23*, 1305-1313.

Bill, J., and Palmer, E. (1989). Positive selection of CD4+ T cells mediated by MHC class ll-bearing stromal cell in the thymic cortex. Nature *341*, 649-651.

Bjorkman, P.J., Saper, M.A., Samraoui, B., Bennett, W.S., Strominger, J.L., and Wiley, D.C. (1987). Structure of the human class I histocompatibility antigen, HLA-A2. Nature *329*, 506-512.

Bolotin, D.A., Shugay, M., Mamedov, I.Z., Putintseva, E.V., Turchaninova, M.A., Zvyagin, I.V., Britanova, O.V., and Chudakov, D.M. (2013). MiTCR: software for T-cell receptor sequencing data analysis. Nat Meth *10*, 813-814.

Bonasio, R., Scimone, M.L., Schaerli, P., Grabie, N., Lichtman, A.H., and von Andrian, U.H. (2006). Clonal deletion of thymocytes by circulating dendritic cells homing to the thymus. Nat Immunol *7*, 1092-1100.

Borrego, F., Kabat, J., Kim, D.-K., Lieto, L., Maasho, K., Peña, J., Solana, R., and Coligan, J.E. (2002). Structure and function of major histocompatibility complex (MHC) class I specific receptors expressed on human natural killer (NK) cells. Molecular Immunology *38*, 637-660.

Bosc, N., and Lefranc, M.-P. (2003). The mouse (Mus musculus) T cell receptor alpha (TRA) and delta (TRD) variable genes. Developmental & Comparative Immunology *27*, 465-497.

Bouillet, P., Purton, J.F., Godfrey, D.I., Zhang, L.-C., Coultas, L., Puthalakath, H., Pellegrini, M., Cory, S., Adams, J.M., and Strasser, A. (2002). BH3-only Bcl-2 family

member Bim is required for apoptosis of autoreactive thymocytes. Nature *415*, 922-926.

Bourlat, S.J., Haenel, Q., Finnman, J., and Leray, M. (2016). Preparation of Amplicon Libraries for Metabarcoding of Marine Eukaryotes Using Illumina MiSeq: The Dual-PCR Method. In Marine Genomics: Methods and Protocols, S.J. Bourlat, ed. (New York, NY: Springer New York), pp. 197-207.

Bowlus, C.L., Ahn, J., Chu, T., and Gruen, J.R. (1999). Cloning of a Novel MHC-Encoded Serine Peptidase Highly Expressed by Cortical Epithelial Cells of the Thymus. Cellular Immunology *196*, 80-86.

Brady, H.J., Salomons, G.S., Bobeldijk, R.C., and Berns, A.J. (1996). T cells from baxalpha transgenic mice show accelerated apoptosis in response to stimuli but do not show restored DNA damage-induced cell death in the absence of p53. The EMBO Journal *15*, 1221-1230.

Bridgeman, J.S., Sewell, A.K., Miles, J.J., Price, D.A., and Cole, D.K. (2012). Structural and biophysical determinants of αβ T-cell antigen recognition. Immunology *135*, 9-18.

Brocker, T., Riedinger, M., and Karjalainen, K. (1997). Targeted Expression of Major Histocompatibility Complex (MHC) Class II Molecules Demonstrates that Dendritic Cells Can Induce Negative but Not Positive Selection of Thymocytes In Vivo. The Journal of Experimental Medicine *185*, 541-550.

Brooks, A., Hartley, S., Kjer-Nielsen, L., Perera, J., Goodnow, C.C., Basten, A., and McCluskey, J. (1991). Class II-restricted presentation of an endogenously derived immunodominant T-cell determinant of hen egg lysozyme. Proceedings of the National Academy of Sciences of the United States of America *88*, 3290-3294.

Brownlie, R.J., and Zamoyska, R. (2013). T cell receptor signalling networks: branched, diversified and bounded. Nat Rev Immunol *13*, 257-269.

Buck, S.B., Bradford, J., Gee, K.R., Agnew, B.J., Clarke, S.T., and Salic, A. (2008). Detection of S-phase cell cycle progression using 5-ethynyl-2′- deoxyuridine incorporation with click chemistry, an alternative to using 5-bromo-2′-deoxyuridine antibodies. BioTechniques *44*, 927-929.

Burnet, M. (1959). Auto-immune Disease: I. Modern Immunological Concepts. British Medical Journal *2*, 645-650.

Burnet, M. (1962). Role of the Thymus and Related Organs in Immunity. British Medical Journal *2*, 807-811.

Cabaniols, J.-P., Fazilleau, N., Casrouge, A., Kourilsky, P., and Kanellopoulos, J.M. (2001). Most α/β T Cell Receptor Diversity Is Due to Terminal Deoxynucleotidyl Transferase. The Journal of Experimental Medicine *194*, 1385.

Cheraghali, A.M., Knaus, E.E., and Wiebe, L.I. (1994). Bioavailability and pharmacokinetic parameters for 5-ethyl-2′-deoxyuridine. Antiviral Research *25*, 259-267.

Chu, H.H., Moon, J.J., Kruse, A.C., Pepper, M., and Jenkins, M.K. (2010). Negative selection and peptide chemistry determine the size of naive foreign peptide-MHC class II-specific CD4+ T cell populations. Journal of immunology *185*, 4705-4713.

Colaert, N., Helsens, K., Martens, L., Vandekerckhove, J., and Gevaert, K. (2009). Improved visualization of protein consensus sequences by iceLogo. Nat Meth *6*, 786-787.

Cole, D.K., Pumphrey, N.J., Boulter, J.M., Sami, M., Bell, J.I., Gostick, E., Price, D.A., Gao, G.F., Sewell, A.K., and Jakobsen, B.K. (2007). Human TCR-Binding Affinity is Governed by MHC Class Restriction. The Journal of Immunology *178*, 5727.

Cole, D.K., Yuan, F., Rizkallah, P.J., Miles, J.J., Gostick, E., Price, D.A., Gao, G.F., Jakobsen, B.K., and Sewell, A.K. (2009). Germ Line-governed Recognition of a Cancer Epitope by an Immunodominant Human T-cell Receptor. Journal of Biological Chemistry *284*, 27281-27289.

Cosgrove, D., Chan, S.H., Waltzinger, C., Benoist, C., and Mathis, D. (1992). The thymic compartment responsible for positive selection of CD4+ T cells. Int Immunol *4*, 707-710.

Cosgrove, D., Gray, D., Dierich, A., Kaufman, J., Lemeur, M., Benoist, C., and Mathis, D. (1991). Mice lacking MHC class II molecules. Cell *66*, 1051-1066.

Cowan, J.E., Jenkinson, W.E., and Anderson, G. (2015). Thymus medulla fosters generation of natural Treg cells, invariant γδ T cells, and invariant NKT cells: What we learn from intrathymic migration. European Journal of Immunology *45*, 652-660.

Cowan, Jennifer E., McCarthy, Nicholas I., and Anderson, G. (2016). CCR7 Controls Thymus Recirculation, but Not Production and Emigration, of Foxp3+ T Cells. Cell Reports *14*, 1041-1048.

Cowan, J.E., McCarthy, N.I., Parnell, S.M., White, A.J., Bacon, A., Serge, A., Irla, M., Lane, P.J.L., Jenkinson, E.J., Jenkinson, W.E., and Anderson, G. (2014). Differential Requirement For CCR4 and CCR7 During The Development of Innate and Adaptive αβT-cells In The Adult Thymus. Journal of immunology (Baltimore, Md. : 1950) *193*, 1204-1212.

Cowan, J.E., Parnell, S.M., Nakamura, K., Caamano, J.H., Lane, P.J.L., Jenkinson, E.J., Jenkinson, W.E., and Anderson, G. (2013). The thymic medulla is required for Foxp3+ regulatory but not conventional CD4+ thymocyte development. The Journal of Experimental Medicine *210*, 675-681.

Cozzo Picca, C., Oh, S., Panarey, L., Aitken, M., Basehoar, A., and Caton, A.J. (2009). Thymocyte deletion can bias Treg formation toward low-abundance self-peptide. European Journal of Immunology *39*, 3301-3306.

Daley, S.R., Hu, D.Y., and Goodnow, C.C. (2013). Helios marks strongly autoreactive CD4+ T cells in two major waves of thymic deletion distinguished by induction of PD-1 or NF-κB. The Journal of Experimental Medicine.

Daley, S.R., Teh, C., Hu, D.Y., Strasser, A., and Gray, D.H.D. (2017). Cell death and thymic tolerance. Immunological Reviews *277*, 9-20.

Daniels, M.A., Teixeiro, E., Gill, J., Hausmann, B., Roubaty, D., Holmberg, K., Werlen, G., Hollander, G.A., Gascoigne, N.R.J., and Palmer, E. (2006). Thymic selection threshold defined by compartmentalization of Ras/MAPK signalling. Nature *444*, 724-729.

Das, G., Gould, D.S., Augustine, M.M., Fragoso, G., Scitto, E., Stroynowski, I., Van Kaer, L., Schust, D.J., Ploegh, H., and Janeway, C.A. (2000). Qa-2–Dependent

Selection of Cd8α/α T Cell Receptor α/β(+) Cells in Murine Intestinal Intraepithelial Lymphocytes. The Journal of Experimental Medicine *192*, 1521-1528.

Dash, P., McClaren, J.L., Oguin, T.H., Rothwell, W., Todd, B., Morris, M.Y., Becksfort, J., Reynolds, C., Brown, S.A., Doherty, P.C., and Thomas, P.G. (2011). Paired analysis of TCRα and TCRβ chains at the single-cell level in mice. The Journal of Clinical Investigation *121*, 288-295.

Davis, M.M., and Bjorkman, P.J. (1988). T-cell antigen receptor genes and T-cell recognition. Nature *334*, 395-402.

de Boer, J., Williams, A., Skavdis, G., Harker, N., Coles, M., Tolaini, M., Norton, T., Williams, K., Roderick, K., Potocnik, A.J., and Kioussis, D. (2003). Transgenic mice with hematopoietic and lymphoid specific expression of Cre. European Journal of Immunology *33*, 314-325.

Dengjel, J., Schoor, O., Fischer, R., Reich, M., Kraus, M., Müller, M., Kreymborg, K., Altenberend, F., Brandenburg, J., Kalbacher, H.*, et al.* (2005). Autophagy promotes MHC class II presentation of peptides from intracellular source proteins. Proceedings of the National Academy of Sciences *102*, 7922-7927.

Derbinski, J., Gäbler, J., Brors, B., Tierling, S., Jonnakuty, S., Hergenhahn, M., Peltonen, L., Walter, J., and Kyewski, B. (2005). Promiscuous gene expression in thymic epithelial cells is regulated at multiple levels. The Journal of Experimental Medicine *202*, 33-45.

Derbinski, J., Schulte, A., Kyewski, B., and Klein, L. (2001). Promiscuous gene expression in medullary thymic epithelial cells mirrors the peripheral self. Nat Immunol *2*, 1032-1039.

Doyle, C., and Strominger, J.L. (1987). Interaction between CD4 and class II MHC molecules mediates cell adhesion. Nature *330*, 256-259.

Dunker, A.K., Silman, I., Uversky, V.N., and Sussman, J.L. (2008). Function and structure of inherently disordered proteins. Current Opinion in Structural Biology *18*, 756-764.

Dzhagalov, I.L., Chen, K.G., Herzmark, P., and Robey, E.A. (2013). Elimination of Self-Reactive T Cells in the Thymus: A Timeline for Negative Selection. PLoS Biol *11*, e1001566.

Egerton, M., Scollay, R., and Shortman, K. (1990). Kinetics of mature T-cell development in the thymus. Proceedings of the National Academy of Sciences of the United States of America *87*, 2579-2582.

Ehrlich, L.I.R., Oh, D.Y., Weissman, I.L., and Lewis, R.S. (2009). Differential Contribution of Chemotaxis and Substrate Restriction to Segregation of Immature and Mature Thymocytes. Immunity *31*, 986-998.

Feng, D., Bond, C.J., Ely, L.K., Maynard, J., and Garcia, K.C. (2007). Structural evidence for a germline-encoded T cell receptor-major histocompatibility complex interaction 'codon'. Nat Immunol *8*, 975-983.

Fernandes-Alnemri, T., Litwack, G., and Alnemri, E.S. (1994). CPP32, a novel human apoptotic protein with homology to Caenorhabditis elegans cell death protein Ced-3 and mammalian interleukin-1 beta-converting enzyme. Journal of Biological Chemistry *269*, 30761-30764.

Florea, B.I., Verdoes, M., Li, N., Van Der Linden, W.A., Geurink, P.P., Van Den Elst, H., Hofmann, T., De Ru, A., Van Veelen, P.A., Tanaka, K.*, et al.* (2010). Activity-based profiling reveals reactivity of the murine thymoproteasome-specific subunit β5t. Chemistry and Biology *17*, 795-801.

Fujiura, Y., Kawaguchi, M., Kondo, Y., Obana, S., Yamamoto, H., Nanno, M., and Ishikawa, H. (1996). Development of CD8 alpha alpha+ intestinal intraepithelial T cells in beta 2-microglobulin- and/or TAP1-deficient mice. The Journal of Immunology *156*, 2710-2715.

Gallegos, A.M., and Bevan, M.J. (2004). Central Tolerance to Tissue-specific Antigens Mediated by Direct and Indirect Antigen Presentation. The Journal of Experimental Medicine *200*, 1039-1049.

Gangadharan, D., Lambolez, F., Attinger, A., Wang-Zhu, Y., Sullivan, B.A., and Cheroutre, H. (2006). Identification of Pre- and Postselection TCRαβ+ Intraepithelial Lymphocyte Precursors in the Thymus. Immunity *25*, 631-641.

Gapin, L., Cheroutre, H., and Kronenberg, M. (1999). Cutting Edge: TCRαβ+ CD8αα+ T Cells Are Found in Intestinal Intraepithelial Lymphocytes of Mice That Lack Classical MHC Class I Molecules. The Journal of Immunology *163*, 4100-4104.

Garcia, K.C. (2012). Reconciling views on T cell receptor germline bias for MHC. Trends in immunology *33*, 429-436.

Garcia, K.C., Adams, J.J., Feng, D., and Ely, L.K. (2009). The molecular basis of TCR germline bias for MHC is surprisingly simple. Nat Immunol *10*, 143-147.

Genolet, R., Stevenson, B.J., Farinelli, L., Østerås, M., and Luescher, I.F. (2012). Highly diverse TCRα chain repertoire of pre-immune CD8+ T cells reveals new insights in gene recombination. The EMBO Journal *31*, 1666.

Germain, R.N. (2002). T-cell development and the CD4-CD8 lineage decision. Nat Rev Immunol *2*, 309-322.

Gherardin, Nicholas A., Keller, Andrew N., Woolley, Rachel E., Le Nours, J., Ritchie, David S., Neeson, Paul J., Birkinshaw, Richard W., Eckle, Sidonia B.G., Waddington, John N., Liu, L.*, et al.* (2016). Diversity of T Cells Restricted by the MHC Class I-Related Molecule MR1 Facilitates Differential Antigen Recognition. Immunity *44*, 32-45.

Godfrey, D.I., Kennedy, J., Suda, T., and Zlotnik, A. (1993). A Developmental Pathway Involving Four Phenotypically and Functionally Distinct Subsets of CD3-CD4-CD8- Triple-Negative Adult Mouse Thymocytes Defined by CD44 and CD25 Expression. Journal of immunology *150*, 4244-4252.

Godfrey, D.I., MacDonald, H.R., Kronenberg, M., Smyth, M.J., and Kaer, L.V. (2004). NKT cells: what's in a name? Nat Rev Immunol *4*, 231-237.

Godfrey, D.I., Stankovic, S., and Baxter, A.G. (2010). Raising the NKT cell family. Nat Immunol *11*, 197-206.

Gommeaux, J., Grégoire, C., Nguessan, P., Richelme, M., Malissen, M., Guerder, S., Malissen, B., and Carrier, A. (2009). Thymus-specific serine protease regulates positive selection of a subset of CD4+ thymocytes. European Journal of Immunology *39*, 956-964.

Gotter, J., Brors, B., Hergenhahn, M., and Kyewski, B. (2004). Medullary Epithelial Cells of the Human Thymus Express a Highly Diverse Selection of Tissue-specific Genes Colocalized in Chromosomal Clusters. The Journal of Experimental Medicine *199*, 155-166.

Gottschalk, R.A., Corse, E., and Allison, J.P. (2012). Expression of Helios in Peripherally Induced Foxp3+ Regulatory T Cells. The Journal of Immunology *188*, 976.

Gratzner, H.G. (1982). Monoclonal antibody to 5-bromo- and 5-iododeoxyuridine: A new reagent for detection of DNA replication. Science *218*, 474.

Gray, D., Abramson, J., Benoist, C., and Mathis, D. (2007). Proliferative arrest and rapid turnover of thymic epithelial cells expressing Aire. The Journal of Experimental Medicine *204*, 2521.

Gray, D.H.D., Chidgey, A.P., and Boyd, R.L. (2002). Analysis of thymic stromal cell populations using flow cytometry. Journal of Immunological Methods *260*, 15-28.

Grusby, M.J., Johnson, R.S., Papaioannou, V.E., and Glimcher, L.H. (1991). Depletion of CD4+ T cells in major histocompatibility complex class II-deficient mice. Science *253*, 1417-1420.

Guidos, C.J., Danska, J.S., Fathman, C.G., and Weissman, I.L. (1990). T cell receptor-mediated negative selection of autoreactive T lymphocyte precursors occurs after commitment to the CD4 or CD8 lineages. The Journal of Experimental Medicine *172*, 835.

Hadeiba, H., Lahl, K., Edalati, A., Oderup, C., Habtezion, A., Pachynski, R., Nguyen, L., Ghodsi, A., Adler, S., and Butcher, Eugene C. (2012). Plasmacytoid Dendritic Cells Transport Peripheral Antigens to the Thymus to Promote Central Tolerance. Immunity *36*, 438-450.

Hale, J.S., and Fink, P.J. (2010). T-cell receptor revision: friend or foe? Immunology *129*, 467-473.

Hansen, J.C., Lu, X., Ross, E.D., and Woody, R.W. (2006). Intrinsic Protein Disorder, Amino Acid Composition, and Histone Terminal Domains. Journal of Biological Chemistry *281*, 1853-1856.

Hayday, A.C., and Pennington, D.J. (2007). Key factors in the organized chaos of early T cell development. Nat Immunol *8*, 137-144.

Heino, M., Peterson, P., Kudoh, J., Nagamine, K., Lagerstedt, A., Ovod, V., Ranki, A., Rantala, I., Nieminen, M., Tuukkanen, J.*, et al.* (1999). Autoimmune Regulator Is Expressed in the Cells Regulating Immune Tolerance in Thymus Medulla. Biochemical and Biophysical Research Communications *257*, 821-825.

Hernandez, J.B., Newton, R.H., and Walsh, C.M. (2010). Life and death in the thymus—cell death signaling during T cell development. Current Opinion in Cell Biology *22*, 865-871.

Hinterberger, M., Aichinger, M., da Costa, O.P., Voehringer, D., Hoffmann, R., and Klein, L. (2010). Autonomous role of medullary thymic epithelial cells in central CD4+ T cell tolerance. Nat Immunol *11*, 512-519.

Ho, W.Y., Cooke, M.P., Goodnow, C.C., and Davis, M.M. (1994). Resting and anergic B cells are defective in CD28-dependent costimulation of naive CD4+ T cells. The Journal of Experimental Medicine *179*, 1539-1549.

Hoffman, E.S., Passoni, L., Crompton, T., Leu, T.M.J., Schatz, D.G., Koff, A., Owen, M.J., and Hayday, A.C. (1996). Productive T-cell receptor β-chain gene rearrangement: Coincident regulation of cell cycle and clonality during development in vivo. Genes and Development *10*, 948-962.

Hogquist, K.A., Baldwin, T.A., and Jameson, S.C. (2005). Central tolerance: learning self-control in the thymus. Nat Rev Immunol *5*, 772-782.

Holling, T.M., Schooten, E., and van Den Elsen, P.J. (2004). Function and regulation of MHC class II molecules in T-lymphocytes: of mice and men. Human Immunology *65*, 282-290.

Honey, K., Nakagawa, T., Peters, C., and Rudensky, A. (2002). Cathepsin L Regulates CD4+ T Cell Selection Independently of Its Effect on Invariant Chain: A Role in the Generation of Positively Selecting Peptide Ligands. The Journal of Experimental Medicine *195*, 1349-1358.

Hsieh, C.-S., Lee, H.-M., and Lio, C.-W.J. (2012). Selection of regulatory T cells in the thymus. Nat Rev Immunol *12*, 157-167.

Hsieh, C.S., Liang, Y., Tyznik, A.J., Self, S.G., Liggitt, D., and Rudensky, A.Y. (2004). Recognition of the peripheral self by naturally arising CD25+ CD4+ T cell receptors. Immunity *21*, 267-277.

Hu, D.Y., Wirasinha, R.C., Goodnow, C.C., and Daley, S.R. (2017). IL-2 prevents deletion of developing T-regulatory cells in the thymus. Cell Death Differ.

Hu, D.Y., Yap, J.Y., Wirasinha, R.C., Howard, D.R., Goodnow, C.C., and Daley, S.R. (2016). A timeline demarcating two waves of clonal deletion and Foxp3 upregulation during thymocyte development. Immunol Cell Biol *94*, 357-366.

Hubert, F.-X., Kinkel, S.A., Davey, G.M., Phipson, B., Mueller, S.N., Liston, A., Proietto, A.I., Cannon, P.Z.F., Forehan, S., Smyth, G.K.*, et al.* (2011). Aire regulates the transfer of antigen from mTECs to dendritic cells for induction of thymic tolerance. Blood *118*, 2462-2472.

Hubert, F.X., Kinkel, S.A., Webster, K.E., Cannon, P., Crewther, P.E., Proeitto, A.I., Wu, L., Heath, W.R., and Scott, H.S. (2008). A Specific Anti-Aire Antibody Reveals Aire Expression Is Restricted to Medullary Thymic Epithelial Cells and Not Expressed in Periphery. The Journal of Immunology *180*, 3824-3832.

Hughes, E.A., Hammond, C., and Cresswell, P. (1997). Misfolded major histocompatibility complex class I heavy chains are translocated into the cytoplasm and degraded by the proteasome. Proceedings of the National Academy of Sciences *94*, 1896-1901.

Huseby, E.S., Crawford, F., White, J., Kappler, J., and Marrack, P. (2003). Negative selection imparts peptide specificity to the mature T cell repertoire. Proceedings of the National Academy of Sciences *100*, 11565-11570.

Huseby, E.S., White, J., Crawford, F., Vass, T., Becker, D., Pinilla, C., Marrack, P., and Kappler, J.W. (2005). How the T Cell Repertoire Becomes Peptide and MHC Specific. Cell *122*, 247-260.Iserte, J.A., Stephan, B.I., Go, #xf1, i, S.E., Borio, C.S., Ghiringhelli,

P.D., and Lozano, M.E. (2013). Family-Specific Degenerate Primer Design: A Tool to Design Consensus Degenerated Oligonucleotides. Biotechnology Research International *2013*, 9.

Jönsson, P., Southcombe, J.H., Santos, A.M., Huo, J., Fernandes, R.A., McColl, J., Lever, M., Evans, E.J., Hudson, A., Chang, V.T.*, et al.* (2016). Remarkably low affinity of CD4/peptide-major histocompatibility complex class II protein interactions. Proceedings of the National Academy of Sciences *113*, 5682-5687.

Kappler, J.W., Roehm, N., and Marrack, P. (1987). T cell tolerance by clonal elimination in the thymus. Cell *49*, 273-280.

Kawahata, K., Misaki, Y., Yamauchi, M., Tsunekawa, S., Setoguchi, K., Miyazaki, J.-i., and Yamamoto, K. (2002). Generation of CD4+CD25+ Regulatory T Cells from Autoreactive T Cells Simultaneously with Their Negative Selection in the Thymus and from Nonautoreactive T Cells by Endogenous TCR Expression. The Journal of Immunology *168*, 4399.

Kieback, E., Hilgenberg, E., Stervbo, U., Lampropoulou, V., Shen, P., Bunse, M., Jaimes, Y., Boudinot, P., Radbruch, A., Klemm, U.*, et al.* (2016). Thymus-Derived Regulatory T Cells Are Positively Selected on Natural Self-Antigen through Cognate Interactions of High Functional Avidity. Immunity *44*, 1114-1126.

Kishimoto, H., and Sprent, J. (1997). Negative Selection in the Thymus Includes Semimature T Cells. The Journal of Experimental Medicine *185*, 263-272.

Kisielow, P., Bluthmann, H., Staerz, U.D., Steinmetz, M., and von Boehmer, H. (1988). Tolerance in T-cell-receptor transgenic mice involves deletion of nonmature CD4+8+ thymocytes. Nature *333*, 742-746.

Kjer-Nielsen, L., Patel, O., Corbett, A.J., Le Nours, J., Meehan, B., Liu, L., Bhati, M., Chen, Z., Kostenko, L., Reantragoon, R.*, et al.* (2012). MR1 presents microbial vitamin B metabolites to MAIT cells. Nature *491*, 717-723.

Klar, D., and Hämmerling, G.J. (1989). Induction of assembly of MHC class I heavy chains with beta 2microglobulin by interferon-gamma. The EMBO Journal *8*, 475-481.

Klarenbeek, P.L., Doorenspleet, M.E., Esveldt, R.E.E., Van Schaik, B.D.C., Lardy, N., Van Kampen, A.H.C., Tak, P.P., Plenge, R.M., Baas, F., De Bakker, P.I.W., and De Vries, N. (2015). Somatic variation of T-cell receptor genes strongly associate with HLA class restriction. PLoS ONE *10*.

Klein, L., Hinterberger, M., Wirnsberger, G., and Kyewski, B. (2009). Antigen presentation in the thymus for positive selection and central tolerance induction. Nat Rev Immunol *9*, 833-844.

Klein, L., Klugmann, M., Nave, K.-A., Tuohy, V.K., and Kyewski, B. (2000). Shaping of the autoreactive T-cell repertoire by a splice variant of self protein expressed in thymic epithelial cells. Nat Med *6*, 56-61.

Klein, L., Kyewski, B., Allen, P.M., and Hogquist, K.A. (2014). Positive and negative selection of the T cell repertoire: what thymocytes see (and don't see). Nat Rev Immunol *14*, 377-391.

Klein, L., Roettinger, B., and Kyewski, B. (2001). Sampling of complementing self-antigen pools by thymic stromal cells maximizes the scope of central T cell tolerance. European Journal of Immunology *31*, 2476-2486.

Klose, Christoph S.N., Blatz, K., d'Hargues, Y., Hernandez, Pedro P., Kofoed-Nielsen, M., Ripka, Juliane F., Ebert, K., Arnold, Sebastian J., Diefenbach, A., Palmer, E., and Tanriver, Y. (2014). The Transcription Factor T-bet Is Induced by IL-15 and Thymic Agonist Selection and Controls CD8αα+ Intraepithelial Lymphocyte Development. Immunity *41*, 230-243.

Koble, C., and Kyewski, B. (2009). The thymic medulla: a unique microenvironment for intercellular self-antigen transfer. The Journal of Experimental Medicine *206*, 1505-1513.

Kochan, G., Escors, D., Breckpot, K., and Guerrero-Setas, D. (2013). Role of non-classical MHC class I molecules in cancer immunosuppression. OncoImmunology *2*.

Koller, B.H., Marrack, P., Kappler, J.W., and Smithies, O. (1990). Normal development of mice deficient in beta 2M, MHC class I proteins, and CD8+ T cells. Science *248*, 1227-1230.

Kozich, J., Westcott, S.L., Baxter, N.T., Highlander, S.K., and Schloss, P.D. (2013). Development of a dual-index sequencing strategy and curation pipeline for analyzing amplicon sequence data on the miseq illumina sequencing platform. Applied and Environmental Microbiology *79*, 5112-5120.

Kurd, N., and Robey, E.A. (2016). T-cell selection in the thymus: a spatial and temporal perspective. Immunological Reviews *271*, 114-126.

Kurioka, A., Walker, L.J., Klenerman, P., and Willberg, C.B. (2016). MAIT cells: new guardians of the liver. Clin Trans Immunol *5*, e98.

Kurts, C., Kosaka, H., Carbone, F.R., Miller, J.F.A.P., and Heath, W.R. (1997). Class I–restricted Cross-Presentation of Exogenous Self-Antigens Leads to Deletion of Autoreactive CD8+ T Cells. The Journal of Experimental Medicine *186*, 239.

Kwan, J., and Killeen, N. (2004). CCR7 Directs the Migration of Thymocytes into the Thymic Medulla. The Journal of Immunology *172*, 3999-4007.

Kyte, J., and Doolittle, R.F. (1982). A simple method for displaying the hydropathic character of a protein. Journal of Molecular Biology *157*, 105-132.

Ladi, E., Schwickert, T.A., Chtanova, T., Chen, Y., Herzmark, P., Yin, X., Aaron, H., Shiao, W.C., Lipp, M., Roysam, B., and Robey, E.A. (2008). Thymocyte-dendritic cell interactions near sources of CCR7 ligands in the thymic cortex. Journal of immunology *181*, 7014-7023.

Le Borgne, M., Ladi, E., Dzhagalov, I., Herzmark, P., Liao, Y.F., Chakraborty, A.K., and Robey, E.A. (2009). The impact of negative selection on thymocyte migration in the medulla. Nat Immunol *10*, 823-830.

Lee, H.-M., Bautista, Jhoanne L., Scott-Browne, J., Mohan, James F., and Hsieh, C.-S. (2012). A Broad Range of Self-Reactivity Drives Thymic Regulatory T Cell Selection to Limit Responses to Self. Immunity *37*, 475-486.

Lei, Y., Ripen, A.M., Ishimaru, N., Ohigashi, I., Nagasawa, T., Jeker, L.T., Bösl, M.R., Holländer, G.A., Hayashi, Y., de Waal Malefyt, R.*, et al.* (2011). Aire-dependent production of XCL1 mediates medullary accumulation of thymic dendritic cells and contributes to regulatory T cell development. The Journal of Experimental Medicine *208*, 383-394.

Leishman, A.J., Gapin, L., Capone, M., Palmer, E., MacDonald, H.R., Kronenberg, M., and Cheroutre, H. (2002). Precursors of Functional MHC Class I- or Class II-Restricted CD8αα+ T Cells Are Positively Selected in the Thymus by Agonist Self-Peptides. Immunity *16*, 355-364.

Li, M.O., and Rudensky, A.Y. (2016). T cell receptor signalling in the control of regulatory T cell differentiation and function. Nat Rev Immunol *16*, 220-233.

Li, Y., Huang, Y., Lue, J., Quandt, J.A., Martin, R., and Mariuzza, R.A. (2005). Structure of a human autoimmune TCR bound to a myelin basic protein self-peptide and a multiple sclerosis-associated MHC class II molecule. The EMBO Journal *24*, 2968-2979.

Liston, A., Gray, D.H.D., Lesage, S., Fletcher, A.L., Wilson, J., Webster, K.E., Scott, H.S., Boyd, R.L., Peltonen, L., and Goodnow, C.C. (2004a). Gene Dosage-limiting Role of Aire in Thymic Expression, Clonal Deletion, and Organ-specific Autoimmunity. The Journal of Experimental Medicine *200*, 1015-1026.

Liston, A., Lesage, S., Gray, D.H.D., Boyd, R.L., and Goodnow, C.C. (2005). Genetic lesions in T-cell tolerance and thresholds for autoimmunity. Immunological Reviews *204*, 87-101.

Liston, A., Lesage, S., Gray, D.H.D., O'Reilly, L.A., Strasser, A., Fahrer, A.M., Boyd, R.L., Wilson, J., Baxter, A.G., Gallo, E.M.*, et al.* (2004b). Generalized Resistance to Thymic Deletion in the NOD Mouse: A Polygenic Trait Characterized by Defective Induction of Bim. Immunity *21*, 817-830.

Liston, A., Lesage, S., Wilson, J., Peltonen, L., and Goodnow, C.C. (2003). Aire regulates negative selection of organ-specific T cells. Nat Immunol *4*, 350-354.

Liston, A., Nutsch, K.M., Farr, A.G., Lund, J.M., Rasmussen, J.P., Koni, P.A., and Rudensky, A.Y. (2008). Differentiation of regulatory Foxp3+ T cells in the thymic cortex. Proceedings of the National Academy of Sciences *105*, 11903-11908.

Livák, F., Tourigny, M., Schatz, D.G., and Petrie, H.T. (1999). Characterization of TCR Gene Rearrangements During Adult Murine T Cell Development. The Journal of Immunology *162*, 2575.

Loi, M., Müller, A., Steinbach, K., Niven, J., Barreira da Silva, R., Paul, P., Ligeon, L.-A., Caruso, A., Albrecht, Randy A., Becker, Andrea C.*, et al.* (2016). Macroautophagy Proteins Control MHC Class I Levels on Dendritic Cells and Shape Anti-viral CD8+ T Cell Responses. Cell Reports *15*, 1076-1087.

Lucas, B., and Germain, R.N. (1996). Unexpectedly complex regulation of CD4/CD8 coreceptor expression supports a revised model for CD4+CD8+ thymocyte differentiation. Immunity *5*, 461-477.

Lucas, B., Vasseur, F., and Penit, C. (1993). Normal sequence of phenotypic transitions in one cohort of 5-bromo-2'-deoxyuridine-pulse-labeled thymocytes. Correlation with T cell receptor expression. The Journal of Immunology *151*, 4574-4582.

Maddelein, D., Colaert, N., Buchanan, I., Hulstaert, N., Gevaert, K., and Martens, L. (2015). The iceLogo web server and SOAP service for determining protein consensus sequences. Nucleic Acids Research *43*, W543-W546.

Malchow, S., Leventhal, D.S., Lee, V., Nishi, S., Socci, N.D., and Savage, P.A. (2016). Aire Enforces Immune Tolerance by Directing Autoreactive T Cells into the Regulatory T Cell Lineage. Immunity *44*, 1102-1113.

Malchow, S., Leventhal, D.S., Nishi, S., Fischer, B.I., Shen, L., Paner, G.P., Amit, A.S., Kang, C., Geddes, J.E., Allison, J.P.*, et al.* (2013). Aire-Dependent Thymic Development of Tumor-Associated Regulatory T Cells. Science *339*, 1219.

Malhotra, D., Linehan, J.L., Dileepan, T., Lee, Y.J., Purtha, W.E., Lu, J.V., Nelson, R.W., Fife, B.T., Orr, H.T., Anderson, M.S.*, et al.* (2016). Tolerance is established in polyclonal CD4+ T cells by distinct mechanisms, according to self-peptide expression patterns. Nat Immunol *17*, 187-195.

Mandal, M., Borowski, C., Palomero, T., Ferrando, A.A., Oberdoerffer, P., Meng, F., Ruiz-Vela, A., Ciofani, M., Zuniga-Pflucker, J.-C., Screpanti, I.*, et al.* (2005). The BCL2A1 gene as a pre–T cell receptor–induced regulator of thymocyte survival. The Journal of Experimental Medicine *201*, 603-614.

Margulies, D.H. (1997). Interactions of TCRs with MHC-peptide complexes: a quantitative basis for mechanistic models. Current Opinion in Immunology *9*, 390-395.

Marrack, P., Lo, D., Brinster, R., Palmiter, R., Burkly, L., Flavell, R.H., and Kappler, J. (1988). The effect of thymus environment on T cell development and tolerance. Cell *53*, 627-634.

Marrack, P., Scott-Browne, J.P., Dai, S., Gapin, L., and Kappler, J.W. (2008). Evolutionarily conserved amino acids that control TCR-MHC interaction. In Annual Review of Immunology, pp. 171-203.

Masella, A.P., Bartram, A.K., Truszkowski, J.M., Brown, D.G., and Neufeld, J.D. (2012). PANDAseq: paired-end assembler for illumina sequences. BMC Bioinformatics *13*, 1-7.

Mathis, D.J., Benoist, C., Williams 2nd, V.E., Kanter, M., and McDevitt, H.O. (1983). Several mechanisms can account for defective E alpha gene expression in different mouse haplotypes. Proceedings of the National Academy of Sciences of the United States of America *80*, 273-277.

Matiašová, A., Ševc, J., Mikeš, J., Jendželovský, R., Daxnerová, Z., and Fedoročko, P. (2014). Flow cytometric determination of 5-bromo-2'-deoxyuridine pharmacokinetics in blood serum after intraperitoneal administration to rats and mice. Histochemistry and Cell Biology *142*, 703-712.

Matsuda, J.L., Naidenko, O.V., Gapin, L., Nakayama, T., Taniguchi, M., Wang, C.-R., Koezuka, Y., and Kronenberg, M. (2000). Tracking the Response of Natural Killer T Cells to a Glycolipid Antigen Using Cd1d Tetramers. The Journal of Experimental Medicine *192*, 741.

Matsui, K., Boniface, J.J., Reay, P.A., Schild, H., Fazekas de St Groth, B., and Davis, M.M. (1991). Low affinity interaction of peptide-MHC complexes with T cell receptors. Science *254*, 1788.

Matsuyama, M., Wiadrowski, M.N., and Metcalf, D. (1966). Autoradiographic analysis of lymphopoiesis and lymphocyte migration in mice bearing multiple thymus grafts. The Journal of Experimental Medicine *123*, 559.

Mayans, S., Stepniak, D., Palida, Sakina F., Larange, A., Dreux, J., Arlian, Britni M., Shinnakasu, R., Kronenberg, M., Cheroutre, H., and Lambolez, F. (2014). αβT Cell Receptors Expressed by CD4−CD8αβ− Intraepithelial T Cells Drive Their Fate into a Unique Lineage with Unusual MHC Reactivities. Immunity *41*, 207-218.

McBlane, J.F., van Gent, D.C., Ramsden, D.A., Romeo, C., Cuomo, C.A., Gellert, M., and Oettinger, M.A. (1995). Cleavage at a V(D)J recombination signal requires only RAG1 and RAG2 proteins and occurs in two steps. Cell *83*, 387-395.

McCaughtry, T.M., Baldwin, T.A., Wilken, M.S., and Hogquist, K.A. (2008). Clonal deletion of thymocytes can occur in the cortex with no involvement of the medulla. The Journal of Experimental Medicine *205*, 2575-2584.

McCaughtry, T.M., Wilken, M.S., and Hogquist, K.A. (2007). Thymic emigration revisited. The Journal of Experimental Medicine *204*, 2513-2520.

McDonald, Benjamin D., Bunker, Jeffrey J., Erickson, Steven A., Oh-Hora, M., and Bendelac, A. (2015). Crossreactive αβ T Cell Receptors Are the Predominant Targets of Thymocyte Negative Selection. Immunity *43*, 859-869.

McDonald, Benjamin D., Bunker, Jeffrey J., Ishizuka, Isabel E., Jabri, B., and Bendelac, A. (2014). Elevated T Cell Receptor Signaling Identifies a Thymic Precursor to the TCRαβ+CD4−CD8β− Intraepithelial Lymphocyte Lineage. Immunity *41*, 219-229.

McGargill, M.A., and Hogquist, K.A. (1999). Antigen-Induced Coreceptor Down-Regulation on Thymocytes Is Not a Result of Apoptosis. The Journal of Immunology *162*, 1237.

McHugh, R.S., Whitters, M.J., Piccirillo, C.A., Young, D.A., Shevach, E.M., Collins, M., and Byrne, M.C. (2002). CD4+CD25+ Immunoregulatory T Cells: Gene Expression Analysis Reveals a Functional Role for the Glucocorticoid-Induced TNF Receptor. Immunity *16*, 311-323.

McNeil, L.K., Starr, T.K., and Hogquist, K.A. (2005). A requirement for sustained ERK signaling during thymocyte positive selection in vivo. Proceedings of the National Academy of Sciences of the United States of America *102*, 13574-13579.

Melichar, H.J., Ross, J.O., Herzmark, P., Hogquist, K.A., and Robey, E.A. (2013). Distinct Temporal Patterns of T Cell Receptor Signaling During Positive Versus Negative Selection in Situ. Sci. Signal. *6*, ra92-.

Melichar, H.J., Ross, J.O., Taylor, K.T., and Robey, E.A. (2015). Stable Interactions and Sustained TCR Signaling Characterize Thymocyte–Thymocyte Interactions that Support Negative Selection. The Journal of Immunology *194*, 1057-1061.

Merwe, P.A.v.d., and Davis, S.J. (2003). Molecular Interactions Mediating T Cell Antigen Recognition. Annual Review of Immunology *21*, 659-684.

Metzger, Todd C., Khan, Imran S., Gardner, James M., Mouchess, Maria L., Johannes, Kellsey P., Krawisz, Anna K., Skrzypczynska, Katarzyna M., and Anderson, Mark S. (2013). Lineage Tracing and Cell Ablation Identify a Post-Aire-Expressing Thymic Epithelial Cell Population. Cell Reports *5*, 166-179.

Miles, J.J., and Burrows, S.R. (2013). Immune parameters to consider when choosing T-cell receptors for therapy. Frontiers in Immunology *4*.

Miles, J.J., Douek, D.C., and Price, D.A. (2011). Bias in the αβ T-cell repertoire: implications for disease pathogenesis and vaccination. Immunol Cell Biol *89*, 375-387.

Miller, J.F.A.P. (1961). Immunological Function of The Thymus. The Lancet *278*, 748-749.

Millet, V., Naquet, P., and Guinamard, R.R. (2008). Intercellular MHC transfer between thymic epithelial and dendritic cells. European Journal of Immunology *38*, 1257-1263.

Miyazawa, S., and Jernigan, R.L. (1996). Residue – Residue Potentials with a Favorable Contact Pair Term and an Unfavorable High Packing Density Term, for Simulation and Threading. Journal of Molecular Biology *256*, 623-644.

Mizushima, N., Yamamoto, A., Matsui, M., Yoshimori, T., and Ohsumi, Y. (2004). In vivo analysis of autophagy in response to nutrient starvation using transgenic mice expressing a fluorescent autophagosome marker. Mol Biol Cell *15*, 1101-1111.

Mombaerts, P., Iacomini, J., Johnson, R.S., Herrup, K., Tonegawa, S., and Papaioannou, V.E. (1992). RAG-1-deficient mice have no mature B and T lymphocytes. Cell *68*, 869-877.

Moran, A.E., and Hogquist, K.A. (2012). T-cell receptor affinity in thymic development. Immunology *135*, 261-267.

Moran, A.E., Holzapfel, K.L., Xing, Y., Cunningham, N.R., Maltzman, J.S., Punt, J., and Hogquist, K.A. (2011). T cell receptor signal strength in Treg and iNKT cell development demonstrated by a novel fluorescent reporter mouse. J Exp Med *208*, 1279-1289.

Murata, S., Sasaki, K., Kishimoto, T., Niwa, S.-i., Hayashi, H., Takahama, Y., and Tanaka, K. (2007). Regulation of CD8+ T Cell Development by Thymus-Specific Proteasomes. Science *316*, 1349-1353.

Naeher, D., Daniels, M.A., Hausmann, B., Guillaume, P., Luescher, I., and Palmer, E. (2007). A constant affinity threshold for T cell tolerance. The Journal of Experimental Medicine *204*, 2553.

Nakagawa, T., Roth, W., Wong, P., Nelson, A., Farr, A., Deussing, J., Villadangos, J.A., Ploegh, H., Peters, C., and Rudensky, A.Y. (1998). Cathepsin L: Critical Role in Ii Degradation and CD4 T Cell Selection in the Thymus. Science *280*, 450-453.

Napier, R.J., Adams, E.J., Gold, M.C., and Lewinsohn, D.M. (2015). The Role of Mucosal Associated Invariant T Cells in Antimicrobial Immunity. Frontiers in Immunology *6*.

Nedjic, J., Aichinger, M., Emmerich, J., Mizushima, N., and Klein, L. (2008). Autophagy in thymic epithelium shapes the T-cell repertoire and is essential for tolerance. Nature *455*, 396-400.

Nedjic, J., Aichinger, M., Mizushima, N., and Klein, L. (2009). Macroautophagy, endogenous MHC II loading and T cell selection: the benefits of breaking the rules. Current Opinion in Immunology *21*, 92-97.

Neefjes, J., Jongsma, M.L.M., Paul, P., and Bakke, O. (2011). Towards a systems understanding of MHC class I and MHC class II antigen presentation. Nat Rev Immunol *11*, 823-836.

Negishi, I., Motoyama, N., Nakayama, K.-i., Nakayama, K., Senju, S., Hatakeyama, S., Zhang, Q., Chan, A.C., and Loh, D.Y. (1995). Essential role for ZAP-70 in both positive and negative selection of thymocytes. Nature *376*, 435-438.

Nicholson, D.W., Ali, A., Thornberry, N.A., Vaillancourt, J.P., Ding, C.K., Gallant, M., Gareau, Y., Griffin, P.R., Labelle, M., Lazebnik, Y.A.*, et al.* (1995). Identification and inhibition of the ICE/CED-3 protease necessary for mammalian apoptosis. Nature *376*, 37-43.

Norment, A.M., Salter, R.D., Parham, P., Engelhard, V.H., and Littman, D.R. (1988). Cell-cell adhesion mediated by CD8 and MHC class I molecules. Nature *336*, 79-81.

Nossal, G.J.V. (1994). Negative selection of lymphocytes. Cell *76*, 229-239.

Oehen, S., Feng, L., Xia, Y., Surh, C.D., and Hedrick, S.M. (1996). Antigen compartmentation and T helper cell tolerance induction. Journal of Experimental Medicine *183*, 2617-2626.

Ogilvy, S., Metcalf, D., Print, C.G., Bath, M.L., Harris, A.W., and Adams, J.M. (1999). Constitutive Bcl-2 expression throughout the hematopoietic compartment affects multiple lineages and enhances progenitor cell survival. Proceedings of the National Academy of Sciences *96*, 14943-14948.

Oh, J., and Shin, J.-S. (2015). The Role of Dendritic Cells in Central Tolerance. Immune Netw *15*, 111-120.

Ohnmacht, C., Pullner, A., King, S.B.S., Drexler, I., Meier, S., Brocker, T., and Voehringer, D. (2009). Constitutive ablation of dendritic cells breaks self-tolerance of CD4 T cells and results in spontaneous fatal autoimmunity. The Journal of Experimental Medicine *206*, 549-559.

Pacholczyk, R., Ignatowicz, H., Kraj, P., and Ignatowicz, L. (2006). Origin and T Cell Receptor Diversity of Foxp3+CD4+CD25+ T Cells. Immunity *25*, 249-259.

Packard Jr, D.S., Menzies, R.A., and Skalko, R.G. (1973). Incorporation of Thymidine and its Analogue, Bromodeoxyuridine, into Embryos and Maternal Tissues of the Mouse. Differentiation *1*, 397-405.

Page, D.M., Kane, L.P., Allison, J.P., and Hedrick, S.M. (1993). Two signals are required for negative selection of CD4+CD8+ thymocytes. The Journal of Immunology *151*, 1868.
Palmer, E. (2003). Negative selection--clearing out the bad apples from the T-cell repertoire. Nat Rev Immunol *3*, 383-391.

Pannetier, C., Cochet, M., Darche, S., Casrouge, A., Zöller, M., and Kourilsky, P. (1993). The sizes of the CDR3 hypervariable regions of the murine T-cell receptor β chains vary as a function of the recombined germ-line segments. Proceedings of the National Academy of Sciences of the United States of America *90*, 4319-4323.

Park, S.-H., Guy-Grand, D., Lemonnier, F.A., Wang, C.-R., Bendelac, A., and Jabri, B. (1999). Selection and Expansion of CD8α/α+ T Cell Receptor αβ+ Intestinal Intraepithelial Lymphocytes in the Absence of Both Classical Major Histocompatibility Complex Class I and Nonclassical CD1 Molecules. The Journal of Experimental Medicine *190*, 885.

Penit, C. (1986). In vivo thymocyte maturation. BUdR labeling of cycling thymocytes and phenotypic analysis of their progeny support the single lineage model. The Journal of Immunology *137*, 2115-2121.

Penit, C. (1988). Localization and phenotype of cycling and post-cycling murine thymocytes studied by simultaneous detection of bromodeoxyuridine and surface antigens. Journal of Histochemistry & Cytochemistry *36*, 473-478.

Pénit, C., Lucas, B., and Vasseur, F. (1995). Cell expansion and growth arrest phases during the transition from precursor (CD4-8-) to immature (CD4+8+) thymocytes in normal and genetically modified mice. The Journal of Immunology *154*, 5103-5113.

Pénit, C., and Vasseur, F. (1997). Expansion of mature thymocyte subsets before emigration to the periphery. The Journal of Immunology *159*, 4848-4856.

Perry, J.S.A., and Hsieh, C.-S. (2016). Development of T-cell tolerance utilizes both cell-autonomous and cooperative presentation of self-antigen. Immunological Reviews *271*, 141-155.

Perry, Justin S.A., Lio, C.-Wang J., Kau, Andrew L., Nutsch, K., Yang, Z., Gordon, Jeffrey I., Murphy, Kenneth M., and Hsieh, C.-S. (2014). Distinct Contributions of Aire and Antigen-Presenting-Cell Subsets to the Generation of Self-Tolerance in the Thymus. Immunity *41*, 414-426.

Petrie, H.T., Livak, F., Burtrum, D., and Mazel, S. (1995). T cell receptor gene recombination patterns and mechanisms: Cell death, rescue, and T cell production. Journal of Experimental Medicine *182*, 121-127.

Ploegh, H.L., Orr, H.T., and Strominger, J.L. (1981). Major histocompatibility antigens: The human (HLA-A,-B,-C) and murine (H-2K, H-2D) class I molecules. Cell *24*, 287-299.

Pobezinsky, L.A., Angelov, G.S., Tai, X., Jeurling, S., Van Laethem, F., Feigenbaum, L., Park, J.-H., and Singer, A. (2012). Clonal deletion and the fate of autoreactive thymocytes that survive negative selection. Nat Immunol *13*, 569-578.

Pommié, C., Levadoux, S., Sabatier, R., Lefranc, G., and Lefranc, M.P. (2004). IMGT standardized criteria for statistical analysis of immunoglobulin V-Region amino acid properties. Journal of Molecular Recognition *17*, 17-32.

Prinz, I., Sansoni, A., Kissenpfennig, A., Ardouin, L., Malissen, M., and Malissen, B. (2006). Visualization of the earliest steps of γδ T cell development in the adult thymus. Nat Immunol *7*, 995-1003.

Rammensee, H.-G., Friede, T., and Stevanović, S. (1995). MHC ligands and peptide motifs: first listing. Immunogenetics *41*, 178-228.

Raulet, D.H. (1989). The structure, function, and molecular genetics of the γ/δ T cell receptor. Annual Review of Immunology *7*, 175-207.

Raviola, E., and Karnovsky, M.J. (1972). Evidence for A Blood-thymus Barrier Using Electron-opaque Tracers. The Journal of Experimental Medicine *136*, 466-498.

Reinherz, E.L., and Wang, J.-h. (2015). Codification of bidentate pMHC interaction with TCR and co-receptor. Trends in immunology *36*, 300-306.

Reith, W., LeibundGut-Landmann, S., and Waldburger, J.-M. (2005). Regulation of MHC class II gene expression by the class II transactivator. Nat Rev Immunol *5*, 793-806.

Rist, M., Smith, C., Bell, M.J., Burrows, S.R., and Khanna, R. (2009). Cross-recognition of HLA DR4 alloantigen by virus-specific CD8+ T cells: a new paradigm for self-/nonself-recognition. Blood *114*, 2244.

Roche, P.A., and Furuta, K. (2015). The ins and outs of MHC class II-mediated antigen processing and presentation. Nat Rev Immunol *15*, 203-216.

Rossjohn, J., Gras, S., Miles, J.J., Turner, S.J., Godfrey, D.I., and McCluskey, J. (2015). T Cell Antigen Receptor Recognition of Antigen-Presenting Molecules. Annual Review of Immunology *33*, 169-200.

Rowley, J.W., Oler, A.J., Tolley, N.D., Hunter, B.N., Low, E.N., Nix, D.A., Yost, C.C., Zimmerman, G.A., and Weyrich, A.S. (2011). Genome-wide RNA-seq analysis of human and mouse platelet transcriptomes. Blood *118*, e101-e111.

Rudolph, M.G., Stanfield, R.L., and Wilson, I.A. (2006). How TCRs bind MHCs, peptides, and coreceptors. In Annual Review of Immunology, pp. 419-466.

Saini, M., Sinclair, C., Marshall, D., Tolaini, M., Sakaguchi, S., and Seddon, B. (2010). Regulation of Zap70 Expression During Thymocyte Development Enables Temporal Separation of CD4 and CD8 Repertoire Selection at Different Signaling Thresholds. Sci. Signal. *3*, ra23-.

Sakaguchi, S., Sakaguchi, N., Asano, M., Itoh, M., and Toda, M. (1995). Immunologic self-tolerance maintained by activated T cells expressing IL-2 receptor alpha-chains (CD25). Breakdown of a single mechanism of self-tolerance causes various autoimmune diseases. The Journal of Immunology *155*, 1151.

Salic, A., and Mitchison, T.J. (2008). A chemical method for fast and sensitive detection of DNA synthesis in vivo. Proceedings of the National Academy of Sciences *105*, 2415-2420.

Salomon, D.R., Mojcik, C.F., Chang, A.C., Wadsworth, S., Adams, D.H., Coligan, J.E., and Shevach, E.M. (1994). Constitutive activation of integrin alpha 4 beta 1 defines a unique stage of human thymocyte development. The Journal of Experimental Medicine *179*, 1573.

Sansom, S.N., Shikama-Dorn, N., Zhanybekova, S., Nusspaumer, G., Macaulay, I.C., Deadman, M.E., Heger, A., Ponting, C.P., and Holländer, G.A. (2014). Population and single-cell genomics reveal the Aire dependency, relief from Polycomb silencing, and distribution of self-antigen expression in thymic epithelia. Genome Research *24*, 1918-1931.

Sant'Angelo, D.B., Lucas, B., Waterbury, P.G., Cohen, B., Brabb, T., Goverman, J., Germain, R.N., and Janeway Jr, C.A. (1998). A Molecular Map of T Cell Development. Immunity *9*, 179-186.

Schmid, D., Pypaert, M., and Munz, C. (2007). Antigen-loading compartments for major histocompatibility complex class II molecules continuously receive input from autophagosomes. Immunity *26*, 79-92.

Scott-Browne, J.P., White, J., Kappler, J.W., Gapin, L., and Marrack, P. (2009). Germline-encoded amino acids in the αβ T-cell receptor control thymic selection. Nature *458*, 1043-1046.

Sha, W.C., Nelson, C.A., Newberry, R.D., Kranz, D.M., Russell, J.H., and Loh, D.Y. (1988). Positive and negative selection of an antigen receptor on T cells in transgenic mice. Nature *336*, 73-76.

Sharon, E., Sibener, L.V., Battle, A., Fraser, H.B., Garcia, K.C., and Pritchard, J.K. (2016). Genetic variation in MHC proteins is associated with T cell receptor expression biases. Nat Genet *48*, 995-1002.

Shi, Y. (2002). Mechanisms of Caspase Activation and Inhibition during Apoptosis. Molecular Cell *9*, 459-470.

Shimoda, M., Mmanywa, F., Joshi, S.K., Li, T., Miyake, K., Pihkala, J., Abbas, J.A., and Koni, P.A. (2006). Conditional Ablation of MHC-II Suggests an Indirect Role for MHC-II in Regulatory CD4 T Cell Maintenance. The Journal of Immunology *176*, 6503-6511.

Shinkai, Y., Koyasu, S., Nakayama, K., Murphy, K.M., Loh, D.Y., Reinherz, E.L., and Alt, F.W. (1993). Restoration of T cell development in RAG-2-deficient mice by functional TCR transgenes. Science *259*, 822.

Shiow, L.R., Rosen, D.B., Brdickova, N., Xu, Y., An, J., Lanier, L.L., Cyster, J.G., and Matloubian, M. (2006). CD69 acts downstream of interferon-α/β to inhibit S1P1 and lymphocyte egress from lymphoid organs. Nature *440*, 540-544.

Shugay, M., Bagaev, D.V., Turchaninova, M.A., Bolotin, D.A., Britanova, O.V., Putintseva, E.V., Pogorelyy, M.V., Nazarov, V.I., Zvyagin, I.V., Kirgizova, V.I.*, et al.* (2015). VDJtools: Unifying Post-analysis of T Cell Receptor Repertoires. PLoS Comput Biol *11*, e1004503.

Sim, B.-C., Zerva, L., Greene, M.I., and Gascoigne, N.R.J. (1996). Control of MHC Restriction by TCR Vα CDR1 and CDR2. Science *273*, 963.

Simmons, K.B., Wubeshet, M., Ames, K.T., McMahan, C.J., Hale, J.S., and Fink, P.J. (2012). Modulation of TCRβ Surface Expression During TCR Revision. Cellular immunology *272*, 124-129.

Sinclair, C., Bains, I., Yates, A.J., and Seddon, B. (2013). Asymmetric thymocyte death underlies the CD4:CD8 T-cell ratio in the adaptive immune system. Proceedings of the National Academy of Sciences.

Sloan, V.S., Cameron, P., Porter, G., Gammon, M., Amaya, M., Mellins, E., and Zaller, D.M. (1995). Mediation by HLA-DM of dissociation of peptides from HLA-DR. Nature *375*, 802-806.

Stadinski, B.D., Shekhar, K., Gómez-Touriño, I., Jung, J., Sasaki, K., Sewell, A.K., Peakman, M., Chakraborty, A.K., and Huseby, E.S. (2016). Hydrophobic CDR3 residues promote the development of self-reactive T cells. Nature Immunology.

Stadinski, B.D., Trenh, P., Duke, B., Huseby, P.G., Li, G., Stern, L.J., and Huseby, E.S. (2014). Effect of CDR3 Sequences and Distal V Gene Residues in Regulating TCR–MHC Contacts and Ligand Specificity. The Journal of Immunology *192*, 6071-6082.

Stadinski, Brian D., Trenh, P., Smith, Rebecca L., Bautista, B., Huseby, Priya G., Li, G., Stern, Lawrence J., and Huseby, Eric S. (2011). A Role for Differential Variable Gene

Pairing in Creating T Cell Receptors Specific for Unique Major Histocompatibility Ligands. Immunity *35*, 694-704.

Stepanek, O., Prabhakar, Arvind S., Osswald, C., King, Carolyn G., Bulek, A., Naeher, D., Beaufils-Hugot, M., Abanto, Michael L., Galati, V., Hausmann, B.*, et al.* (2014). Coreceptor Scanning by the T Cell Receptor Provides a Mechanism for T Cell Tolerance. Cell *159*, 333-345.

Straus, D.B., and Weiss, A. (1992). Genetic evidence for the involvement of the lck tyrosine kinase in signal transduction through the T cell antigen receptor. Cell *70*, 585-593.

Straus, D.B., and Weiss, A. (1993). The CD3 chains of the T cell antigen receptor associate with the ZAP-70 tyrosine kinase and are tyrosine phosphorylated after receptor stimulation. The Journal of Experimental Medicine *178*, 1523.

Stritesky, G.L., Jameson, S.C., and Hogquist, K.A. (2012). Selection of self-reactive T cells in the thymus. In Annual Review of Immunology, pp. 95-114.

Stritesky, G.L., Xing, Y., Erickson, J.R., Kalekar, L.A., Wang, X., Mueller, D.L., Jameson, S.C., and Hogquist, K.A. (2013). Murine thymic selection quantified using a unique method to capture deleted T cells. Proceedings of the National Academy of Sciences *110*, 4679-4684.

Stumptner-Cuvelette, P., and Benaroch, P. (2002). Multiple roles of the invariant chain in MHC class II function. Biochimica et Biophysica Acta (BBA) - Molecular Cell Research *1542*, 1-13.

Sun, S., Zhang, X., Tough, D.F., and Sprent, J. (1998). Type I Interferon-mediated Stimulation of T Cells by CpG DNA. The Journal of Experimental Medicine *188*, 2335-2342.

Surh, C.D., and Sprent, J. (1994). T-cell apoptosis detected in situ during positive and negative selection in the thymus. Nature *372*, 100-103.

Swat, W., Ignatowicz, L., von Boehmer, H., and Kisielow, P. (1991). Clonal deletion of immature CD4+8+ thymocytes in suspension culture by extrathymic antigen-presenting cells. Nature *351*, 150-153.

Takaba, H., Morishita, Y., Tomofuji, Y., Danks, L., Nitta, T., Komatsu, N., Kodama, T., and Takayanagi, H. (2015). Fezf2 Orchestrates a Thymic Program of Self-Antigen Expression for Immune Tolerance. Cell *163*, 975-987.

Takahama, Y. (2006). Journey through the thymus: stromal guides for T-cell development and selection. Nat Rev Immunol *6*, 127-135.

Takahama, Y., Ohigashi, I., Baik, S., and Anderson, G. (2017). Generation of diversity in thymic epithelial cells. Nat Rev Immunol *17*, 295-305.

Takahashi, T., Tagami, T., Yamazaki, S., Uede, T., Shimizu, J., Sakaguchi, N., Mak, T.W., and Sakaguchi, S. (2000). Immunologic Self-Tolerance Maintained by Cd25+Cd4+ Regulatory T Cells Constitutively Expressing Cytotoxic T Lymphocyte–Associated Antigen 4. The Journal of Experimental Medicine *192*, 303.

Takeda, I., Ine, S., Killeen, N., Ndhlovu, L.C., Murata, K., Satomi, S., Sugamura, K., and Ishii, N. (2004). Distinct Roles for the OX40-OX40 Ligand Interaction in Regulatory and Nonregulatory T Cells. The Journal of Immunology *172*, 3580.

Taniguchi, R.T., DeVoss, J.J., Moon, J.J., Sidney, J., Sette, A., Jenkins, M.K., and Anderson, M.S. (2012). Detection of an autoreactive T-cell population within the polyclonal repertoire that undergoes distinct autoimmune regulator (Aire)-mediated selection. Proceedings of the National Academy of Sciences *109*, 7847-7852.

Taylor, M.J., Husain, K., Gartner, Z.J., Mayor, S., and Vale, R.D. (2017). A DNA-Based T Cell Receptor Reveals a Role for Receptor Clustering in Ligand Discrimination. Cell *169*, 108-119.e120.

Testi, R., Phillips, J.H., and Lanier, L.L. (1989). Leu 23 induction as an early marker of functional CD3/T cell antigen receptor triggering. Requirement for receptor cross-linking, prolonged elevation of intracellular [Ca++] and stimulation of protein kinase C. The Journal of Immunology *142*, 1854-1860.

Thiault, N., Darrigues, J., Adoue, V., Gros, M., Binet, B., Perals, C., Leobon, B., Fazilleau, N., Joffre, O.P., Robey, E.A.*, et al.* (2015). Peripheral regulatory T lymphocytes recirculating to the thymus suppress the development of their precursors. Nat Immunol *16*, 628-634.

Thornton, A.M., Korty, P.E., Tran, D.Q., Wohlfert, E.A., Murray, P.E., Belkaid, Y., and Shevach, E.M. (2010). Expression of Helios, an Ikaros Transcription Factor Family Member, Differentiates Thymic-Derived from Peripherally Induced Foxp3+ T Regulatory Cells. The Journal of Immunology *184*, 3433.

Tikhonova, Anastasia N., Van Laethem, F., Hanada, K.-i., Lu, J., Pobezinsky, Leonid A., Hong, C., Guinter, Terry I., Jeurling, Susanna K., Bernhardt, G., Park, J.-H.*, et al.* (2012). αβ T Cell Receptors that Do Not Undergo Major Histocompatibility Complex-Specific Thymic Selection Possess Antibody-like Recognition Specificities. Immunity *36*, 79-91.

Tomaru, U., Ishizu, A., Murata, S., Miyatake, Y., Suzuki, S., Takahashi, S., Kazamaki, T., Ohara, J., Baba, T., Iwasaki, S.*, et al.* (2009). Exclusive expression of proteasome subunit β5t in the human thymic cortex. Blood *113*, 5186.

Turner, J.M., Brodsky, M.H., Irving, B.A., Levin, S.D., Perlmutter, R.M., and Littman, D.R. (1990). Interaction of the unique N-terminal region of tyrosine kinase p56lck with cytoplasmic domains of CD4 and CD8 is mediated by cysteine motifs. Cell *60*, 755-765.

Ueno, T., Saito, F., Gray, D.H.D., Kuse, S., Hieshima, K., Nakano, H., Kakiuchi, T., Lipp, M., Boyd, R.L., and Takahama, Y. (2004). CCR7 Signals Are Essential for Cortex–Medulla Migration of Developing Thymocytes. The Journal of Experimental Medicine *200*, 493-505.

Uversky, V.N., Gillespie, J.R., and Fink, A.L. (2000). Why are 'natively unfolded' proteins unstructured under physiologic conditions? Proteins: Structure, Function and Genetics *41*, 415-427.

Van Laethem, F., Sarafova, S.D., Park, J.-H., Tai, X., Pobezinsky, L., Guinter, Terry I., Adoro, S., Adams, A., Sharrow, S.O., Feigenbaum, L., and Singer, A. (2007). Deletion of CD4 and CD8 Coreceptors Permits Generation of αβT Cells that Recognize Antigens Independently of the MHC. Immunity *27*, 735-750.

Van Laethem, F., Tikhonova, Anastasia N., Pobezinsky, Leonid A., Tai, X., Kimura, Motoko Y., Le Saout, C., Guinter, Terry I., Adams, A., Sharrow, Susan O., Bernhardt, G.*, et al.* (2013). Lck Availability during Thymic Selection Determines the Recognition Specificity of the T Cell Repertoire. Cell *154*, 1326-1341.

van Meerwijk, J.P.M., Marguerat, S., Lees, R.K., Germain, R.N., Fowlkes, B.J., and MacDonald, H.R. (1997). Quantitative Impact of Thymic Clonal Deletion on the T Cell Repertoire. The Journal of Experimental Medicine *185*, 377-384.

Van Parijs, L., Peterson, D.A., and Abbas, A.K. (1998). RETRACTED: The Fas/Fas Ligand Pathway and Bcl-2 Regulate T Cell Responses to Model Self and Foreign Antigens. Immunity *8*, 265-274.

Vantourout, P., and Hayday, A. (2013). Six-of-the-best: unique contributions of γδ T cells to immunology. Nat Rev Immunol *13*, 88-100.

Vasquez, N.J., Kaye, J., and Hedrick, S.M. (1992). In vivo and in vitro clonal deletion of double-positive thymocytes. The Journal of Experimental Medicine *175*, 1307.

Veillette, A., Bookman, M.A., Horak, E.M., and Bolen, J.B. (1988). The CD4 and CD8 T cell surface antigens are associated with the internal membrane tyrosine-protein kinase p56lck. Cell *55*, 301-308.

Veillette, A., Zúñiga-Pflücker, J.C., Bolen, J.B., and Kruisbeek, A.M. (1989). Engagement of CD4 and CD8 expressed on immature thymocytes induces activation of intracellular tyrosine phosphorylation pathways. The Journal of Experimental Medicine *170*, 1671.

von Boehmer, H. (2004). Selection of the T-Cell Repertoire: Receptor-Controlled Checkpoints in T-Cell Development. In Advances in Immunology (Academic Press), pp. 201-238.

von Boehmer, H. (2005). Unique features of the pre-T-cell receptor [alpha]-chain: not just a surrogate. Nat Rev Immunol *5*, 571-577.

Wang, X., Laan, M., Bichele, R., Kisand, K., Scott, H.S., and Peterson, P. (2012). Post-Aire maturation of thymic medullary epithelial cells involves selective expression of keratinocyte-specific autoantigens. Frontiers in Immunology *3*.

Weathers, E.A., Paulaitis, M.E., Woolf, T.B., and Hoh, J.H. (2004). Reduced amino acid alphabet is sufficient to accurately recognize intrinsically disordered protein. FEBS Letters *576*, 348-352.

Webb, L.V., Ley, S.C., and Seddon, B. (2016). TNF activation of NF-κB is essential for development of single-positive thymocytes. The Journal of Experimental Medicine *213*, 1399.

Williams, O., Norton, T., Halligey, M., Kioussis, D., and Brady, H.J.M. (1998). The Action of Bax and Bcl-2 on T Cell Selection. The Journal of Experimental Medicine *188*, 1125-1133.

Wilson, A., Held, W., and MacDonald, H.R. (1994). Two waves of recombinase gene expression in developing thymocytes. The Journal of Experimental Medicine *179*, 1355.

Wirnsberger, G., Mair, F., Klein, L., and Cantor, H. (2009). Regulatory T Cell Differentiation of Thymocytes Does Not Require a Dedicated Antigen-Presenting Cell but Is under T Cell-Intrinsic Developmental Control. Proceedings of the National Academy of Sciences of the United States of America *106*, 10278-10283.

Wolf, B.B., Schuler, M., Echeverri, F., and Green, D.R. (1999). Caspase-3 Is the Primary Activator of Apoptotic DNA Fragmentation via DNA Fragmentation Factor-

45/Inhibitor of Caspase-activated DNase Inactivation. Journal of Biological Chemistry *274*, 30651-30656.

Wong, J., Obst, R., Correia-Neves, M., Losyev, G., Mathis, D., and Benoist, C. (2007). Adaptation of TCR repertoires to self-peptides in regulatory and nonregulatory CD4+ T cells. Journal of immunology *178*, 7032-7041.

Wu, L., and Shortman, K. (2005). Heterogeneity of thymic dendritic cells. Seminars in Immunology *17*, 304-312.

Xing, Y., and Hogquist, K.A. (2012). T-cell tolerance: central and peripheral. Cold Spring Harbor perspectives in biology *4*.

Xing, Y., Wang, X., Jameson, S.C., and Hogquist, K.A. (2016). Late stages of T cell maturation in the thymus involve NF-κB and tonic type I interferon signaling. Nat Immunol *17*, 565-573.

Yamano, T., Nedjic, J., Hinterberger, M., Steinert, M., Koser, S., Pinto, S., Gerdes, N., Lutgens, E., Ishimaru, N., Busslinger, M.*, et al.* (2015). Thymic B Cells Are Licensed to Present Self Antigens for Central T Cell Tolerance Induction. Immunity *42*, 1048-1061.

Yang, S., Fujikado, N., Kolodin, D., Benoist, C., and Mathis, D. (2015). Regulatory T cells generated early in life play a distinct role in maintaining self-tolerance. Science *348*, 589-594.

Yano, M., Kuroda, N., Han, H., Meguro-Horike, M., Nishikawa, Y., Kiyonari, H., Maemura, K., Yanagawa, Y., Obata, K., Takahashi, S.*, et al.* (2008). Aire controls the differentiation program of thymic epithelial cells in the medulla for the establishment of self-tolerance. The Journal of Experimental Medicine *205*, 2827-2838.

Yin, L., Huseby, E., Scott-Browne, J., Rubtsova, K., Pinilla, C., Crawford, F., Marrack, P., Dai, S., and Kappler, John W. (2011). A Single T Cell Receptor Bound to Major Histocompatibility Complex Class I and Class II Glycoproteins Reveals Switchable TCR Conformers. Immunity *35*, 23-33.

Yu, Y., Arora, A., Min, W., Roifman, C.M., and Grunebaum, E. (2009). EdU incorporation is an alternative non-radioactive assay to [3H]thymidine uptake for in vitro measurement of mice T-cell proliferations. Journal of Immunological Methods *350*, 29-35.

Yui, M.A., and Rothenberg, E.V. (2014). Developmental gene networks: a triathlon on the course to T cell identity. Nat Rev Immunol *14*, 529-545.

Zamyatnin, A.A. (1972). Protein volume in solution. Progress in Biophysics and Molecular Biology *24*, 107-123.

Ziętara, N., Łyszkiewicz, M., Puchałka, J., Witzlau, K., Reinhardt, A., Förster, R., Pabst, O., Prinz, I., and Krueger, A. (2015). Multicongenic fate mapping quantification of dynamics of thymus colonization. The Journal of Experimental Medicine *212*, 1589-1601.

Zijlstra, M., Bix, M., Simister, N.E., Loring, J.M., Raulet, D.H., and Jaenisch, R. (1990). β2-Microglobulin deficient mice lack CD4-8+ cytolytic T cells. Nature *344*, 742-746.

Zinkernagel, R.M., and Doherty, P.C. (1974). Restriction of in vitro T cell-mediated cytotoxicity in lymphocytic choriomeningitis within a syngeneic or semiallogeneic system. Nature *248*, 701-702.